

# Advances

## in Clinical and Experimental Medicine

MONTHLY ISSN 1899-5276 (PRINT) ISSN 2451-2680 (ONLINE)

[advances.umw.edu.pl](http://advances.umw.edu.pl)

2023, Vol. 32, No. 3 (March)

Impact Factor (IF) – 1.736  
Ministry of Science and Higher Education – 70 pts  
Index Copernicus (ICV) – 168.52 pts



WROCLAW  
MEDICAL UNIVERSITY

Advances  
in Clinical and Experimental  
Medicine



# Advances in Clinical and Experimental Medicine

ISSN 1899-5276 (PRINT)

ISSN 2451-2680 (ONLINE)

advances.umw.edu.pl

**MONTHLY 2023**  
**Vol. 32, No. 3**  
**(March)**

Advances in Clinical and Experimental Medicine (*Adv Clin Exp Med*) publishes high-quality original articles, research-in-progress, research letters and systematic reviews and meta-analyses of recognized scientists that deal with all clinical and experimental medicine.

## Editorial Office

ul. Marcinkowskiego 2–6  
50-368 Wrocław, Poland  
Tel.: +48 71 784 12 05  
E-mail: redakcja@umw.edu.pl

## Publisher

Wrocław Medical University  
Wybrzeże L. Pasteura 1  
50-367 Wrocław, Poland

Online edition is the original version  
of the journal

## Editor-in-Chief

Prof. Donata Kurpas

## Deputy Editor

Prof. Wojciech Kosmala

## Managing Editor

Marek Misiak, MA

## Statistical Editors

Wojciech Bombała, MSc  
Anna Kopszak, MSc  
Dr. Krzysztof Kujawa

## Manuscript editing

Marek Misiak, MA, Jolanta Krzyżak, MA

## Scientific Committee

Prof. Sabine Bährer-Kohler  
Prof. Antonio Cano  
Prof. Breno Diniz  
Prof. Erwan Donal  
Prof. Chris Fox  
Prof. Naomi Hachiya  
Prof. Carol Holland  
Prof. Markku Kurkinen  
Prof. Christos Lionis

Prof. Raimundo Mateos  
Prof. Zbigniew W. Raś  
Prof. Jerzy W. Rozenblit  
Prof. Silvana Santana  
Prof. James Sharman  
Prof. Jamil Shibli  
Prof. Michał Toborek  
Prof. László Vécsei  
Prof. Cristiana Vitale

## Section Editors

### Anesthesiology

Prof. Marzena Zielińska

### Basic Sciences

Prof. Iwona Bil-Lula  
Prof. Bartosz Kempisty  
Dr. Wiesława Kranc  
Dr. Anna Lebedeva  
Dr. Maciej Sobczyński

### Clinical Anatomy, Legal Medicine, Innovative Technologies

Prof. Rafael Boscolo-Berto

### Dentistry

Prof. Marzena Dominiak  
Prof. Tomasz Gedrange  
Prof. Jamil Shibli

### Dermatology

Prof. Jacek Szepietowski

### Emergency Medicine, Innovative Technologies

Prof. Jacek Smereka

### Gynecology and Obstetrics

Prof. Olimpia Sipak-Szmigiel

### Histology and Embryology

Dr. Mateusz Olbromski

### Internal Medicine

#### Angiology

Dr. Angelika Chachaj

#### Cardiology

Prof. Wojciech Kosmala  
Dr. Daniel Morris

#### Endocrinology

Prof. Marek Bolanowski

### Gastroenterology

Assoc. Prof. Katarzyna Neubauer

### Hematology

Prof. Andrzej Deptała

Prof. Dariusz Wołowicz

### Nephrology and Transplantology

Assoc. Prof. Dorota Kamińska

Assoc. Prof. Krzysztof Letachowicz

### Pulmonology

Prof. Anna Brzecka

### Microbiology

Prof. Marzenna Bartoszewicz

Assoc. Prof. Adam Junka

### Molecular Biology

Dr. Monika Bielecka

Prof. Jolanta Saczko

### Neurology

Assoc. Prof. Magdalena Koszewicz

Assoc. Prof. Anna Pokryszko-Dragan

Dr. Masaru Tanaka

### Neuroscience

Dr. Simone Battaglia

### Oncology

Prof. Andrzej Deptała

Dr. Marcin Jędryka

### Gynecological Oncology

Dr. Marcin Jędryka

### Orthopedics

Prof. Paweł Reichert

### Otolaryngology

Assoc. Prof. Tomasz Zatoński

### Pediatrics

#### Pediatrics, Metabolic Pediatrics, Clinical Genetics, Neonatology, Rare Disorders

Prof. Robert Śmigiel

#### Pediatric Nephrology

Prof. Katarzyna Kiliś-Pstrusińska

#### Pediatric Oncology and Hematology

Assoc. Prof. Marek Ussowicz

### Pharmaceutical Sciences

Assoc. Prof. Marta Kepinska

Prof. Adam Matkowski

### Pharmacoeconomics, Rheumatology

Dr. Sylwia Szafraniec-Buryło

### Psychiatry

Prof. Jerzy Leszek

### Public Health

Prof. Monika Sawhney

Prof. Izabella Uchmanowicz

### Qualitative Studies, Quality of Care

Prof. Ludmiła Marcinowicz

### Radiology

Prof. Marek Szaśniadek

### Rehabilitation

Dr. Elżbieta Rajkowska-Labon

### Surgery

Assoc. Prof. Mariusz Chabowski

Prof. Renata Tabała

### Telemedicine, Geriatrics, Multimorbidity

Assoc. Prof. Maria Magdalena

Bujnowska-Fedak

## Editorial Policy

Advances in Clinical and Experimental Medicine (Adv Clin Exp Med) is an independent multidisciplinary forum for exchange of scientific and clinical information, publishing original research and news encompassing all aspects of medicine, including molecular biology, biochemistry, genetics, biotechnology and other areas. During the review process, the Editorial Board conforms to the "Uniform Requirements for Manuscripts Submitted to Biomedical Journals: Writing and Editing for Biomedical Publication" approved by the International Committee of Medical Journal Editors ([www.ICMJE.org](http://www.ICMJE.org)). The journal publishes (in English only) original papers and reviews. Short works considered original, novel and significant are given priority. Experimental studies must include a statement that the experimental protocol and informed consent procedure were in compliance with the Helsinki Convention and were approved by an ethics committee.

For all subscription-related queries please contact our Editorial Office: [redakcja@umw.edu.pl](mailto:redakcja@umw.edu.pl)

For more information visit the journal's website: [advances.umw.edu.pl](http://advances.umw.edu.pl)

Pursuant to the ordinance of the Rector of Wrocław Medical University No. 12/XVI R/2023, from February 1, 2023, authors are required to pay a fee for each manuscript accepted for publication in the journal Advances in Clinical and Experimental Medicine. The fee amounts to 990 EUR for original papers and meta-analyses, 700 EUR for reviews, and 350 EUR for research-in-progress (RIP) papers and research letters.

Advances in Clinical and Experimental Medicine has received financial support from the resources of Ministry of Science and Higher Education within the "Social Responsibility of Science – Support for Academic Publishing" project based on agreement No. RCN/SP/0584/2021.



Ministry of Education and Science  
Republic of Poland

Czasopismo Advances in Clinical and Experimental Medicine korzysta ze wsparcia finansowego ze środków Ministerstwa Edukacji i Nauki w ramach programu „Społeczna Odpowiedzialność Nauki – Rozwój Czasopism Naukowych” na podstawie umowy nr RCN/SP/0584/2021.



Ministerstwo  
Edukacji i Nauki

Indexed in: MEDLINE, Science Citation Index Expanded, Journal Citation Reports/Science Edition, Scopus, EMBASE/Excerpta Medica, Ulrich's™ International Periodicals Directory, Index Copernicus

Typographic design: Piotr Gil, Monika Kołęda

DTP: Wydawnictwo UMW

Cover: Monika Kołęda

Printing and binding: Drukarnia I-BiS Bierońscy Sp.k.



## Contents

### Editorials

- 267 Dominika Filipiak-Strzecka, Piotr Lipiec, Jarosław D. Kasprzak  
**Handheld ultrasound in cardiology: Current perspective**

### Meta-analyses

- 275 Xing Chen, Lihong Yang  
**A systematic review and meta-analysis of the relationship between T-lymphocytes and respiratory tract infection in children**
- 285 Zhen Chen, Hui Zhang  
**A meta-analysis on the role of brain-derived neurotrophic factor in Parkinson's disease patients**

### Original papers

- 297 Çağdaş Özgökçe, Aydın Öcal, Işıl Sezen Ermiş  
**Expression of NF- $\kappa$ B and VEGF in normal placenta and placenta previa patients**
- 307 Zan-Xiong Chen, Hong-Qian Liu, Zhen-Hua Wu, Jun-Lian He, Hao-Jie Zhong  
**Type 3 innate lymphoid cells as an indicator of renal dysfunction and serum uric acid in hyperuricemia**
- 315 Yu-Juan Zhang, Wen-Kai Zhu, Fa-Ying Qi, Feng-Yuan Che  
**CircHIPK3 promotes neuroinflammation through regulation of the miR-124-3p/STAT3/NLRP3 signaling pathway in Parkinson's disease**
- 331 Emilia Błeszyńska-Marunowska, Łukasz Wierucki, Kacper Jagiełło, Krzysztof Rewiuk, Katarzyna Mitręga, Zbigniew Kalarus  
**Prevalence and factors predisposing to potential drug–drug interactions in a Polish community-dwelling geriatric population: An observational, cross-sectional study**
- 341 Bartosz Paweł Wojtera, Agnieszka Sobecka, Mateusz Szewczyk, Piotr Machczyński, Wiktoria Maria Suchorska, Wojciech Golusiński  
**CLIC1 plasma concentration is associated with lymph node metastases in oral squamous cell carcinoma**
- 349 Mengxi Wang, Yanfen Qiu, Lili Gao, Feng Qi, Liangjia Bi  
**The impact of IGF-1 on alveolar bone remodeling and BMP-2 expression in orthodontic tooth movement in diabetic rats**
- 357 Lili Guo, Ming Liu, Tao Duan  
**Hydrogen suppresses oxidative stress by inhibiting the p38 MAPK signaling pathway in preeclampsia**
- 369 Wenhao Cheng, Yumo Lu, Renqiong Chen, Hong Ren, Wenlong Hu  
**The role of the 47-kDa membrane lipoprotein of *Treponema pallidum* in promoting maturation of peripheral blood monocyte-derived dendritic cells without enhancing C-C chemokine receptor type 7-mediated dendritic cell migration**

### Research letters

- 379 Kannan Sridharan, Rashed Abdulla Al Banna, Aisha Husain  
**Time-to-event modeling for achieving a stable warfarin dose using genetic and non-genetic covariates**
- 385 Monika Stępień, Natalia Świątoniowska-Lonc, Brygida Knysz, Beata Jankowska-Polańska, Amadeusz Kuźniarski, Agnieszka Piwowar, Małgorzata Zalewska  
**An epidemiological and retrospective study in a cohort qualified for SARS-CoV-2 vaccination in the region of Lower Silesia, Poland**



# Handheld ultrasound in cardiology: Current perspective

Dominika Filipiak-Strzecka<sup>B,D</sup>, Piotr Lipiec<sup>E,F</sup>, Jarosław D. Kasprzak<sup>E,F</sup>

Chair and Department of Cardiology, Bieganski Hospital, Medical University of Lodz, Poland

A – research concept and design; B – collection and/or assembly of data; C – data analysis and interpretation;  
D – writing the article; E – critical revision of the article; F – final approval of the article

Advances in Clinical and Experimental Medicine, ISSN 1899–5276 (print), ISSN 2451–2680 (online)

*Adv Clin Exp Med.* 2023;32(3):267–274

## Address for correspondence

Dominika Filipiak-Strzecka  
E-mail: dominika.filipiak@gmail.com

## Funding sources

None declared

## Conflict of interest

None declared

Received on December 12, 2022

Accepted on December 26, 2022

Published online on March 28, 2023

## Abstract

The advantages of ultrasonography do not need to be discussed. It is suitable for use in diverse clinical settings and environments by operators with different backgrounds. Recent technological advances have led not only to the enhancement of the diagnostic capabilities of stationary ultrasound systems but also to miniaturization, which in turn led to the introduction of smartphone-sized handheld ultrasound devices (HUDs), designed to be used at bedside to improve and extend the scope of physical examination. Although diagnostic capabilities of HUDs are expanding, according to guidelines, they cannot be perceived as a tool suitable for performing full echocardiographic examination. However, their ultraportability made them essential for the bedside assessment, with the particular emphasis on the bedside focus cardiac ultrasound (FoCUS)-goal-oriented, limited echocardiographic screening. Clinically relevant cardiological targets suggested for HUDs include the assessment of left ventricular (LV) systolic function and size, assessment of other cardiac chambers, identification of gross valvular abnormalities, and detection of the pathological masses within the heart cavities. Handheld ultrasound devices may be also helpful in identifying pleural effusion or subpleural consolidations; furthermore, brief ultrasonographic assessment of “lung comets” enables the estimation of the level of congestion. Ultrasound screening for certain vascular abnormalities also appears promising. The limitations of HUDs are rather obvious and caution is needed to distinguish the role of HUD-based bedside-limited scan from comprehensive stationary echocardiography. It appears that the right approach is to treat them as complementary tools proving their capabilities in diverse clinical scenarios.

**Key words:** handheld ultrasound device, FoCUS, echocardiography

## Cite as

Filipiak-Strzecka D, Lipiec P, Kasprzak JD. Handheld ultrasound in cardiology: Current perspective. *Adv Clin Exp Med.* 2023;32(3):267–274. doi:10.17219/acem/158555

## DOI

10.17219/acem/158555

## Copyright

Copyright by Author(s)

This is an article distributed under the terms of the Creative Commons Attribution 3.0 Unported (CC BY 3.0) (<https://creativecommons.org/licenses/by/3.0/>)

## Introduction

The advantages of ultrasonography are unquestionable and its widespread application requires no justification. It is probably the most versatile imaging method in medicine, and its unique characteristics – availability, portability, low cost, and absence of side effects – make it suitable for use in diverse clinical settings and environments by operators with different backgrounds, to examine numerous structures of the human body. Additionally, the fast image acquisition and the possibility for immediate image interpretation can provide relevant clinical information with direct impact on patient management.

Recent technological advances have led not only to the enhancement of the diagnostic capabilities of stationary ultrasound systems. With different clinical scenarios requiring diversified tools, the path of development began to diverge. On the one hand, echocardiographers expect top imaging quality with the implementation of the most sophisticated imaging methods. On the other, when used in a fast-paced reality of emergency room, such traits are left underused and undervalued – it is the portability and simplified yet prompt assessment of patient's status that counts. Conventional high-end systems, even though designed as mobile, in reality prove difficult to transport. The necessity for bedside examination would result in a time-consuming and impractical transfers of heavy and delicate devices. Thus, the development within the echocardiographic realm may mean more cutting-edge imaging technology but also fitting basic modalities into take-me-everywhere portable devices. While discussing various stages of miniaturization, we should mention the creation of mobile echocardiographs – slightly trimmed down in size yet not in 2D-imaging capabilities group of devices which are more easily transported; laptop-sized portable echocardiographs with slightly limited array of imaging modalities but still sufficient to perform full echo, and finally smartphone-sized handheld ultrasound devices (HUDs) designed for use at bedside to extend and improve physical examination beyond the stethoscope rather than replace standard echocardiography.<sup>1,2</sup>

Visual stethoscope was a theoretical concept first mentioned and then implemented in a real diagnostic device in 1970s by Roelandt et al. (Minivisor).<sup>3,4</sup> However, brilliant ideas may require the technology to catch up and it was not until the beginning of 2000s when the first, “pocket size imaging ultrasonograph” suitable for cardiac imaging was introduced (Acuson P10; Siemens AG, Munich, Germany). Other problem which brilliant ideas usually face is that they have to prevail old routines. Two hundred years ago, it was commonly doubted whether the recently invented stethoscope “will ever come into general use, notwithstanding its value<sup>5</sup>” – and now it has become a symbol of a physician and the diagnostic process.

Fortunately, it is an exaggeration to compare the above-mentioned anecdote and the current position of HUDs in modern medicine. However, the question of their status

in cardiology is quite intriguing, and finding new possibilities for augmenting diagnostic process with ultrasonography appears very tempting.<sup>6,7</sup>

## Technical evolution

Finding a niche in a world of imaging diagnostics required investigating uncharted waters. The HUD manufacturers implemented various ideas to meet clinicians needs that other devices could not fulfill. The user interface of HUDs was simplified, with limited image adjustments, as examination was supposed to be based on the predefined presets, optimally with ease of a single-handed operation. Pioneer HUD enabled only 2D imaging with most basic area and distance measurement tools. Initially used 3.7-inch screen now seems outdated, as the technology utilized then does not compare favorably with screens of currently used smartphones. Significant improvements made throughout the years of development included:

- Addition of color – Doppler modality (visual assessment of cardiac valve competence was made possible).
  - Introduction of a dual probe combining the features of a sector and linear probe, which enabled the assessment of more superficially positioned structures.
  - Radical change of design – certain HUDs are just a probe which could either be connected by a cord or wirelessly with the smartphone/tablet with a dedicated application installed. Such approach had numerous benefits: possibility of fitting the screen size to the clinician's needs; no risk of the prolonged use of the outdated technology as the screen could be “replaced” with the purchase of a new smart device; easy firmware updates that could fix potential software issues; less complicated disinfection of the device (which proved vital during the coronavirus disease (COVID-19) pandemic).
  - Implementation of M-mode imaging capabilities.
  - Streaming a real-time examination for a second opinion or consult, which might prove essential if the HUD operator is an entry-level sonographer.<sup>8</sup>
  - Introduction of the downloadable apps that assist in obtaining correct projections or enable automated evaluation of certain cardiac parameters with the use of machine learning technology. With sufficient computing power of HUDs, it is possible to automatically calculate the left ventricular ejection fraction (LVEF) using an artificial intelligence (AI) module. The first iteration of the software requires only a single 4-chamber view with no border tracing editing. Currently, there are HUDs with more advanced LVEF assessment algorithm which uses 2 apical views: 4-chamber and 2-chamber. Furthermore, manual correction of endocardial borders is possible.
- Manufacturers still search for the optimal size of the HUD screen. At first, the miniaturization was perceived as a paramount goal and the devices were constantly becoming smaller and easy for one-handed operation. However, at a certain

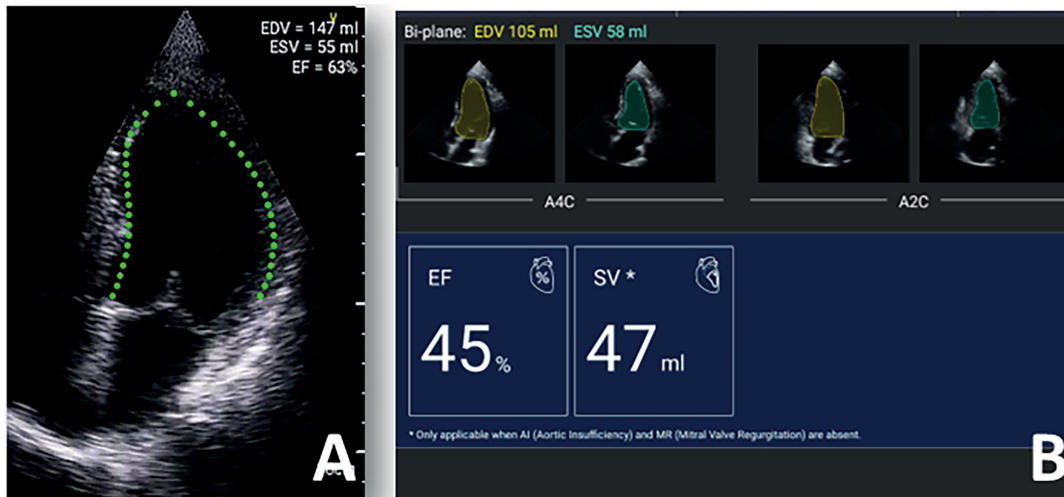


**Fig. 1.** AI-enhanced assessment of LVEF. A. LVivo application; measurement based on 4-chamber apical view only; B. Assessment based on 4-chamber and 2-chamber apical views; manual endocardium border editing available

AI – artificial intelligence; LVEF – left ventricular ejection fraction.

point, the desired ultraportability clashed with the limited visibility of echocardiographic projections on tiny screens. It appears that a larger device with better screen resolution and equipped with a widened set of diagnostic functions but still not exceeding more or less the size of a tablet combines the best features from both worlds. While it will not fit a white coat pocket, it still remains very lightweight and portable. Most recent HUDs may be slightly bigger than other devices from this group, but are equipped with color Doppler, M-mode, pulsed wave and continuous wave spectral Doppler, previously mentioned AI module for LVEF assessment, and systems tutoring and aiding inexperienced sonographers.<sup>9</sup> This makes the separation of a “HUD study” from a “standard study in the lab” less obvious; however, the main objective of using HUDs is improved initial diagnosis rather than replacing comprehensive echocardiography.

## Clinical targets for HUDs

The search for the optimal clinical application of HUDs became a focus of numerous published studies. Many of those papers present cardiologists’ outlook on the subject.<sup>10,11</sup> According to the European Association of Cardiovascular Imaging (EACVI) guidelines,<sup>1,2</sup> the following findings should be emphasized.

### Assessment of LV systolic function and size

In the majority of cases, the assessment of LV systolic function is qualitative, based on visual estimation of LVEF and regional wall motion. This task proved to be one of main interests of authors attempting to make HUD-acquired echocardiography analysis a fully automated process. Certain HUDs (e.g., VScan Extend; GE Healthcare, Lincoln Park, USA) offer a downloadable application which enables an automated edge detection of left myocardial wall and calculates the end-systolic and

end-diastolic left ventricular volumes and LVEF using apical 4-chamber views. Good agreement between HUD and 3D measurement of LVEF on stationary echocardiography was identified<sup>12,13</sup>; however, the results largely depended on the quality of acquired images. Furthermore, in almost 12% of patients, the software failed to calculate LVEF.<sup>12</sup> A more advanced algorithm available on other device (Kosmos; Echonus, Redmond, USA) performed an automated EF calculation from 2 apical projections, which showed good agreement with measurements using Simpson’s method. Other clinical benefits of this software include high-specificity and high-sensitivity detection of patients with decreased LVEF.<sup>14</sup> Improvements to the algorithm also enable a semi-automated EF by editing the endocardial borders, which might prove clinically relevant but requires further validation (Fig. 1).

## Assessment of other cardiac chambers

Right ventricle (RV) visualization with HUDs proves more challenging. Variable correlations between HUD and high-end systems to identify RV dysfunction have been reported. Some studies showed that HUDs proved feasible in the initial assessment of patients with suspected pulmonary embolism. It was concluded that rapid imaging protocols with HUDs, based, among others, on RV enlargement, allow for improved initial evaluation of patients with suspected pulmonary embolism and increase the diagnostic accuracy of clinical risk assessment scores (Fig. 2).<sup>15,16</sup>

Several studies confirmed the feasibility of HUDs in assessing the width and collapsibility of the inferior vena cava (IVC) parameters used for estimating right atrial filling pressures, also in the setting of critical care unit. It is worth noting that in few studies, HUD operators were trained nurses.<sup>17–19</sup> The presence of left atrium (LA) dilatation as a marker of increased LA pressures was proposed as one of the parameters to be evaluated in critically ill patients when performing their initial assessment.<sup>20</sup>



## Gross valvular abnormalities

Initially, a valvular assessment could only be qualitative and based on the visual detection of morphologic abnormalities, such as significant calcification or dilated valvular ring. Due to the introduction of the color Doppler modality, such assessment, although still qualitative, became more accurate. Quantitative analysis was recently made available with the implementation of spectral Doppler to a HUD. It was already confirmed that experienced operators can reliably detect clinically significant aortic stenosis (AS) and facilitate AS grading with the use of this HUD, and this modality might prove promising (Fig. 3).<sup>21</sup>

## Other specific echo findings

The HUD-derived projections are of sufficient quality to enable the detection of the pathological masses within heart cavities. Although scientific data are mainly obtained from case studies, they show that thrombus in LV,<sup>22</sup> masses suggesting the presence of tumors (e.g., myxoma<sup>23</sup>),

or thrombus in transit in right atrium (RA) and RV<sup>24</sup> could all be identified. There is a good overall concordance with the conventional echocardiography in the detection and assessment of pericardial effusion (Fig. 4).<sup>25,26</sup>

## Extracardiac findings

The HUD-performed lung ultrasonography became a particularly interesting diagnostic option in the time of COVID-19 pandemic.<sup>27,28</sup> Besides the identification of pleural effusion or subpleural consolidations, brief ultrasonographic assessment of “lung comets” allows the estimation of the level of congestion, which is vital in patients with heart failure (HF) (Fig. 5).<sup>29</sup>

Ultrasound screening for certain vascular abnormalities can also prove clinically relevant. Handheld ultrasound devices proved their feasibility in carotid stenosis evaluation,<sup>30,31</sup> accessing site complications screening after the femoral artery puncture<sup>32</sup> or a detection of the aortic root dilatation as a marker of aortic dissection in symptomatic patients. Abdominal aneurysm screening may also be feasible in patients with good substernal visibility.

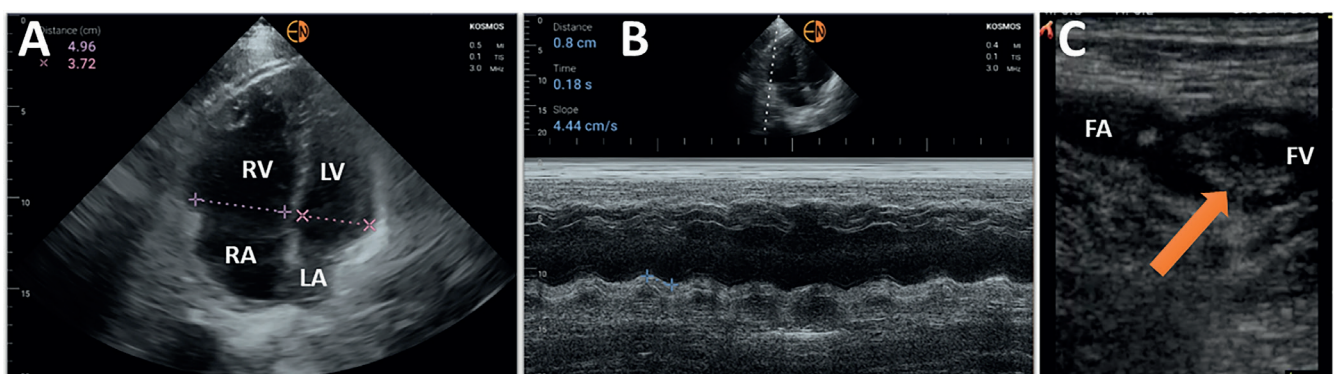


Fig. 2. Bedside HUD examination in patients with suspected pulmonary embolism. A. 4-chamber apical view, RV/LV ratio >1; B. M-mode presentation, decreased TAPSE indicating RV dysfunction; C. Positive result of compression ultrasound, specific for thrombus in femoral vein (marked with an arrow)

HUD – handheld ultrasound device; RV – right ventricle; RA – right atrium; LV – left ventricle; LA – left atrium; FA – femoral artery; FV – femoral vein; TAPSE – tricuspid annular plane systolic excursion.

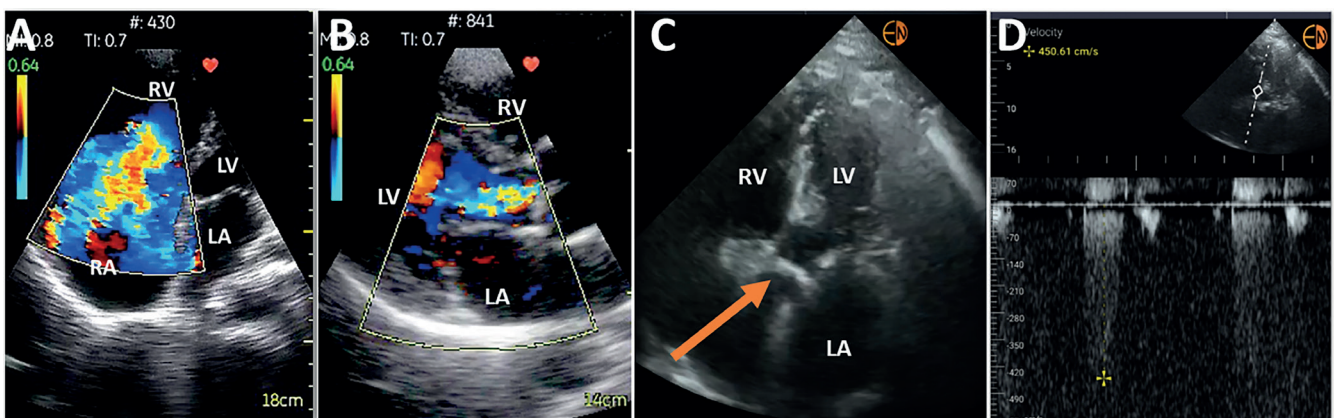


Fig. 3. Valve abnormalities registered with the use of a HUD. A. Massive tricuspid insufficiency; B. Moderate aortic insufficiency; C,D. Significant AS; continuous wave Doppler modality used to confirm severity of stenosis

HUD – handheld ultrasound device; RV – right ventricle; RA – right atrium; LV – left ventricle; LA – left atrium; AS – aortic stenosis.

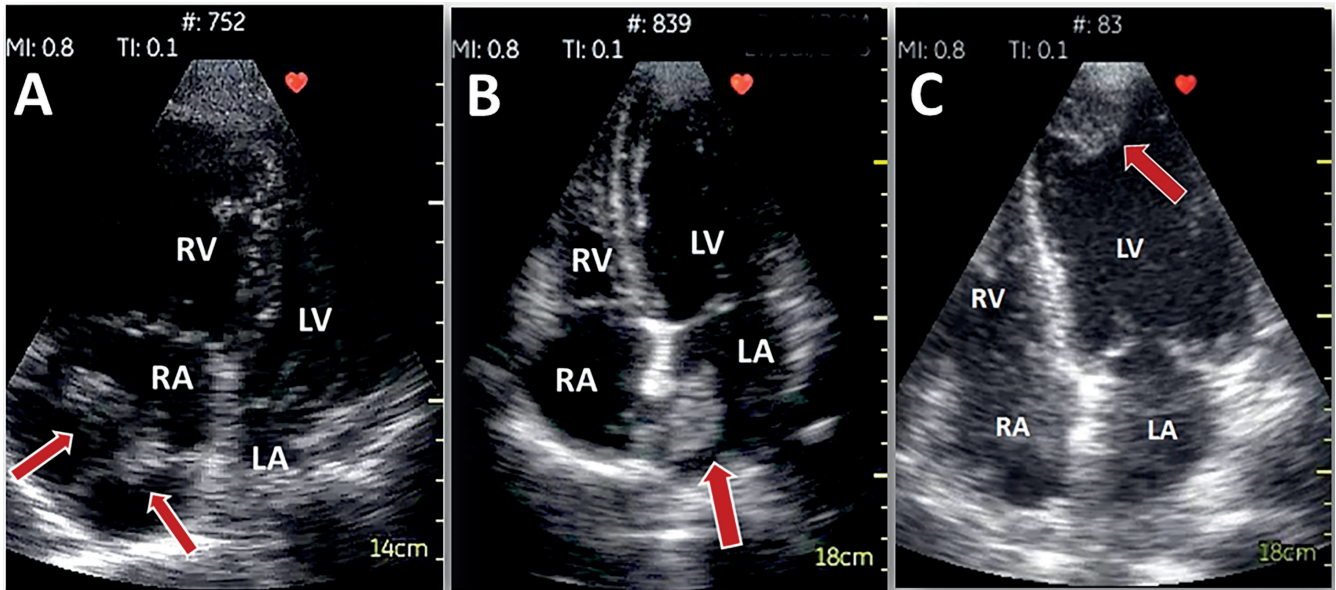


Fig. 4. Intracardiac pathological masses detected with a HUD. A. “Thrombus in transit”; B. LA tumor, later diagnosed as myxoma; C. Thrombus in the apical part of the LV

HUD – handheld ultrasound device; RV – right ventricle; RA – right atrium; LV – left ventricle; LA – left atrium.

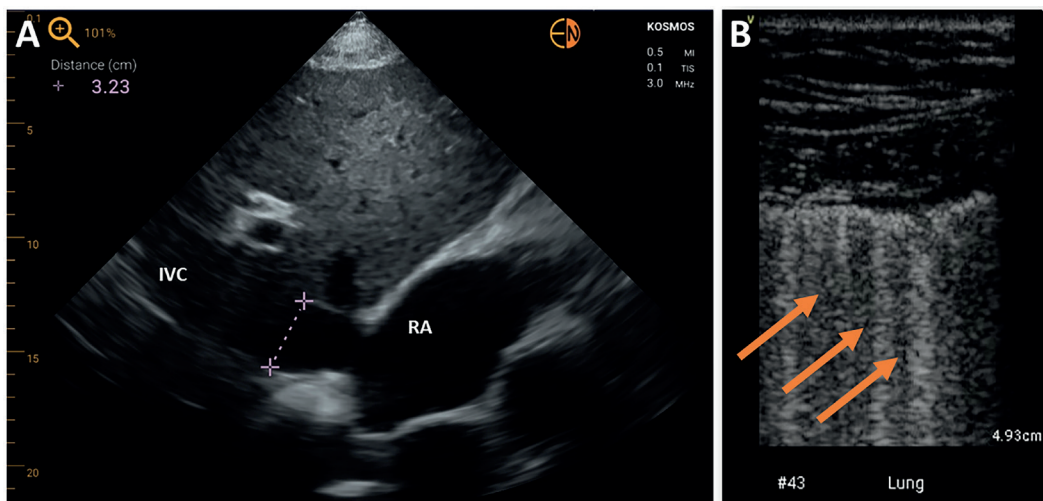


Fig. 5. Bedside HUD examination in a patient with symptoms of HF.

A. IVC dilatation, suggestive of fluid retention; B. Lung ultrasonography – B-lines marked with arrows show pulmonary congestion

HUD – handheld ultrasound device; IVC – inferior vena cava; RA – right atrium; HF – heart failure.

### FoCUS examination

Due to limited diagnostic capabilities of HUDs, it was impossible, according to guidelines, to perceive them as tools that could be used for full echocardiographic examination. However, their ultraportability made them essential tools for the bedside examination, with the particular emphasis on the bedside focus cardiac ultrasound (FoCUS)-goal-oriented, limited echocardiographic examination.<sup>33</sup> Such procedure should be treated as an extension of the physical examination. It can be performed in any environment, with a predefined limited protocol, by an operator not necessarily trained in comprehensive echocardiography, but appropriately trained in FoCUS and usually responsible for decision-making and/or treatment process.

### Who needs the HUDs?

Non-cardiologist use of ultrasound for rapid, bedside structural assessment of the heart in critically ill patients drew widespread attention for the first time in the early 1990s. It was shown that a readily available, limited echocardiogram carried out by emergency physicians could confer a mortality benefit to those with penetrating cardiac injuries.<sup>34</sup> From this narrow scope, non-traditional users of echocardiography such as critical care physicians have expanded the applications of cardiac ultrasound to address a broad array of important clinical questions at the bedside.

The EACVI guidelines emphasize that FoCUS should only be used by the operators who have completed appropriate education and training program, and who fully



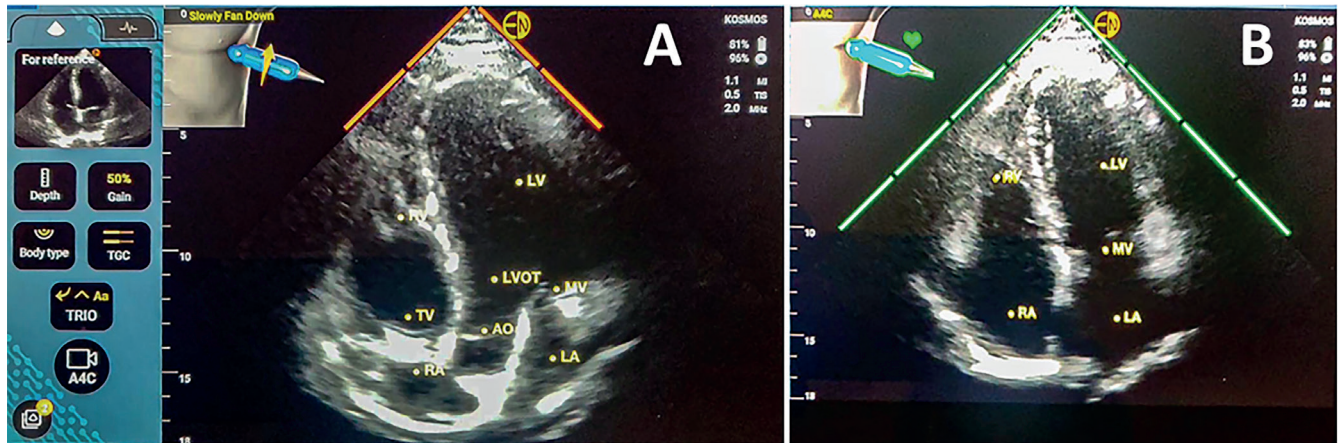


Fig. 6. AI-enhanced auto-labeling and auto-guiding modality (Kosmos; Echonus, Redmond, USA). A. The task was to acquire 4-chamber apical view; projection was assessed as incorrect (orange indicators); probe clockwise rotation suggested; B. Correct 4-chamber apical view; all indicators green

AI – artificial intelligence; RV – right ventricle; RA – right atrium; LV – left ventricle; LA – left atrium; LVOT – left ventricular outflow tract; TV – tricuspid valve; MV – mitral valve; AO – aorta.

understand and respect its scope and limitations.<sup>33</sup> The FoCUS utilizes a highly restricted protocol that represents a small part of the standard comprehensive echocardiographic examination. Although cardiologists who have completed basic echocardiography training outlined in the EACVI recommendations are qualified to perform echocardiography in all emergency situations, for optimal use of FoCUS, they should be familiar with the FoCUS scope, approach and Core Curriculum. In this regard, they could also benefit from additional training, e.g., in basic lung ultrasound (LUS) and the use of cardiac ultrasound in critical care. In case of other medical professionals, theoretical and practical training is vital; it was observed that learning curve for FoCUS is relatively steep.<sup>35</sup>

Novel HUDs introduced machine-learning tutorials for the less experienced operators – modality of real-time labelling of the visualized structures. Apical projections can also be assessed using the software algorithm, and in case of the suboptimal quality hints regarding the proper probe orientation are displayed on the device screen (Fig. 6).

## Other implementations of HUDs

Apart from their clinical usefulness, HUDs are an unequivocally valuable tools for educating and hands-on training of medical students. It was previously confirmed that even a brief training of medical students results in the reliably performed basic ultrasonographic screening augmenting the physical examination.<sup>36,37</sup> Importantly, the learning curve is steep. Proposed use of HUDs by anesthesiologists for the purpose of point-of-care ultrasound (POCUS) learning also proved effective.<sup>38</sup> The HUDs were also introduced as a tool used in numerous screening programs in schools, workplaces and in social campaigns.<sup>39–42</sup> They may also play a prominent role in the development of the contemporary

telemedicine – in a study conducted by Dykes et al., the parents of pediatric patients after heart transplant were trained in acquiring images in parasternal short-axis and apical views, which were subsequently sent to an experienced sonographer for assessment. Interestingly, acquired projections were sufficient for the qualitative assessment of LV function.<sup>43</sup> Finally, HUDs are efficient, cost-effective screening tool to detect patients requiring full echocardiography.<sup>44,45</sup>

## Conclusions

In a world where the consumer needs are being created rather than correctly identified, it may be difficult to tell apart between a gadget and a useful tool that might actually improve certain aspects of our lives. Things become even more convoluted in medicine, where the stakes are especially high. The HUDs at first may seem “gimmicky” and having no real substance to back their widespread use. But in reality, they are still passing the test of time being widely used by numerous medical professionals, who would not otherwise be able to introduce the elements of imaging diagnostics into the treatment process. Moving limited echocardiogram out of echocardiography rooms to the bedside created a real challenge to the traditional ‘just a stethoscope’ approach towards more robust bedside screening. Expert sonographers may frown upon the limited set of features, but even them, when facing an immediate threat to patient’s life in a setting of an emergency ward, would be more than happy to perform basic echocardiography rather than rely on a limited set of diagnostic data. The limitations of HUDs are obvious and effort is needed to distinguish indications for the HUD-based bedside-limited scan and comprehensive, in many cases decisive standard state-of-the-art echocardiography. This is, however, the skill of picking the right tool for the job.



## ORCID iDs

Dominika Filipiak-Strzecka  <https://orcid.org/0000-0001-5760-1243>  
 Piotr Lipiec  <https://orcid.org/0000-0001-5959-2109>  
 Jarosław D. Kasprzak  <https://orcid.org/0000-0002-5850-8187>

## References

- Cardim N, Dalen H, Voigt JU, et al. The use of handheld ultrasound devices: A position statement of the European Association of Cardiovascular Imaging (2018 update). *Eur Heart J Cardiovasc Imaging*. 2019; 20(3):245–252. doi:10.1093/ehjci/jej145
- Sicari R, Galderisi M, Voigt JU, et al. The use of pocket-size imaging devices: A position statement of the European Association of Echocardiography. *Eur J Echocardiogr*. 2011;12(2):85–87. doi:10.1093/ejecho card/jeq184
- Ligtvoet C, Rusterborgh H, Kappen L, Bom N. Real time ultrasonic imaging with a hand-held scanner part I: Technical description. *Ultrasound Med Biol*. 1978;4(2):91–92. doi:10.1016/0301-5629(78) 90033-9
- Roelandt J, Wladimiroff JW, Baars AM. Ultrasonic real time imaging with a hand-held-scanner part II: Initial clinical experience. *Ultrasound Med Biol*. 1978;4(2):93–97. doi:10.1016/0301-5629(78) 90034-0
- Mehta M, Kaul S. Reply: Handheld ultrasound is a valuable bedside tool which can supplement the bedside cardiac exam but not replace it. *JACC Cardiovasc Imaging*. 2015;8(5):622. doi:10.1016/j.jcmg. 2015.01.016
- Hsieh A, Baker MB, Phalen JM, et al. Handheld point-of-care ultrasound: Safety considerations for creating guidelines. *J Intensive Care Med*. 2022;37(9):1146–1151. doi:10.1177/08850666221076041
- Chamsi-Pasha MA, Sengupta PP, Zoghbi WA. Handheld echocardiography: Current state and future perspectives. *Circulation*. 2017; 136(22):2178–2188. doi:10.1161/CIRCULATIONAHA.117.026622
- Wejner-Mik P, Teneta A, Jankowski M, et al. Feasibility and clinical utility of real-time tele-echocardiography using personal mobile device-based pocket echocardiograph. *Arch Med Sci*. 2019;18(4):998–1003. doi:10.5114/aoms.2019.83136
- Stewart JE, Goudie A, Mukherjee A, Dwivedi G. Artificial intelligence-enhanced echocardiography in the emergency department. *Emerg Med Australas*. 2021;33(6):1117–1120. doi:10.1111/1742-6723.13847
- Wejner-Mik P, Kasprzak JD, Filipiak-Strzecka D, Miśkowiec D, Lorens A, Lipiec P. Personal mobile device-based pocket echocardiograph: The diagnostic value and clinical utility. *Adv Med Sci*. 2019;64(1): 157–161. doi:10.1016/j.advms.2018.11.003
- Michalski B, Kasprzak JD, Szymczyk E, Lipiec P. Diagnostic utility and clinical usefulness of the pocket echocardiographic device: Diagnostic utility and clinical usefulness of the pocket echocardiographic device. *Echocardiography*. 2012;29(1):1–6. doi:10.1111/j.1540-8175. 2011.01553.x
- Filipiak-Strzecka D, Kasprzak JD, Wejner-Mik P, Szymczyk E, Wdowiak-Okrojek K, Lipiec P. Artificial intelligence-powered measurement of left ventricular ejection fraction using a handheld ultrasound device. *Ultrasound Med Biol*. 2021;47(4):1120–1125. doi:10.1016/j.ultrasmedbio.2020.12.003
- Hjorth-Hansen AK, Magelssen MI, Andersen GN, et al. Real-time automatic quantification of left ventricular function by hand-held ultrasound devices in patients with suspected heart failure: A feasibility study of a diagnostic test with data from general practitioners, nurses and cardiologists. *BMJ Open*. 2022;12(10):e063793. doi:10.1136/bmjopen-2022-063793
- Papadopoulou SL, Sachpekidis V, Kantartzis V, Styliadis I, Nihoyannopoulos P. Clinical validation of an artificial intelligence-assisted algorithm for automated quantification of left ventricular ejection fraction in real time by a novel handheld ultrasound device. *Eur Heart J Digital Health*. 2022;3(1):29–37. doi:10.1093/ehjdh/ztac001
- Filipiak-Strzecka D, Kasprzak JD, Lipiec P. Brief cardiovascular imaging with pocket-size ultrasound devices improves the accuracy of the initial assessment of suspected pulmonary embolism. *Int J Cardiovasc Imaging*. 2018;34(10):1595–1605. doi:10.1007/s10554-018-1382-5
- Dresden S, Mitchell P, Rahimi L, et al. Right ventricular dilatation on bedside echocardiography performed by emergency physicians aids in the diagnosis of pulmonary embolism. *Ann Emerg Med*. 2014; 63(1):16–24. doi:10.1016/j.annemergmed.2013.08.016
- Zisis G, Yang Y, Huynh Q, et al. Nurse-provided lung and inferior vena cava assessment in patients with heart failure. *J Am Coll Cardiol*. 2022;80(5):513–523. doi:10.1016/j.jacc.2022.04.064
- Gundersen GH, Norekval TM, Haug HH, et al. Adding point of care ultrasound to assess volume status in heart failure patients in a nurse-led outpatient clinic: A randomised study. *Heart*. 2016;102(1):29–34. doi:10.1136/heartjnl-2015-307798
- Liebo MJ, Israel RL, Lillie EO, Smith MR, Rubenson DS, Topol EJ. Is pocket mobile echocardiography the next-generation stethoscope? A cross-sectional comparison of rapidly acquired images with standard transthoracic echocardiography. *Ann Intern Med*. 2011;155(1):33. doi:10.7326 /0003-4819-155-1-201107050-00005
- Mai TV, Shaw DJ, Amundson SA, Agan DL, Kimura BJ. Learning to apply the pocket ultrasound device on the critically ill: Comparing six “quick-look” signs for quality and prognostic values during initial use by novices. *Crit Care*. 2013;17(5):448. doi:10.1186/cc12875
- Sachpekidis V, Papadopoulou SL, Kantartzis V, Styliadis I, Nihoyannopoulos P. A novel handheld echocardiography device with continuous-wave Doppler capability: Implications for the evaluation of aortic stenosis severity. *J Am Soc Echocardiogr*. 2022;35(12):1273–1280. doi:10.1016/j.echo.2022.08.012
- Shamoun F, Narichania A. Handheld echocardiography saves the brain: A serendipitously found left ventricular thrombus. *J Cardiovasc Echography*. 2015;25(2):53. doi:10.4103/2211-4122.161780
- Pourdjabbar A, Hibbert B, Maze R, Lai C, Le May MR. Left atrial myxoma: A rare cause of dyspnea. *Can J Cardiol*. 2014;30(4):465.e1–465.e2. doi:10.1016/j.cjca.2013.11.017
- Wejner-Mik P, Filipiak-Strzecka D, Kasprzak JD, Lipiec P. Intracardiac thrombus in a patient with pulmonary embolism: The use of handheld ultrasound. *Folia Cardiol*. 2016;11(4):347. [https://journals.viamedica.pl/fovia\\_cardiologica/article/view/FC.2016.0058/37779](https://journals.viamedica.pl/fovia_cardiologica/article/view/FC.2016.0058/37779)
- Kennedy Hall M, Coffey EC, Herbst M, et al. The “5Es” of emergency physician-performed focused cardiac ultrasound: A protocol for rapid identification of effusion, ejection, equality, exit, and entrance. *Acad Emerg Med*. 2015;22(5):583–593. doi:10.1111/acem.12652
- Kimura BJ, Yogo N, O’Connell CW, Phan JN, Showalter BK, Wolfson T. Cardiopulmonary limited ultrasound examination for “quick-look” bedside application. *Am J Cardiol*. 2011;108(4):586–590. doi:10.1016/j.amjcard.2011.03.091
- Dadon Z, Levi N, Alpert EA, et al. The quality, safety, feasibility, and interpretive accuracy of echocardiographic and lung ultrasound assessment of COVID-19 patients using a hand-held ultrasound. *Echocardiography*. 2022;39(7):886–894. doi:10.1111/echo.15372
- Dadon Z, Levi N, Orlev A, et al. The utility of handheld cardiac and lung ultrasound in predicting outcomes of hospitalised patients with COVID-19. *Can J Cardiol*. 2022;38(3):338–346. doi:10.1016/j.cjca. 2021.11.016
- Johannessen Ø, Myhre PL, Omland T. Assessing congestion in acute heart failure using cardiac and lung ultrasound: A review. *Exp Rev Cardiovasc Ther*. 2021;19(2):165–176. doi:10.1080/14779072.2021.1865155
- Filipiak-Strzecka D, Kasprzak JD, Szymczyk E, Wejner-Mik P, Lipiec P. Bedside screening with the use of pocket-size imaging device can be useful for ruling out carotid artery stenosis in patients scheduled for cardiac surgery. *Echocardiography*. 2017;34(5):716–722. doi:10.1111/echo.13507
- Jin L, Tong LY, Sha L, et al. Handheld versus conventional ultrasound for assessing carotid artery in routine volunteers. *Clin Hemorheol Microcirc*. 2022;82(3):255–263. doi:10.3233/CH-221521
- Filipiak-Strzecka D, Michalski B, Kasprzak JD, Lipiec P. Pocket-size imaging devices allow for reliable bedside screening for femoral artery access site complications. *Ultrasound Med Biol*. 2014;40(12):2753–2758. doi:10.1016/j.ultrasmedbio.2014.06.022
- Neskovic AN, Skinner H, Price S, et al. Focus cardiac ultrasound core curriculum and core syllabus of the European Association of Cardiovascular Imaging. *Eur Heart J Cardiovasc Imaging*. 2018;19(5):475–481. doi:10.1093/ehjci/jej006
- Plummer D, Brunette D, Asinger R, Ruiz E. Emergency department echocardiography improves outcome in penetrating cardiac injury. *Ann Emerg Med*. 1992;21(6):709–712. doi:10.1016/S0196-0644(05)82784-2
- Jujo S, Sakka BI, Lee-Jayaram JJ, et al. Medical student medium-term skill retention following cardiac point-of-care ultrasound training based on the American Society of Echocardiography curriculum framework. *Cardiovasc Ultrasound*. 2022;20(1):26. doi:10.1186/s12947-022-00296-z

36. Filipiak-Strzecka D, John B, Kasprzak J, Michalski B, Lipiec P. Pocket-size echocardiograph: A valuable tool for non-experts or just a portable device for echocardiographers? *Adv Med Sci.* 2013;58(1):67–72. doi:10.2478/v10039-012-0054-2
37. Kameda T, Koibuchi H, Konno K, Taniguchi N. Self-learning followed by telepresence instruction of focused cardiac ultrasound with a handheld device for medical students: A preliminary study. *J Med Ultrasonics.* 2022;49(3):415–423. doi:10.1007/s10396-022-01233-3
38. Moharir A, Tobias JD. The role of a handheld ultrasound device to facilitate remote learning for a point-of-care ultrasound certificate program. *Adv Med Educ Pract.* 2021;12:1043–1048. doi:10.2147/AMEP.S328625
39. Esposito R, Ilardi F, Schiano Lomoriello V, et al. Identification of the main determinants of abdominal aorta size: A screening by pocket size imaging device. *Cardiovasc Ultrasound.* 2017;15(1):2. doi:10.1186/s12947-016-0094-z
40. Saxena A. Rheumatic heart disease screening by “point-of-care” echocardiography: An acceptable alternative in resource limited settings? *Transl Pediatr.* 2015;4(3):210–213. doi:10.3978/j.issn.2224-4336.2015.06.01
41. Abe Y, Ito M, Tanaka C, et al. A novel and simple method using pocket sized echocardiography to screen for aortic stenosis. *J Am Soc Echocardiogr.* 2013;26(6):589–596. doi:10.1016/j.echo.2013.03.008
42. Hosseini S, Samiei N, Tabib A, et al. Prevalence of structural heart diseases detected by handheld echocardiographic device in school-age children in Iran: The SHED LIGHT Study. *Global Health.* 2022;17(1):39. doi:10.5334/gh.1121
43. Dykes JC, Kipps AK, Chen A, Nourse S, Rosenthal DN, Selamet Tierney ES. Parental acquisition of echocardiographic images in pediatric heart transplant patients using a handheld device: A pilot telehealth study. *J Am Soc Echocardiogr.* 2019;32(3):404–411. doi:10.1016/j.echo.2018.10.007
44. Gianstefani S, Catibog N, Whittaker AR, et al. Pocket-size imaging device: Effectiveness for ward-based transthoracic studies. *Eur Heart J Cardiovasc Imaging.* 2013;14(12):1132–1139. doi:10.1093/ehjci/jet091
45. Prinz C, Voigt JU. Diagnostic accuracy of a hand-held ultrasound scanner in routine patients referred for echocardiography. *J Am Soc Echocardiogr.* 2011;24(2):111–116. doi:10.1016/j.echo.2010.10.017

# A systematic review and meta-analysis of the relationship between T-lymphocytes and respiratory tract infection in children

Xing Chen<sup>1,A–D,F</sup>, Lihong Yang<sup>2,A–E</sup>

<sup>1</sup> Department of Paediatrics, Huzhou Central Hospital, Affiliated Central Hospital Huzhou University, China

<sup>2</sup> Department of General Practice, Huzhou Central Hospital, Affiliated Central Hospital Huzhou University, China

A – research concept and design; B – collection and/or assembly of data; C – data analysis and interpretation; D – writing the article; E – critical revision of the article; F – final approval of the article

Advances in Clinical and Experimental Medicine, ISSN 1899–5276 (print), ISSN 2451–2680 (online)

*Adv Clin Exp Med.* 2023;32(3):275–284

## Address for correspondence

Lihong Yang

E-mail: yanglihong2006@126.com

## Funding sources

None declared

## Conflict of interest

None declared

Received on May 11, 2022

Reviewed on July 4, 2022

Accepted on September 23, 2022

Published online on December 8, 2022

## Abstract

The objective of this paper was to investigate the relationship between T-lymphocytes and respiratory tract infection in children. A meta-analysis was performed of studies related to virus-infected respiratory illnesses in children, and the change in the ratio of their T-lymphocyte subsets CD4<sup>+</sup>/CD8<sup>+</sup>. A systematic literature review was performed using MEDLINE (through PubMed), CINAHL (via Ebsco), Scopus, and Web of Science, for studies describing change in T-lymphocyte levels in children suffering from acute respiratory illnesses. Studies were included as per the Population, Intervention, Comparison, Outcomes and Study (PICOS) criteria, and relevant event data were extracted. A risk of publication bias and a risk of bias assessment were performed, and a funnel plot was designed using RevMan software. A column histogram was designed to compare the adverse effects. A total of 12 studies from the years 2000–2022 were included in the meta-analysis, containing information about 1111 patients. The current meta-analysis has a low risk of publication bias with the Egger's test p-value being 0.583 ( $p > 0.05$ ) and the Begg's test p-value being 0.772 ( $p > 0.05$ ). The odds ratio (OR) value was 3.66 (95% confidence interval (95% CI): 1.08–12.43), the risk ratio (RR) value was 1.91 (95% CI: 1.07–3.40) and the significance level was  $p < 0.05$ , which indicates that an alteration in T-lymphocyte levels occurs in respiratory infections.

T-lymphocyte levels are altered during infection, and the association between T-lymphocytes and respiratory diseases in children was investigated in this study. Based on statistically significant data ( $p < 0.05$ ), we concluded that T-lymphocyte levels are adjusted in the event of viral respiratory sickness in children to alleviate the infection.

**Key words:** T-lymphocytes, respiratory tract infections, COVID-19, respiratory illnesses among children, T-lymphocyte subsets CD4<sup>+</sup>

## Cite as

Chen X, Yang L. A systematic review and meta-analysis of the relationship between T-lymphocytes and respiratory tract infection in children.

*Adv Clin Exp Med.* 2023;32(3):275–284.

doi:10.17219/acem/154881

## DOI

10.17219/acem/154881

## Copyright

Copyright by Author(s)

This is an article distributed under the terms of the Creative Commons Attribution 3.0 Unported (CC BY 3.0) (<https://creativecommons.org/licenses/by/3.0/>)

## Introduction

Acute respiratory tract infections (ARTIs) are quite common in young people. Children, for example, are more susceptible to upper respiratory infections, such as the common cold, influenza and croup,<sup>1,2</sup> or lower respiratory infections, such as bronchitis and pneumonia.<sup>3,4</sup> The upper respiratory system includes the trachea and bronchi airways, as well as the paranasal sinuses and middle ear.<sup>5,6</sup> The lower respiratory tract includes the airways from the trachea and bronchi, as well as the bronchioles and alveoli. Bacteria, fungi and viruses can cause acute respiratory infections, which can either stay limited to the respiratory tract or spread throughout the body due to infection or microbial toxins.<sup>7-9</sup> When a foreign body or pathogen enters the body, the immune system recognizes the antigen and activates the immune system, causing certain cells to proliferate and differentiate to make antibodies. Antibodies work by destroying the antigen and fighting the infection. Similarly, it is thought that when children have a respiratory ailment, their T-lymphocyte level changes in comparison to their usual level, allowing the pathogen to be eliminated and the infection to be cleared. T-lymphocytes are major players in the immune system that target specific foreign particles. They will not generically attack any antigens, but they will circulate in the blood until they encounter their specific antigen and then trigger the immune response. As such, T-lymphocytes play a critical part in immunity to foreign substances, as shown in Fig. 1. It is obvious that CD8<sup>+</sup> and CD4<sup>+</sup> T-lymphocyte cells are necessary for facilitating the clearance of pathogens following many acute viral infections of the lung. This is the case because both types of T-lymphocytes are involved in the immune response and in providing the protection against secondary infections. Hence, the combined induction of virus-specific CD8<sup>+</sup> and CD4<sup>+</sup> T-lymphocyte cells and antibody production is essential for the development of optimal protective immunity.

Several review articles and case studies also reported that the change in T-lymphocyte levels in children with recurrent respiratory infections is most likely. In their review

study, Chen and John Wherry<sup>12</sup> observed that individuals with severe coronavirus disease 2019 (COVID-19) have altered T-lymphocyte responses that are either insufficient or overactive. Lambert and Culley<sup>13</sup> discovered that the levels of T-helper cells and CD8<sup>+</sup> cells alter during respiratory infections. In 2013, Tan et al.<sup>14</sup> identified changes in circulating T-lymphocytes in children with obstructive lung disorders. According to Zimmermann and Curtis,<sup>15</sup> COVID-19 is less severe in youngsters because of its significant potential to change T-lymphocyte levels and antibody production. In light of these findings, we conducted a systematic review and meta-analysis to look into the link between T-lymphocytes and respiratory tract infections in children, analyzing 12 case-control studies<sup>16-27</sup> that compared the change in T-lymphocyte levels in children with respiratory illness to healthy controls. Although bacteria, viruses and fungi can all cause respiratory infections in children, this study focuses solely on viral respiratory disorders and their influence on T-lymphocyte numbers. All of the analyzed studies used flow cytometry to evaluate the changes in T-lymphocyte levels in terms of changing T-lymphocyte subsets: CD4<sup>+</sup> and CD8<sup>+</sup> levels.

He et al.<sup>16</sup> reported an increase in T-lymphocyte count in children with acute respiratory infections, but Munteanu et al.<sup>21</sup> and Gul et al.<sup>22</sup> found a decrease in T-lymphocyte count. Similarly, Li et al.<sup>23</sup> and Cosgrove et al.<sup>24</sup> described an increase in T-lymphocyte levels in children with lower respiratory tract infections such as pneumonia and upper respiratory tract infections such as rhinorrhea, respectively, while Calapodopulos et al.<sup>25</sup> found a decrease in T-lymphocyte count in children with upper respiratory tract infections such as tonsillitis and sinusitis. Lu et al.<sup>26</sup> and Mahmoudi et al.<sup>27</sup> showed an increase in T-lymphocyte count in their studies on the latest pandemic, the 2019 novel coronavirus (2019-nCoV), which causes lower respiratory tract infections like pneumonia.

Considering all these contradictory reports, the present meta-analysis was conducted to evaluate whether the combined induction of virus-specific T-lymphocyte cells and enhanced antibody production occurred in children with acute respiratory illness or not. Data from the 12 selected

Respiratory illnesses in children	Types and causative virus of different respiratory tract infections	Immune response
<ul style="list-style-type: none"> <li>• Children are prone to respiratory tract infections caused by viruses</li> <li>• These infections may affect either upper or lower respiratory tract</li> </ul>	<ul style="list-style-type: none"> <li>• <b>Upper respiratory tract infections:</b> <ul style="list-style-type: none"> <li>• Common cold – rhino virus</li> <li>• Influenza – influenza virus</li> </ul> </li> <li>• <b>Lower respiratory tract infections:</b> <ol style="list-style-type: none"> <li>1. Croup – parainfluenza virus</li> <li>2. Bronchitis – adenovirus</li> <li>3. Pneumonia – respiratory syncytial virus (RSV), SARS-CoV-2</li> </ol> </li> </ul>	<ul style="list-style-type: none"> <li>• To alleviate the viral infection, immune response is activated which results in change in T-lymphocytes level</li> <li>• The change in T-lymphocyte is detected in terms of T-cell subsets CD4<sup>+</sup> and CD8<sup>+</sup> through flow cytometry</li> </ul>

Fig. 1. Respiratory illnesses in children

SARS-CoV-2 – severe acute respiratory syndrome coronavirus 2.

studies were retrieved, statistically evaluated and analyzed in order to determine the significant link between the T-lymphocyte levels in children with acute respiratory illness.

## Objectives

Through the evaluation of the combined induction of virus-specific T-lymphocyte cells and enhanced antibody production for optimal immunity, the purpose of this research is to investigate the link between T-lymphocytes and ARTIs in children. Specifically, this investigation will focus on children.

## Materials and methods

In the current investigation (registration at Huzhou University, China, No. HZ #/IRB/2021/2220), we followed the normative requirements of Preferred Reporting Items for Systematic Reviews and Meta-analyses (PRISMA).

### Search methodology

A comprehensive search was undertaken in the databases of MEDLINE (through PubMed), CINAHL (via Ebsco), Scopus, and Web of Science, concerning studies published between 2000 and 2022 and using the following keywords: “upper respiratory tract infections”, “lower respiratory tract infections”, “common cold”, “croup”, “pneumonia”, “COVID-19”, “influenza”, “viral infections”, “respiratory syncytial virus”, “rhinovirus”, “influenza virus”, “T-lymphocytes”, “T-lymphocyte subsets CD4<sup>+</sup> and CD8<sup>+</sup>”, “immune response”, “immunity”, and “antibody production”. All included papers followed the PRISMA guidelines, and studies were chosen at random, regardless of language, publication status or study type (prospective, retrospective or clinical trial). The event data from the included studies and the demographics of patients<sup>16–27</sup> were collected and used for the meta-analysis.

Separately, 2 writers (XC and LY) scanned pertinent sources for similar investigations. Full-text articles were analyzed, and abstracts were included only if they contained enough information for the meta-analysis. Obsolete references were removed, and studies that met the inclusion criteria were taken into consideration. Two researchers (XC and LY) separately obtained the event data with useful variables.

### Inclusion and exclusion criteria

Studies from the years 2000–2022 that indicated the changes in T-lymphocyte levels in children during acute respiratory tract infections were included. In this analysis, only full-text articles with sufficient event data for the 2 × 2 DerSimonian and Laird method were selected, while studies with insufficient data and papers published before 2000 were excluded.

## Analytical standard evaluation and heterogeneity sources

Two reviewers (XC and LY) independently assessed the methodological soundness and calculated the experimental heterogeneity. The Cochran’s Q statistic and I<sup>2</sup> index were estimated using RevMan software v. 4.1 (<https://training.cochrane.org/online-learning/core-software/rev-man>) to evaluate the heterogeneity.<sup>28</sup> The use of different case-control, prospective and retrospective studies, different number of patients, and assessment of different viral infections, either upper respiratory tract infections like the common cold, influenza, or lower respiratory tract infections like pneumonia, croup and other viruses, were all investigated as sources of heterogeneity.

### Statistical analyses

The diagnostic odds ratio (OR) was determined using the DerSimonian and Laird approach for statistical analysis.<sup>29</sup> The event data were used to create a 2 × 2 table, and RevMan software was used to perform a meta-analysis. The Mantel–Haenszel (M–H) test with the random bivariate model was used to obtain the pooled diagnostic OR with 95% confidence interval (95% CI) and the risk ratio (RR) with 95% CI.<sup>30</sup> The heterogeneity of included research (Tau<sup>2</sup>,  $\chi^2$  value, Q value, degrees of freedom (df) value, I<sup>2</sup> value, and p-value) was assessed using RevMan software together with their corresponding forest plots. To analyze the risk of publication bias, RevMan software was used to provide a risk of bias summary and a risk of bias graph. The publication bias of the included studies was assessed using the Begg’s test and the Egger’s test. The Deek’s funnel plot<sup>31</sup> was performed by plotting the log risk ratio of each study against its standard error using MedCalc software v. 20.118 (MedCalc Software Ltd., Ostend, Belgium). The CD4<sup>+</sup>/CD8<sup>+</sup> ratio in children with respiratory tract infections compared to healthy controls was evaluated, and a column histogram was created to compare the change in T-lymphocyte subsets.

## Results

### Results of literature searches

A total of 1448 studies have been retrieved from various databases. By reviewing the titles and abstracts of these investigations, we were able to eliminate 285 studies, leaving 1163 records to be assessed further. We also eliminated 642 studies due to faulty references and duplication, leaving only 521 for the final screening. Due to inclusion criteria, 395 of the 521 studies were removed, and for the remaining 126 papers, eligibility was further determined. Inadequate evidence and improper comparison criteria for creating 2 × 2 tables for the review were the main reasons for



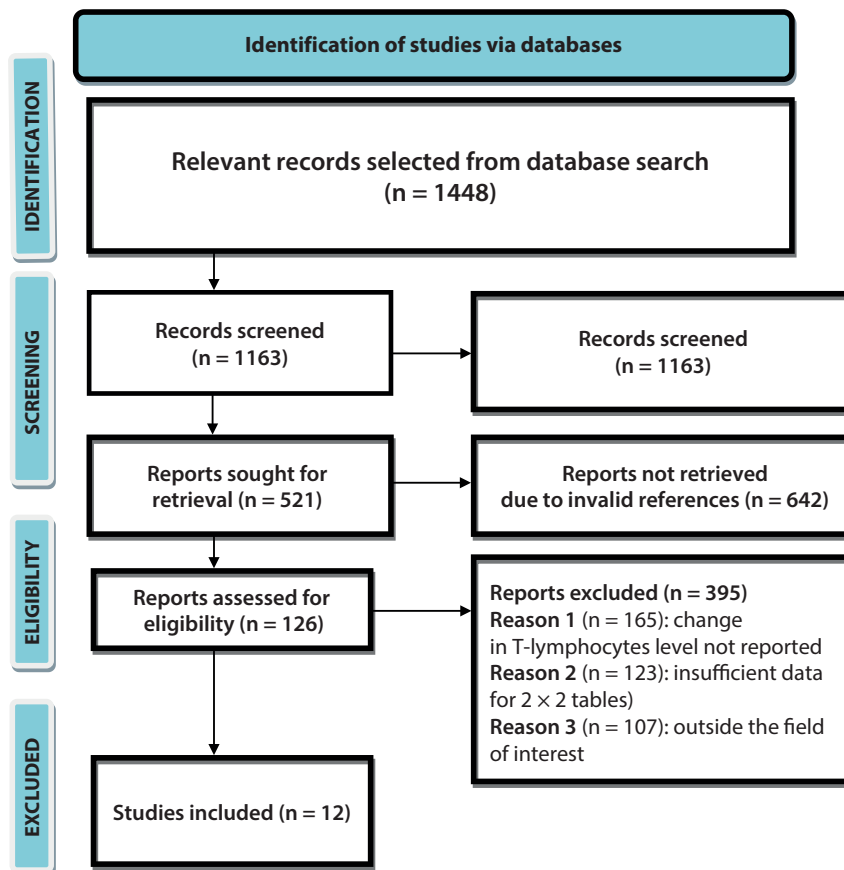


Fig. 2. Flow diagram of the study group

the omission. Finally, 12 papers from the years 2000–2022 that fit the inclusion criteria, namely a change in T-lymphocyte levels in children with recurrent respiratory infections, were incorporated into the meta-analysis, as shown in Fig. 2.

The trials included 1111 children who were recruited at random, and reported changes in CD4<sup>+</sup> and CD8<sup>+</sup> T-lymphocyte subsets in children with ARTIs compared to healthy controls. Each of the studied children suffered from an acute respiratory illness, such as cystic fibrosis or pneumonia. Their T-lymphocyte levels were compared with levels in healthy children of the same age group to assess changes in T-lymphocyte levels due to viral infection. Table 1 shows the demographic characteristics of the studies included in this meta-analysis. It lists the authors of each study, publication year, journal title, kind of respiratory tract infection, causative virus, number of patients and healthy controls, change in the T-lymphocyte subset ratio (CD4<sup>+</sup>/CD8<sup>+</sup>), significance level (p-value), and study conclusion. A meta-analysis was performed based on the event data from these studies, including the number of patients and healthy controls, as well as the change in their CD4<sup>+</sup>/CD8<sup>+</sup> ratio.

## Meta-analysis findings

RevMan software was used to conduct a meta-analysis. Table 2 shows the risk of bias for the included studies. The risk of bias graph in Fig. 3 and the risk of bias summary

in Fig. 4 reveal that the current meta-analysis has a low risk of bias. A funnel plot was created using RevMan software to detect publication bias or systematic heterogeneity. The current meta-analysis has a low risk of publication bias, as apparent from the symmetric inverted funnel shape plot (Fig. 5), which shows a well-conducted data collection with little chance of publication bias. It is also evident from the results of both the Egger's test and the Begg's test as the p-values of both tests are greater than 0.050 and therefore are not statistically significant. The Egger's test p-value is 0.583 ( $p > 0.050$ ) and the Begg's test p-value is 0.772 ( $p > 0.050$ ).

The OR of the included studies was evaluated using RevMan software to assess the link between changes in T-lymphocyte levels in children with acute upper or lower respiratory infections compared to healthy children. Figure 6 depicts the forest plot of ORs as well as data heterogeneity. The position of diamonds in the forest plot toward diseased children confirms that the likelihood of alteration in T-lymphocyte levels is higher in sick children as compared to healthy controls. As the diamond shape is not touching the line of no effect, it confirms that the difference between the 2 groups studied is statistically significant. We calculated a pooled OR of 3.66 and a 95% CI of 1.08–12.43, with heterogeneity of Tau<sup>2</sup> value of 4.51, a  $\chi^2$  value of 390.49, a df value of 11, an I<sup>2</sup> value of 97%, a Z value of 2.08, and a p-value of 0.040. An OR greater than 1 indicates that the condition or event is more likely

**Table 1.** Demographic summary of included studies

Study ID and year	Journal title	Respiratory illness	Causative virus	Age of patients [years]	Sample collected	Cells studied	Estimation technique	Observations				Conclusion T-lymphocyte level in respiratory illness	
								Number of patients	CD4 <sup>+</sup> /CD8 <sup>+</sup> ratio	Number of healthy controls	CD4 <sup>+</sup> /CD8 <sup>+</sup> ratio		p-value
He et al. 2005 [16]	<i>The International Journal of Infectious Diseases</i>	lower respiratory tract infections: severe acute respiratory syndrome pneumonia	SARS-associated coronavirus	<18	blood sample	T-cell subsets CD4 <sup>+</sup> and CD8 <sup>+</sup>	flow cytometry	271	1.51 ±0.73	51	1.57 ±0.44	0.05	increases
Karsh et al. 2005 [17]	<i>Allergy, Asthma &amp; Clinical Immunology</i>	lower respiratory tract infections: asthma, bronchitis	SARS-associated coronavirus	<18	blood sample	T-cell subsets CD4 <sup>+</sup> and CD8 <sup>+</sup>	flow cytometry	30	2.28 ±1.3	25	4.0 ±1.3	0.005	increases
Pinto et al. 2006 [18]	<i>Pediatrics</i>	lower respiratory tract infections: bronchitis	respiratory syncytial virus	<1	blood sample	T-cell subsets CD4 <sup>+</sup> and CD8 <sup>+</sup>	flow cytometry	42	2.5 ±2.01	21	3.7 ±0.65	0.001	increases
Kim et al. 2011 [19]	<i>Korean Journal of Pediatrics</i>	lower respiratory tract infections: bronchitis, pneumonia	influenza A virus (H1N1)	<18	blood sample	T-cell subsets CD4 <sup>+</sup> and CD8 <sup>+</sup>	flow cytometry	16	0.86 ±0.24	13	1.61 ±0.49	0.01	increases
Connors et al. 2018 [20]	<i>Journal of Immunology</i>	lower respiratory tract infections: bronchitis	respiratory syncytial virus	<10	blood sample	T-cell subsets CD4 <sup>+</sup> and CD8 <sup>+</sup>	flow cytometry	113	0.34 ±0.09	21	0.51 ±0.24	0.001	increases
Munteanu et al. 2019 [21]	<i>Experimental and Therapeutic Medicine</i>	lower respiratory tract infections: bronchitis	respiratory syncytial virus	<7	blood sample	T-cell subsets CD4 <sup>+</sup> and CD8 <sup>+</sup>	flow cytometry	30	2 ±1	10	1.5 ±0.2	0.002	decreases
Gul et al. 2020 [22]	<i>Saudi Journal of Biological Sciences</i>	lower respiratory tract infections: bronchitis, pneumonia	HPIV	<12	throat or naso-pharyngeal swab	T-cell subsets CD4 <sup>+</sup> and CD8 <sup>+</sup>	flow cytometry	58	3.12 ±0.59	20	2.18 ±0.654	0.001	decreases
Li et al. 2020 [23]	<i>Journal of Infection</i>	lower respiratory tract infections: pneumonia	2019-nCoV	<6	blood sample	T-cell subsets CD4 <sup>+</sup> and CD8 <sup>+</sup>	flow cytometry	40	1.57 ±0.69	16	1.73 ±0.57	0.424	increases
Cosgrove et al. 2021 [24]	<i>Pediatric Research</i>	upper respiratory tract infection: cough, congestion, rhinorrhea	rhinovirus	<18	nasal mucosa	T-cell subsets CD4 <sup>+</sup> and CD8 <sup>+</sup>	flow cytometry	54	3.58 ±2.07	9	4.98 ±2.32	0.0001	increases
Calapodopulos et al. 2021 [25]	<i>Jornal de Pediatria</i>	upper respiratory tract infection: tonsillitis, sinusitis	rhinovirus, influenza virus	<6	blood sample	T-cell subsets CD4 <sup>+</sup> and CD8 <sup>+</sup>	flow cytometry	39	2.05 ±0.9	56	1.92 ±0.8	0.05	decreases
Lu et al. 2021 [26]	<i>BMC Pediatrics</i>	lower respiratory tract infections: pneumonia	2019-nCoV	<6	blood sample	T-cell subsets CD4 <sup>+</sup> and CD8 <sup>+</sup>	flow cytometry	20	1.7 ±1.4	101	2.9 ±1.5	0.001	increases
Mahmoudi et al. 2021 [27]	<i>Frontiers in Pediatrics</i>	lower respiratory tract infections: pneumonia	2019-nCoV	<8	blood sample	T-cell subsets CD4 <sup>+</sup> and CD8 <sup>+</sup>	flow cytometry	34	1.1 ±0.47	21	1.4 ±0.8	0.063	increases

SARS – severe acute respiratory syndrome; HPIV – human parainfluenza virus; 2019-nCoV – 2019 novel coronavirus.

Table 2. Risk assessment for included studies

Study ID and year of publication	He et al. 2005 [16]	Karsh et al. 2005 [17]	Pinto et al. 2006 [18]	Kim et al. 2011 [19]	Connors et al. 2018 [20]	Munteanu et al. 2019 [21]	Gul et al. 2020 [22]	Li et al. 2020 [23]	Cosgrove et al. 2021 [24]	Calapodopulos et al. 2021 [25]	Lu et al. 2021 [26]	Mahmoudi et al. 2021 [27]
Was a consecutive or random sample of patients enrolled?	Y	Y	Y	Y	Y	Y	Y	Y	Y	Y	Y	Y
Did the study avoid inappropriate exclusions?	Y	Y	Y	Y	Y	Y	Y	Y	Y	Y	Y	Y
Did all patients receive the same reference standard?	Y	Y	Y	Y	Y	Y	Y	Y	Y	Y	Y	Y
Were all patients included in the analysis?	N	N	N	N	N	N	N	N	N	N	N	N
Was the sample frame appropriate to address the target population?	Y	Y	Y	Y	Y	Y	Y	Y	Y	Y	Y	Y
Were study participants sampled in an appropriate way?	Y	Y	Y	Y	Y	Y	Y	Y	Y	Y	Y	Y
Were the study subjects and the setting described in detail?	Y	Y	Y	Y	Y	Y	Y	Y	Y	Y	Y	Y
Were valid methods used for the identification of the condition?	Y	Y	Y	Y	Y	Y	Y	Y	Y	Y	Y	Y
Was the condition measured in a standard, reliable way for all participants?	Y	Y	Y	Y	Y	Y	Y	Y	Y	Y	Y	Y
Was there appropriate statistical analysis?	Y	Y	Y	Y	Y	Y	Y	Y	Y	Y	Y	Y

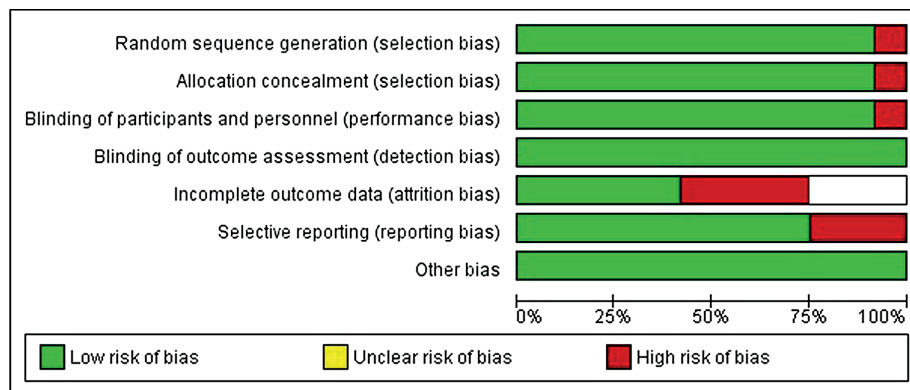


Fig. 3. Risk of bias graph

to occur. Because our calculated OR is also greater than 1, i.e., 3.66 with 95% CI ranging from 1.08 to 12.43, it confirms the increased likelihood of change in T-lymphocyte levels in children suffering from different respiratory tract infections. The high  $I^2$  value of 97% indicates a high degree of heterogeneity of the data and a p-value of less than 0.05 indicates that the results of this meta-analysis are statistically significant. This proved that when a child has an acute respiratory tract infection (ARTI), the number of T-lymphocytes changes as an immune response to the virus.

The RR of the included studies was also calculated using RevMan software, and the resulting forest plot is displayed in Fig. 7. The location of diamonds in the OR and RR forest plots confirms that the likelihood of alteration in T-lymphocyte levels is higher in sick children as compared to healthy controls. Also, as the diamond shape is not touching the line of no effect, it confirms that the difference in the RR between the 2 study groups is statistically significant. We calculated a pooled RR of 1.91, with 95% CI ranging from 1.07 to 3.40. The RR was greater than 1, indicating that ill patients are more likely than healthy controls to exhibit changes in T-lymphocyte counts. Moreover,

the heterogeneity was high with a  $\tau^2$  value of 0.99, a  $\chi^2$  value of 283.45, a df value of 11, a Z value of 2.19, and a p-value of 0.030. These numbers point to a random sampling of data and the use of categorical research variables. A p-value of less than 0.05 indicates that the meta-analysis results are statistically significant. Hence, we can conclude that a change in T-lymphocyte levels in children with acute respiratory illness is more likely to occur.

## Discussion

Pathogens cause severe illnesses and numerous complications when they invade our systems. However, the pathogen does not always triumph. Instead, our immune response is triggered, and soon after recognizing the invader, and winning immunogenicity over pathogenicity, it restores health. Children's immune systems are more active and respond faster by producing pathogen-specific antibodies via activated T-lymphocytes; in consequence, they combat the disease more effectively.

In their review article, Simon et al. state that innate and adaptive immune systems of a child are active and



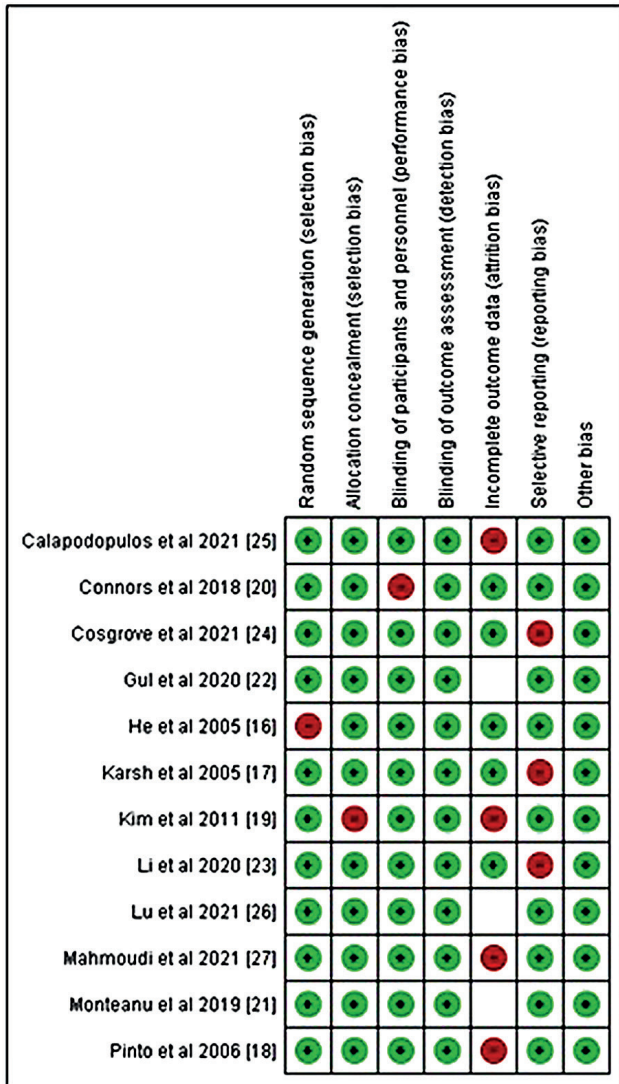
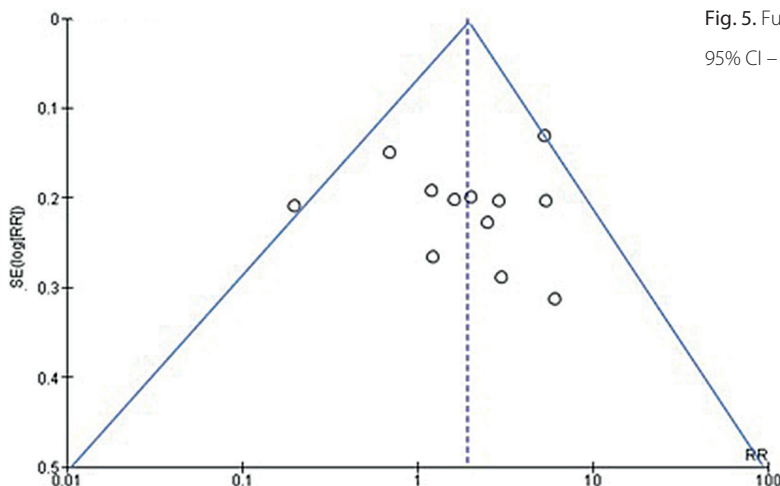


Fig. 4. Risk of bias summary

immature, but their efficacy diminishes with age.<sup>32</sup> Similarly, Tosif et al. found that children are more sensitive to COVID-19 but, on account of their active immunity, they can mount an efficient immune response to severe



acute respiratory syndrome coronavirus 2 (SARS-CoV-2) and prevent the infection with the virus.<sup>33</sup> The activity of the immune system can be measured by the number of B-cells, T-helper cells, cytotoxic T-lymphocytes, neutrophils, macrophages, and other immune response cells. The T-helper cells stimulate B-cells via their cytokines and help in the production of specific antibodies, hence the change in T-lymphocyte levels is usually measured in terms of the ratio of T-lymphocyte subsets CD4<sup>+</sup> and CD8<sup>+</sup> to assess the activated immune response.<sup>34,35</sup> The CD4<sup>+</sup>/CD8<sup>+</sup> ratio is the proportion of T-helper cells with CD4 on their surface to cytotoxic T-lymphocytes with CD8 on their surface.

Considering these reports, we also compared the change in the CD4<sup>+</sup>/CD8<sup>+</sup> ratio reported in the included studies in children with recurrent respiratory illness when compared to healthy controls, measured with flow cytometry (it is presented in a column histogram in Fig. 8). The figure indicates that T-lymphocyte levels are altered and that is why we found the CD4<sup>+</sup>/CD8<sup>+</sup> ratio either reduced or increased as compared to controls. Therefore, as a result of the altered CD4<sup>+</sup>/CD8<sup>+</sup> ratio in the studies that were included, the OR value of 3.66 (95% CI: 1.08–12.43), the RR value of 1.91 (95% CI: 1.07–3.40), and the significance level of p 0.05, this meta-analysis came to the conclusion that T-lymphocyte levels are altered in children with acute respiratory illnesses, which is a symptomatic of infection and indicative of an activated immune response.

### Limitations

The diversity of the respiratory tract infections analyzed, and the flow cytometry tests performed by different technicians may increase the likelihood of misleading concentration values, are the drawbacks of this study. Evaluating the comparative accuracy has an effect on the findings because many studies that reported equivalent T-lymphocyte values with healthy controls were not included in the analysis. Data from other relevant studies that indicate changes in T-lymphocyte levels

Fig. 5. Funnel plot for publication bias

95% CI – 95% confidence interval; RR – risk ratio; SE – standard error.

Publication Bias	
Egger's test	
Intercept	2.5959
95% CI	0.7216 to 4.4702
Significance level	P = 0.583
Begg's test	
Kendall's Tau	0.1429
Significance level	P = 0.772

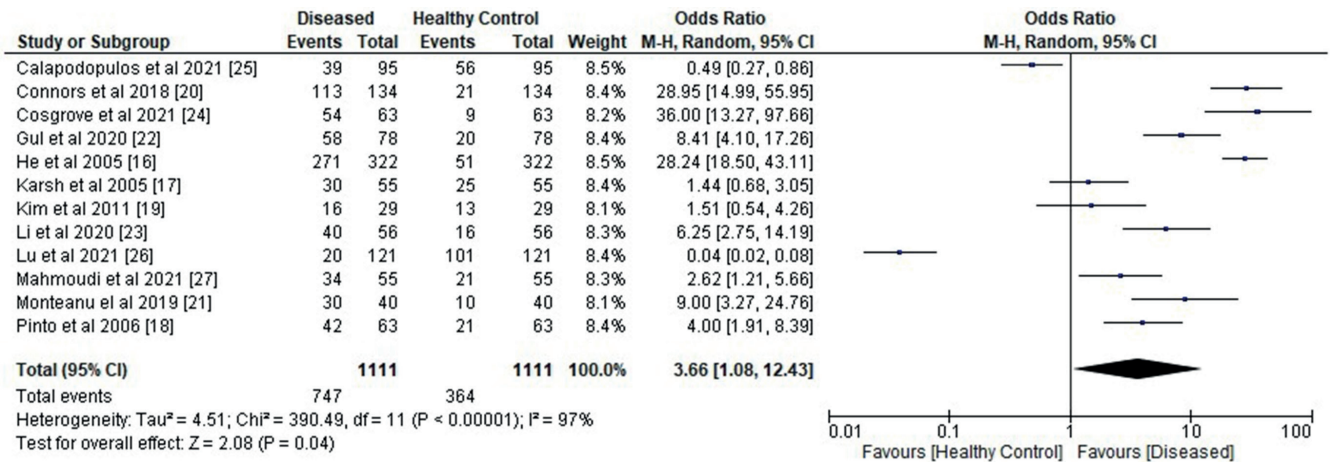


Fig. 6. Forest plot for odds ratio (OR)

95% CI – 95% confidence interval; df – degrees of freedom; M–H – Mantel–Haenszel.

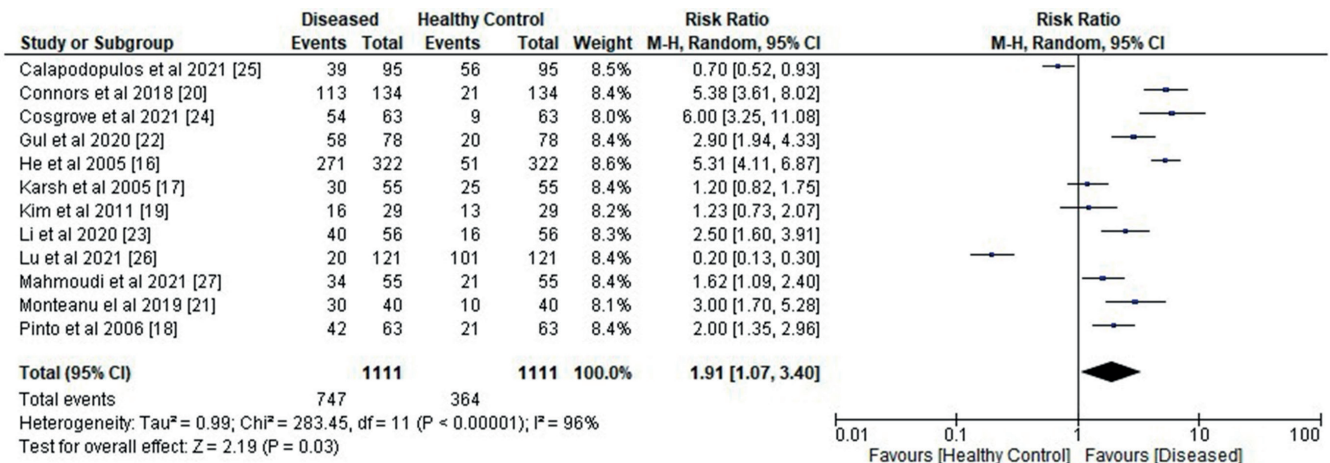


Fig. 7. Forest plot for risk ratio (RR)

95% CI – 95% confidence interval; df – degrees of freedom; M–H – Mantel–Haenszel.

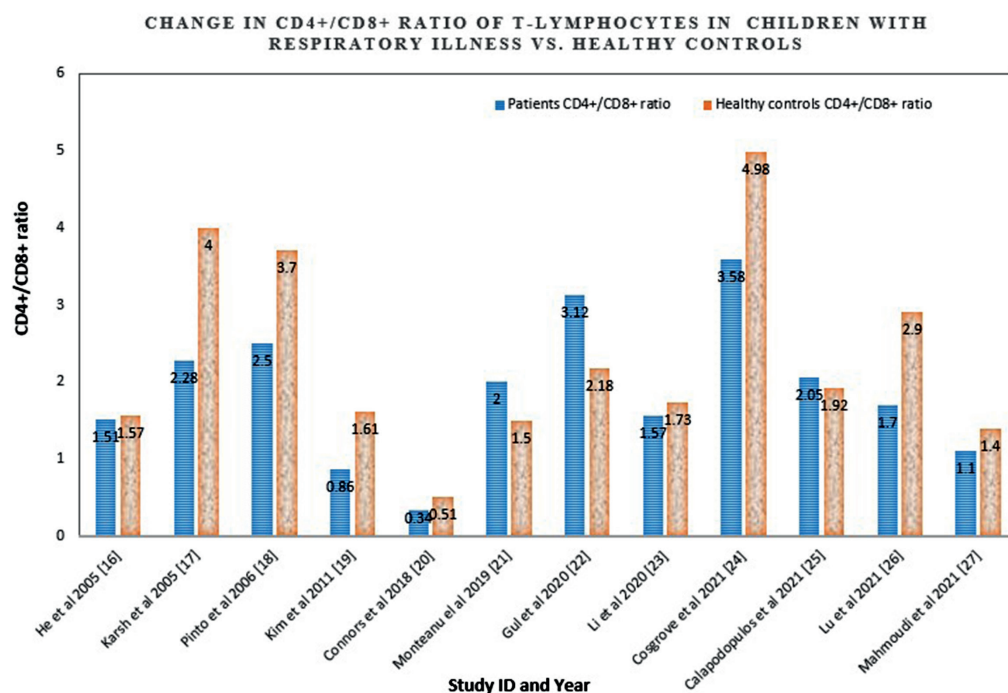


Fig. 8. Column histogram for change in T-lymphocyte subsets ratio


in children with recurrent respiratory disease can also be included to better illustrate the association. The role changed T-lymphocyte levels and acute respiratory disorders in children can be better elucidated if specific data on the patient's case history, physical examination and pathological tests are also used in the analyzes.

## Conclusions

Since the T-lymphocyte levels are altered during infection, the association between T-lymphocytes and respiratory diseases in children was investigated in this systematic review and meta-analysis. Based on the statistically significant data ( $p < 0.05$ ), we concluded that there is a strong link between T-lymphocyte levels and acute respiratory tract infections in children. The combined induction of virus-specific T-lymphocyte cells and enhanced antibody production in children with acute respiratory illness play a significant role in alleviating the infection at a faster rate by boosting their immunity.

### ORCID iDs

Xing Chen  <https://orcid.org/0000-0002-7694-2606>

Lihong Yang  <https://orcid.org/0000-0001-6514-146X>

### References

- Monto AS. Epidemiology of viral respiratory infections. *Disease-a-Month*. 2003;49(3):160–174. doi:10.1067/mda.2003.17
- Dagne H, Andualem Z, Dagne B, Taddese AA. Acute respiratory infection and its associated factors among children under-five years attending pediatrics ward at University of Gondar Comprehensive Specialized Hospital, Northwest Ethiopia: Institution-based cross-sectional study. *BMC Pediatr*. 2020;20(1):93. doi:10.1186/s12887-020-1997-2
- Khan MA. Epidemiological studies on lower respiratory tract infection in children in the District Bannu, Khyber Pakhtunkhwa, Pakistan. *Egypt J Bronchol*. 2022;16(1):17. doi:10.1186/s43168-022-00119-9
- van Woensel JBM. Viral lower respiratory tract infection in infants and young children. *BMJ*. 2003;327(7405):36–40. doi:10.1136/bmj.327.7405.36
- Soccal PM, Aubert JD, Bridevaux PO, et al. Upper and lower respiratory tract viral infections and acute graft rejection in lung transplant recipients. *Clin Infect Dis*. 2010;51(2):163–170. doi:10.1086/653529
- Patwa A, Shah A. Anatomy and physiology of respiratory system relevant to anaesthesia. *Indian J Anaesth*. 2015;59(9):533. doi:10.4103/0019-5049.165849
- Knobbe RB, Diallo A, Fall A, et al. Pathogens causing respiratory tract infections in children less than 5 years of age in Senegal. *Microbiol Insights*. 2019;12:117863611989088. doi:10.1177/1178636119890885
- Bhuyan GS, Hossain MA, Sarker SK, et al. Bacterial and viral pathogen spectra of acute respiratory infections in under-5 children in hospital settings in Dhaka city. *PLoS One*. 2017;12(3):e0174488. doi:10.1371/journal.pone.0174488
- Sonawane AA, Shastri J, Bavdekar SB. Respiratory pathogens in infants diagnosed with acute lower respiratory tract infection in a tertiary care hospital of western India using multiplex real-time PCR. *Indian J Pediatr*. 2019;86(5):433–438. doi:10.1007/s12098-018-2840-8
- Dhochak N, Singhal T, Kabra SK, Lodha R. Pathophysiology of COVID-19: Why children fare better than adults? *Indian J Pediatr*. 2020;87(7):537–546. doi:10.1007/s12098-020-03322-y
- Zhou L, Fu F, Wang Y, et al. Interlocked feedback loops balance the adaptive immune response. *Math Biosci Eng*. 2022;19(4):4084–4100. doi:10.3934/mbe.2022188
- Chen Z, John Wherry E. T cell responses in patients with COVID-19. *Nat Rev Immunol*. 2020;20(9):529–536. doi:10.1038/s41577-020-0402-6
- Lambert L, Culley FJ. Innate immunity to respiratory infection in early life. *Front Immunol*. 2017;8:1570. doi:10.3389/fimmu.2017.01570
- Tan HL, Gozal D, Wang Y, et al. Alterations in circulating T-cell lymphocyte populations in children with obstructive sleep apnea. *Sleep*. 2013;36(6):913–922. doi:10.5665/sleep.2724
- Zimmermann P, Curtis N. Why is COVID-19 less severe in children? A review of the proposed mechanisms underlying the age-related difference in severity of SARS-CoV-2 infections. *Arch Dis Child*. 2021;106(5):429–439. doi:10.1136/archdischild-2020-320338
- He Z, Zhao C, Dong Q, et al. Effects of severe acute respiratory syndrome (SARS) coronavirus infection on peripheral blood lymphocytes and their subsets. *Int J Infect Dis*. 2005;9(6):323–330. doi:10.1016/j.ijid.2004.07.014
- Karsh J, Angel JB, Young CD, et al. Association of the frequency of respiratory illness in early childhood with a change in the distribution of blood lymphocyte subpopulations. *All Asth Clin Immun*. 2005;1(4):135. doi:10.1186/1710-1492-1-4-135
- Pinto RA, Arredondo SM, Bono MR, Gaggero AA, Díaz PV. T helper 1/T helper 2 cytokine imbalance in respiratory syncytial virus infection is associated with increased endogenous plasma cortisol. *Pediatrics*. 2006;117(5):e878–e886. doi:10.1542/peds.2005-2119
- Kim JE, Bauer S, La KS, et al. CD4<sup>+</sup>/CD8<sup>+</sup> T lymphocytes imbalance in children with severe 2009 pandemic influenza A (H1N1) pneumonia. *Korean J Pediatr*. 2011;54(5):207. doi:10.3345/kjp.2011.54.5.207
- Connors TJ, Baird JS, Yopes MC, et al. Developmental regulation of effector and resident memory T cell generation during pediatric viral respiratory tract infection. *J Immunol*. 2018;201(2):432–439. doi:10.4049/jimmunol.1800396
- Munteanu A, Surcel M, Huică R, et al. Peripheral immune cell markers in children with recurrent respiratory infections in the absence of primary immunodeficiency. *Exp Ther Med*. 2019;18(3):1693–1700. doi:10.3892/etm.2019.7714
- Gul A, Khan S, Arshad M, et al. Peripheral blood T cells response in human parainfluenza virus-associated lower respiratory tract infection in children. *Saudi J Biol Sci*. 2020;27(10):2847–2852. doi:10.1016/j.sjbs.2020.07.005
- Li H, Chen K, Liu M, Xu H, Xu Q. The profile of peripheral blood lymphocyte subsets and serum cytokines in children with 2019 novel coronavirus pneumonia. *J Infect*. 2020;81(1):115–120. doi:10.1016/j.jinf.2020.04.001
- Cosgrove PR, Redhu NS, Tang Y, Monuteaux MC, Horwitz BH. Characterizing T cell subsets in the nasal mucosa of children with acute respiratory symptoms. *Pediatr Res*. 2021;90(5):1023–1030. doi:10.1038/s41390-021-01364-2
- Calapodopulos NVI, Sawan-Mendonça MM, da Silva MV, et al. Association of recurrent upper respiratory tract infections with low production of oxygen intermediates in children. *J Pediatr (Rio J)*. 2022;98(4):399–405. doi:10.1016/j.jpeds.2021.09.008
- Lu W, Yang L, Li X, et al. Early immune responses and prognostic factors in children with COVID-19: A single-center retrospective analysis. *BMC Pediatr*. 2021;21(1):181. doi:10.1186/s12887-021-02561-y
- Mahmoudi S, Yaghmaei B, Sharifzadeh Ekbatani M, et al. Effects of coronavirus disease 2019 (COVID-19) on peripheral blood lymphocytes and their subsets in children: Imbalanced CD4<sup>+</sup>/CD8<sup>+</sup> T cell ratio and disease severity. *Front Pediatr*. 2021;9:643299. doi:10.3389/fped.2021.643299
- Tawfik GM, Dila KAS, Mohamed MYF, et al. A step-by-step guide for conducting a systematic review and meta-analysis with simulation data. *Trop Med Health*. 2019;47(1):46. doi:10.1186/s41182-019-0165-6
- Jackson D, Law M, Barrett JK, et al. Extending DerSimonian and Laird's methodology to perform network meta-analyses with random inconsistency effects. *Stat Med*. 2016;35(6):819–839. doi:10.1002/sim.6752
- Efthimiou O, Rücker G, Schwarzer G, Higgins JPT, Egger M, Salanti G. Network meta-analysis of rare events using the Mantel-Haenszel method. *Stat Med*. 2019;38(16):2992–3012. doi:10.1002/sim.8158
- Viswanathan M, Patnode CD, Berkman ND, et al. Recommendations for assessing the risk of bias in systematic reviews of health-care interventions. *J Clin Epidemiol*. 2018;97:26–34. doi:10.1016/j.jclinepi.2017.12.004
- Simon AK, Hollander GA, McMichael A. Evolution of the immune system in humans from infancy to old age. *Proc Biol Sci*. 2015;282(1821):20143085. doi:10.1098/rspb.2014.3085

33. Tosif S, Neeland MR, Sutton P, et al. Immune responses to SARS-CoV-2 in three children of parents with symptomatic COVID-19. *Nat Commun.* 2020;11(1):5703. doi:10.1038/s41467-020-19545-8
34. Yin Y, Qin J, Dai Y, Zeng F, Pei H, Wang J. The CD4<sup>+</sup>/CD8<sup>+</sup> ratio in pulmonary tuberculosis: Systematic and meta-analysis article. *Iran J Public Health.* 2015;44(2):185–193. PMID:25905052.
35. Huang W, Berube J, McNamara M, et al. Lymphocyte subset counts in COVID-19 patients: A meta-analysis. *Cytometry.* 2020;97(8):772–776. doi:10.1002/cyto.a.24172



# A meta-analysis on the role of brain-derived neurotrophic factor in Parkinson's disease patients

Zhen Chen<sup>A–F</sup>, Hui Zhang<sup>A–F</sup>

Department of Neurology, Xuzhou Central Hospital, China

A – research concept and design; B – collection and/or assembly of data; C – data analysis and interpretation; D – writing the article; E – critical revision of the article; F – final approval of the article

Advances in Clinical and Experimental Medicine, ISSN 1899–5276 (print), ISSN 2451–2680 (online)

*Adv Clin Exp Med.* 2023;32(3):285–295

## Address for correspondence

Hui Zhang  
E-mail: Zhanghui\_sci@outlook.com

## Funding sources

None declared

## Conflict of interest

None declared

Received on July 23, 2022

Reviewed on September 3, 2022

Accepted on September 26, 2022

Published online on November 18, 2022

## Abstract

**Background.** Brain-derived neurotrophic factor (BDNF) is essential for the development of dopaminergic neurons in the substantia nigra.

**Objectives.** To investigate the level of BDNF among Parkinson's disease (PD) subjects and the influence of depression on BDNF levels.

**Materials and methods.** A total of 1920 subjects were included in the analysis; of these, 1034 had PD and 886 were healthy controls. A thorough literature search up to May 2022 was conducted. The mean difference (MD) of BDNF levels and 95% confidence intervals (95% CIs) were calculated with random or fixed effects models.

**Results.** Compared to healthy controls, levels of BDNF were significantly lower in patients with PD (MD =  $-1.60$ , 95% CI ( $-2.49$ ,  $-0.70$ ),  $p < 0.001$ ). Patients with PD and depression had significantly lower levels of BDNF (MD =  $-3.39$ , 95% CI ( $-5.55$ ,  $-1.23$ ),  $p = 0.002$ ), as well as those with PD without depression (MD =  $-0.80$ , 95% CI ( $-1.56$ ,  $-0.03$ ),  $p = 0.04$ ). However, there was no discernible change in BDNF levels (MD =  $-0.82$ , 95% CI ( $1.75$ ,  $0.10$ ),  $p = 0.08$ ) between the participants with PD and depression compared to the PD patients alone.

**Conclusions.** Compared with healthy controls, BDNF levels were significantly lower in the subjects with PD combined with depression, and PD without depression. However, there was no discernible difference in BDNF levels between subjects with PD with depression compared to those with PD without depression.

**Key words:** Parkinson's disease, BDNF, depression, dopaminergic neurons, substantia nigra

## Cite as

Chen Z, Zhang H. A meta-analysis on the role of brain-derived neurotrophic factor in Parkinson's disease patients. *Adv Clin Exp Med.* 2023;32(3):285–295. doi:10.17219/acem/154955

## DOI

10.17219/acem/154955

## Copyright

Copyright by Author(s)

This is an article distributed under the terms of the Creative Commons Attribution 3.0 Unported (CC BY 3.0) (<https://creativecommons.org/licenses/by/3.0/>)

## Introduction

Parkinson's disease (PD) is a degenerative neurological illness. Recent research has suggested that inflammatory processes are involved in PD, which contradicts the monoamine depletion hypothesis (the traditional approach to depression).<sup>1,2</sup> Given this, we might speak of an inflammatory hypothesis to explain the serotonergic, noradrenergic and dopaminergic dysfunctions that are characteristic of depression.<sup>3</sup> In addition, low-quality diets are linked to the aforementioned negative physical, mental and cognitive health effects. Many different processes, including oxidative stress, plasticity, the microbiota–gut–brain axis, and most notably, inflammatory responses, are modulated by diet, which makes it a major risk factor for chronic diseases.<sup>4</sup> The ventrolateral cell groups (i.e., A9 or nigrostriatal pathway) in the substantia nigra are the most susceptible to damage, whereas the dorsal and medial cell groups (i.e., A10 or mesolimbic pathway) are the most resilient ones.<sup>5</sup> It has been hypothesized that the pacemaker-like features of dopaminergic neurons, which cause frequent intracellular calcium transients are the molecular basis for the selective vulnerability of these cells. There is some evidence that A9 neurons have impaired calcium buffering, which can contribute to cellular stress and, ultimately, the disruption of cellular homeostasis. The first affected neurons are those in the olfactory bulb (anterior olfactory nucleus) and dorsal motor nucleus of the vagus (medulla), then those in the pons (locus ceruleus), and finally those in the substantia nigra (dopaminergic neurons).<sup>5</sup> In addition, recent evidence from studies on action control conducted on healthy individuals supported a causal role of dopamine in action control, and others addressed how PD is accompanied by impairments in covert cognitive processes.<sup>6,7</sup> Still, other studies investigated underlying goal-directed motor functioning (e.g., action planning, conflict adaptation, motor inhibition)<sup>8,9</sup> and how dopaminergic medication may modulate these action control components.

The symptoms of PD can be divided into motor symptoms and non-motor symptoms (NMSs). Motor-related symptoms include muscle rigidity, tremors and changes in speech. Sensory complaints, mental abnormalities, sleep disturbances, and autonomic dysfunction are common NMSs experienced by people with PD. Non-motor symptoms can occur in the earliest stages of the disease, even before motor impairment is clinically apparent. Depression is a notable NMS that is particularly prevalent in the early stages of the disease. It has a substantial influence on the quality of life and disability.<sup>10</sup> The loss of dopamine-producing cells and the development of Lewy bodies in the brain commonly lead to NMSs in PD, which decreases the quality of life and presents significant hurdles in disease management. The modulation of autonomic nervous system responses is crucial for behavioral regulation.<sup>11,12</sup> Synuclein aggregations and the denervation of the dopaminergic nigrostriatal system are thought to play major roles in the pathophysiology of PD.<sup>13,14</sup> Anxiety disorders

respond well to antidepressants, such as selective serotonin reuptake inhibitors and serotonin noradrenaline reuptake inhibitors, because of their proposed shared neurobiological basis: alterations in prefrontal-limbic pathways<sup>15,16</sup> and serotonergic projections arising from the raphe nuclei.<sup>17</sup> However, current transcranial magnetic stimulation (TMS) has pinpointed 2 separate circuit targets for symptom clusters of depression (i.e., sorrow) and anxiety (i.e., irritability). Transcranial magnetic stimulation of the dorsomedial prefrontal cortex lowers depression symptoms and alleviates anxiety symptoms.<sup>18</sup> Depression and other non-motor symptoms, such as reduced nonverbal communication and expressivity, may present themselves early in people with PD. Depression and other NMSs may be triggered by quinolinic acid. Research has shown that the neurotoxicity of the quinolinic acid contributes to the etiology of PD.<sup>19</sup> The uncertainty associated with PD and coronavirus disease 2019 (COVID-19) magnified each other, and the cancellation of clinical appointments and restrictions on physical activity had substantial adverse effects on the well-being of this group of individuals.<sup>20</sup>

Neuropeptides and neurohormones play an important role in cognitive, emotional, social, and arousal functions, and are biomarkers to help evaluate risk, diagnosis, disease course, and therapeutic outcomes of a disease.<sup>21</sup> Prior research has demonstrated that the levels of A42 and tau protein in the serum of PD patients are highly variable and do not correlate with the mean scores on tests used to evaluate the severity of cognitive disorders. Therefore, A42 and tau protein in serum cannot be used as biomarkers of neurodegenerative changes in PD with cognitive impairment.<sup>22</sup> On the other hand, patients with neurodegenerative diseases such as PD or psychiatric disorders such as depression have decreased levels of kynurenic acid.<sup>23</sup>

In adult brains, the neurotrophin known as the brain-derived neurotrophic factor (BDNF) promotes dendrite morphogenesis, synaptic plasticity, arborization, and even neurogenesis.<sup>24,25</sup> Brain-derived neurotrophic factor is essential for the development of dopaminergic neurons in the substantia nigra,<sup>24</sup> which are widely dispersed in cortical and subcortical regions. Brain-derived neurotrophic factor stimulates neurite growth and supports the survival of nigral dopaminergic neurons within the substantia nigra. Therefore, blocking the expression of BDNF results in the death of adult dopaminergic neurons.<sup>26</sup> Parkinson's disease patients have a lower expression of BDNF in the pars compacta of the substantia nigra,<sup>27–29</sup> reducing trophic support for dopaminergic neurons. At the same time, the remaining dopaminergic neurons in the substantia nigra produce dwindling levels of BDNF.<sup>30</sup>

## Objectives

The aim of the current meta-analysis is to investigate the level of BDNF among PD subjects and the influence of comorbid depressive symptoms on BDNF levels.

## Materials and methods

### Study design

This meta-analysis consisted of clinical research studies that were a part of the epidemiological declaration<sup>31</sup> and had a set study protocol. For data collection and analysis, a wide variety of databases were consulted, including PubMed, Ovid, Cochrane Library, Embase, and Google Scholar.

### Data collection

Data were collected from clinical trials as well as human observational research papers that were written in any language. Studies were used regardless of sample size. Articles that did not give an association measurement, such as reviews, editorials or research letters, were not included.

### Identification

According to the PICOS principle, a protocol of search strategies was developed<sup>32</sup> and defined as follows: 1) patients (P): subjects diagnosed with PD; 2) intervention/exposure (I): BDNF; 3) comparison (C): BDNF in various subject groups; 4) outcome (O): PD compared to controls, PD with depression compared to controls, PD without depression compared to controls, and PD with depression compared to PD without depression; 5) study design (S): no restriction.<sup>33</sup>

Using the keywords and associated phrases listed in Table 1 (search strategies for different databases),

Table 1. Search strategy for each database

Database	Search strategy
PubMed	#1 "Parkinson's disease" (MeSH terms) OR "brain-derived neurotrophic factor" (all fields) #2 "brain" (MeSH terms) OR "depression" (all fields) #3 #1 AND #2
Ovid	#1 "Parkinson's disease" (all fields) OR "brain-derived neurotrophic factor" (all fields) #2 "brain" (all fields) OR "depression" (all fields) #3 #1 AND #2
Google Scholar	#1 "Parkinson's disease" OR "brain-derived neurotrophic factor" #2 "brain" OR "depression" #3 #1 AND #2
Embase	#1 "Parkinson's disease"/exp OR "brain-derived neurotrophic factor" #2 "brain"/exp OR "depression" #3 #1 AND #2
Cochrane Library	#1 "Parkinson's disease": ti, ab, kw; "brain-derived neurotrophic factor": ti, ab, kw (word variations have been searched) #2 "brain": ti, ab, kw OR "depression": ti, ab, kw (word variations have been searched) #3 #1 AND #2

ti, ab, kw – terms in either title or abstract or keyword fields; exp – exploded indexing term.

we conducted a complete search of the PubMed, Ovid, Cochrane Library, Embase, and Google Scholar databases up to May 2022. The titles and abstracts of the collected publications that did not link the levels of BDNF to PD were excluded from the analysis. Two authors, ZC and HZ, acted as reviewers to identify suitable studies.

### Eligibility and inclusion

The following criteria had to be met for an article to be considered for the inclusion in the meta-analysis:

1. The study was either prospective, observational, randomized, or retrospective;
2. The target intervention population consisted of individuals with PD;
3. The intervention regimen of the included studies was based on plasma samples of BDNF;
4. The study examined BDNF levels in several subject categories.

Exclusion criteria were:

1. Studies that failed to identify the plasma levels of BDNF in PD patients;
2. Studies that did not focus on the impact of comparison outcomes.

Figure 1 illustrates our selection process.

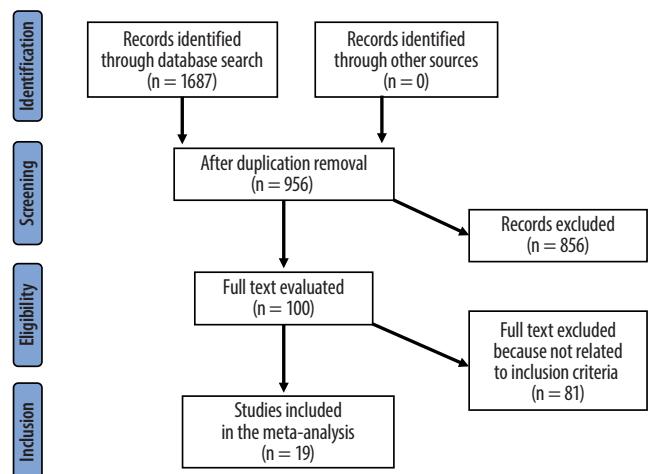


Fig. 1. Schematic diagram of the study procedure

### Identification

Data extracted from the studies included: study- and subject-related features in a standard format; the surname of the first author; the period of the study, the year of publication; the country of the study; the design of the study; the population type recruited in the study; the total number of subjects; categories; qualitative and quantitative evaluation method; demographic data; clinical and treatment characteristics; information source; outcome evaluation; and statistical analysis.<sup>34</sup> A single study evaluating BDNF in PD patients yielded inconsistent results, so it was

isolated. Each study was assessed for bias, and the methodological quality of the chosen studies was evaluated by the 2 authors in a blinded fashion using the risk of bias tool from the Cochrane Handbook for Systematic Reviews of Interventions, v. 5.1.0.<sup>35</sup>

The Newcastle-Ottawa Scale (NOS), a quality and bias assessment tool developed specifically for observational research, was also used to evaluate the bias. The NOS examines the sample, the comparability of cases and controls, and the exposure in observational studies, with studies being assigned values between 0 and 9. Studies with a rating of 7–9 are of the highest quality and have the lowest risk of bias compared to those of lower ratings. Studies with a quality and bias risk rating from 4 to 6 are considered to have moderate quality. Each study was reviewed by the 2 authors.

## Statistical analyses

The mean difference (MD) with a 95% confidence interval (95% CI) was calculated using a random or fixed effects model. All groups were analyzed using the random effects model due to high heterogeneity, whereas the use of fixed effects model required the confirmation of high similarity between the included study and a low heterogeneity ( $I^2$ ) level. The  $I^2$  index (determined using Reviewer Manager and expressed in forest plots), expressed as a numeric value ranging from 0 to 100, was calculated (as a percentage). Percentages ranging from 0% to 25%, 25% to 50%, 50% to 75%, and 75% to 100% indicated no, low, moderate, and high heterogeneity, respectively.<sup>36</sup> Fixed effects models were used when the heterogeneity was low. As previously stated, the subcategory analysis was performed by stratifying the initial evaluation into result categories. The publication bias was investigated quantitatively with the Begg's test (the publication bias was

considered present if  $p < 0.05$ ).<sup>37</sup> A two-tailed test was used to calculate the p-value. The statistical analysis and graphs were created with the Reviewer Manager v. 5.3 software (The Cochrane Collaboration, Copenhagen, Denmark) and Jamovi software v. 2.3 (<https://www.jamovi.org/>) using a continuous model.

## Results

Nineteen articles (out of 1765 reviewed) published between 2009 and 2022 satisfied the inclusion criteria and were included in the meta-analysis.<sup>38–61</sup> Table 2 summarizes the findings of these investigations. Ultimately, more than 1000 people had PD and 886 were healthy controls. Number of subjects in the included studies ranged from 29 to 369.

### PD patients compared to controls

Fifteen studies, which included 634 subjects, reported data stratified according to PD compared to the control group (Fig. 2). Parkinson's disease was associated with significantly lower levels of BDNF compared to controls (MD = -1.60, 95% CI [-2.49, -0.70],  $p < 0.001$ ), with a heterogeneity of 99%.

### PD patients with depression compared to controls

Five studies, which included 232 subjects, reported data stratified according to PD with depression (Fig. 3). Parkinson's disease with depression was associated with significantly lower levels of BDNF (MD = -3.39, 95% CI [-5.55, -1.23],  $p = 0.002$ ), with a heterogeneity of 99%.

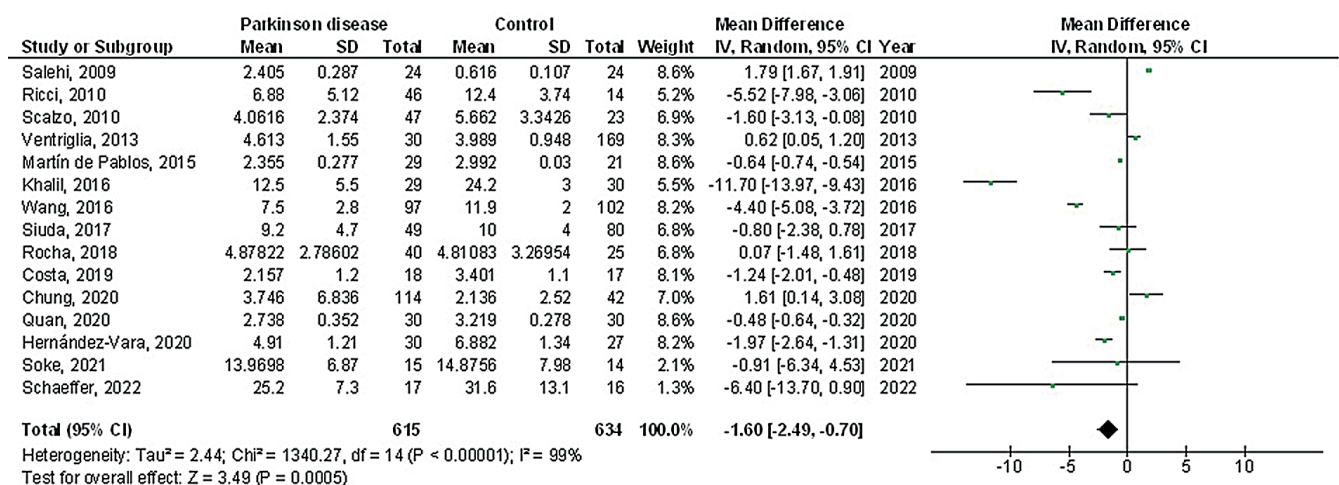


Fig. 2. Forest plot of brain-derived neurotrophic factor (BDNF) levels in Parkinson's disease (PD) patients compared with healthy controls

SD – standard deviation; 95% CI – 95% confidence interval; df – degrees of freedom.



**Table 2.** Characteristics of the selected studies included in the meta-analysis

Study and year	Country	Total	Parkinson's disease	Control	Age	Gender (M/F)	Disease duration	H&Y in PD	UPDRS part III in PD	Depression scale	NOS	Sampling time
Salehi and Mashayekhi, 2009 <sup>38</sup>	Iran	48	24	24	65.3 ±7.2	–	–	–	–	–	3	–
Scalzo et al., 2010 <sup>39</sup>	Brazil	70	47	23	65.7 ±8.8	32/38	7.6 ±4.5	2	34.5 ±23.3	–	7	morning
Ricci et al., 2010 <sup>40</sup>	Italy	60	46	14	63.7 ±8.87	29/31	8.05 ±2.41	2.7 ±0.7	–	16 ≤ HAM-D	7	–
Pålhagen et al., 2010 <sup>41</sup>	Sweden	25	11	14	65.3 ±7.2	14/11	6.9 ±2.4	1.8 ±0.4	22.6 ±10.1	–	7	–
Ventriglia et al., 2013 <sup>42</sup>	Italy	199	30	169	67.6 ±8.4	114/91	–	16 ≤ HAM-D score	–	–	6	morning
Martín de Pablos et al., 2015 <sup>43</sup>	Spain	50	29	21	63.4 ±0.9	27/23	–	2.16 ±1.04	–	–	4	–
Khalil et al., 2016 <sup>44</sup>	Jordan	59	29	30	59.4 ±13.1	35/24	4.4 ±2.7	2.4 ±0.7	49.2 ±16.5	–	7	–
Wang et al., 2016 <sup>45</sup>	China	199	97	102	63.6 ±9.32	112/87	4.23 ±3.1	1.59 ±0.43	–	–	8	morning
Siuda et al., 2017 <sup>46</sup>	Poland	129	49	80	63.3 ±10.5	63/66	8.41 ±5.8	2.7 ±0.7	–	19 ≤ BDI score	8	morning
Wang et al., 2017 <sup>47</sup>	China	198	96	102	61.64 ±8.87	113/85	3.76 ±2.56	1.6 ±0.7	–	53 ≤ SDS score	7	morning
Rocha et al., 2018 <sup>48</sup>	Brazil	65	40	25	68.71 ±10.7	46/19	5.45 ±4.13	2.44 ±0.69	34.57 ±18.43	–	8	evening
Costa et al., 2019 <sup>49</sup>	Brazil	35	18	17	68 (62.5–71.5)	22/13	4.5 (3–14.25)	2.16 ±0.44	–	HAM-D r = –0.44	8	morning
Hernández-Vara et al., 2020 <sup>50</sup>	Spain	57	30	27	63.97 ±9.59 (38–77)	36/21	1 (0.92–1.5)	1 (1–2)	16.5 (12.75–22.00)	mean HAM-D: 5.63, SD = 3.79	6	morning
Quan et al., 2020 <sup>51</sup>	China	60	30	30	67.19 ±8.12	32/28	4.13 ±1.50	2.12 ±0.75	–	–	5	morning
Chung et al., 2020 <sup>52</sup>	Taiwan	156	114	42	69.67 ±8.44	91/65	2.70 ±2.45	–	22.89 ±10.00	–	8	–
Shi et al., 2021 <sup>53</sup>	China	79	53	26	65.04 ±10.55	37/42	2 ±2.6	1.33 ±2.89	–	–	7	morning
Soke et al., 2021 <sup>54</sup>	Turkey	29	15	14	57.07 ±8.18	19/10	8.13 ±4.81	–	8.13 ±4.81	–	6	morning
Huang et al., 2021 <sup>55</sup>	China	369	259	110	62.84 ±8.73	199/170	4.96 ±2.09	2.07 ±1.02	33.78 ±8.31	HAM-D: 17 (33.78 ±8.31)	8	morning
Schaeffer, 2022 <sup>56</sup>	Germany	33	17	16	58 ±10	17/16	5.6 ±5.0	1.85 ±0.42	25 ±10	–	6	–
Total		1920	1034	886	–	–	–	–	–	–	–	–

PD – patients with Parkinson's disease; H&Y – Hoehn and Yahr's motor stage; UPDRS – Unified Parkinson's Disease Rating Scale; NOS – Newcastle-Ottawa Scale; HAM-D – Hamilton Depression Rating Scale; SD – standard deviation; BDI – Beck Depression Inventory; SDS – Self-Rating Depression Scale.

### PD patients without depression compared to controls

Five studies, which included 259 subjects, reported data stratified according to PD without depression (Fig. 4). Parkinson's disease without depression was associated with significantly lower levels of BDNF (MD = –0.80, 95% CI (–1.56, –0.03), p = 0.04), with a heterogeneity of 94%.

### PD patients with depression compared to PD patients without depression

Seven studies, which included 305 subjects, reported data stratified according to PD with depression compared to PD without depression (Fig. 5). Parkinson's disease patients with depression and PD patients without depression had no statistically significant difference in BDNF levels (MD = –0.82, 95% CI (–1.75, 0.10), p = 0.08) and a heterogeneity of 95%.

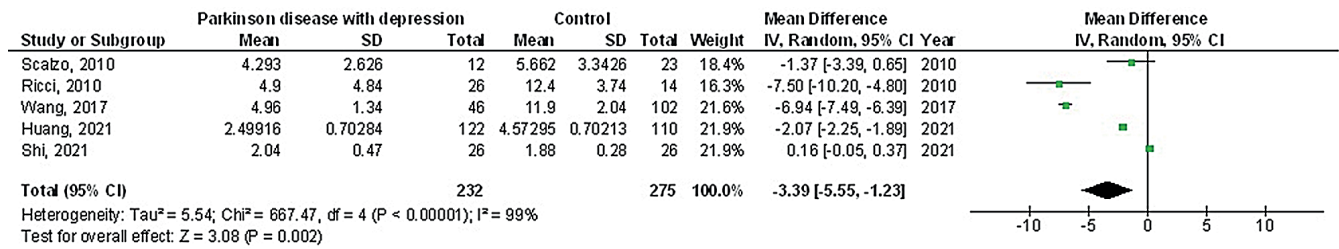


Fig. 3. Forest plot of brain-derived neurotrophic factor (BDNF) levels in Parkinson's disease (PD) patients with depression compared with healthy controls  
SD – standard deviation; 95% CI – 95% confidence interval; df – degrees of freedom.

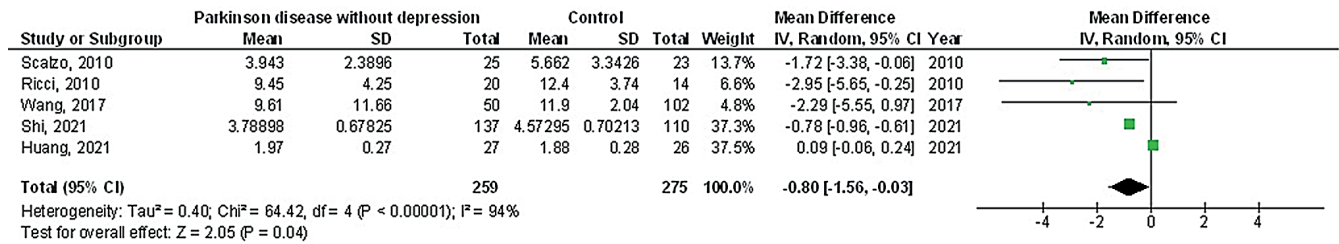


Fig. 4. Forest plot of brain-derived neurotrophic factor (BDNF) levels in Parkinson's disease (PD) patients without depression compared with healthy controls  
SD – standard deviation; 95% CI – 95% confidence interval; df – degrees of freedom.

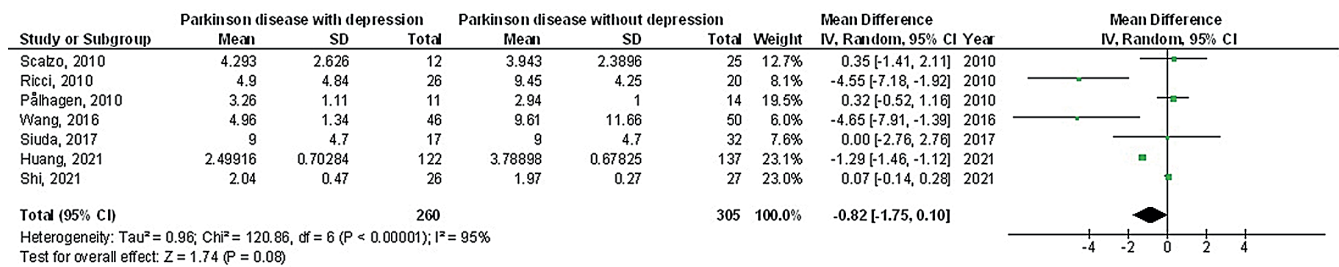


Fig. 5. Forest plot of brain-derived neurotrophic factor (BDNF) levels in Parkinson's disease (PD) patients with depression compared with PD patients without depression

SD – standard deviation; 95% CI – 95% confidence interval; df – degrees of freedom.

## Analysis of other potential covariates/factors

The analysis of studies with defined sampling time (morning) similarly found significantly lower BDNF levels in PD patients compared with controls (Fig. 6) (MD = -1.24, 95% CI (-2.30, -0.17),  $p = 0.002$ ), with a heterogeneity of 95%.

It was not possible to assess the impact of individual characteristics such as gender and ethnicity on the comparison results as data on these variables were not collected. In addition, the publication bias was found to not be statistically different for PD subjects compared with controls ( $p = 0.62$ ). Similarly, the analysis of studies with defined sampling time (i.e., morning) failed to identify statistically significant bias ( $p = 0.61$ ). In addition, the results of the Begg's test for PD patients with depression, PD patients without depression, and PD patients with depression compared to PD patients without depression were  $p = 0.82$ ,  $p = 0.99$  and  $p = 0.77$ , respectively, indicating a lack of publication bias.

The risk of bias assessment was evaluated with NOS (Table 2). Twelve studies were found to have a score between 7 and 9 points, which reflects a low risk of bias. Six studies showed a moderate risk of bias, with scores ranging from 4 to 6 points. Only one study scored 3 points, reflecting a high risk of bias resulting from low quality methodology.

## Discussion

A total of 1920 individuals, 1034 of whom were diagnosed with PD and 886 of whom were healthy controls, were included in the current meta-analysis.<sup>38–56</sup> Parkinson's disease patients, both with and without depression, had lower levels of BDNF than healthy controls. Parkinson's disease patients with depression did not have lower levels of BDNF than PD patients without depression. It is important to be cautious when interpreting the results comparing PD patients with and without depression, as these data come from relatively small sample sizes (13 out of 19) and a limited number of studies (<100).

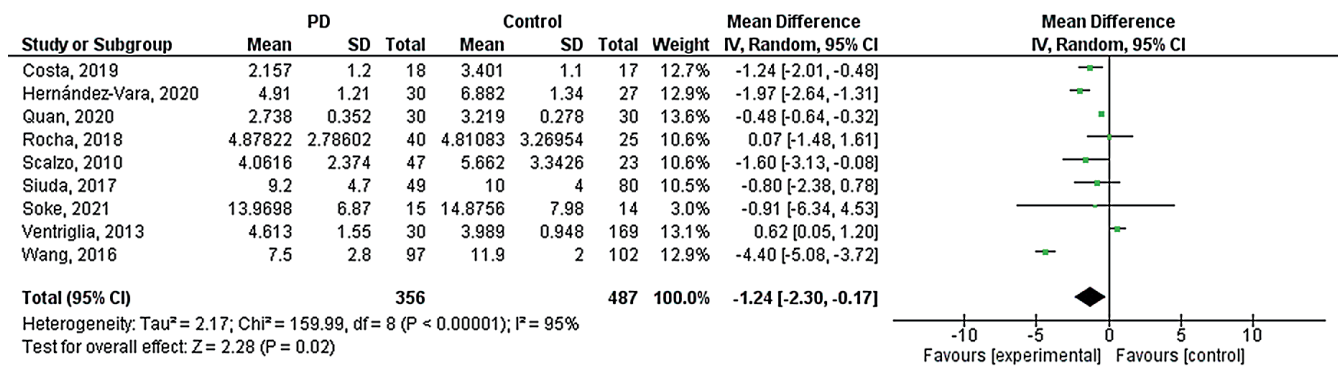


Fig. 6. Forest plot of the morning samples BDNF levels in Parkinson's disease (PD) patients compared with healthy controls

SD – standard deviation; 95% CI – 95% confidence interval; df – degrees of freedom.

It is critical to determine if circulating BDNF levels may be used as a surrogate for BDNF expression in the central nervous system and neurons, given the role of this factor in PD. The association between blood levels of BDNF and hippocampal BDNF is highest in mice ( $R^2 = 0.81$ ).<sup>37</sup> However, whether this association applies to people remains debated. We know that BDNF is produced by glial cells, like astrocytes and microglia, as well as extra-central nervous system cell types, such as endothelium cells and peripheral blood mononuclear cells.<sup>57</sup> Circulating BDNF appears to originate mainly in the central nervous system, given that it may cross the blood–brain barrier and that endothelial and mononuclear cells express extremely low quantities of it.<sup>58</sup> Therefore, studying the levels of BDNF in the serum of PD patients as a surrogate for its expression in the central nervous system is now possible. Due to their inherent ability to retain proteins, platelets are the principal source of BDNF in the blood.

Patients with PD had a lower BDNF expression and more dopamine in their striatum, according to the dopamine transporter scans.<sup>59</sup> The expression of BDNF can be affected by a wide range of factors, including the 196 A/G single nucleotide polymorphism. This 196 A/G polymorphism, which results in a Val66Met substitution, was initially discovered by Momose et al. as a possible homozygote mutation linked to an increased risk of PD.<sup>60</sup> This mutation was confirmed to consistently downregulate the expression of BDNF<sup>61</sup> and it was the subject of future research to determine its link to PD risk.<sup>62,63</sup>

Reduced expression of BDNF, irrespective of nigral dopaminergic expression, alters dopaminergic outflow to the striatum and mimics the motor symptoms of PD in mice.<sup>64</sup> In addition, synuclein, the primary component of Lewy body fibrils in people with Parkinson's disease, inhibits BDNF's neurotrophic action in the substantia nigra by first downregulating BDNF expression<sup>65</sup> and then, by competitively inhibiting BDNF signaling at the receptor level.<sup>66</sup> Exogenous BDNF lowers the loss of dopaminergic neurons in PD models employing 6-hydroxydopamine hydrobromide and 1-methyl-4-phenyl-1,2,3,6-tetrahydropyridine as well as neuronal cultures, according to the majority

of research.<sup>67–70</sup> Extensive data are suggesting the protective effect of BDNF on the dopaminergic substantia nigra population in PD and its downregulation in individuals with PD.<sup>71</sup> On the flip side, the development of PD has been associated with increasing levels of BDNF in blood and cerebrospinal fluid.<sup>38,39</sup> Also, an important role of physical training and exercise had been recognized, since acute exercise can boost blood levels of BDNF and then improve cognitive function shortly after exercise.<sup>72</sup> Memory enhancement is more noticeable and strongest shortly following training matched to other cognitive areas. In addition, it was shown that both dopamine replacement therapy and anti-parkinsonism medicines upregulate BDNF to a small degree.<sup>73</sup> As noted, these findings have sparked tremendous interest in the potential for exercise-induced alterations in BDNF to arrest neurodegeneration in Parkinson's disease.<sup>74</sup> Several studies reveal reduced serum levels of BDNF in PD subjects.<sup>38–56,75–79</sup> The Val66Met polymorphisms were not identified as predictors of PD risk except for a slight increase in risk linked with the AA+AG genotype.<sup>80</sup> Even though some research suggests that the Val66Met variant can alter the expression of BDNF in PD, a growing body of evidence suggests that acute exercise can increase the serum levels of BDNF and alleviate the symptoms of Parkinson's disease.<sup>81</sup> For many, the cognitive benefits of exercise can be attributed to an increase in serum BDNF.<sup>82,83</sup> Parikh et al. found that the BDNF regulates the striatal dopamine levels in mice, specifically affecting the balance of glutamate and the ability to adapt cognitively and executively.<sup>84</sup>

The benefits of exercise on neuroplasticity and protection from 1-methyl-4-phenyl-1,2,3,6-tetrahydropyridine-induced neurotoxicity were lost in animals with a complete deletion or insufficient expression of BDNF.<sup>85,86</sup> It is possible that the alleviation of depression and motor symptoms due to continuous exercise may also be due to an increase in BDNF protein in the striatum of mice.<sup>87</sup>

One study found a paradoxical increase in serum BDNF with increased depression duration and decreased motor capacity, whereas another study found no difference in serum BDNF when considering patients' physical capacity.<sup>88</sup> Brain-derived neurotrophic factor levels are higher in patients with

PD who have had long-term dopamine replacement therapy, according to a study by Scalzo et al.<sup>39</sup> This suggests that the increased expression of BDNF in advanced PD is not only due to medication-induced release of the pool of BDNF.

It is hoped that nonpharmaceutical interventions, such as exercise, can reduce the symptoms of PD. Hirsch et al. found that regulated exercise could improve blood BDNF levels and decrease Rating Scale III (RS-III) scores in individuals with PD.<sup>88</sup> These data support the efficacy of non-pharmacological methods to induce BDNF in PD. Serum BDNF rises incrementally in the early stages of PD, most likely due to a compensatory increase in the production of BDNF by the surviving dopaminergic neurons. According to Hirsch et al., exercising a few times a week can help PD patients improve their motor scores and increase their blood levels of BDNF.<sup>88</sup> Despite the findings stating that physical training and BDNF levels increase as PD symptoms decrease, it is unclear if this is mediated by BDNF. The findings of Scalzo et al. contradict the results of this study; however, the authors do not acknowledge or explain this discrepancy.<sup>39</sup> Furthermore, it is important to point out that the aforementioned research supports the idea that exercise can improve depressive symptoms in PD patients by promoting BDNF expression and signaling. The effects of medications must be considered when analyzing data from PD patients. Even though numerous studies have qualitatively documented the use of common medications in study groups, many of these studies have not controlled for the effect of dosage or frequency of use. For example, it is thought that increased levels of BDNF are a contributing component in treating depression with serotonin reuptake inhibitors.<sup>89</sup> Selegiline, an inhibitor of monoamine oxidase, an agonist of the N-methyl-D-aspartate receptor, and metformin, a tricyclic antidepressant, have been shown to have neuroprotective characteristics.<sup>90–93</sup> Many studies offered only a dichotomous assessment of depression in PD patients and did not use psychological tests to establish a quantitative score.

The results of this meta-analysis indicate that BDNF levels are decreased in patients with PD and perhaps in PD patients with depression.<sup>89–98</sup> For these potential connections to be demonstrated and compared with other subjects in terms of the examined consequences, further research is needed. Larger and more uniform samples are required for this type of study.<sup>99–103</sup> A previous meta-analysis similarly showed that BDNF had favorable advantages in treating PD and reducing PD with depression.<sup>104–110</sup> To determine whether age and ethnicity are connected to the outcomes of our study, well-conducted randomized controlled trials are needed.

## Limitations

While this study may have been skewed by excluding so many trials from our meta-analysis, these studies failed to meet our rigorous inclusion criteria. Of the 19 papers

analyzed, 13 had sample sizes of less than 100 people. In addition, some of the included studies did not mention the sampling time of BDNF. There is no way to tell if the results are due to gender or ethnicity, as data on these variables were not included in our study. Patients with PD were evaluated for BDNF using data from previous research, which may have been skewed due to a lack of relevant information. Uncollected variables such as the respondents' age, gender and nutritional status may have also skewed the results.

## Conclusions

Parkinson's disease combined with depression, and PD patients without depression had significantly lower levels of BDNF than healthy controls. Parkinson's disease patients with depression did not have lower levels of BDNF than PD patients without depression. In individuals with PD, acute exercise and physical training are consistently associated with increased serum BDNF and, by extension, better motor function and lower Unified Parkinson Disease Rating Scale (UPDRS) stage III scores. Our research suggests that depression, a major comorbidity in PD, and PD both have the capacity to downregulate the expression of BDNF. In addition, possible drug effects, such as antidepressants and dopamine replacement treatment, are reflected here as well.

### ORCID iDs

Zhen Chen  <https://orcid.org/0000-0003-3886-2493>

Hui Zhang  <https://orcid.org/0000-0002-4234-9062>

### References

1. Tanaka M, Spekker E, Szabó Á, Polyák H, Vécsei L. Modelling the neurodevelopmental pathogenesis in neuropsychiatric disorders: Bioactive kynurenes and their analogues as neuroprotective agents. In celebration of 80<sup>th</sup> birthday of Professor Peter Riederer. *J Neural Transm.* 2022;129(5–6):627–642. doi:10.1007/s00702-022-02513-5
2. Rosenblat JD, Cha DS, Mansur RB, McIntyre RS. Inflamed moods: A review of the interactions between inflammation and mood disorders. *Prog Neuropsychopharmacol Biol Psychiatry.* 2014;53:23–34. doi:10.1016/j.pnpbp.2014.01.013
3. Carrera-González M del P, Cantón-Habas V, Rich-Ruiz M. Aging, depression and dementia: The inflammatory process. *Adv Clin Exp Med.* 2022;31(5):469–473. doi:10.17219/acem/149897
4. Hepsomali P, Coxon C. Inflammation and diet: Focus on mental and cognitive health. *Adv Clin Exp Med.* 2022;31(8):821–825. doi:10.17219/acem/152350
5. Dickson DW. Neuropathology of Parkinson disease. *Parkinsonism Relat Disord.* 2018;46:530–533. doi:10.1016/j.parkreldis.2017.07.033
6. Battaglia S, Cardellicchio P, Di Fazio C, Nazzi C, Fracasso A, Borgomaneri S. The influence of vicarious fear-learning in “infecting” reactive action inhibition. *Front Behav Neurosci.* 2022;16:946263. doi:10.3389/fnbeh.2022.946263
7. Borgomaneri S, Serio G, Battaglia S. Please, don't do it! Fifteen years of progress of non-invasive brain stimulation in action inhibition. *Cortex.* 2020;132:404–422. doi:10.1016/j.cortex.2020.09.002
8. Battaglia S, Serio G, Scarpazza C, D'Ausilio A, Borgomaneri S. Frozen in (e)motion: How reactive motor inhibition is influenced by the emotional content of stimuli in healthy and psychiatric populations. *Behav Res Ther.* 2021;146:103963. doi:10.1016/j.brat.2021.103963
9. Mazzoni P, Shabbott B, Cortes JC. Motor control abnormalities in Parkinson's disease. *Cold Spring Harb Perspect Med.* 2012;2(6):a009282. doi:10.1101/cshperspect.a009282



10. Cao X, Yang F, Zheng J, Wang X, Huang Q. Aberrant structure MRI in Parkinson's disease and comorbidity with depression based on multinomial tensor regression analysis. *J Pers Med*. 2022;12(1):89. doi:10.3390/jpm12010089
11. Ellena G, Battaglia S, Ládavas E. The spatial effect of fearful faces in the autonomic response. *Exp Brain Res*. 2020;238(9):2009–2018. doi:10.1007/s00221-020-05829-4
12. Borgomaneri S, Vitale F, Battaglia S, Avenanti A. Early right motor cortex response to happy and fearful facial expressions: A TMS motor-evoked potential study. *Brain Sci*. 2021;11(9):1203. doi:10.3390/brainsci11091203
13. Tanaka M, Szabó Á, Spekker E, Polyák H, Tóth F, Vécsei L. Mitochondrial impairment: A common motif in neuropsychiatric presentation? The link to the tryptophan–kynurenine metabolic system. *Cells*. 2022;11(16):2607. doi:10.3390/cells11162607
14. Byeon H. Development of a stacking-based ensemble machine learning for detection of depression in Parkinson's disease: Preliminary research. *Biol Life Sci Forum*. 2021;9:10857. doi:10.3390/ECCM-10857
15. McTeague LM, Rosenberg BM, Lopez JW, et al. Identification of common neural circuit disruptions in emotional processing across psychiatric disorders. *Am J Psychiatry*. 2020;177(5):411–421. doi:10.1176/appi.ajp.2019.18111271
16. Kovner R, Oler JA, Kalin NH. Cortico-limbic interactions mediate adaptive and maladaptive responses relevant to psychopathology. *Am J Psychiatry*. 2019;176(12):987–999. doi:10.1176/appi.ajp.2019.19101064
17. An Y, Chen C, Inoue T, et al. Mirtazapine exerts an anxiolytic-like effect through activation of the median raphe nucleus-dorsal hippocampal 5-HT pathway in contextual fear conditioning in rats. *Prog Neuropsychopharmacol Biol Psychiatry*. 2016;70:17–23. doi:10.1016/j.pnpbp.2016.04.014
18. Chen C. Recent advances in the study of the comorbidity of depressive and anxiety disorders. *Adv Clin Exp Med*. 2022;31(4):355–358. doi:10.17219/acem/147441
19. Hestad K, Alexander J, Rootwelt H, Aaseth JO. The role of tryptophan dysmetabolism and quinolinic acid in depressive and neurodegenerative diseases. *Biomolecules*. 2022;12(7):998. doi:10.3390/biom12070998
20. Holland C, Garner I, Simpson J, et al. Impacts of COVID-19 lockdowns on frailty and wellbeing in older people and those living with long-term conditions. *Adv Clin Exp Med*. 2021;30(11):1111–1114. doi:10.17219/acem/144135
21. Tanaka M, Vécsei L. Editorial of Special Issue 'Dissecting Neurological and Neuropsychiatric Diseases: Neurodegeneration and Neuroprotection.' *Int J Mol Sci*. 2022;23(13):6991. doi:10.3390/ijms23136991
22. Chojdak-Łukasiewicz J, Małodobra-Mazur M, Zimny A, Noga L, Paradowski B. Plasma tau protein and Aβ42 level as markers of cognitive impairment in patients with Parkinson's disease. *Adv Clin Exp Med*. 2020;29(1):115–121. doi:10.17219/acem/112058
23. Martos D, Tuka B, Tanaka M, Vécsei L, Telegdy G. Memory enhancement with kynurenic acid and its mechanisms in neurotransmission. *Biomedicines*. 2022;10(4):849. doi:10.3390/biomedicines10040849
24. Porritt MJ, Batchelor PE, Howells DW. Inhibiting BDNF expression by antisense oligonucleotide infusion causes loss of nigral dopaminergic neurons. *Exp Neurol*. 2005;192(1):226–234. doi:10.1016/j.expneurol.2004.11.030
25. Nagahara AH, Tuszynski MH. Potential therapeutic uses of BDNF in neurological and psychiatric disorders. *Nat Rev Drug Discov*. 2011;10(3):209–219. doi:10.1038/nrd3366
26. Murer MG, Yan Q, Raisman-Vozari R. Brain-derived neurotrophic factor in the control human brain, and in Alzheimer's disease and Parkinson's disease. *Prog Neurobiol*. 2001;63(1):71–124. doi:10.1016/S0301-0082(00)00014-9
27. Howells DW, Porritt MJ, Wong JYF, et al. Reduced BDNF mRNA expression in the Parkinson's disease substantia nigra. *Exp Neurol*. 2000;166(1):127–135. doi:10.1006/exnr.2000.7483
28. Mogi M, Togari A, Kondo T, et al. Brain-derived growth factor and nerve growth factor concentrations are decreased in the substantia nigra in Parkinson's disease. *Neurosci Lett*. 1999;270(1):45–48. doi:10.1016/S0304-3940(99)00463-2
29. Parain K, Murer MG, Yan Q, et al. Reduced expression of brain-derived neurotrophic factor protein in Parkinson's disease substantia nigra. *Neuroreport*. 1999;10(3):557–561. doi:10.1097/00001756-199902250-00021
30. Collier TJ, Dung Ling Z, Carvey PM, et al. Striatal trophic factor activity in aging monkeys with unilateral MPTP-induced parkinsonism. *Exp Neurol*. 2005;191:560–567. doi:10.1016/j.expneurol.2004.08.018
31. Stroup DF. Meta-analysis of observational studies in epidemiology: A proposal for reporting. *JAMA*. 2000;283(15):2008. doi:10.1001/jama.283.15.2008
32. Higgins JPT. Measuring inconsistency in meta-analyses. *BMJ*. 2003;327(7414):557–560. doi:10.1136/bmj.327.7414.557
33. Liberati A, Altman DG, Tetzlaff J, et al. The PRISMA statement for reporting systematic reviews and meta-analyses of studies that evaluate health care interventions: Explanation and elaboration. *J Clin Epidemiol*. 2009;62(10):e1–e34. doi:10.1016/j.jclinepi.2009.06.006
34. Gupta A, Das A, Majumder K, et al. Obesity is independently associated with increased risk of hepatocellular cancer-related mortality: A systematic review and meta-analysis. *Am J Clin Oncol*. 2018;41(9):874–881. doi:10.1097/COC.0000000000000388
35. Higgins JPT, Altman DG, Gotzsche PC, et al. The Cochrane Collaboration's tool for assessing risk of bias in randomised trials. *BMJ*. 2011;343:d5928. doi:10.1136/bmj.d5928
36. Sheikhbahaei S, Trahan TJ, Xiao J, et al. FDG-PET/CT and MRI for evaluation of pathologic response to neoadjuvant chemotherapy in patients with breast cancer: A meta-analysis of diagnostic accuracy studies. *Oncologist*. 2016;21(8):931–939. doi:10.1634/theoncologist.2015-0353
37. Klein AB, Williamson R, Santini MA, et al. Blood BDNF concentrations reflect brain-tissue BDNF levels across species. *Int J Neuropsychopharm*. 2011;14(3):347–353. doi:10.1017/S1461145710000738
38. Salehi Z, Mashayekhi F. Brain-derived neurotrophic factor concentrations in the cerebrospinal fluid of patients with Parkinson's disease. *J Clin Neurosci*. 2009;16(1):90–93. doi:10.1016/j.jocn.2008.03.010
39. Scalzo P, Kümmer A, Bretas TL, Cardoso F, Teixeira AL. Serum levels of brain-derived neurotrophic factor correlate with motor impairment in Parkinson's disease. *J Neurol*. 2010;257(4):540–545. doi:10.1007/s00415-009-5357-2
40. Ricci V, Pomponi M, Martinotti G, et al. Antidepressant treatment restores brain-derived neurotrophic factor serum levels and ameliorates motor function in Parkinson disease patients. *J Clin Psychopharmacol*. 2010;30(6):751–753. doi:10.1097/JCP.0b013e3181fc2ec7
41. Pålhagen S, Qi H, Mårtensson B, Wälinder J, Granérus AK, Svenningsson P. Monoamines, BDNF, IL-6 and corticosterone in CSF in patients with Parkinson's disease and major depression. *J Neurol*. 2010;257(4):524–532. doi:10.1007/s00415-009-5353-6
42. Ventriglia M, Zanardini R, Bonomini C, et al. Serum brain-derived neurotrophic factor levels in different neurological diseases. *Biomed Res Int*. 2013;2013:901082. doi:10.1155/2013/901082
43. Martín de Pablos A, García-Moreno JM, Fernández E. Does the cerebrospinal fluid reflect altered redox state but not neurotrophic support loss in Parkinson's disease? *Antioxid Redox Signal*. 2015;23(11):893–898. doi:10.1089/ars.2015.6423
44. Khalil H, Alomari MA, Khabour OF, Al-Hieshan A, Bajwa JA. Relationship of circulating BDNF with cognitive deficits in people with Parkinson's disease. *J Neurosci*. 2016;362:217–220. doi:10.1016/j.jns.2016.01.032
45. Wang Y, Liu H, Zhang BS, Soares JC, Zhang XY. Low BDNF is associated with cognitive impairments in patients with Parkinson's disease. *Parkinsonism Relat Disord*. 2016;29:66–71. doi:10.1016/j.parkreldis.2016.05.023
46. Siuda J, Patalong-Ogiewa M, Żmuda W, et al. Cognitive impairment and BDNF serum levels. *Neurol Neurochir Pol*. 2017;51(1):24–32. doi:10.1016/j.pjnns.2016.10.001
47. Wang Y, Liu H, Du XD, et al. Association of low serum BDNF with depression in patients with Parkinson's disease. *Parkinsonism Relat Disord*. 2017;41:73–78. doi:10.1016/j.parkreldis.2017.05.012
48. Rocha NP, Ferreira JPS, Scalzo PL, et al. Circulating levels of neurotrophic factors are unchanged in patients with Parkinson's disease. *Arq Neuropsiquiatr*. 2018;76(5):310–315. doi:10.1590/0004-282x.20180035
49. Costa CM, de Oliveira GL, Fonseca ACS, Lana R de C, Polese JC, Pernambuco AP. Levels of cortisol and neurotrophic factor brain-derived in Parkinson's disease. *Neurosci Lett*. 2019;708:134359. doi:10.1016/j.neulet.2019.134359
50. Hernández-Vara J, Sáez-Francés N, Lorenzo-Bosquet C, et al. BDNF levels and nigrostriatal degeneration in "drug naïve" Parkinson's disease patients. An "in vivo" study using I-123-FP-CIT SPECT. *Parkinsonism Relat Disord*. 2020;78:31–35. doi:10.1016/j.parkreldis.2020.06.037

51. Quan Y, Wang J, Wang S, Zhao J. Association of the plasma long non-coding RNA MEG3 with Parkinson's disease. *Front Neurol.* 2020;11:532891. doi:10.3389/fneur.2020.532891
52. Chung CC, Huang PH, Chan L, Chen JH, Chien LN, Hong CT. Plasma exosomal brain-derived neurotrophic factor correlated with the postural instability and gait disturbance-related motor symptoms in patients with Parkinson's disease. *Diagnostics.* 2020;10(9):684. doi:10.3390/diagnostics10090684
53. Shi MY, Ma CC, Chen FF, et al. Possible role of glial cell line-derived neurotrophic factor for predicting cognitive impairment in Parkinson's disease: A case-control study. *Neural Regen Res.* 2021;16(5):885. doi:10.4103/1673-5374.297091
54. Soke F, Kocer B, Fidan I, Keskinoglu P, Guclu-Gunduz A. Effects of task-oriented training combined with aerobic training on serum BDNF, GDNF, IGF-1, VEGF, TNF- $\alpha$ , and IL-1 $\beta$  levels in people with Parkinson's disease: A randomized controlled study. *Exp Gerontol.* 2021;150:111384. doi:10.1016/j.exger.2021.111384
55. Huang Y, Huang C, Zhang Q, Wu W, Sun J. Serum BDNF discriminates Parkinson's disease patients with depression from without depression and reflect motor severity and gender differences. *J Neurol.* 2021;268(4):1411–1418. doi:10.1007/s00415-020-10299-3
56. Schaeffer E, Roeben B, Granert O, et al. Effects of exergaming on hippocampal volume and brain-derived neurotrophic factor levels in Parkinson's disease. *Eur J Neurol.* 2022;29(2):441–449. doi:10.1111/ene.15165
57. Quesseveur G, David DJ, Gaillard MC, et al. BDNF overexpression in mouse hippocampal astrocytes promotes local neurogenesis and elicits anxiolytic-like activities. *Transl Psychiatry.* 2013;3(4):e253. doi:10.1038/tp.2013.30
58. Karege F, Schwald M, Cisse M. Postnatal developmental profile of brain-derived neurotrophic factor in rat brain and platelets. *Neurosci Lett.* 2002;328(3):261–264. doi:10.1016/S0304-3940(02)00529-3
59. Ziebell M, Khalid U, Klein AB, et al. Striatal dopamine transporter binding correlates with serum BDNF levels in patients with striatal dopaminergic neurodegeneration. *Neurobiol Aging.* 2012;33(2):428.e1–428.e5. doi:10.1016/j.neurobiolaging.2010.11.010
60. Momose Y, Murata M, Kobayashi K, et al. Association studies of multiple candidate genes for Parkinson's disease using single nucleotide polymorphisms. *Ann Neurol.* 2002;51(1):133–136. doi:10.1002/ana.10079
61. Egan MF, Kojima M, Callicott JH, et al. The BDNF val66met polymorphism affects activity-dependent secretion of BDNF and human memory and hippocampal function. *Cell.* 2003;112(2):257–269. doi:10.1016/S0092-8674(03)00035-7
62. Dai L, Wang D, Meng H, et al. Association between the *BDNF* G196A and C270T polymorphisms and Parkinson's disease: A meta-analysis. *Int J Neurosci.* 2013;123(10):675–683. doi:10.3109/00207454.2013.798784
63. Dluzen DE, Anderson LI, McDermott JL, Kucera J, Walro JM. Striatal dopamine output is compromised within +/- BDNF mice. *Synapse.* 2002;43(2):112–117. doi:10.1002/syn.10027
64. Yuan Y, Sun J, Zhao M, et al. Overexpression of  $\alpha$ -synuclein down-regulates BDNF expression. *Cell Mol Neurobiol.* 2010;30(6):939–946. doi:10.1007/s10571-010-9523-y
65. Kang SS, Zhang Z, Liu X, et al. TrkB neurotrophic activities are blocked by  $\alpha$ -synuclein, triggering dopaminergic cell death in Parkinson's disease. *Proc Natl Acad Sci U S A.* 2017;114(40):10773–10778. doi:10.1073/pnas.1713969114
66. Mocchetti I, Bachis A, Nosheny RL, Tanda G. Brain-derived neurotrophic factor expression in the substantia nigra does not change after lesions of dopaminergic neurons. *Neurotox Res.* 2007;12(2):135–143. doi:10.1007/BF03033922
67. Goldberg NRS, Caesar J, Park A, et al. Neural stem cells rescue cognitive and motor dysfunction in a transgenic model of dementia with Lewy bodies through a BDNF-dependent mechanism. *Stem Cell Rep.* 2015;5(5):791–804. doi:10.1016/j.stemcr.2015.09.008
68. Yoshimoto Y, Lin Q, Collier TJ, Frim DM, Breakefield XO, Bohn MC. Astrocytes retrovirally transduced with BDNF elicit behavioral improvement in a rat model of Parkinson's disease. *Brain Res.* 1995;691(1–2):25–36. doi:10.1016/0006-8993(95)00596-1
69. Zhao L, He LX, Huang SN, et al. Protection of dopamine neurons by vibration training and upregulation of brain-derived neurotrophic factor in a MPTP mouse model of Parkinson's disease. *Physiol Res.* 2014;63(5):649–657. doi:10.33549/physiolres.932743
70. Ferreira RN, de Miranda AS, Rocha NP, Simoes e Silva AC, Teixeira AL, da Silva Camargos ER. Neurotrophic factors in Parkinson's disease: What have we learned from preclinical and clinical studies? *Curr Med Chem.* 2018;25(31):3682–3702. doi:10.2174/09298673255666180313101536
71. Onerup A, Angenete E, Bock D, et al. The effect of pre- and post-operative physical activity on recovery after colorectal cancer surgery (PHYSSURG-C): Study protocol for a randomised controlled trial. *Trials.* 2017;18(1):212. doi:10.1186/s13063-017-1949-9
72. Okazawa H, Murata M, Watanabe M, Kamei M, Kanazawa I. Dopamine stimulation up-regulates the in vivo expression of brain-derived neurotrophic factor (BDNF) in the striatum. *FEBS Lett.* 1992;313(2):138–142. doi:10.1016/0014-5793(92)81430-T
73. Campos C, Rocha NBF, Lattari E, Paes F, Nardi AE, Machado S. Exercise-induced neuroprotective effects on neurodegenerative diseases: The key role of trophic factors. *Exp Rev Neurother.* 2016;16(6):723–734. doi:10.1080/14737175.2016.1179582
74. Angelucci F, Peppe A, Carlesimo GA, et al. A pilot study on the effect of cognitive training on BDNF serum levels in individuals with Parkinson's disease. *Front Hum Neurosci.* 2015;9:130. doi:10.3389/fnhum.2015.00130
75. Frazzitta G, Maestri R, Ghilardi MF, et al. Intensive rehabilitation increases BDNF serum levels in Parkinsonian patients: A randomized study. *Neurorehabil Neural Repair.* 2014;28(2):163–168. doi:10.1177/1545968313508474
76. Khalil H, Alomari MA, Khabour O, Al-Hieshan A, Bajwa JA. The association between physical activity with cognitive function and brain-derived neurotrophic factor in people with Parkinson's disease: A pilot study. *J Aging Phys Act.* 2017;25(4):646–652. doi:10.1123/japa.2016-0121
77. Marusiak J, Żeligowska E, Mencil J, et al. Interval training-induced alleviation of rigidity and hypertonia in patients with Parkinson's disease is accompanied by increased basal serum brain-derived neurotrophic factor. *J Rehabil Med.* 2015;47(4):372–375. doi:10.2340/16501977-1931
78. Sajatovic M, Ridgel A, Walter E, et al. A randomized trial of individual versus group-format exercise and self-management in individuals with Parkinson's disease and comorbid depression. *Patient Prefer Adherence.* 2017;11:965–973. doi:10.2147/PPA.S135551
79. Zoladz JA, Majerczak J, Żeligowska E, et al. Moderate-intensity interval training increases serum brain-derived neurotrophic factor level and decreases inflammation in Parkinson's disease patients. *J Physiol Pharmacol.* 2014;65(3):441–448. PMID:24930517
80. Lee YH, Song GG. *BDNF* 196 G/A and 270 C/T polymorphisms and susceptibility to Parkinson's disease: A meta-analysis. *J Mot Behav.* 2014;46(1):59–66. doi:10.1080/00222895.2013.862199
81. Phillips C. Brain-derived neurotrophic factor, depression, and physical activity: Making the neuroplastic connection. *Neural Plast.* 2017;2017:260130. doi:10.1155/2017/260130
82. de Assis GG, de Almondes KM. Exercise-dependent BDNF as a modulatory factor for the executive processing of individuals in course of cognitive decline: A systematic review. *Front Psychol.* 2017;8:584. doi:10.3389/fpsyg.2017.00584
83. Etnier JL, Labban JD, Karper WB, et al. Innovative research exploring the effects of physical activity and genetics on cognitive performance in community-based older adults. *J Aging Phys Act.* 2015;23(4):559–568. doi:10.1123/japa.2014-0221
84. Parikh V, Naughton SX, Yegla B, Guzman DM. Impact of partial dopamine depletion on cognitive flexibility in BDNF heterozygous mice. *Psychopharmacology.* 2016;233(8):1361–1375. doi:10.1007/s00213-016-4229-6
85. Gerecke KM, Jiao Y, Pagala V, Smeyne RJ. Exercise does not protect against MPTP-induced neurotoxicity in BDNF haploinsufficient mice. *PLoS One.* 2012;7(8):e43250. doi:10.1371/journal.pone.0043250
86. Ieraci A, Madaio AI, Mallei A, Lee FS, Popoli M. Brain-derived neurotrophic factor Val66Met human polymorphism impairs the beneficial exercise-induced neurobiological changes in mice. *Neuropsychopharmacology.* 2016;41(13):3070–3079. doi:10.1038/npp.2016.120
87. Tuon T, Valvassori SS, Dal Pont GC, et al. Physical training prevents depressive symptoms and a decrease in brain-derived neurotrophic factor in Parkinson's disease. *Brain Res Bull.* 2014;108:106–112. doi:10.1016/j.brainresbull.2014.09.006

88. Hirsch MA, van Wegen EEH, Newman MA, Heyn PC. Exercise-induced increase in brain-derived neurotrophic factor in human Parkinson's disease: A systematic review and meta-analysis. *Transl Neurodegener.* 2018;7(1):7. doi:10.1186/s40035-018-0112-1
89. Kishi T, Yoshimura R, Ikuta T, Iwata N. Brain-derived neurotrophic factor and major depressive disorder: Evidence from meta-analyses. *Front Psychiatry.* 2018;8:308. doi:10.3389/fpsy.2017.00308
90. Paumier KL, Sortwell CE, Madhavan L, et al. Chronic amitriptyline treatment attenuates nigrostriatal degeneration and significantly alters trophic support in a rat model of Parkinsonism. *Neuropsychopharmacology.* 2015;40(4):874–883. doi:10.1038/npp.2014.262
91. Zhao Q, Cai D, Bai Y. Selegiline rescues gait deficits and the loss of dopaminergic neurons in a subacute MPTP mouse model of Parkinson's disease. *Int J Mol Med.* 2013;32(4):883–891. doi:10.3892/ijmm.2013.1450
92. Bustos G, Abarca J, Bustos V, et al. NMDA receptors mediate an early up-regulation of brain-derived neurotrophic factor expression in substantia nigra in a rat model of presymptomatic Parkinson's disease. *J Neurosci Res.* 2009;87(10):2308–2318. doi:10.1002/jnr.22063
93. Patil SP, Jain PD, Ghumatkar PJ, Tambe R, Sathaye S. Neuroprotective effect of metformin in MPTP-induced Parkinson's disease in mice. *Neuroscience.* 2014;277:747–754. doi:10.1016/j.neuroscience.2014.07.046
94. Elgendy MO, Hassan AH, Saeed H, Abdelrahim ME, Eldin RS. Asthmatic children and MDI verbal inhalation technique counseling. *Pulm Pharmacol Ther.* 2020;61:101900. doi:10.1016/j.pupt.2020.101900
95. Osama H, Abdullah A, Gamal B, et al. Effect of honey and royal jelly against cisplatin-induced nephrotoxicity in patients with cancer. *J Am Coll Nutr.* 2017;36(5):342–346. doi:10.1080/07315724.2017.1292157
96. Sayed AM, Khalaf AM, Abdelrahim MEA, Elgendy MO. Repurposing of some anti-infective drugs for COVID-19 treatment: A surveillance study supported by an in silico investigation. *Int J Clin Pract.* 2021;75(4):e13877. doi:10.1111/ijcp.13877
97. Saeed H, Elberry AA, Eldin AS, Rabea H, Abdelrahim MEA. Effect of nebulizer designs on aerosol delivery during non-invasive mechanical ventilation: A modeling study of in vitro data. *Pulm Ther.* 2017;3(1):233–241. doi:10.1007/s41030-017-0033-7
98. Saeed H, Abdelrahim ME, Rabea H, Salem HF. Impact of advanced patient counseling using a training device and smartphone application on asthma control. *Respir Care.* 2020;65(3):326–332. doi:10.4187/respcare.06903
99. Madney YM, Laz NI, Elberry AA, Rabea H, Abdelrahim MEA. The influence of changing interfaces on aerosol delivery within high flow oxygen setting in adults: An in-vitro study. *J Drug Deliv Sci Technol.* 2020;55:101365. doi:10.1016/j.jddst.2019.101365
100. Hassan A, Rabea H, Hussein RRS, et al. In-vitro characterization of the aerosolized dose during non-invasive automatic continuous positive airway pressure ventilation. *Pulm Ther.* 2016;2(1):115–126. doi:10.1007/s41030-015-0010-y
101. Harb HS, Laz NI, Rabea H, Abdelrahim MEA. First-time handling of different inhalers by chronic obstructive lung disease patients. *Exp Lung Res.* 2020;46(7):258–269. doi:10.1080/01902148.2020.1789903
102. Abdelrahim ME, Assi KH, Chrystyn H. Relative bioavailability of terbutaline to the lung following inhalation, using urinary excretion. *Br J Clin Pharmacol.* 2011;71(4):608–610. doi:10.1111/j.1365-2125.2010.03873.x
103. Harb HS, Elberry AA, Rabea H, Fathy M, Abdelrahim MEA. Is Combihaler usable for aerosol delivery in single limb non-invasive mechanical ventilation? *J Drug Deliv Sci Technol.* 2017;40:28–34. doi:10.1016/j.jddst.2017.05.022
104. Karimi N, Ashourizadeh H, Akbarzadeh Pasha B, et al. Blood levels of brain-derived neurotrophic factor (BDNF) in people with multiple sclerosis (MS): A systematic review and meta-analysis. *Multiple Scler Relat Dis.* 2022;65:103984. doi:10.1016/j.msard.2022.103984
105. D'Souza T, Rajkumar AP. Systematic review of genetic variants associated with cognitive impairment and depressive symptoms in Parkinson's disease. *Acta Neuropsychiatr.* 2020;32(1):10–22. doi:10.1017/neu.2019.28
106. Wang Q, Liu J, Guo Y, Dong G, Zou W, Chen Z. Association between BDNF G196A (Val66Met) polymorphism and cognitive impairment in patients with Parkinson's disease: A meta-analysis. *Braz J Med Biol Res.* 2019;52(8):e8443. doi:10.1590/1414-431x20198443
107. Jiang L, Zhang H, Wang C, Ming F, Shi X, Yang M. Serum level of brain-derived neurotrophic factor in Parkinson's disease: A meta-analysis. *Prog Neuropsychopharmacol Biol Psychiatry.* 2019;88:168–174. doi:10.1016/j.pnpbp.2018.07.010
108. You T, Ogawa EF. Effects of meditation and mind-body exercise on brain-derived neurotrophic factor: A literature review of human experimental studies. *Sports Med Health Sci.* 2020;2(1):7–9. doi:10.1016/j.smhs.2020.03.001
109. Mojtavavi H, Shaka Z, Momtazmanesh S, Ajdari A, Rezaei N. Circulating brain-derived neurotrophic factor as a potential biomarker in stroke: A systematic review and meta-analysis. *J Transl Med.* 2022;20(1):126. doi:10.1186/s12967-022-03312-y
110. Rahmani F, Saghazadeh A, Rahmani M, et al. Plasma levels of brain-derived neurotrophic factor in patients with Parkinson disease: A systematic review and meta-analysis. *Brain Res.* 2019;1704:127–136. doi:10.1016/j.brainres.2018.10.006





# Expression of NF- $\kappa$ B and VEGF in normal placenta and placenta previa patients

Çağdaş Özgökçe<sup>1,A–F</sup>, Aydın Öcal<sup>1,A–F</sup>, Işıl Sezen Ermiş<sup>2,A–F</sup>

<sup>1</sup> Department of Perinatology, İstanbul Zeynep Kamil Women's and Children's Disease Training and Research Hospital, İstanbul, Turkey

<sup>2</sup> Department of Obstetrics and Gynecology, Faculty of Medicine, Harran University, Şanlıurfa, Turkey

A – research concept and design; B – collection and/or assembly of data; C – data analysis and interpretation; D – writing the article; E – critical revision of the article; F – final approval of the article

Advances in Clinical and Experimental Medicine, ISSN 1899–5276 (print), ISSN 2451–2680 (online)

Adv Clin Exp Med. 2023;32(3):297–306

## Address for correspondence

Çağdaş Özgökçe

E-mail: drcozgoke@gmail.com

## Funding sources

None declared

## Conflict of interest

None declared

Received on March 23, 2022

Reviewed on August 29, 2022

Accepted on September 22, 2022

Published online on November 14, 2022

## Cite as

Özgökçe Ç, Öcal A, Ermiş IS. Expression of NF- $\kappa$ B and VEGF in normal placenta and placenta previa patients.

Adv Clin Exp Med. 2023;32(3):297–306.

doi:10.17219/acem/154858

## DOI

10.17219/acem/154858

## Copyright

Copyright by Author(s)

This is an article distributed under the terms of the Creative Commons Attribution 3.0 Unported (CC BY 3.0)

(<https://creativecommons.org/licenses/by/3.0/>)

## Abstract

**Background.** Placenta previa is a pregnancy condition associated with the development of complications related to placental insufficiency, including hypertension, preeclampsia and perinatal mortality. Dysfunction in uteroplacental arteries causes the release of cytokines, leukotrienes and immunomodulatory hormones, which leads to an inflammatory reaction.

**Objectives.** The nuclear factor kappa-light-chain-enhancer of activated B cells (NF- $\kappa$ B) pathway and vascular endothelial growth factor (VEGF) are known to play crucial roles in inflammation and angiogenic regulation. This study aimed to demonstrate the morphometric and immunohistochemical effects on inflammation and angiogenesis underlying placenta previa.

**Materials and methods.** Twenty pregnant patients with placenta previa and 20 healthy pregnant patients, all between 30 and 38 weeks gestational age, were included in the study. The gestational age of the pregnancies was determined according to the last date of menstruation and/or ultrasonographic measurements. Blood samples and clinical data were obtained from the prenatal patient groups. Samples were taken from the connecting stem region from both groups.

**Results.** The mean difference between the control and placenta previa patients was statistically significant for the parameters of blood vessels in villi, diameter of floating small villus, decidual cells, syncytial knots, congestion in blood vessels, fibrinoid accumulation, and inflammation. Significant degeneration and apoptotic changes in the syncytial cells of the root villi and an increase in syncytial nodes and bridges were observed in the placenta previa specimens. In the connecting stem region of the placenta previa samples, blood vessel dilatation, endothelial cell hyperplasia and a higher number of syncytial nodes were observed. In the immunohistochemical examination of the placenta previa samples, an increase in NF- $\kappa$ B and VEGF expression was observed in the endothelial cells, syncytial cells and Hofbauer cells.

**Conclusions.** Vascular endothelial growth factor was found to stimulate endothelial cell proliferation and migration, and to significantly affect angiogenesis during the developmental process of the placenta and remodeling of the uterine vessels, inducing NF- $\kappa$ B signaling and apoptotic development during cytotrophoblastic invasion in the vascularization of the placenta.

**Key words:** VEGF, NF- $\kappa$ B, placenta previa, chorionic villus

## Background

Placenta previa is an obstetric condition in which there is atypical localization of the placenta around the internal cervical os. It is accompanied by painless vaginal bleeding in the 3<sup>rd</sup> trimester. It is a gynecological disease that can partially or completely obscure the cervical opening, with the placenta localized in the lower part of the uterus.<sup>1</sup> Placenta previa is known to occur in 1 out of 200 pregnant women. It is important to detect this condition in the early stages of pregnancy because of the essential role of the follow-up. Placenta previa can complicate delivery and lead to life-threatening complications for the mother and baby, especially when it occurs close to the birth. There has been a remarkable increase in the incidence of placenta previa in recent years. It has been reported that cesarean section techniques, surgical interventions to the uterus, births at advanced age, high parity, tobacco and substance use, and in vitro techniques can trigger this disease.<sup>1-3</sup>

It is known that placenta previa can lead to cardiac problems due to pregnancy, prolapse of the placenta and accompanying mortality.<sup>4,5</sup> Dysfunction in arterial nutrition leads to the inability of the uterus and placenta to receive enough blood. These findings suggest that placental factors help in immune modulation, which is essentially required for successful pregnancy completion. There is a regulated balance between pro-inflammatory and anti-inflammatory factors. The emergence of regulatory T cells is induced with a suppressive effect against autoreactive T cell effectors. Indeed, a functioning neuropeptide system contributes to overall health, and changes in the expression of these neuropeptides and/or their receptors result in altered susceptibility to inflammatory and autoimmune diseases.<sup>6</sup> Surgery may cause damage to the endometrium and myometrium of the uterus, increasing the risk of placenta previa.<sup>2</sup>

The signaling pathway leading to the eventual activation of nuclear factor kappa-light-chain-enhancer of activated B cells (NF- $\kappa$ B) plays an important role in immune and inflammatory responses.<sup>7</sup> Regulation of maternal T cells during pregnancy is mediated by NF- $\kappa$ B p65; studies have reported that the degradation of p65 in maternal T cells is induced by the activation of fatty acid synthase (Fas). Placental exosomes expressing the Fas ligand (a type II membrane protein that belongs to the tumor necrosis factor superfamily) have been implicated as having an immunomodulatory function during pregnancy.<sup>8</sup> In a study on congenital Zika syndrome in pregnant women, it was reported that Smaducin-6 (a membrane-bound Smad6-derived peptide) blocked the NF- $\kappa$ B activation mechanism via Pellino E3 ubiquitin protein ligase 1 but had no direct effect on congenital Zika syndrome.<sup>9</sup> Olmos-Ortiz et al. observed that prolactin, toll-like receptor 4 (TLR4) expression, and mechanisms related to NF- $\kappa$ B phosphorylation provide and organize the upregulation of lipopolysaccharides. They reported that prolactin may play an important

role in limiting inflammatory responses to lipopolysaccharides in the human placenta and inhibiting immune responses against infections that may threaten the outcomes of pregnancy. It is the first evidence of this mechanism for the anti-inflammatory activity of prolactin in the human placenta.<sup>10</sup> They showed that infection of *Listeria monocytogenes* upregulates TLR2 and cytosolic DNA sensing pathways, as well as the downstream pro-inflammatory circuit in which NF- $\kappa$ B is involved.<sup>11</sup> The effects of fatty acids on the placental inflammatory cytokines in relation to TLR4/NF- $\kappa$ B were investigated in a study in which trophoblast cells isolated from 14 normal-term human placentas were incubated with fatty acids. According to the study, the long-chain saturated fatty acids – stearic acid and palmitic acid – stimulated the secretion and synthesis of tumor necrosis factor- $\alpha$  (TNF- $\alpha$ ) and interleukin (IL)-6 and 8 by trophoblast cells at a statistically significant level. The authors stated that unsaturated fatty acids do not change cytokine expression and that palmitate-induced inflammatory effects are accompanied by TLR4 activation, NF- $\kappa$ B phosphorylation and nuclear translocation.<sup>12</sup> Pro-inflammatory stimulation of macrophage colony-stimulating factor (M-CSF) secreted by free 1<sup>st</sup>-trimester decidual cells in pregnant women and its relationship with macrophage development were investigated. It has been found that in free 1<sup>st</sup>-trimester decidual cells, IL-1 $\beta$  and TNF- $\alpha$  signal along the NF- $\kappa$ B pathway to induce M-CSF.<sup>13</sup> It has been suggested that the interaction between Nestin and cyclin-dependent kinase 5 may lead to the progression of placenta previa by regulating NF- $\kappa$ B.<sup>14</sup>

In recent years, a great deal of research has focused on the relationship between abnormal angiogenesis and placenta previa.<sup>3</sup> Vascular endothelial growth factor (VEGF) is known as a signaling protein that stimulates vasculogenesis and angiogenesis.<sup>15,16</sup> Chehroudi et al. stated that umbilical cord inflammatory cytokines and VEGF have not been extensively studied in terms of pregnancy disorders or maternal/neonatal causes. In that study, maternal and neonatal variables, as well as VEGF-A, VEGF-C and VEGF-D expression in umbilical cord lysates were examined. The authors determined that VEGF-A is strongly suppressed in adverse pregnancy cases.<sup>17</sup> In another study, choroidal neovascularization was induced by laser and immune cells, and the neovascularization was analyzed using polymerase chain reaction (PCR). In the early inflammatory phase after the laser exposure, anti-placental growth factor, VEGF-A, was reported to be significantly upregulated. They observed that the increase in VEGF-A was limited to the scar, while anti-placental growth factor showed a wider spread.<sup>18</sup> The expression of VEGF in hypertension, preeclampsia and preterm birth cases has been examined in various studies. It has been reported that the expression level of VEGF decreased due to hypertension,<sup>19</sup> the level of VEGF receptors increased in preeclampsia,<sup>20</sup> and the expression level of VEGF was very high in cases of premature delivery.<sup>21,22</sup>

Vascular endothelial growth factor plays a role in angiogenic regulation and is secreted during pregnancy in sufficient amounts from cell groups outside the placental villi; it promotes proliferation, adhesion and/or invasion.<sup>23</sup> Human deciduas from the 1<sup>st</sup>, 2<sup>nd</sup> and 3<sup>rd</sup> trimesters were examined via immunocytochemistry. The viability of total decidual cells and different cell isolates was not affected by triiodothyronine. In the 1<sup>st</sup> trimester, triiodothyronine was reported to reduce VEGF-A secretion by total decidual cells and to increase angiopoietin-2 secretion by stromal-depleted cells.<sup>24</sup> They suggested that VEGF and soluble fms-like tyrosine kinase-1 levels are important for diagnosing placenta previa and can be considered additional parameters to differentiate between placenta accreta and increta.<sup>25</sup> Moreover, the increase in the expression of high mobility group box protein 1 in the placenta may be related to the pathogenesis of placenta previa by regulating the expression of the proangiogenic factor VEGF.<sup>26</sup> In another study, VEGF and leptin levels in 2<sup>nd</sup>-trimester amniotic fluid samples taken between 16 and 20 weeks of pregnancy were compared with a control group at 37 weeks. According to their results, amniotic fluid VEGF levels in the 2<sup>nd</sup> trimester predict preterm delivery better than leptin levels.<sup>27</sup>

The first blood vessel formation begins when angioblasts of mesenchymal origin gather in groups from the yolk sac of the embryo and develop the endothelial tube. The first developing veins reform an existing circulatory system, and both regional proliferation and regression, as well as branching and migration, are observed. With angiogenesis forming the new vascular system, mature endothelial cells divide and new capillaries are formed. It is known that VEGF signaling must be activated for vasculogenesis and angiogenesis to occur fully.<sup>28,29</sup>

## Objectives

This study aimed to determine the expression levels of NF- $\kappa$ B and VEGF in the placenta in order to understand the possible morphometric and immunohistochemical effects on inflammation and angiogenesis underlying placenta previa.

## Materials and methods

### Study population

This study was carried out at Van Özel Akdamar Hospital, Department of Obstetrics and Gynecology, between May 2021 and February 2022. It was approved by the ethics committee of Van Akdamar Hospital, Van, Turkey. The study included 20 pregnant patients with placenta previa and 20 healthy pregnant patients between 30 and 38 weeks gestational age.

The gestational ages of the pregnancies were determined by the last date of menstruation and/or ultrasonographic measurements. Blood samples and clinical data were obtained from the prenatal patient groups and compared. Placental samples from both the normal placenta and placenta previa groups were taken from under the connecting stem region and evaluated (Fig. 1).

### Histological analysis

For both groups, placental tissue samples (1 cm  $\times$  1 cm  $\times$  1 cm) were taken from around the umbilical cord under sterile conditions immediately after delivery and dissected. After soaking in 10% formol saline for at least 1 day, the samples were kept in 70% ethanol. The placental specimens were dehydrated in a routine ascending series of alcohol, cleared in terpineol, and then embedded in paraffin wax. For histological examination, 4–6- $\mu$ m thick transverse sections were obtained and stained with hematoxylin and eosin (H&E).

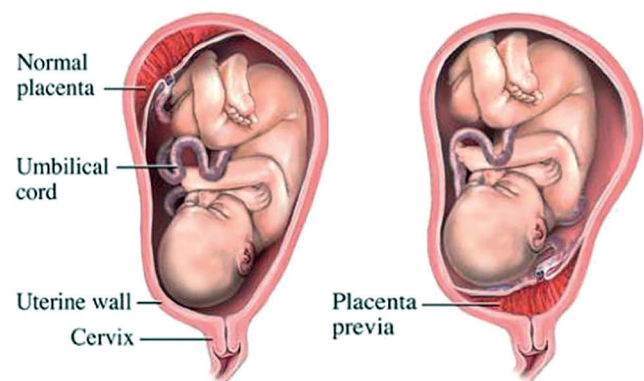


Fig. 1. Schematic diagram of the normal location of the placenta and of placenta previa

### Immunohistochemistry staining

The sections were left in distilled water and washed for 3–5 min in phosphate-buffered saline (PBS) (catalog No. 10010023; Thermo Fisher Scientific, Fremont, USA). Antigen uptake was performed in a microwave (700 W; Bosch®, Gerlingen, Germany) for 3 min at 90°C. For proteolysis, the sections were heated in a microwave oven at 700 W in a citrate buffer (pH 6) solution. The sections were washed for 3–5 min in PBS and incubated for 20 min in hydrogen peroxide (H<sub>2</sub>O<sub>2</sub>) (K-40677109, 64271; Merck, Darmstadt, Germany) (3 mL 30% H<sub>2</sub>O<sub>2</sub> + 27 mL methanol). The sections were then washed for 3–5 min in PBS and blocked for 8 min with Ultra V Block (lot: PHL150128; Thermo Fisher Scientific). After drainage, primary antibodies (NF- $\kappa$ B antibodies, mouse monoclonal antibodies (1/100) and VEGF antibodies) were applied. The sections were incubated and kept at 4°C overnight. Then, they were washed for 3–5 min in PBS and reincubated with applied secondary antibodies (Histostain-Plus Kit; Invitrogen, Carlsbad, USA) for 20 min. Next, the sections washed with PBS were exposed



to streptavidin peroxidase (lot: PHL150128; Thermo Fisher Scientific) for 20 min. The sections were washed for 3–5 min in PBS and treated with 3,3'-diaminobenzidine (DAB) (lot: HD36221; Thermo Fisher Scientific) for 3–10 min (it was kept for minimal and maximal times between 3 and 10 min depending on the intensity of expression). The slides showing the reaction were stopped in PBS. After counterstaining with Harris Haematoxylin for 45 s, the slides were dried with residual alcohol and cleaned in xylene. The slides were mounted with Entellan (Sigma-Aldrich, St. Louis, USA), and histopathological examinations were performed using an Olympus BH-2 light microscope (Olympus Corp., Tokyo, Japan). Semiquantitative scaling of immunoreactivity was carried out. The intensity of staining was graded from 0 to 4 (0 – no staining, 1 – faint staining, 2 – moderate staining, 3 – intense staining, and 4 – highly intense staining). The values of 0–2 were considered one group, and the values of 3–4 were considered the other group.

## Statistical analyses

The IBM SPSS Statistics for Windows v. 21.0 (IBM Corp., Armonk, USA) software was used for statistical analyses. Measured variables were presented as mean  $\pm$  standard deviation ( $M \pm SD$ ) and median (interquartile range (IQR)). Categorical variables were presented as numbers and percentages (%). The conformity of the data to normal distribution was analyzed using the Shapiro–Wilk test and Q–Q plots. The Student's *t*-test was used for normally distributed variables, the bootstrap test for means was used for not normally distributed variables, and the Welch's *t*-test was used when equal variances were not assumed to compare the control and placenta previa groups. The Fisher's exact test was used for the comparison of qualitative histologic parameter variables in the control and placenta previa groups. The hypotheses were taken in 2 directions, and  $p \leq 0.05$  was considered statistically significant.

## Results

### Histopathological examination

In the control group, the main root villi at cell junctions and syncytial cells in free villi were observed. Chromatin-rich nuclei were located in the cell center. Cytotrophoblast cells were oval in appearance, and the blood vessels in the villi were lined with squamous endothelial cells with regular lumens. There were a few syncytial nodes and bridges in the villi, and decidual cells with polygonal chromatin density were also observed polygonally (Fig. 2A).

In the placenta previa group, a notable degeneration and apoptotic changes in the syncytial cells of the root villi and an increase in syncytial nodes and bridges were observed. Excessive expansion and occlusion in blood vessels, hyperplastic endothelial cells, and thinning and degenerative

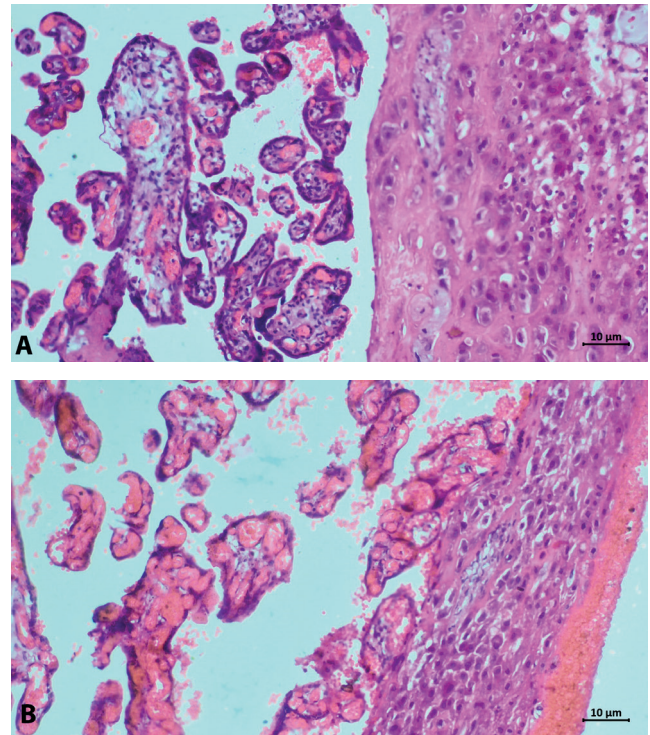


Fig. 2. A. Control group. Chromatin-rich nuclei of syncytial cells in the main stem villi. Cytotrophoblast cells are oval, blood vessels in the villi are composed of squamous endothelial cells with regular lumens, a few syncytial nodes and bridges in the villus, and decidual cells with polygonal chromatin density (hematoxylin and eosin (H&E) staining). B. Placenta previa group. Significant deterioration and apoptotic changes in root villus syncytial cells, increases in syncytial nodes and bridges, excessive expansion and occlusion of blood vessels, and hyperplastic endothelial cells (H&E staining)

differences in the connective tissue fibers of the villi were observed (Fig. 2B).

### Immunohistochemical examination of NF- $\kappa$ B expression

In the control group, the expression of NF- $\kappa$ B was mild in the syncytial cells of the root and free villi, and moderate in the vascular endothelial cells, macrophages and fibroblasts in the connective tissue cells (Fig. 3A).

In the placenta previa group, an increase in the NF- $\kappa$ B expression was observed in the large root villi in the connecting stem region and in the syncytial nodes and bridges of mature chorionic villi. The NF- $\kappa$ B protein expression was significantly positive in Hofbauer cells, endothelial cells and connective tissue cells located in small-scale blood vessels (Fig. 3B).

### Immunohistochemical examination of VEGF expression

In the control group, the expression of VEGF was moderate in the root villi and blood vessel endothelial cells, syncytial cells, as well as some Hofbauer cells outside the decidual area region (Fig. 3C).

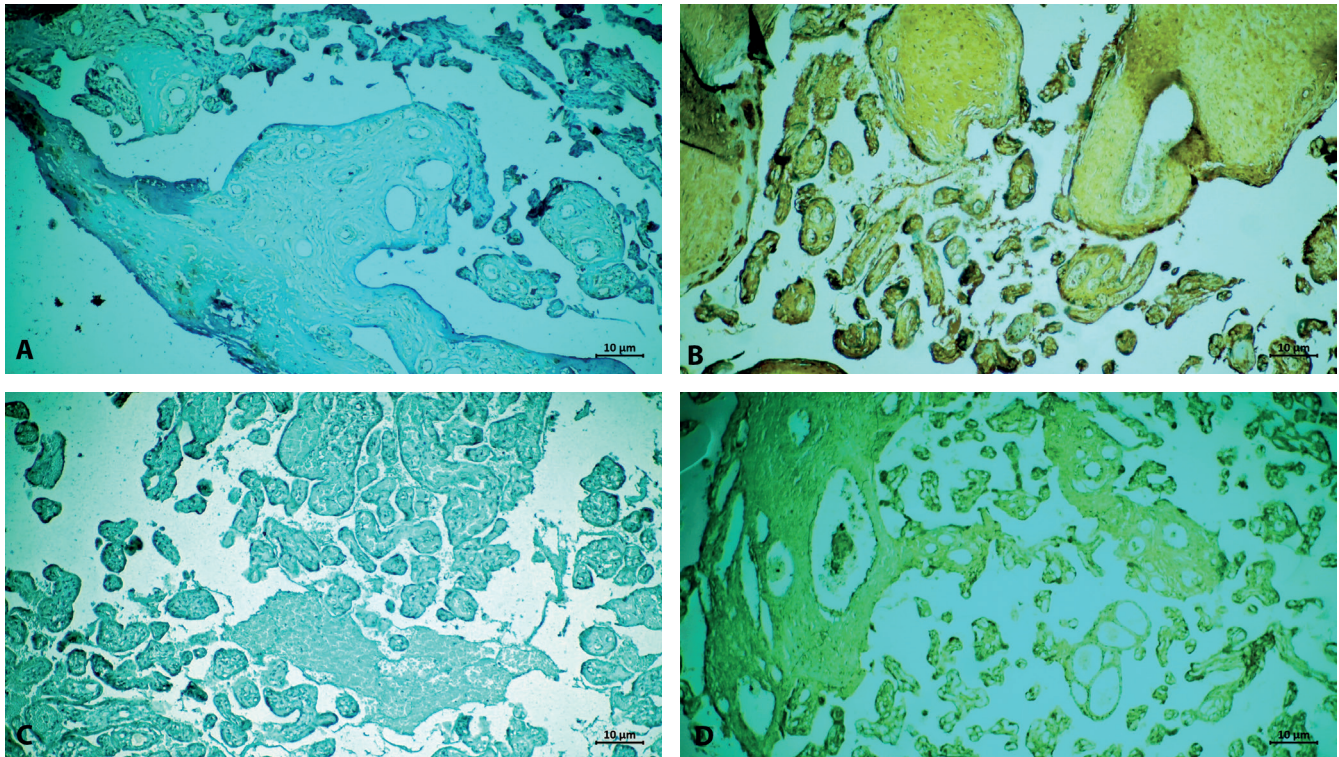


**Fig. 3.** A. Control group. Mild nuclear factor kappa-light-chain-enhancer of activated B cells (NF- $\kappa$ B) expression in syncytial cells in root and free villi, moderate NF- $\kappa$ B expression in vascular endothelial cells, macrophages, and fibroblast cells in connective tissue cells (NF- $\kappa$ B immunostaining). B. Placenta previa group. An increase in NF- $\kappa$ B expression was observed in the large root villi in the connecting stem region and in the syncytial nodes and bridges of the mature chorionic villi (NF- $\kappa$ B immunostaining). C. Control group. Vascular endothelial growth factor (VEGF) expression in root villi and blood vessel endothelial cells, syncytial cells and some Hofbauer cells outside the decidual cell area region (VEGF immunostaining). D. Placenta previa group. A remarkable increase in VEGF expression in the root villi, free villi, blood vessel endothelial cells, syncytial nodes and bridges, and Hofbauer cells (VEGF immunostaining)

In the placenta previa group, a significant increase in the VEGF expression was observed in the root villi, free villi, blood vessel endothelial cells, syncytial nodes and bridges, as well as Hofbauer cells (Fig. 3D).

In the transverse section of the stem villus in the control group, cytotrophoblast cell nuclei in the heterochromatin structure, membrane thickness and organelle structures were normal, as well as mitochondria and endoplasmic reticulum structures in the decidual cell cytoplasm. The nuclei of the blood vessel endothelial cells protruded toward the heterochromatin and lumen, and Hofbauer cells were seen in a regular structure outside. Basement membrane thicknesses were normal (Fig. 4A). In the placenta previa group, degenerative changes in cytotrophoblast cell nuclei were observed. The dilatation of endoplasmic reticulum structures in the cytoplasm, deterioration in the structure of mitochondrial cristae, and hyalinized areas in the villus connective tissue were observed (Fig. 4B).

## Statistical results

Statistical analysis of the parameters belonging to the control and placenta previa patients is shown in Table 1,2. The mean differences between the control and placenta previa patients were statistically significant for the parameters of epithelial thickness in villi, diameter

of floating small villi, diameter of blood vessels in villi, diameter of decidual cells, syncytial knots, congestion in blood vessels, fibrinoid accumulation, inflammation, degeneration in decidual cells, VEGF and NF- $\kappa$ B expression, maternal age, gravida, parity, and gestational age. Differences in significance levels between parameters are provided in detail in Table 1,2.

The diameters of floating small villi, epithelial thickness in villi, diameter of blood vessels in villi, diameter of decidual cells, parity, gestational age, age, and gravida values of both groups are also given as a boxplot (Fig. 5).

## Discussion

It has been reported that inflammation is triggered by placental malformations, differentiation of the uterine endometrium and significant scarring in the uterus due to surgical approaches or other gynecological operations.<sup>15</sup> It is known that the presence of scar tissue can lead to the development of inflammation in epithelial tissue, as well as vascular insufficiency in the cells of the placenta, such that the tissues cannot benefit from oxygen sufficiently.<sup>30</sup> Inflammatory factors initiate the morphology of the uterine spiral vessels. In the lower segment of the uterus, the presence of pelvic adhesions causes atypical blastocyst



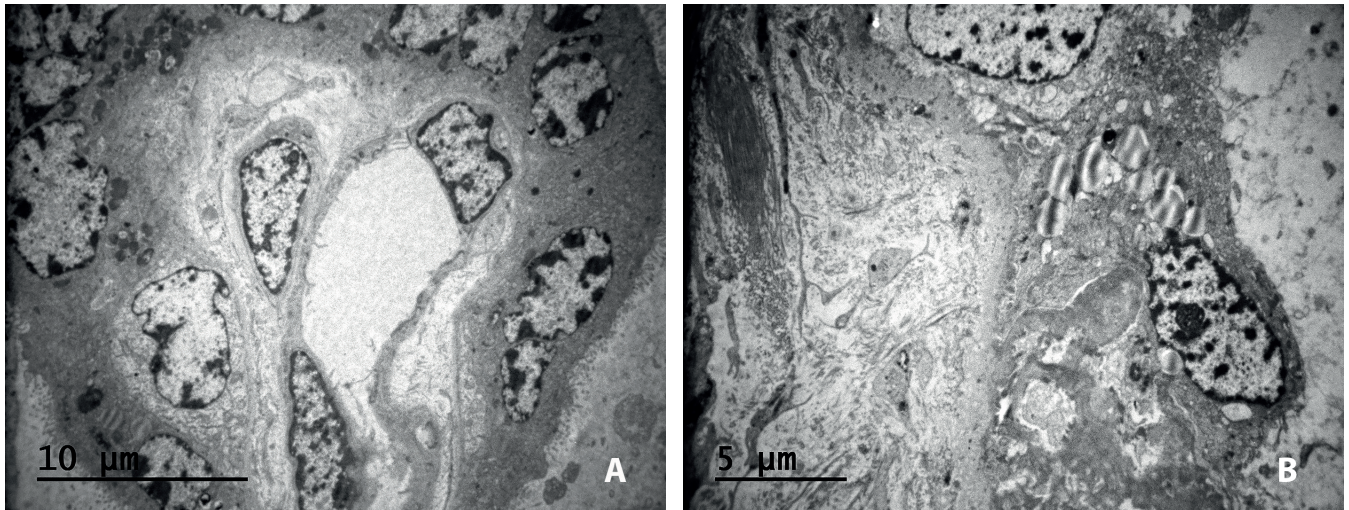


Fig. 4. A. Control group. Cytotrophoblast cell nuclei, membrane thickness, organelle structures, heterochromatin structure in stem villus, and mitochondria and endoplasmic reticulum structures in decidua cell cytoplasm were normal (uranyl acetate and lead citrate staining). B. Placenta previa group. Degenerative changes in cytotrophoblast cell nuclei, dilatation in endoplasmic reticulum structures in the cytoplasm, disruption in mitochondrial cristae structure, and hyalinized areas in villus connective tissue (uranyl acetate and lead citrate staining)

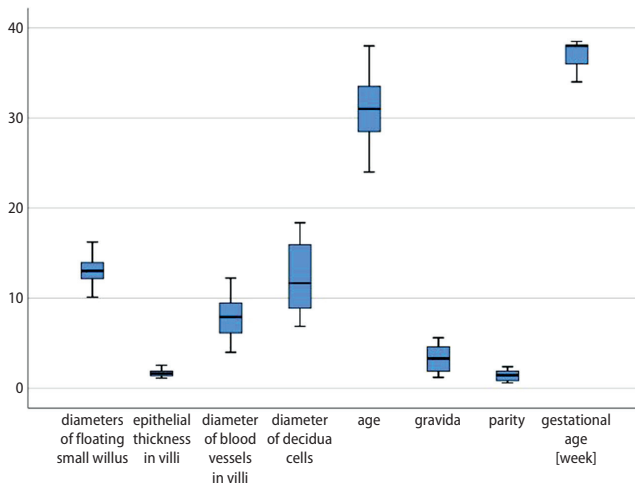


Fig. 5. Boxplot of the parameters of both groups

implantation and dysperistalsis of uterine contraction to form placenta previa.<sup>31</sup> Trophoblast cell infiltration and molecular regulation of placental angiogenesis play an important role in the molecular mechanisms underlying placenta previa.

The NF- $\kappa$ B has been shown to regulate many genes involved in important cellular responses, such as inflammation, migration, proliferation, and apoptosis. It has been noted that the early cytoplasmic events leading to the release and translocation of NF- $\kappa$ B are insufficient to explain the complex nature of NF- $\kappa$ B biology.<sup>32,33</sup> The NF- $\kappa$ B protein expression is also manifested in other diseases characterized by high oxidative stress and inflammatory factors, such as acquired immunodeficiency syndrome (AIDS), atherosclerosis, rheumatoid arthritis, osteoporosis, Alzheimer's disease, and ischemia/reperfusion injury.<sup>34</sup> In another clinical study, Atic and Devenci

stated that endothelin-1 expression induced NF- $\kappa$ B levels in macrophage cells in the development of diabetic foot ulcers.<sup>35</sup>

It has been reported that NF- $\kappa$ B protein expression is lower in normal placentas compared to preeclamptic placentas. Also, the relationship between NF- $\kappa$ B expression and leukocytes and vascular tissue has been demonstrated, especially in preeclampsia.<sup>7,36,37</sup> Another studies determined that an increase in the expression of NF- $\kappa$ B protein in the placenta can change the expression of different genes in preeclampsia and contribute to the pathogenesis of the disease. The activation of placental NF- $\kappa$ B in preeclampsia supports this observation, as it increases placental TNF- $\alpha$ , cyclooxygenase-2 and thromboxane levels.<sup>38,39</sup> Li et al. used quantitative PCR, western blot and immunofluorescence techniques to study the placental tissue of patients with diabetes mellitus and autophagy. They reported that women with gestational diabetes mellitus have an increased risk of neonatal infection through placental inflammation and autophagy. According to their quantitative PCR results, due to gestational diabetes mellitus, hypoxia-inducible factor-1 $\alpha$  and the TLR4/myeloid differential protein-88/NF- $\kappa$ B pathway increase protein expression levels. In western blot results, they reported that NF- $\kappa$ B inhibitor alpha and NF- $\kappa$ B P65 expression in the placenta significantly increased due to gestational diabetes mellitus.<sup>40</sup> Similarly, insulin resistance was investigated to understand morphological changes in gestational diabetes mellitus. The TLR4/ myeloid differential protein-88/NF- $\kappa$ B pathway can play an important role in the emergence of insulin resistance in the placentas of pregnant women with gestational diabetes mellitus.<sup>41</sup> The TLR4/myeloid differential protein-88/NF- $\kappa$ B pathway has been examined in other experimental studies. It has been reported that these protein expressions are

**Table 1.** Comparison of morphometric measurement values of the control group and placenta previa patients

Histologic parameters	Group	n	M ±SD	Median (IQR)	p-value
Diameters of floating small villus [µm]	1	20	13.93 ±1.13	13.34 (1.81)	0.001 <sup>b</sup>
	2	20	12.16 ±1.22	12.18 (4.39)	
Epithelial thickness in villi [µm]	1	20	1.56 ±0.29	1.54 (0.39)	0.034 <sup>a</sup>
	2	20	1.80 ±0.40	1.76 (0.46)	
Diameter of blood vessels in villi [µm]	1	20	9.84 ±0.92	9.45 (0.57)	0.001 <sup>b</sup>
	2	20	6.02 ±0.74	6.15 (0.57)	
Parity	1	20	0.94 ±0.27	0.85 (0.40)	0.001 <sup>b</sup>
	2	20	1.90 ±0.25	1.90 (0.40)	
Gestational age [weeks]	1	20	38.19 ±0.16	38.10 (0.17)	0.001 <sup>c</sup>
	2	20	35.80 ±1.40	36.00 (2.75)	
Diameter of decidual cells [µm]	1	20	15.57 ±1.28	15.93 (1.65)	<0.001 <sup>a</sup>
	2	20	8.89 ±1.05	8.90 (1.87)	
Age [years]	1	20	29.10 ±2.77	30.00 (4.50)	0.001 <sup>b</sup>
	2	20	33.00 ±2.96	33.00 (4.50)	
Gravida	1	20	1.91 ±0.39	1.90 (0.63)	<0.001 <sup>a</sup>
	2	20	4.69 ±0.42	4.60 (0.67)	

1 – control group; 2 – placenta previa group; M ±SD – mean ± standard deviation; IQR – interquartile range; <sup>a</sup> Student’s t-test; <sup>b</sup> Bootstrap test for means; <sup>c</sup> Welch-corrected variant of t-test.

**Table 2.** Comparison of morphometric, clinical and immunohistochemical measurement values of the control group and placenta previa patients (Fisher’s exact test)

Histologic parameters	Groups		p-value	
	1, n (%)	2, n (%)		
Syncytial knot	no staining + faint staining + moderate staining	20 (90.9)	2 (9.1)	<0.001
	intense staining + high intense staining	0 (0.0)	18 (100.0)	
Congestion in blood vessels	no staining + faint staining + moderate staining	20 (90.9)	2 (9.1)	<0.001
	intense staining + high intense staining	0 (0.0)	18 (100.0)	
Fibrinoid accumulation	no staining + faint staining + moderate staining	20 (90.9)	2 (9.1)	<0.001
	intense staining + high intense staining	0 (0.0)	18 (100.0)	
Inflammation	no staining + faint staining + moderate staining	20 (87.0)	3 (13.0)	<0.001
	intense staining + high intense staining	0 (0.0)	17 (100.0)	
Degeneration in decidual cells	no staining + faint staining + moderate staining	20 (87.0)	3 (13.0)	<0.001
	intense staining + high intense staining	0 (0.0)	17 (100.0)	
VEGF	no staining + faint staining + moderate staining	20 (95.2)	1 (4.8)	<0.001
	intense staining + high intense staining	0 (0.0)	19 (100.0)	
PSTAT-3	no staining + faint staining + moderate staining	20 (100.0)	0 (0.0)	<0.001
	intense staining + high intense staining	0 (0.0)	20 (100.0)	

1 – control group; 2 – placenta previa group; VEGF – vascular endothelial growth factor; PSTAT-3 – phosphorylated signal transducer and activator of transcription 3.

significantly increased in experimental animals due to diabetes mellitus.<sup>42–44</sup> High-mobility group box 1, receptors for advanced glycation end products (AGEs), and the NF-κB p65 pathway, which are genes related to mRNA levels, were analyzed with PCR in 61 normotensive pregnant women and 64 women with severe preeclampsia. In the comparison between the 2 groups, the mRNA levels of high-mobility group box 1, receptors for AGEs, and NF-κB p65 were higher in the severe preeclamptic placentas.<sup>45</sup>

In this study, it was observed that NF-κB protein expression was prominent in the connective root region of placenta previa and in the large root villi in the syncytial nodes and bridges of mature chorionic villi. There was also a significant increase in the NF-κB protein expression in Hofbauer cells, endothelial cells and connective tissue cells located in small-scale blood vessels (Fig. 3B). We determined that the increase in cytokine signaling that developed after the increased inflammatory

reaction may be due to an increase in the inductive effect of macrophages.

Chantraine et al. compared the total area occupied by vessels in normal and placenta-increta placental beds. They reported that the vessels in placenta increta were significantly less frequent and larger. They stated that the vascular location is more heterogeneous, especially in placenta increta.<sup>46</sup> Another study investigated the effects of maternal serum levels of VEGF, placental growth factor and soluble fms-like tyrosine kinase 1 on patients with and without complete placenta previa. According to the study findings, there was a decrease in the serum level of VEGF but an increase in the tissue level in the placenta. As a result of electrophoresis performed in placenta previa, VEGF level increased.<sup>25,47</sup> It has been reported that VEGF, which increases in response to placental hypoxia, is not functional during the pathogenesis of preeclampsia. Moreover, since the ligand-receptor binding is impaired, the amount of free VEGF in the preeclamptic placenta increases, impairing vascular function as a result of endothelial cell damage.<sup>48</sup> A significant increase in VEGF expression was observed in the root villi, free villi, blood vessel endothelial cells, syncytial nodes and bridges, and Hofbauer cells due to the hypoxia effect after placenta previa.

It has been stated that cytotrophoblast cell degeneration can be explained by placental ischemia and that other etiological factors are not important. According to the histopathological findings of our study, there was a significant decrease in the transfer and synthetic activity of trophoblasts. Cellular respiration was also affected.<sup>49</sup> Thickening of the basal lamina, increase in intervillous collagen and marked differentiation in mitochondrial structure were noted, with great damage to the multinucleated protoplasm masses, which lost their cell membranes under hypoxic conditions and became single cells. Significant degenerative changes in cytotrophoblast cell nuclei were observed in the placenta previa group in our study. Dilatation in endoplasmic reticulum structures in the cytoplasm, deterioration in the mitochondrial cristae structure and the appearance of hyalinized areas in the villus connective tissue were evaluated as negative images for cell and villus integrity disruption and trophoblast invasion, as well as for angiogenesis (Fig. 4B). Faraji et al. evaluated maternal characteristics, VEGF and placental growth factor in the placenta accreta spectrum. The placental growth factor serum level was found to be statistically significantly higher in the placenta accreta spectrum and placenta accreta spectrum subgroups compared to the normal placenta group. They also stated that the previa status of the placenta accreta spectrum patients did not affect serum levels of VEGF and placental growth factor.<sup>50</sup> Faraji et al. also stated that insufficient VEGF secretion and invasion of interstitial extravillous trophoblasts to a metastable cell phenotype and advanced myometrial invasion causes placenta previa. In a study of VEGF and phosphotyrosine immunostaining, it was

reported that epithelial–mesenchymal invasion, especially the expression of vimentin and cytokeratin-7, was predominant in extravillous trophoblasts.<sup>47</sup> Biberoglu et al. compared abnormal and normal placentation and data in terms of fms-like tyrosine kinase 1 and VEGF. They did not find a statistically significant result in maternal serum values of fms-like tyrosine kinase 1, placental growth factor, fms-like tyrosine kinase 1/placental growth factor ratio, and VEGF in the abnormal placenta groups.<sup>51</sup> However, another study reported that amniotic fluid VEGF and leptin levels were the highest in women with placenta previa and the lowest in women with intrauterine growth retardation and pregnancy-induced hypertension.<sup>27</sup>

## Limitations


The 2 main limitations are that the study focused on a relatively small group, and it was composed only of Turkish women. The NF- $\kappa$ B and VEGF signaling pathways were not detected at serum level. Examination at tissue levels was performed at immunohistochemistry and ultrastructural level. More extensive research is needed for a greater understanding of this phenomenon.


## Conclusions

Vascular endothelial growth factor was found to stimulate endothelial cell proliferation and migration and significantly affect angiogenesis during the developmental process of the placenta and remodeling of the uterine vessels. Imbalances in VEGF can lead to aberrant placental vascular development. We determined that VEGF affects trophoblastic invasion by increasing NF- $\kappa$ B signaling as a result of hypoxia occurring after placenta previa and induces apoptotic development, which is critically important during cytotrophoblastic invasion in the vascularization of the placenta.

## ORCID iDs

Çağdaş Özgökçe  <https://orcid.org/0000-0003-4960-4625>

Aydın Öcal  <https://orcid.org/0000-0002-6027-1094>

Işıl Sezen Ermiş  <https://orcid.org/0000-0002-9714-4670>

## References

1. Ahmed SR. Major placenta previa: Rate, maternal and neonatal outcomes experience at a tertiary maternity hospital, Sohag, Egypt. A prospective study. *J Clin Diagn Res.* 2015;9(11):QC17–QC19. doi:10.7860/JCDR/2014/14930.6831
2. Jauniaux E, Alfirevic Z, Bhide A, et al. Placenta praevia and placenta accreta: Diagnosis and management. Green-Top Guideline No. 27a. *BJOG.* 2019;126(1):e1–e48. doi:10.1111/1471-0528.15306
3. Silver RM. Abnormal placentation: Placenta previa, vasa previa, and placenta accreta. *Obstet Gynecol.* 2015;126(3):654–668. doi:10.1097/AOG.0000000000001005
4. Sheiner E, Shoham-Vardi I, Hallak M, Hershkowitz R, Katz M, Mazor M. Placenta previa: Obstetric risk factors and pregnancy outcome. *J Matern Fetal Neonatal Med.* 2001;10(6):414–419. doi:10.1080/jmf.10.6.414.419
5. Rosenberg T, Pariente G, Sergienko R, Wiznitzer A, Sheiner E. Critical analysis of risk factors and outcome of placenta previa. *Arch Gynecol Obstet.* 2011;284(1):47–51. doi:10.1007/s00404-010-1598-7



6. Yang L, Liu CC, Zheng H, et al. LRP1 modulates the microglial immune response via regulation of JNK and NF- $\kappa$ B signaling pathways. *J Neuroinflammation*. 2016;13(1):304. doi:10.1186/s12974-016-0772-7
7. Tak PP, Firestein GS. NF- $\kappa$ B: A key role in inflammatory diseases. *J Clin Invest*. 2001;107(1):7–11. doi:10.1172/JCI11830
8. Ariyakumar G, Morris JM, McKelvey KJ, Ashton AW, McCracken SA. NF- $\kappa$ B regulation in maternal immunity during normal and IUGR pregnancies. *Sci Rep*. 2021;11(1):20971. doi:10.1038/s41598-021-00430-3
9. Luo H, Li G, Wang B, et al. Pel1 signaling blockade attenuates congenital zika syndrome. *PLoS Pathog*. 2020;16(6):e1008538. doi:10.1371/journal.ppat.1008538
10. Olmos-Ortiz A, Déciga-García M, Preciado-Martínez E, et al. Prolactin decreases LPS-induced inflammatory cytokines by inhibiting TLR-4/NF $\kappa$ B signaling in the human placenta. *Mol Hum Reprod*. 2019;25(10):660–667. doi:10.1093/molehr/gaz038
11. Johnson LJ, Azari S, Webb A, et al. Human placental trophoblasts infected by *Listeria monocytogenes* undergo a pro-inflammatory switch associated with poor pregnancy outcomes. *Front Immunol*. 2021;12:709466. doi:10.3389/fimmu.2021.709466
12. Yang X, Haghiac M, Glazebrook P, Minium J, Catalano PM, Hauguel-de Mouzon S. Saturated fatty acids enhance TLR4 immune pathways in human trophoblasts. *Hum Reprod*. 2015;30(9):2152–2159. doi:10.1093/humrep/dev173
13. Li M, Piao L, Chen CP, et al. Modulation of decidual macrophage polarization by macrophage colony-stimulating factor derived from first-trimester decidual cells. *Am J Pathol*. 2016;186(5):1258–1266. doi:10.1016/j.ajpath.2015.12.021
14. Li L, Zhang J, Gao H, Ma Y. Nestin is highly expressed in foetal spinal cord isolated from placenta previa patients and promotes inflammation by enhancing NF- $\kappa$ B activity. *Biomarkers*. 2018;23(6):597–602. doi:10.1080/1354750X.2018.1468824
15. Japan Environment and Children's Study Group, Tsuji M, Shibata E, et al. Associations between metal concentrations in whole blood and placenta previa and placenta accreta: The Japan Environment and Children's Study (JECS). *Environ Health Prev Med*. 2019;24(1):40. doi:10.1186/s12199-019-0795-7
16. Umapathy A, Chamley LW, James JL. Reconciling the distinct roles of angiogenic/anti-angiogenic factors in the placenta and maternal circulation of normal and pathological pregnancies. *Angiogenesis*. 2020;23(2):105–117. doi:10.1007/s10456-019-09694-w
17. Chehroudi C, Kim H, Wright TE, Collier AC. Dysregulation of inflammatory cytokines and inhibition of VEGFA in the human umbilical cord are associated with negative pregnancy outcomes. *Placenta*. 2019;87:16–22. doi:10.1016/j.placenta.2019.09.002
18. Crespo-García S, Corkhill C, Roubéix C, et al. Inhibition of placenta growth factor reduces subretinal mononuclear phagocyte accumulation in choroidal neovascularization. *Invest Ophthalmol Vis Sci*. 2017;58(12):4997. doi:10.1167/iovs.16-21283
19. Bhavina K, Radhika J, Pandian SS. VEGF and eNOS expression in umbilical cord from pregnancy complicated by hypertensive disorder with different severity. *BioMed Res Int*. 2014;2014:982159. doi:10.1155/2014/982159
20. Almasry SM, Elfayomy AK, Hashem HE. Ultrastructure and histomorphometric analysis of human umbilical cord vessels in preeclampsia: A potential role of VEGF, VEGFR-1 and VEGFR-2. *Rom J Morphol Embryol*. 2016;57(2 Suppl):681–689. PMID:27833959.
21. Krukier II, Pogorelova TN. Production of vascular endothelial growth factor and endothelin in the placenta and umbilical cord during normal and complicated pregnancy. *Bull Exp Biol Med*. 2006;141(2):216–218. doi:10.1007/s10517-006-0131-2
22. Kaukola T, Räsänen J, Herva R, Patel DD, Hallman M. Suboptimal neurodevelopment in very preterm infants is related to fetal cardiovascular compromise in placental insufficiency. *Am J Obstet Gynecol*. 2005;193(2):414–420. doi:10.1016/j.ajog.2004.12.005
23. Knflier M. Critical growth factors and signalling pathways controlling human trophoblast invasion. *Int J Dev Biol*. 2010;54(2–3):269–280. doi:10.1387/ijdb.082769mk
24. Vasilopoulou E, Loubière LS, Lash GE, et al. Triiodothyronine regulates angiogenic growth factor and cytokine secretion by isolated human decidual cells in a cell-type specific and gestational age-dependent manner. *Hum Reprod*. 2014;29(6):1161–1172. doi:10.1093/humrep/deu046
25. Wang N, Shi D, Li N, Qi H. Clinical value of serum VEGF and sFlt-1 in pernicious placenta previa. *Ann Med*. 2021;53(1):2041–2049. doi:10.1080/07853890.2021.1999492
26. Xie H, Qiao P, Lu Y, et al. Increased expression of high mobility group box protein 1 and vascular endothelial growth factor in placenta previa. *Mol Med Rep*. 2017;16(6):9051–9059. doi:10.3892/mmr.2017.7682
27. Hong SN, Joo BS, Chun S, Kim A, Kim HY. Prediction of preterm delivery using levels of vascular endothelial growth factor and leptin in amniotic fluid from the second trimester. *Arch Gynecol Obstet*. 2015;291(2):265–271. doi:10.1007/s00404-014-3439-6
28. Coultas L, Chawengsaksophak K, Rossant J. Endothelial cells and VEGF in vascular development. *Nature*. 2005;438(7070):937–945. doi:10.1038/nature04479
29. Byrd N, Becker S, Maye P, et al. Hedgehog is required for murine yolk sac angiogenesis. *Development*. 2002;129(2):361–372. doi:10.1242/dev.129.2.361
30. Ratiu AC, Crisan DC. A prospective evaluation and management of different types of placenta praevia using parallel vertical compression suture to preserve uterus. *Medicine (Baltimore)*. 2018;97(46):e13253. doi:10.1097/MD.00000000000013253
31. Gasparri ML, Nirgianakis K, Taghavi K, Papadia A, Mueller MD. Placenta previa and placental abruption after assisted reproductive technology in patients with endometriosis: A systematic review and meta-analysis. *Arch Gynecol Obstet*. 2018;298(1):27–34. doi:10.1007/s00404-018-4765-x
32. Basith S, Manavalan B, Gosu V, Choi S. Evolutionary, structural and functional interplay of the I $\kappa$ B family members. *PLoS One*. 2013;8(1):e54178. doi:10.1371/journal.pone.0054178
33. Lawrence T. The nuclear factor NF- $\kappa$ B pathway in inflammation. *Cold Spring Harb Perspect Biol*. 2009;1(6):a001651. doi:10.1101/cshperspect.a001651
34. Ahn KS. Transcription factor NF- $\kappa$ B: A sensor for smoke and stress signals. *Ann N Y Acad Sci*. 2005;1056(1):218–233. doi:10.1196/annals.1352.026
35. Atic R, Deveci E. Endothelin 1, NF- $\kappa$ B, and ADAM-15 expression in diabetic foot wounds. *Bratisl Med J*. 2019;120(1):58–64. doi:10.4149/BLM\_2019\_009
36. Luppi P, Tse H, Lain KY, Markovic N, Piganelli JD, DeLoia JA. Preeclampsia activates circulating immune cells with engagement of the NF- $\kappa$ B pathway. *Am J Reprod Immunol*. 2006;56(2):135–144. doi:10.1111/j.1600-0897.2006.00386.x
37. Takacs P, Kauma SW, Sholley MM, Walsh SW, Dinsmoor MJ, Green K. Increased circulating lipid peroxides in severe preeclampsia activate NF- $\kappa$ B and upregulate ICAM-1 in vascular endothelial cells. *FASEB J*. 2001;15(2):279–281. doi:10.1096/fj.00-0549fje
38. Vaughan JE, Walsh SW. Activation of NF- $\kappa$ B in placentas of women with preeclampsia. *Hypertens Pregnancy*. 2012;31(2):243–251. doi:10.3109/10641955.2011.642436
39. Shah TJ, Walsh SW. Activation of NF- $\kappa$ B and expression of COX-2 in association with neutrophil infiltration in systemic vascular tissue of women with preeclampsia. *Am J Obstet Gynecol*. 2007;196(1):48.e1–48.e8. doi:10.1016/j.ajog.2006.08.038
40. Li YX, Long DL, Liu J, et al. Gestational diabetes mellitus in women increased the risk of neonatal infection via inflammation and autophagy in the placenta. *Medicine (Baltimore)*. 2020;99(40):e22152. doi:10.1097/MD.00000000000022152
41. Feng H, Su R, Song Y, et al. Positive correlation between enhanced expression of TLR4/MyD88/NF- $\kappa$ B with insulin resistance in placentae of gestational diabetes mellitus. *PLoS One*. 2016;11(6):e0157185. doi:10.1371/journal.pone.0157185
42. Shen Z, Yang C, Zhu P, Tian C, Liang A. Protective effects of syringin against oxidative stress and inflammation in diabetic pregnant rats via TLR4/MyD88/NF- $\kappa$ B signaling pathway. *Biomed Pharmacother*. 2020;131:110681. doi:10.1016/j.biopha.2020.110681
43. Yao J, Li Y, Jin Y, Chen Y, Tian L, He W. Synergistic cardioprotection by tilianin and syringin in diabetic cardiomyopathy involves interaction of TLR4/NF- $\kappa$ B/NLRP3 and PGC1 $\alpha$ /SIRT3 pathways. *Int Immunopharmacol*. 2021;96:107728. doi:10.1016/j.intimp.2021.107728
44. Liu T, Zheng W, Wang L, Wang L, Zhang Y. TLR4/NF- $\kappa$ B signaling pathway participates in the protective effects of apocynin on gestational diabetes mellitus induced placental oxidative stress and inflammation. *Reprod Sci*. 2020;27(2):722–730. doi:10.1007/s43032-019-00078-5

45. Zhu L, Zhang Z, Zhang L, et al. HMGB1–RAGE signaling pathway in severe preeclampsia. *Placenta*. 2015;36(10):1148–1152. doi:10.1016/j.placenta.2015.08.006
46. Chantraine F, Blacher S, Berndt S, et al. Abnormal vascular architecture at the placental-maternal interface in placenta increta. *Am J Obstet Gynecol*. 2012;207(3):188.e1–188.e9. doi:10.1016/j.ajog.2012.06.083
47. Wehrum MJ, Buhimschi IA, Salafia C, et al. Accreta complicating complete placenta previa is characterized by reduced systemic levels of vascular endothelial growth factor and by epithelial-to-mesenchymal transition of the invasive trophoblast. *Am J Obstet Gynecol*. 2011;204(5):411.e1–411.e11. doi:10.1016/j.ajog.2010.12.027
48. İrtegün S, Ağaçayak E, Deveci E. Examining the expression level of VEGF and vimentin by immunohistochemistry and western blot in preeclamptic and normotensive placentas [in Turkish]. *Dicle Med J*. 2016;43(3):400–405. [http://www.diclemedj.org/ozet.php?makale\\_id=2976&dil=en](http://www.diclemedj.org/ozet.php?makale_id=2976&dil=en)
49. Jones CJP, Fox H. An ultrastructural and ultrahistochemical study of the human placenta in maternal pre-eclampsia. *Placenta*. 1980;1(1):61–76. doi:10.1016/S0143-4004(80)80016-6
50. Faraji A, Akbarzadeh-Jahromi M, Bahrami S, et al. Predictive value of vascular endothelial growth factor and placenta growth factor for placenta accreta spectrum. *J Obstet Gynaecol*. 2022;42(5):900–905. doi:10.1080/01443615.2021.1955337
51. Biberoglu E, Kirbas A, Daglar K, et al. Serum angiogenic profile in abnormal placentation. *J Matern Fetal Neonatal Med*. 2016;29(19):3193–3197. doi:10.3109/14767058.2015.1118044



# Type 3 innate lymphoid cells as an indicator of renal dysfunction and serum uric acid in hyperuricemia

Zan-Xiong Chen<sup>1,C-F</sup>, Hong-Qian Liu<sup>2,B,C,F</sup>, Zhen-Hua Wu<sup>3,C,D,F</sup>, Jun-Lian He<sup>2,E,F</sup>, Hao-Jie Zhong<sup>2,4,A,C-F</sup>

<sup>1</sup> Hospital Office, Maoming People's Hospital, China

<sup>2</sup> Department of Gastroenterology, The First Affiliated Hospital of Guangdong Pharmaceutical University, China

<sup>3</sup> Department of Gastroenterology, Maoming People's Hospital, China

<sup>4</sup> School of Biology and Biological Engineering, South China University of Technology, Guangzhou, China

A – research concept and design; B – collection and/or assembly of data; C – data analysis and interpretation;

D – writing the article; E – critical revision of the article; F – final approval of the article

Advances in Clinical and Experimental Medicine, ISSN 1899–5276 (print), ISSN 2451–2680 (online)

*Adv Clin Exp Med.* 2023;32(3):307–313

## Address for correspondence

Hao-Jie Zhong

E-mail: jaxzhong@126.com

## Funding sources

This study was supported by the China Postdoctoral Science Foundation (grant No. 2021M700034) and High-level Hospital Construction Research Project of Maoming People's Hospital, China.

## Conflict of interest

None declared

Received on May 26, 2022

Reviewed on July 10, 2022

Accepted on September 15, 2022

Published online on October 17, 2022

## Abstract

**Background.** Type 3 innate lymphoid cells (ILC3s) are a newly identified group of innate immune cells that participate in the progression of several metabolic diseases by secreting interleukin (IL)-17 and IL-22. These cytokines are associated with hyperuricemia (HUA) severity and development; however, the relationship between ILC3s and HUA remains unclear.

**Objectives.** To determine the characteristics of circulating ILC3s in patients with HUA.

**Materials and methods.** Type 3 innate lymphoid cells and their subsets were detected using flow cytometry in peripheral blood mononuclear cells (PBMCs) of 80 HUA patients and 30 healthy controls (HC). Plasma levels of IL-17A and IL-22 were measured with enzyme-linked immunosorbent assay (ELISA). Clinical data of enrolled subjects were collected from electronic medical records.

**Results.** In patients with HUA, the frequency of circulating ILC3s was elevated and positively correlated with levels of serum uric acid and serum creatinine (Scr). Although there was no significant difference in the plasma concentration of IL-17A between the patients with HUA and healthy controls, positive correlations between plasma IL-17A and the concentration of serum uric acid and frequency of circulating ILC3s were observed in the patients with HUA.

**Conclusions.** In patients with HUA, positive correlations were detected between circulating ILC3 levels, plasma IL-17A and serum uric acid. Therefore, ILC3s and IL-17A may be useful indicators of disease severity, and are potential new therapeutic targets in HUA.

**Key words:** uric acid, innate immunity, interleukin-17, creatinine, hyperuricemia

## Cite as

Chen ZX, Liu HQ, Wu ZH, He JL, Zhong HJ. Type 3 innate lymphoid cells as an indicator of renal dysfunction and serum uric acid in hyperuricemia. *Adv Clin Exp Med.* 2023;32(3):307–313. doi:10.17219/acem/154625

## DOI

10.17219/acem/154625

## Copyright

Copyright by Author(s)

This is an article distributed under the terms of the Creative Commons Attribution 3.0 Unported (CC BY 3.0) (<https://creativecommons.org/licenses/by/3.0/>)

## Background

Hyperuricemia (HUA) is a prerequisite for the development of gout,<sup>1</sup> the most prevalent form of inflammatory arthritis,<sup>2,3</sup> and is primarily caused by impaired urate excretion.<sup>4</sup> Although the reported prevalence of HUA in the Chinese population has increased to 13.3% and is gradually rising,<sup>5</sup> factors accounting for the pathogenesis and development of HUA are not fully understood.

As the kidney is the major organ that mediates uric acid (UA) excretion, HUA in humans is closely associated with kidney damage and kidney diseases.<sup>6</sup> Furthermore, emerging evidence has highlighted the role of the intestine in HUA and gout development.<sup>7,8</sup> The gut is responsible for 1/3 of total UA excretion,<sup>9</sup> with HUA patients and murine models of the condition often exhibiting intestinal microbiota dysbiosis and barrier dysfunction, both of which contribute to the progression of HUA.<sup>10,11</sup> The studies highlighted above indicate that factors involved in maintaining homeostasis of the intestine might affect the excretion of UA.

A newly defined group of innate immune cells expressing the retinoic acid receptor-related orphan nuclear receptor gamma transcription factor, called type 3 innate lymphoid cells (ILC3s), are thought to play an important role in mucosal immunity.<sup>12</sup> They were identified as abundant in the intestinal mucosa and are associated with gut microbiota tolerance and intestinal barrier integrity.<sup>12,13</sup> Additionally, similar to T helper 17 cells, ILC3s produce a variety of distinct cytokines, including interleukin (IL)-17 and IL-22, that are associated with HUA severity and development.<sup>14,15</sup> Nonetheless, the association between HUA and ILC3s remains unclear.

## Objectives

This study aimed to determine the characteristics of circulating ILC3s in patients with HUA, and to explore whether or not the proportion of circulating ILC3s and the concentration of ILC3-related cytokines (IL-17A and IL-22) correlate with disease severity.

## Materials and methods

### Subjects

In this cross-sectional study, adult patients with HUA and healthy controls (HC) were recruited from the First Affiliated Hospital of Guangdong Pharmaceutical University, China, between September 2020 and August 2021. Hyperuricemia was defined as a serum UA  $\geq 420 \mu\text{mol/L}$  (7.0 mg/dL) in men and  $\geq 360 \mu\text{mol/L}$  (6.0 mg/dL) in women.<sup>16</sup> Patients suffering from carcinoma and intestinal diseases (such as Crohn's disease and ulcerative colitis) were excluded. Demographic data and UA-associated parameters

(serum UA, serum creatinine (Scr) and blood urea nitrogen (BUN)) were collected from electronic medical records. This study was approved by the Ethics Committee of the First Affiliated Hospital of Guangdong Pharmaceutical University, China (approval No. 2021146). Informed consent was obtained from each patient.

### Separation of peripheral blood mononuclear cells and plasma

Morning fasting blood samples were collected from each subject using a heparin anticoagulant tube (Huabo Medical Instrument Co. Ltd., Heze, China) to isolate peripheral blood mononuclear cells (PBMCs) and plasma. Peripheral blood mononuclear cells were obtained using density gradient centrifugation (Ficoll-Paque™ PLUS; GE Healthcare, Chicago, USA) (400 × g, 30 min, room temperature). Plasma was isolated by centrifugation of whole blood (800 × g, 20 min, room temperature) and stored at  $-80^\circ\text{C}$  for further use in enzyme-linked immunosorbent assay (ELISA).

### Flow cytometry

Peripheral blood mononuclear cells were stained using the following antibodies: anti-CD3-FITC (clone: HIT3a), anti-CD5-FITC (clone: UCHT2), anti-CD11c-FITC (clone: 3.9), anti-CD16-FITC (clone: B73.1), anti-CD19-FITC (clone: HIB19), anti-TCR $\alpha\beta$ -FITC (clone: IP26), anti-CD117-PE (clone: A3C6E2), anti-CD127-PE/Cyanine7 (clone: A019D5), anti-CD294-APC (clone: BM16), and anti-CD45-APC/Cyanine7 (clone: H130) (all from BioLegend, Beijing, China). Dead cells were stained with 7-aminocincomycin D (7-AAD) viability staining solution (BioLegend). Total ILCs were identified as 7-AAD<sup>-</sup> CD45<sup>+</sup> lineage (CD3, CD5, CD11c, CD16, CD19, and TCR $\alpha\beta$ )<sup>-</sup> CD127<sup>+</sup> lymphocytes. The ILC1s were CD117<sup>-</sup> CD294<sup>-</sup>, whilst ILC2s were CD294<sup>+</sup>, and ILC3s were CD117<sup>+</sup> CD294<sup>-</sup>. Flow cytometry was performed using a CytoFLEX flow cytometer (Beckman Coulter, Brea, USA), and data were analyzed using CytoExpert v. 2.3 software (Beckman Coulter).

### Enzyme-linked immunosorbent assay

Plasma levels of IL-17A and IL-22 were measured using the ELISA MAX™ Deluxe Set Human IL-17A (No. 433914) and the ELISA MAX™ Deluxe Set Human IL-22 (No. 434504) (both from BioLegend), according to the manufacturer's instructions.

### Statistical analyses

Statistical analyses were performed using GraphPad Prism v. 8.0 software (GraphPad Software, San Diego, USA.). Data distributions were assessed using the Shapiro–Wilk test (Table 1). Normally distributed data are presented as mean  $\pm$  standard deviation (M  $\pm$  SD), whereas

Table 1. Results of normality test

Variable	W-value	p-value
Patients with hyperuricemia		
ILCs/lymphocytes [%]	0.8518	<0.0001
ILC1s/ILCs [%]	0.9510	0.0039
ILC2s/ILCs [%]	0.9623	0.0187
ILC3s/ILCs [%]	0.9571	0.0090
Plasma IL-17A [pg/mL]	0.9533	0.2760
Plasma IL-22 [pg/mL]	0.5434	<0.0001
Serum uric acid [ $\mu$ mol/L]	0.9174	<0.0001
Scr [ $\mu$ mol/L]	0.6294	<0.0001
Blood urea nitrogen [mmol/L]	0.8111	<0.0001
Healthy controls		
ILCs/lymphocytes [%]	0.8040	<0.0001
ILC1s/ILCs [%]	0.9657	0.4301
ILC2s/ILCs [%]	0.9724	0.6065
ILC3s/ILCs [%]	0.9873	0.9695
Plasma IL-17A [pg/mL]	0.8487	0.0021

ILCs – innate lymphoid cells; IL – interleukin; Scr – serum creatinine. Data distribution was assessed using the Shapiro–Wilk test.

non-normally distributed data are presented as median (interquartile range (IQR)). The Spearman’s rank-order correlation was used for nonparametric correlations. The value of  $p < 0.05$  was considered statistically significant.

## Results

### The frequency of circulating ILC3s was increased in patients with HUA

A total of 80 patients with HUA (mean age  $52.85 \pm 15.99$  years, 49 males (61.25%) and 30 HC (mean age  $37.57 \pm 12.37$  years, 9 males (30.00%)) were included in the study. A positive correlation between serum UA and Scr concentrations was found in patients with HUA ( $r_s = 0.501$ ,  $p < 0.001$ ), which suggests an association between HUA and the impairment of renal function. The gating strategy used to separate ILCs and their subgroups is shown in Fig. 1A. First, the levels of ILCs and their subgroups in PBMCs were compared between HC and patients with HUA. Statistical comparisons showed that the percentage of total ILCs in the live lymphocyte population did not differ significantly between the 2 groups (0.09% (0.05–0.17%) compared to 0.07% (0.05–0.10%),  $U = 959.5$ ,  $p = 0.07$ ; Fig. 1B). For ILC subgroups, a marked elevated frequency of circulating ILC3s (22.27% (11.28–32.32%) compared to 17.11% (10.83–21.29%),  $U = 868$ ,  $p = 0.03$ ) was observed in HUA patients, although the frequencies of circulating ILC1s (23.24% (13.83–38.20%) compared to 32.80% (18.91–54.08%),  $U = 924.5$ ,  $p = 0.06$ ) and ILC2s (46.87% (31.37–67.91%) compared to 48.32% (27.26–66.32%),  $U = 1139$ ,  $p = 0.69$ ) did not differ significantly between the 2 groups (Fig. 1C and Table 2).

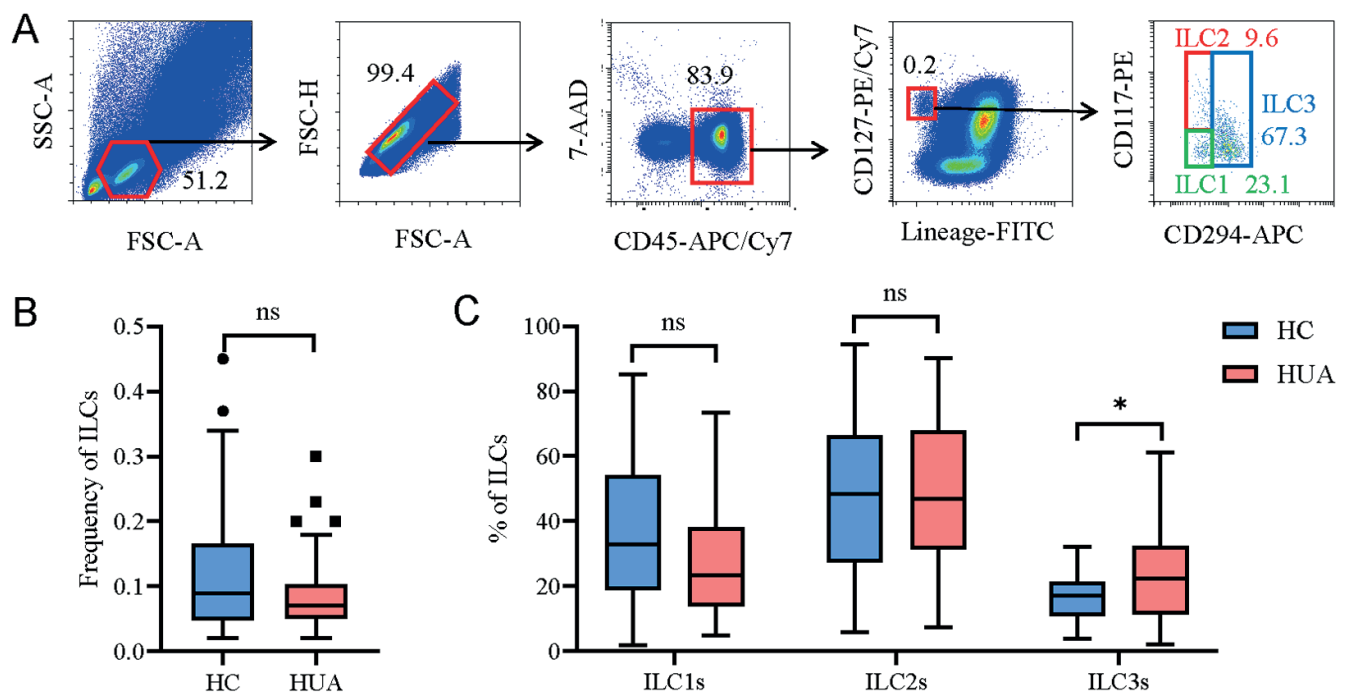
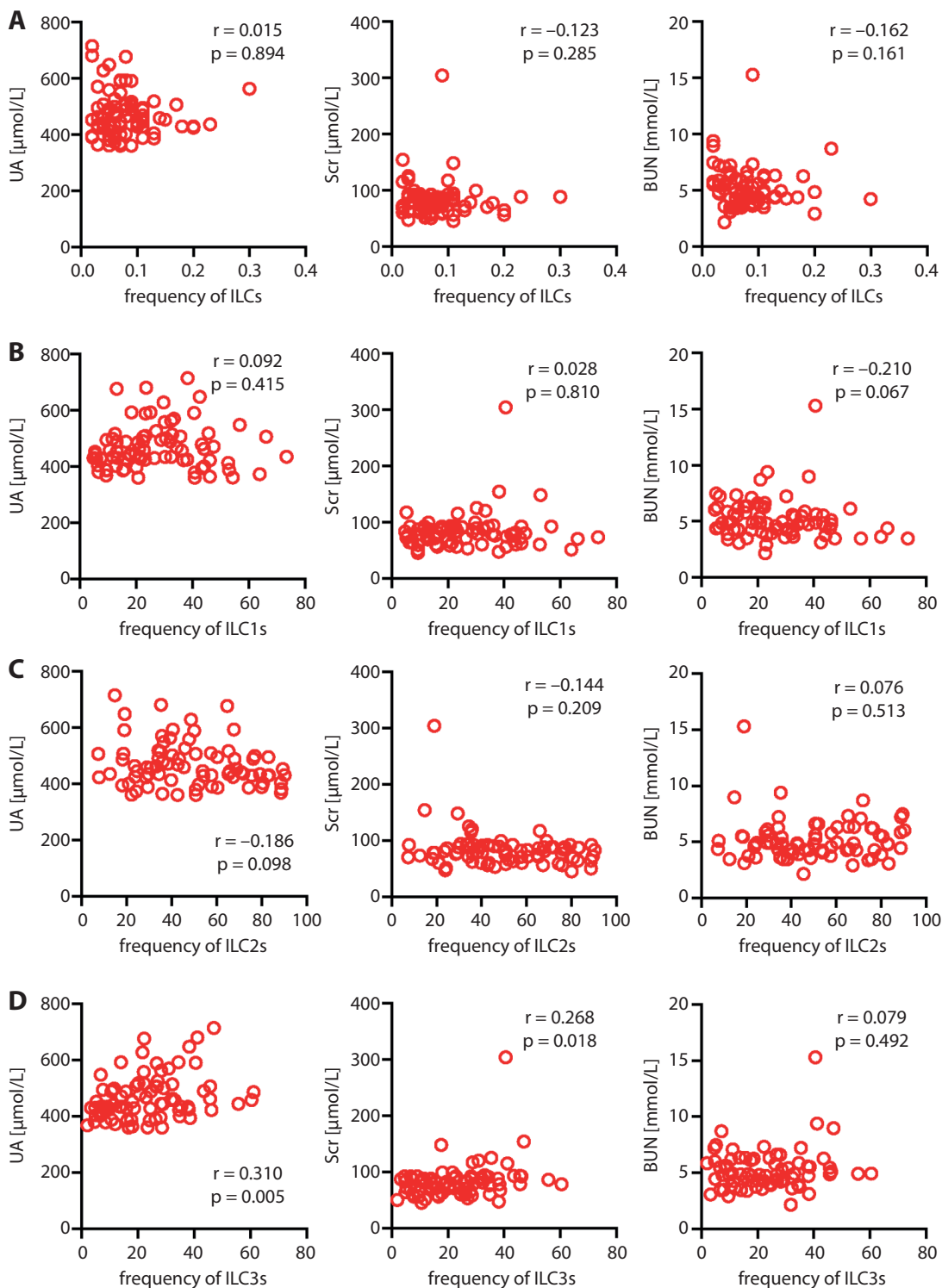


Fig. 1. Circulating type 3 innate lymphoid cells (ILC3s) increased in patients with hyperuricemia. A. Representative dot plots showing the gating strategy used to identify ILC3s among human peripheral blood mononuclear cells (PBMCs). Percentages of ILCs (B) and their subsets (C) in PBMCs from healthy controls (HC) and patients with hyperuricemia (HUA) (Mann–Whitney U test). Lineage = CD3, CD5, CD11c, CD16, CD19, TCR $\alpha$  $\beta$ . Boxplots represent median, interquartile ranges (IQRs) and Tukey-style whiskers. Data points beyond the whiskers represent outliers

\*  $p < 0.05$ ; ns – not significant.



**Fig. 2.** Frequency of circulating type 3 innate lymphoid cells (ILC3s) positively correlated with serum uric acid (UA) and serum creatinine (Scr) in patients with hyperuricemia. Spearman correlation coefficients between the frequencies of circulating ILCs (A), ILC1s (B), ILC2s (C), ILC3s (D), and concentrations of serum UA, Scr and blood urea nitrogen (BUN) in patients with hyperuricemia

### Circulating ILC3s positively correlated with serum UA and Scr levels in patients with HUA

Correlations between the levels of circulating ILCs and their subgroups with UA-associated parameters (serum UA, Scr and blood urea nitrogen) in patients with HUA were assessed. As shown in Fig. 2A–C, no significant correlations were found between the frequencies of circulating ILCs, ILC1s or ILC2s, and UA-associated parameters. In contrast, the frequency

of ILC3s in PBMCs from patients with HUA positively correlated with serum levels of UA ( $r_s = 0.310$ ,  $p = 0.005$ ) and Scr ( $r_s = 0.268$ ,  $p = 0.018$ ) (Fig. 2D).

### Plasma IL-17A positively correlated with the frequency of circulating type ILC3s and serum UA levels

Plasma concentrations of ILC3-related cytokines (IL-17A and IL-22) were compared between the 2 groups, with

**Table 2.** The proportion of circulating ILC subgroups and the concentrations of plasma cytokines between healthy controls and patients with hyperuricemia

Variable	Healthy controls	Patients with hyperuricemia	U-value	p-value
ILCs/lymphocytes [%]	0.09 (0.05–0.17)	0.07 (0.05–0.10)	959.5	0.07
ILC1s/ILCs [%]	32.80 (18.91–54.08)	23.24 (13.83–38.20)	924.5	0.06
ILC2s/ILCs [%]	48.32 (27.26–66.32)	46.87 (31.37–67.91)	1139	0.69
ILC3s/ILCs [%]	17.11 (10.83–21.29)	22.27 (11.28–32.32)	868	0.03
Plasma IL-17A [pg/mL]	3.36 (2.47–4.70)	3.26 (2.75–4.00)	289	0.66
Plasma IL-22 [pg/mL]	29.25 (12.31–49.13)	45.15 (16.69–86.51)	186.5	0.14

ILCs – innate lymphoid cells; IL – interleukin. Data are presented as median (interquartile range (IQR)). Differences between the 2 groups were assessed with Mann–Whitney U tests.

samples from 26 HUA patients and 24 HC being available for ELISA analysis. Although no differences in plasma IL-17A (3.36 (2.47–4.70) compared to 3.26 (2.75–4.00) pg/mL, U = 289, p = 0.66) or IL-22 (29.25 (12.31–49.13) compared to 45.15 (16.69–86.51) pg/mL, U = 186.5, p = 0.14, Table 2) concentrations were detected between the 2 groups, a positive correlation was observed between plasma IL-17A concentration and the frequency of circulating ILC3s in patients with HUA (Fig. 3).

Finally, the associations between ILC3-related cytokines and UA-associated parameters were assessed with

the Spearman’s rank-order correlation. Plasma IL-17A positively correlated with serum UA levels ( $r_s = 0.445$ , p = 0.023); however, no correlations were observed between IL-22 and UA-associated parameters (Fig. 4).

## Discussion

In the present study, the expansion of circulating ILC3s was observed in patients with HUA. Moreover, the proportion of ILC3s among PBMCs positively correlated with

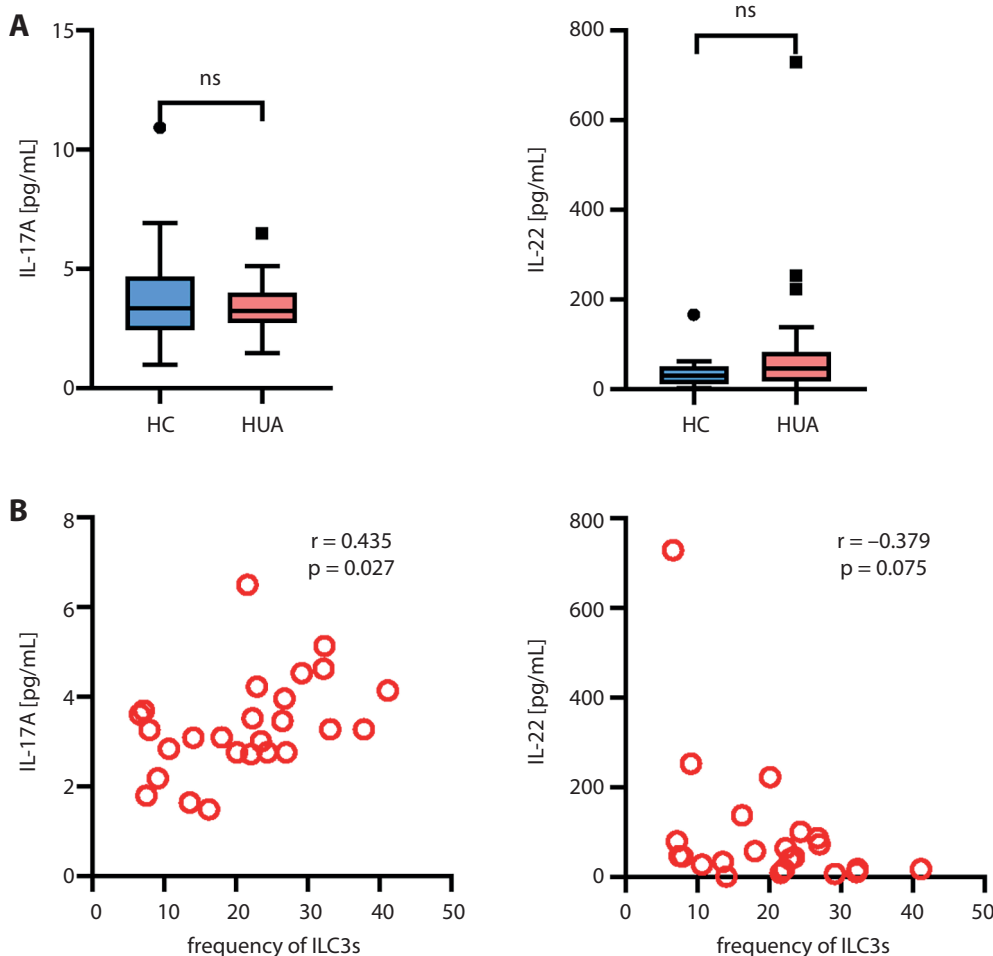


**Fig. 3.** Plasma interleukin (IL)-17A concentration positively correlated with circulating type 3 innate lymphoid cell (ILC3) frequency in patients with hyperuricemia. A. Quantitative analysis of the plasma concentrations of IL-17A and IL-22 in healthy controls (HC) and patients with hyperuricemia (HUA) (Mann–Whitney U test); B. Spearman correlation coefficients between plasma IL-17A and IL-22 levels, and the frequency of circulating ILC3s in patients with HUA. Boxplots represent median, interquartile ranges (IQRs) and Tukey-style whiskers. Data points beyond the whiskers represent outliers

ns – not significant.



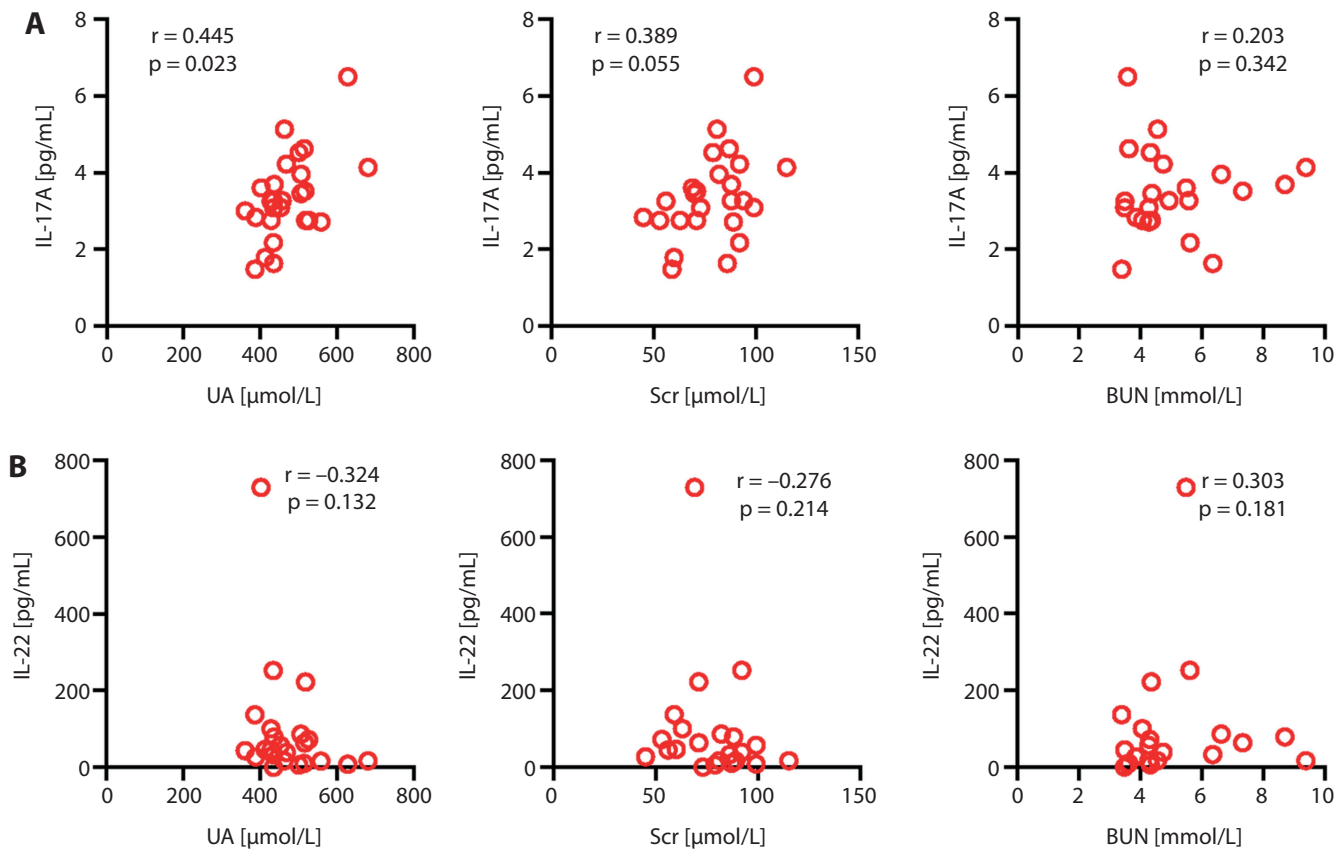


Fig. 4. Plasma interleukin (IL)-17A concentration positively correlated with serum uric acid (UA) level in patients with hyperuricemia (HUA). Spearman's rank-order correlation analysis between the concentrations of plasma IL-17A (A) and IL-22 (B) with serum UA, serum creatinine (Scr) and blood urea nitrogen (BUN) in patients with HUA

serum UA and Scr concentrations, indicating that circulating ILC3s could serve as an indicator of HUA severity. To the best of our knowledge, this is the first study to determine the characteristics of circulating ILC3s in patients with HUA.

Multiple mechanisms could explain the findings of this study. First, HUA may result in increased levels of ILC3s. Recent studies have revealed gut microbiota dysbiosis, characterized by a decrease in species diversity and an increased abundance of inflammation-related microbiota, in HUA patients and mouse models.<sup>8,11,17</sup> In addition, HUA can lead to intestinal barrier dysfunction that presents as enhanced intestinal permeability and gut inflammation.<sup>11,18,19</sup> Such gut dysbiosis and intestinal barrier injury can contribute to the enrichment of ILC3s.<sup>20,21</sup> Furthermore, ILC3s can secrete several pro-inflammatory cytokines, including IL-17 and granulocyte-macrophage colony-stimulating factor,<sup>22</sup> which may promote kidney and intestine inflammation,<sup>22–24</sup> reduce UA excretion and subsequently exacerbate UA accumulation in patients with HUA. Thus, targeting ILC3s may be a novel therapeutic strategy for HUA.

Alterations of ILC3s have been reported in several metabolic diseases. Both the frequency and absolute number of ILC3s were significantly increased in small intestinal lamina propria of nonobese diabetic mice compared to healthy mice, which was accompanied by intestinal

dysbiosis and an impaired intestinal barrier.<sup>25</sup> Furthermore, increased proportions of IL-22<sup>+</sup>ILC3s and IL-17A<sup>+</sup>NKp44<sup>-</sup> ILC3s were detected among PBMCs from patients with axial spondyloarthritis and dyslipidemia.<sup>26</sup> Conversely, type 2 diabetes patients infected with tuberculosis exhibited an obvious reduction in circulating ILC3s relative to those without diabetes.<sup>27</sup> Additionally, ILC3s have been shown to participate in the progression of other metabolic diseases, such as fatty liver disease.<sup>28</sup> Despite the increased levels of circulating ILC3s in HUA patients observed in this study, whether or not ILC3s contribute to HUA development requires further investigation.

The IL-17, a distinct cytokine produced by ILC3s, is widely reported to be associated with acute gout arthritis. Liu et al. showed that serum IL-17 levels were significantly elevated in patients with acute gout arthritis, which positively correlated with disease severity.<sup>29</sup> Furthermore, targeting IL-17 with neutralizing antibodies reduced leukocyte infiltration, decreased pro-inflammatory cytokine levels and attenuated arthritis.<sup>15</sup> However, plasma IL-17 levels did not differ markedly between patients with intercritical gout and HC.<sup>30</sup> Similarly, we found no significant difference in plasma IL-17A concentration between patients with HUA and HC, whereas in patients with HUA, positive correlations were observed between plasma IL-17A, serum UA and frequency of circulating

ILC3s. This suggests that HUA may induce ILC3 expansion and activation, and that plasma IL-17A could be a useful indicator of HUA severity.

## Limitations

The present study had several limitations. Only 2 of the enrolled HUA patients had gout, meaning the association between ILC3s and gout could not be assessed. Also, as this was a cross-sectional study, only the associations between UA level, IL-17 and ILC3 could have been investigated. Indeed, it could not be determined if the relationship between UA level, IL-17 and ILC3s was causal. Furthermore, the sample size was relatively small, particularly for the HC group. Thus, studies with a larger sample size should be conducted to validate our findings.

## Conclusions

In conclusion, we demonstrated that patients with HUA have an elevated frequency of circulating ILC3s. Furthermore, circulating ILC3 levels and plasma IL-17A concentration were positively correlated with HUA severity. Therefore, ILC3s and IL-17A could be useful indicators of HUA severity and have potential as new therapeutic targets in this disease.

## ORCID iDs

Zan-Xiong Chen  <https://orcid.org/0000-0002-3480-2680>  
 Hong-Qian Liu  <https://orcid.org/0000-0003-0269-6892>  
 Zhen-Hua Wu  <https://orcid.org/0000-0001-6916-5549>  
 Jun-Lian He  <https://orcid.org/0000-0002-8844-871X>  
 Hao-Jie Zhong  <https://orcid.org/0000-0001-6586-756X>

## References

- Diaz-Torne C, Ortiz MA, Garcia-Guillen A, et al. The inflammatory role of silent urate crystal deposition in intercritical gout. *Rheumatology*. 2021;60(11):5463–5472. doi:10.1093/rheumatology/keab335
- Dalbeth N, Gosling AL, Gaffo A, Abhishek A. Gout. *Lancet*. 2021;397(10287):1843–1855. doi:10.1016/S0140-6736(21)00569-9
- Dalbeth N, Choi HK, Joosten LAB, et al. Gout. *Nat Rev Dis Primers*. 2019;5(1):69. doi:10.1038/s41572-019-0115-y
- Major TJ, Dalbeth N, Stahl EA, Merriman TR. An update on the genetics of hyperuricaemia and gout. *Nat Rev Rheumatol*. 2018;14(6):341–353. doi:10.1038/s41584-018-0004-x
- Liu R, Han C, Wu D, et al. Prevalence of hyperuricemia and gout in mainland China from 2000 to 2014: A systematic review and meta-analysis. *BioMed Res Int*. 2015;2015:762820. doi:10.1155/2015/762820
- Li H, Zhang H, Yan F, et al. Kidney and plasma metabolomics provide insights into the molecular mechanisms of urate nephropathy in a mouse model of hyperuricemia. *Biochim Biophys Acta Mol Basis Dis*. 2022;1868(6):166374. doi:10.1016/j.bbdis.2022.166374
- Vieira AT, Macia L, Galvão I, et al. A role for gut microbiota and the metabolite-sensing receptor GPR43 in a murine model of gout. *Arthritis Rheum*. 2015;67(6):1646–1656. doi:10.1002/art.39107
- Song S, Lou Y, Mao Y, et al. Alteration of gut microbiome and correlated amino acid metabolism contribute to hyperuricemia and Th17-driven inflammation in Uox-KO mice. *Front Immunol*. 2022;13:804306. doi:10.3389/fimmu.2022.804306
- Yun Y, Yin H, Gao Z, et al. Intestinal tract is an important organ for lowering serum uric acid in rats. *PLoS One*. 2017;12(12):e0190194. doi:10.1371/journal.pone.0190194
- Wang J, Chen Y, Zhong H, et al. The gut microbiota as a target to control hyperuricemia pathogenesis: Potential mechanisms and therapeutic strategies. *Crit Rev Food Sci Nutr*. 2022;62(14):3979–3989. doi:10.1080/10408398.2021.1874287
- Lv Q, Xu D, Zhang X, et al. Association of hyperuricemia with immune disorders and intestinal barrier dysfunction. *Front Physiol*. 2020;11:524236. doi:10.3389/fphys.2020.524236
- Chun E, Lavoie S, Fonseca-Pereira D, et al. Metabolite-sensing receptor Ffar2 regulates colonic group 3 innate lymphoid cells and gut immunity. *Immunity*. 2019;51(5):871.e6–884.e6. doi:10.1016/j.immuni.2019.09.014
- Zhou L, Zhou W, Joseph AM, et al. Group 3 innate lymphoid cells produce the growth factor HB-EGF to protect the intestine from TNF-mediated inflammation. *Nat Immunol*. 2022;23(2):251–261. doi:10.1038/s41590-021-01110-0
- Chen Y, Ma H, Du Y, et al. Functions of 1,25-dihydroxy vitamin D3, vitamin D3 receptor and interleukin-22 involved in pathogenesis of gout arthritis through altering metabolic pattern and inflammatory responses. *PeerJ*. 2021;9:e12585. doi:10.7717/peerj.12585
- Rauci F, Iqbal AJ, Saviano A, et al. IL-17A neutralizing antibody regulates monosodium urate crystal-induced gouty inflammation. *Pharmacol Res*. 2019;147:104351. doi:10.1016/j.phrs.2019.104351
- Li H, Zeng R, Liao Y, et al. Prevalence and risk factors of left ventricular diastolic dysfunction in patients with hyperthyroidism. *Front Endocrinol*. 2021;11:605712. doi:10.3389/fendo.2020.605712
- Sheng S, Chen J, Zhang Y, et al. Structural and functional alterations of gut microbiota in males with hyperuricemia and high levels of liver enzymes. *Front Med*. 2021;8:779994. doi:10.3389/fmed.2021.779994
- Xu D, Lv Q, Wang X, et al. Hyperuricemia is associated with impaired intestinal permeability in mice. *Am J Physiol Gastrointest Liver Physiol*. 2019;317(4):G484–G492. doi:10.1152/ajpgi.00151.2019
- Guo Y, Li H, Liu Z, et al. Impaired intestinal barrier function in a mouse model of hyperuricemia. *Mol Med Rep*. 2019;20(4):3292–3300. doi:10.3892/mmr.2019.10586
- Seidelin JB, Bahl MI, Licht TR, et al. Acute experimental barrier injury triggers ulcerative colitis-specific innate hyperresponsiveness and ulcerative colitis-type microbiome changes in humans. *Cell Mol Gastroenterol Hepatol*. 2021;12(4):1281–1296. doi:10.1016/j.jcmgh.2021.06.002
- Valiente GR, Munir A, Hart ML, et al. Gut dysbiosis is associated with acceleration of lupus nephritis. *Sci Rep*. 2022;12(1):152. doi:10.1038/s41598-021-03886-5
- Zheng M, Zhu J. Innate lymphoid cells and intestinal inflammatory disorders. *Int J Mol Sci*. 2022;23(3):1856. doi:10.3390/ijms23031856
- Paquissi FC, Abensur H. The Th17/IL-17 axis and kidney diseases, with focus on lupus nephritis. *Front Med*. 2021;8:654912. doi:10.3389/fmed.2021.654912
- Wang C, Li Q, Lv J, et al. Alpha-hemolysin of uropathogenic *Escherichia coli* induces GM-CSF-mediated acute kidney injury. *Mucosal Immunol*. 2020;13(1):22–33. doi:10.1038/s41385-019-0225-6
- Miranda MCG, Oliveira RP, Torres L, et al. Frontline Science: Abnormalities in the gut mucosa of non-obese diabetic mice precede the onset of type 1 diabetes. *J Leukoc Biol*. 2019;106(3):513–529. doi:10.1002/JLB.3HI0119-024RR
- Min HK, Moon J, Lee SY, et al. Expanded IL-22<sup>+</sup> group 3 innate lymphoid cells and role of oxidized LDL-C in the pathogenesis of axial spondyloarthritis with dyslipidaemia. *Immune Netw*. 2021;21(6):e43. doi:10.4110/in.2021.21.e43
- Ssekamatte P, Nakibuule M, Nabatanzi R, et al. Type 2 diabetes mellitus and latent tuberculosis infection moderately influence innate lymphoid cell immune responses in Uganda. *Front Immunol*. 2021;12:716819. doi:10.3389/fimmu.2021.716819
- Hamaguchi M, Okamura T, Fukuda T, et al. Group 3 innate lymphoid cells protect steatohepatitis from high-fat diet induced toxicity. *Front Immunol*. 2021;12:648754. doi:10.3389/fimmu.2021.648754
- Liu Y, Zhao Q, Yin Y, McNutt MA, Zhang T, Cao Y. Serum levels of IL-17 are elevated in patients with acute gouty arthritis. *Biochem Biophys Res Commun*. 2018;497(3):897–902. doi:10.1016/j.bbrc.2018.02.166
- Yang QB, He YL, Zhang QB, Mi QS, Zhou JG. Downregulation of transcription factor T-Bet as a protective strategy in monosodium urate-induced gouty inflammation. *Front Immunol*. 2019;10:1199. doi:10.3389/fimmu.2019.01199



# CircHIPK3 promotes neuroinflammation through regulation of the miR-124-3p/STAT3/NLRP3 signaling pathway in Parkinson's disease

Yu-Juan Zhang<sup>1,2,A,C,D,F</sup>, Wen-Kai Zhu<sup>3,B,C</sup>, Fa-Ying Qi<sup>3,B-D</sup>, Feng-Yuan Che<sup>1,3,A,C,F</sup>

<sup>1</sup> Institute of Clinical Medicine College, Guangzhou University of Chinese Medicine, China

<sup>2</sup> Department of Acupuncture, Linyi People's Hospital, China

<sup>3</sup> Department of Neurology, Linyi People's Hospital, China

A – research concept and design; B – collection and/or assembly of data; C – data analysis and interpretation;

D – writing the article; E – critical revision of the article; F – final approval of the article

Advances in Clinical and Experimental Medicine, ISSN 1899–5276 (print), ISSN 2451–2680 (online)

*Adv Clin Exp Med.* 2023;32(3):315–329

## Address for correspondence

Feng-Yuan Che

E-mail: chefy2020@163.com

## Funding sources

The study was funded by Linyi Science and Technology Development Project, Shandong, China (grant No. 202020021).

## Conflict of interest

None declared

Received on April 19, 2022

Reviewed on July 31, 2022

Accepted on September 16, 2022

Published online on October 28, 2022

## Cite as

Zhang YJ, Zhu WK, Qi FY, Che FY. CircHIPK3 promotes neuroinflammation through regulation of the miR-124-3p/STAT3/NLRP3 signaling pathway in Parkinson's disease.

*Adv Clin Exp Med.* 2023;32(3):315–329.

doi:10.17219/acem/154658

## DOI

10.17219/acem/154658

## Copyright

Copyright by Author(s)

This is an article distributed under the terms of the Creative Commons Attribution 3.0 Unported (CC BY 3.0) (<https://creativecommons.org/licenses/by/3.0/>)

## Abstract

**Background.** Parkinson's disease (PD) is characterized as a neurodegenerative disease; however, the mechanisms regarding its pathogenesis have not been fully explored.

**Objectives.** To explore the role of circular RNA homeodomain interacting protein kinase 3 (circHIPK3) in the progression of PD.

**Materials and methods.** The circHIPK3 and microRNA-124 (miR-124) expression in human serum and cerebral fluid was detected using real-time quantitative reverse transcription polymerase chain reaction (qRT-PCR) in 92 PD patients and 95 controls. The circHIPK3 was overexpressed and/or silenced in cells to explore its molecular mechanisms and effects on neuroinflammation. The production of intracellular reactive oxygen species (ROS) was assessed using 2',7'-dichlorodihydrofluorescein diacetate (DCFH-DA) staining. Interleukin 6 (IL-6), IL-1 $\beta$  and tumor necrosis factor alpha (TNF- $\alpha$ ) production in BV2 cells after the indicated treatment was measured using enzyme-linked immunosorbent assay (ELISA). The protein expression of microglia markers (cluster of differentiation molecule 11b (CD11b) and ionized calcium-binding adapter molecule 1 (Iba-1)), pyroptosis-related factors, NLR family pyrin domain containing 3 (NLRP3), apoptosis-associated speck-like protein containing C-terminal caspase recruitment domain (ASC), and caspase-1, signal transducer and activator of transcription 3 (STAT3), and phosphorylated STAT3 (p-STAT3) were examined using western blot analysis. Furthermore, the interaction between circHIPK3, miR-124 and STAT3 was predicted with bioinformatics and examined using fluorescence in situ hybridization (FISH), luciferase reporter assays, RNA pull-down, and RNA immunoprecipitation (RIP).

**Results.** The expression of circHIPK3 in human serum and cerebral fluids was significantly higher than in controls, whereas miR-124 expression was drastically reduced. In addition, lipopolysaccharide (LPS)-treated BV2 cells exhibited higher expression of circHIPK3 and lower miR-124 expression. The SH-SY5Y cells exhibited a significantly impaired viability and elevated apoptotic rate, along with an upregulation of circHIPK3 and a downregulation of miR-124 expression after being treated with supernatants collected from LPS-treated BV2 cells. The upregulation of circHIPK3 increased IL-6, IL-1 $\beta$  and TNF- $\alpha$  secretion in BV2 cells. The protein expressions of microglia markers (CD11b and Iba-1), as well as pyroptosis-related factors, NLRP3, caspase-1, and ASC, were also increased following the expression of circHIPK3. All these effects were reversed by the addition of miR-124.

**Conclusions.** The circHIPK3 enhances neuroinflammation by sponging miR-124 and regulating the miR-124-mediated STAT3/NLRP3 pathway in PD.

**Key words:** Parkinson's disease, NLRP3, miR-124, neuroinflammation, circHIPK3

## Background

Parkinson's disease (PD) is characterized as a progressive and chronic neurodegenerative disease that affects middle-aged and elderly people.<sup>1</sup> Based on reports, the incidence of PD is 1% in people over 65 years of age and 5% in those older than 85.<sup>1</sup> The loss of dopaminergic neurons in the substantia nigra pars compacta (SNpc) leads to the development of the clinical features of PD.<sup>2</sup> These include motor symptoms, such as bradykinesia, akinesia, resting tremor, postural instability, and rigidity. In addition, non-motor features include fatigue, pain, olfactory dysfunction, autonomic dysfunction, sleep disorders, psychiatric symptoms, and cognitive impairment.<sup>3</sup> Although many studies have been performed, the pathogenesis of PD is not completely understood, and no drugs are available to alleviate the progression of the disease.

In recent years, neuroinflammation has been identified as a major factor associated with the pathogenesis of PD.<sup>4</sup> Compared to healthy controls, the samples of cerebrospinal fluid (CSF) and substantia nigra (SN) collected from PD patients exhibited relatively high levels of cytokines and complement.<sup>5</sup> Inflammasomes, specifically the NLR family pyrin domain containing 3 (NLRP3) inflammasome generated by caspase-1, apoptosis-associated speck-like protein containing C-terminal caspase recruitment domain (ASC) adaptor protein and NLRP3 are significantly involved in the pathogenesis and progression of PD.<sup>6</sup> As one of the innate immune cells which reside in the central nervous system (CNS), microglia are involved in both normal and pathologic conditions of the CNS. Additionally, the protective and toxic effects of neuroinflammation caused by the activation of microglia in the brain have been observed.<sup>7,8</sup> Studies have also identified that the NLRP3 inflammasome functions in microglia but not in astrocytes.<sup>9</sup> Therefore, the inhibition of microglia inflammation by targeting NLRP3 may be a potential treatment option in PD.

As a non-coding RNA, circular RNAs (circRNAs) are generated by back-splicing from precursor messenger RNA (mRNA) and expressed in specific tissues in mammals.<sup>10,11</sup> Accumulating evidence indicates that circRNAs exert specific biological functions and participate in various pathophysiological and physiologic processes in neoplastic cells.<sup>12</sup> It has also been proven that because of the existence of binding sites with microRNA (miRNA), circRNAs exert a regulatory role in diseases by controlling the expression of miRNA associated with diseases through a direct interaction.<sup>12</sup>

Growing evidence has implicated circRNAs to significantly participate in the pathogenesis of Alzheimer's disease,<sup>13</sup> stroke,<sup>14</sup> PD,<sup>15</sup> etc. Recently, circRNAs were considered potential targets for PD treatment because of their changing expression during the development of PD.<sup>16</sup> For example, an elevated expression of circSLC8A1 was observed in PD patients and cells after oxidative stress.<sup>17</sup> In another study, the significant upregulation and close connection of circ-zip-2 with the pathogenesis of PD was found.<sup>18</sup> Moreover,

Ghosal et al. indicated that ciRS-7 was significantly involved in the nucleoprotein enrichment pattern of miR-7 in PD.<sup>19</sup>

The circRNA homeodomain interacting protein kinase 3 (circHIPK3, circRNA ID: hsa\_circ\_0000284) has been implicated to facilitate inflammation in various disease states.<sup>20</sup> Through a direct interaction with miR-561 and miR-192, circHIPK3 powerfully enhances the activation of the toll-like receptor 4 (TLR4) pathway and macrophage NLRP3 inflammasomes in gouty arthritis.<sup>21</sup> At the same time, a significant increase in the expression of circHIPK3 in lipopolysaccharide (LPS)-treated H9c2 cells and LPS-induced myocarditis in animals was observed *in vitro* and *in vivo*, and the LPS-induced myocarditis was improved by silencing circHIPK3.<sup>22</sup> An increased expression of circHIPK3 was positively correlated with the degree of neuropathic pain in type II diabetic patients.<sup>23</sup> In diabetic rats, the downregulation of circHIPK3 effectively attenuated neuropathic pain, suggesting the involvement of circHIPK3 in neuroinflammation.<sup>23</sup> However, whether circHIPK3 promotes neuroinflammation following microglia activation in PD remains unknown.

The miR-124 has been the focus of studies on the progression of PD. The microRNA-124 (miR-124) expression was identified in human brain tissues, and the involvement of miR-124 in neurotransmission, synapse morphology and neurogenesis has been found.<sup>24</sup> Previous studies have also shown that miR-124 regulates oxidative damage, mitochondrial dysfunction, neuroinflammation, autophagy, and cell survival in PD.<sup>25</sup> Decreased concentrations of miR-124 in plasma may be considered a diagnostic marker for PD.<sup>26</sup> These findings suggested that miR-124 performs a neuroprotective role in PD and has a therapeutic value.<sup>27</sup>

The signal transducer and activator of transcription 3 (STAT3) is associated with controlling inflammation and immunity, including those in microglia.<sup>28</sup> The activation of STAT3 enhances the expression of inflammation-associated genes and can induce a reduction in dopaminergic neurons, subsequently leading to PD symptoms in mice.<sup>29,30</sup> In addition, through direct interaction with the promoter of NLRP3, STAT3 can enhance the expression of NLRP3 and promote neuronal pyroptosis, leading to neuronal damage.<sup>31</sup>

## Objectives

This study aims to explore the potential molecular mechanisms regulating circHIPK3, miR-124 and NLRP3 in inflammation observed in PD patients.

## Materials and methods

### Patients

The expression of circHIPK3 and miR-124 in blood samples obtained from 92 PD patients was determined. Patients with other neurodegenerative diseases such as Alzheimer's



disease, Huntington's disease and amyotrophic lateral sclerosis were excluded from the study. Additionally, patients with unstable comorbidities, a history of receiving deep brain stimulation and younger than 18 years were also excluded. A lumbar puncture, blood sample collection, standardized detailed neurologic examination, and other ancillary investigations, such as magnetic resonance imaging (MRI), as well as structured interviews, were performed for all patients before the beginning of the study. The protocols for this study were reviewed and approved before the initiation of the study by the Linyi People's Hospital ethics committee (No. of approval 20210045). Patients (n = 95, age > 40) without any neurological and inflammatory disorders were enrolled as a control group. Patients from the control group underwent a lumbar puncture to exclude any potential or suspected neurological disorders. Written informed consent was signed by the patients enrolled in this study. This study complied with the Declaration of Helsinki.

### Sample preparation and real-time quantitative reverse transcription polymerase chain reaction

Lumbar puncture was performed using the standard technique. Collected CSF without blood contamination was immediately frozen at  $-80^{\circ}\text{C}$  and kept for further usage. The numbers of leukocytes and erythrocytes in the collected CSF samples were no more than 5 cells/ $\mu\text{L}$  and 200 cells/ $\mu\text{L}$ , respectively. After overnight fasting and incubation for 2–3 h at room temperature (RT), the venous blood was centrifuged at 1900 g for 20 min. Then, the serum was stored for further analysis at  $-80^{\circ}\text{C}$ . The total RNA in the serum samples was extracted using the TaKaRa RNA Extraction Kit (TaKaRa, Tokyo, Japan).

The purity and concentrations of RNA were evaluated using the Nanodrop-1000 (Thermo Fisher Scientific, Waltham, USA). A PrimeScript<sup>TM</sup> RT reagent Kit (TaKaRa) was employed to perform a reverse transcription of the extracted mRNA to complementary DNA (cDNA). The SYBR<sup>®</sup> Premix Ex Taq<sup>TM</sup> II (TaKaRa) was used to perform the real-time quantitative reverse transcription polymerase chain reaction (qRT-PCR). The primers were designed using Primer Premier v. 6.0 software (PREMIER Biosoft, San Francisco, USA) and the sequences of these primers were listed as follows: circHIPK3 forward: 5'-TATGTTGGTGGATCCTGTTC-GGCA-3', reverse: 5'-TGGTGGGTAGACCAAGACTT-GTGA-3'; glyceraldehyde-3-phosphate dehydrogenase (GAPDH) forward: 5'-ACCACAGTCCATGCCATCAC-3', reverse: 5'-TCCACCACCCTGTTGCTGTA-3'; miR-124 forward: 5'-TCTTTAAGGCACGCGGTG-3', reverse: 5'-TATGGTTTTGACGACTGTGTGAT-3'; and U6 forward: 5'-CTCGCTTCGGCAGCACA-3', reverse: 5'-AAC-GCTTCACGAATTTGCGT-3'. The circHIPK3 and miR-124 expressions were calculated using the  $2^{-\Delta\Delta\text{Ct}}$  method. The GAPDH and U6 expressions were used to normalize the circHIPK3 and miR-124 expressions, respectively.

### Cells and cell culture

The SH-SY5Y and BV2 cells were cultured in Roswell Park Memorial Institute (RPMI) 1640 medium (Gibco, Waltham, USA) containing glucose (5 mM), fetal bovine serum (FBS, 10%; Gibco) and streptomycin/penicillin (1%; Gibco). The medium was replaced every 2 days and the cells that reached 80% confluence were collected for further experiments.

### Conditioned medium-induced neurotoxicity

After 48 h of incubation with LPS (1  $\mu\text{g}/\text{mL}$ ), the supernatants of the BV2 were collected. To remove the cellular debris, 5-min centrifugation at 2500 rpm was conducted. The collected supernatants were then stored at  $-80^{\circ}\text{C}$  and used as the conditioned medium (CM) in further experiments. For CM-induced neurotoxicity, the SH-SY5Y cells were incubated with CM for another 24 h after a 24-hour culture in a normal medium. The neuronal viability was then assessed.

### Measurement of cell viability

The cells were cultured overnight before the measurement. After a 4-hour incubation with 500  $\mu\text{g}/\text{mL}$  of MTT solution at  $37^{\circ}\text{C}$  in the dark, the medium was replaced with dimethyl sulfoxide (DMSO). After a 10-minute shaking, the absorbance was read using a microplate reader (BioTek, Winooski, USA) at 450 nm.

### Determination of cell apoptosis

Annexin V staining was conducted to evaluate the apoptosis rate of SH-SY5Y cells. Briefly, after washing and centrifugation, the cells were suspended in a  $1\times$  Annexin V binding buffer PI (5  $\mu\text{L}$ ; BioVision, Waltham, USA) and Annexin V (5  $\mu\text{L}$ ) was added and stained at RT for 15 min. The apoptosis rate was detected using flow cytometry.

### Cell transfection

A miR-124 mimic was obtained from Guangzhou Riobo-Bio Co., Ltd. (Guangzhou, China). A siRNA (5'-CUACAG-GUAUGGCCUCACA-3') specifically targeted to circHIPK3 was transfected into the BV2 cells to silence the expression of circHIPK3. The cell transfection was conducted using Lipofectamine<sup>TM</sup> 3000 (Thermo Fisher Scientific).

### Detection of reactive oxygen species

Reactive oxygen species (ROS) in the cells were evaluated by 2',7'-dichlorodihydrofluorescein diacetate (DCFH-DA) staining. Briefly, after a 30-minute culture with 10  $\mu\text{M}$  of DCFH-DA at  $37^{\circ}\text{C}$ , the level of ROS in the BV2 cells with different treatments was measured at excitation/emission = 485/535 nm.

## Western blot analysis

After a 20-minute centrifugation at 12,000 g, the protein concentrations of the supernatant were determined. The samples (30 µg per sample) were loaded into a 10–12% sodium dodecyl-sulfate polyacrylamide gel electrophoresis (SDS–PAGE). Next, after transferring onto a polyvinylidene difluoride (PVDF) membrane, the protein bands were blocked in 5% fat-free milk for 1 h at RT. Then, after overnight incubation with the indicated primary antibodies at 4°C, washing 3 times with phosphate-buffered saline with Tween® detergent (PBST), and a 1-hour incubation with horseradish peroxidase (HRP)-conjugated secondary antibodies at RT, the protein bands and signals were detected using an enhanced chemiluminescence detection system (Pierce, Rockford, USA). The antibodies used were as follows: GAPDH (1:1000; Abcam, Cambridge, UK), phosphorylated STAT3 (p-STAT3, 1:1000; Abcam), STAT3 (1:1000; Abcam), ASC (1:1000; Cell Signaling Technology, Danvers, USA), caspase-1 (1:800; Cell Signaling Technology), NLRP3 (1:1000; Cell Signaling Technology), ionized calcium-binding adapter molecule 1 (Iba-1, 1:800; Abcam), and cluster of differentiation molecule 11b (CD11b, 1:1000; Abcam). All protein expressions were normalized to GAPDH.

## Enzyme-linked immunosorbent assay

The enzyme-linked immunosorbent assay (ELISA) kits for tumor necrosis factor alpha (TNF-α), interleukin-1β (IL-1β) and IL-6 (R&D Systems, Minneapolis, USA) were purchased to examine their production from BV2 cells in the supernatant.

## Luciferase assay

The cDNA of circHIPK3 containing predicted binding or mutation sites was obtained using PCR amplification. The purified PCR fragment was then inserted into a pGL3 vector (Promega, Madison, USA) at XhoI/KpnI sites in order to generate the target luciferase reporter plasmid. We named these vectors circHIPK3-WT and circHIPK3-MUT, respectively. Similarly, the magnification of miR-124 3'-UTR of the wild-type STAT3 was performed using PCR, and then it was loaded on a pGL3 vector immediately downstream to the firefly luciferase reporter gene. The complex was called pGL3-WT-STAT3-3'UTR. Next, we mutated the miR-124 binding site of STAT3 3'-UTR using the Site-Directed Mutagenesis Kit (Abcam, Cambridge, UK) and inserted it into another PGL3 at the same location. The mutant is known as PGL3-MUT-STAT3-3'UTR. Forty-eight well plates were used to inoculate BV2 cells. When the convergence reached 50%, 500 ng of luciferase reporter vector was co-transfected with 30 nM of miR-124 mimic or negative control (NC)-mimic using Lipofectamine™ 2000 (Thermo Fisher Scientific). After 48 h of culture, the relative luciferase activities were determined.

## Fluorescence in situ hybridization

The circHIPK3 was labeled with Cy5, the DNA Oligo Probe (GenePharma, Suzhou, China) was labeled with 5-carboxyfluorescein (FAM), and the nucleus was back-stained with 4,6-diamidino-2-phenylindole dihydrochloride (DAPI; GenePharma), which was used for fluorescence in situ hybridization (FISH) detection. After staining, the results were observed and the images were captured under a Leica SP5 confocal microscope (Leica, Wetzlar, Germany).

## RNA immunoprecipitation (RIP)

After overnight incubation with anti-immunoglobulin G (IgG) (Merck Millipore, Burlington, USA) or anti-STAT3 (Ago2) antibodies, the RNA-protein complex was precipitated with protein A agarose beads, followed by RNA extraction and qRT-PCR detection. The negative control was normal IgG.

## RNA pull-down assay

We lysed human BV2 cells transfected with miR-124 mimics and incubated them with a circHIPK3 biotin-conjugated probe that was bound to magnetic beads for 2 h to pull down the miR-124. Then, the pulled-down RNA was purified. The miR-124 biotin-conjugated probe was treated as before.

## Northern blot

The RNA samples were separated using a polyacrylamide gel and transferred to Amersham™ Hybond™-N+ nylon membrane (Amersham Biosciences, Amersham, UK). After fixation with purple coupling, PerfectHyb™ (Sigma-Aldrich, St. Louis, USA) was pre-hybridized and incubated with P32 probes generated using the StarFire® Nucleic Acid Labeling System (Integrated DNA Technologies, Coralville, USA). The U6 or β-actin were used as the control.

## Statistical analyses

All the obtained data were processed and analyzed using GraphPad Prism v. 7.0 (GraphPad Software, San Diego, USA). Shapiro–Wilk test was used to test the normal distribution, whereas F-test was applied to check the homogeneity variance among the groups (Supplementary File). The  $\chi^2$  test was used to investigate the distribution of sexes. Mann–Whitney U test was conducted for the comparisons between the 2 groups in terms of gene expression collected in clinical samples. When 3 or more groups were compared, Kruskal–Wallis test was used, followed by Dunn's test for post hoc analysis. For cell experiments, given that the sample size was very small and that checking the normal distribution has little power, nonparametric tests were used (Mann–Whitney U test or Kruskal–Wallis test followed

by Dunn's test). The values were expressed as median (interquartile range (IQR)) or data point plots (central tendency measure and interval). Spearman's analysis was used to test the correlation between the expression of 2 genes. A value of  $p < 0.05$  was considered statistically significant.

## Results

### CircHIPK3 expression was elevated in PD patients, LPS-induced BV2 cells and conditioned SH-SY5Y medium

The demographic data of PD patients and controls are listed in Table 1. There were no significant differences with regard to age, sex distribution and body mass index (BMI) between PD patients and controls (Table 1).

The expression of circHIPK3 and miR-124 in human blood and CSF was detected with qRT-PCR. The qRT-PCR analysis showed that the expression of circHIPK3 in blood and CSF samples was significantly increased in PD patients compared to controls (blood: Mann–Whitney U test,  $U = 0$ ,  $p < 0.001$ ; CSF: Mann–Whitney U test,  $U = 0$ ,  $p < 0.001$ ; Fig. 1A,C). On the other hand, the expression of miR-124 in the blood and CSF samples was markedly decreased in PD patients compared to controls (blood: Mann–Whitney U test,  $U = 0$ ,  $p < 0.001$ ; CSF: Mann–Whitney U test,  $U = 0$ ,  $p < 0.001$ ; Fig. 1B,D; Table 2 – No. 1–4). Both circHIPK3 expression in blood and CSF samples were negatively correlated with miR-124 expression (blood: Spearman's correlation,  $r = -0.402$ ,  $p < 0.001$ ; CSF: Spearman's correlation,  $r = -0.447$ ,  $p < 0.001$ ; Fig. 1E,F; Table 2 – No. 5,6).

On the other hand, the expression of circHIPK3 was significantly higher in cells after LPS treatment compared to cells without the addition of LPS (Mann–Whitney U test,  $U = 0$ ,  $p = 0.002$ ), where miR-124 expression was drastically decreased (Mann–Whitney U test,  $U = 0$ ,  $p = 0.004$ ; Fig. 2A,B). In addition, a significantly reduced cell viability (Mann–Whitney U test,  $U = 0$ ,  $p = 0.002$ ) and increased cell apoptosis (Mann–Whitney U test,  $U = 0$ ,  $p = 0.007$ ) were observed in SH-SY5Y cells after CM treatment in comparison to non-treated control cells (Fig. 2C–F). In addition, circHIPK3 was upregulated (Fig. 2C; Mann–Whitney U test,  $U = 0$ ,  $p = 0.002$ ) and miR-124 expression was decreased (Mann–Whitney U test,  $U = 1$ ,  $p = 0.007$ ; Fig. 2D; Table 2 – No. 7–12).

### CircHIPK3 enhanced ROS production

To clarify the regulatory roles of circHIPK3 on oxidative stress in cells, ROS content was evaluated. In comparison to control cells, the cells treated with LPS exhibited significantly higher levels of ROS (Kruskal–Wallis test,  $H(4) = 27.87$ ,  $p < 0.001$ ; Dunn's post hoc test,  $p < 0.001$ ; Fig. 3A,B,F). The overexpression of circHIPK3 in transfection cells promoted significantly higher ROS levels (Dunn's post hoc test,  $p < 0.001$ ), while adding miR-124 mimic stopped the LPS-stimulated production of ROS (Fig. 3C,E,F). In contrast, the silencing of circHIPK3 drastically decreased the LPS-stimulated production of ROS (Dunn's post hoc test,  $p = 0.008$ ; Fig. 3D,F). These findings indicate that increases ROS levels in BV2 cells (Table 2 – No. 13).

### CircHIPK3 promoted microglial activation and pyroptosis through the activation of STAT3 signaling

The association of circHIPK3 with inflammation and the activation of microglia was explored through the overexpression or knocking down of circHIPK3 in BV2 cells following LPS stimulation for 12 h. In comparison to the control cells, LPS-stimulated cells exhibited significantly increased CD11b, Iba-1, pyroptosis-related factors, NLRP3, caspase-1, and ASC expression (CD11b: Kruskal–Wallis test,  $H(4) = 25.16$ ,  $p < 0.001$ ; Iba-1: Kruskal–Wallis test,  $H(4) = 24.13$ ,  $p < 0.001$ ; NLRP3: Kruskal–Wallis test,  $H(4) = 22.58$ ,  $p < 0.001$ ; caspase-1: Kruskal–Wallis test,  $H(4) = 24.13$ ,  $p < 0.001$ ; ASC: Kruskal–Wallis test,  $H(4) = 28.47$ ,  $p < 0.001$ ). The results of Dunn's post hoc test were  $p = 0.024$ ,  $p = 0.036$ ,  $p = 0.017$ ,  $p = 0.02$ , and  $p = 0.027$ , respectively. The upregulation of circHIPK3 further increased CD11b and Iba-1 expression as well as NLRP3, caspase-1 and ASC (Dunn's post hoc test:  $p = 0.018$ ,  $p = 0.009$ ,  $p = 0.019$ ,  $p = 0.034$ ,  $p = 0.016$ , respectively). The addition of miR-124 mimic reversed these effects. On the other hand, the LPS-induced expression of CD11b, Iba-1 and pyroptosis-related factors was dramatically reduced by the downregulation of circHIPK3 in LPS-treated cells (Dunn's post hoc test:  $p = 0.034$ ,  $p = 0.024$ ,  $p = 0.036$ ,  $p = 0.018$ ,  $p = 0.038$ , respectively; Fig. 4A–C). Last, we found that LPS stimulation significantly upregulated the expression of total STAT3 and p-STAT3 in comparison to control cells (STAT3: Kruskal–Wallis test,  $H(4) = 20.15$ ,  $p < 0.001$ ; p-STAT3: Kruskal–Wallis test,  $H(4) = 22.46$ ,  $p < 0.001$ ;

Table 1. Basic comparison between Parkinson's disease (PD) patients and controls

Demographic items	PD (n = 92)	Controls (n = 95)	$U/\chi^2$	p-value
Age	66.2 (60.1–71.5)	65.0 (60.0–69.2)	$U = 3659$	0.066
Sex (female/male)	38/54	40/55	$0.012$ (df = 1)	0.911
BMI [kg/cm <sup>2</sup> ]	21.7 (19.6–23.4)	22.5 (19.9–25.5)	$U = 3894$	0.103
Disease duration since first symptoms [months]	22.0 (15.9–29.5)	–	–	–

df – degrees of freedom; BMI – body mass index. Age, BMI and disease duration were expressed as median (interquartile range (IQR)).

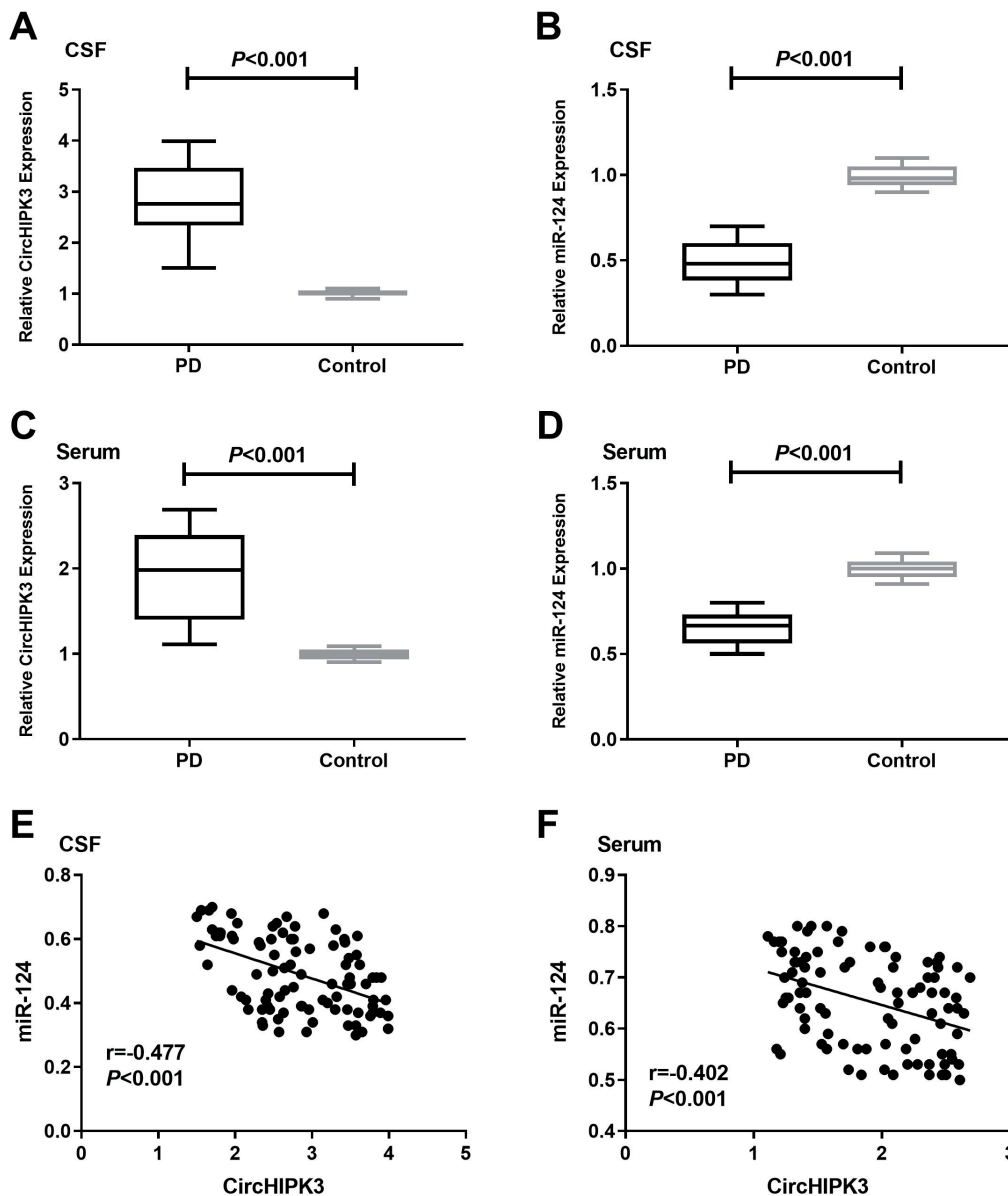


**Fig. 1.** A. Relative cerebrospinal fluid (CSF) circular RNA homeodomain interacting protein kinase 3 (circHIPK3) expression between Parkinson's disease (PD) patients and control group; B. Relative microRNA-124 (miR-124) expression between PD and control group; C. Relative serum circHIPK3 expression between PD and control group. Results were statistically analyzed using Mann–Whitney U test. Data were expressed as median, Q3 (75% percentile), Q1 (25% percentile), interquartile range (Q3–Q1), and minimum and maximum values; D. Relative serum miR-124 expression between PD and control group; E. Correlation of miR-124 and circHIPK3 expression in CSF; F. Correlation of miR-124 and circHIPK3 expression in serum. Results were statistically analyzed using Spearman's correlation

Dunn's post hoc test:  $p = 0.005$  and  $p = 0.008$ , respectively; Table 2 – No. 14–18). The overexpression of circHIPK3 further enhanced LPS-stimulated total STAT3 and p-STAT3 expression (Dunn's post hoc test:  $p = 0.036$ ,  $p = 0.021$ , respectively), while adding miR-124 mimic could reverse these effects. Silencing of circHIPK3 decreased the expression of total STAT3 and p-STAT3 expression compared to the LPS group (Dunn's post hoc test:  $p = 0.027$ ,  $p = 0.015$ , respectively; Fig. 4A,D; Table 2 – No. 19,20). Based on our results, we concluded that circHIPK3 exerted its promotive effect on the activation and pyroptosis of LPS-treated BV2 cells through the regulation of STAT3 signaling.

### CircHIPK3 promoted inflammatory cytokine levels in BV2 cells

As shown in Fig. 4, in comparison to the control cells, the cells after LPS treatment exhibited a significantly

enhanced expression of IL-6, IL-1 $\beta$  and TNF- $\alpha$  (IL-6: Kruskal–Wallis test,  $H(4) = 23.15$ ,  $p < 0.001$ ; IL-1 $\beta$ : Kruskal–Wallis test,  $H(4) = 29.18$ ,  $p < 0.001$ ; TNF- $\alpha$ : Kruskal–Wallis test,  $H(4) = 30.23$ ,  $p < 0.001$ ; Dunn's post hoc test:  $p = 0.005$ ,  $p = 0.008$ ,  $p = 0.004$ , respectively). Additionally, the secretion of IL-6, IL-1 $\beta$  and TNF- $\alpha$  stimulated by LPS was significantly enhanced and impaired by the overexpression of circHIPK3 and miR-124 mimic transfection, respectively (Dunn's post hoc test:  $p < 0.001$ ,  $p = 0.006$ ,  $p < 0.001$ , respectively). On the other hand, silencing circHIPK3 significantly decreased the production of IL-6, IL-1 $\beta$  and TNF- $\alpha$  stimulated by LPS (Dunn's post hoc test:  $p = 0.023$ ,  $p = 0.016$ ,  $p = 0.041$ , respectively; Fig. 5A–C; Table 2 – No. 21–23).

### STAT3 was the target gene of miR-124

To predict the potential targets and binding sites of miR-124, TargetScan (<http://www.targetscan.org>) was used.



Table 2. Statistical results

Comparison items	Statistical method	Statistical value	p-value
1. CircHIPK3 CSF (PD vs controls) (Fig. 1A)	Mann–Whitney U test	U = 0	<0.001
2. MiR-124 CSF (PD vs controls) (Fig. 1B)	Mann–Whitney U test	U = 0	<0.001
3. CircHIPK3 serum (PD vs controls) (Fig. 1C)	Mann–Whitney U test	U = 0	<0.001
4. MiR-124 serum (PD vs controls) (Fig. 1D)	Mann–Whitney U test	U = 0	<0.001
5. Correlation of circHIPK3 expression and miR-124 expressions in CSF (Fig. 1E)	Spearman's correlation	r = –0.447	<0.001
6. Correlation of circHIPK3 expression and miR-124 expressions in serum (Fig. 1F)	Spearman's correlation	r = –0.402	<0.001
7. CircHIPK3 expression between BV2 and LPS-induced BV2 (Fig. 2A)	Mann–Whitney U test	U = 0	0.002
8. MiR-124 expression between BV2 and LPS-induced BV2 (Fig. 2B)	Mann–Whitney U test	U = 0	0.004
9. CircHIPK3 expression between SH-SY5Y and SH-SY5Y+LPS BV2 (Fig. 2C)	Mann–Whitney U test	U = 0	0.002
10. MiR-124 expression between SH-SY5Y and SH-SY5Y+LPS BV2 (Fig. 2D)	Mann–Whitney U test	U = 1	0.007
11. MTT between SH-SY5Y and SH-SY5Y+LPS BV2 (Fig. 2E)	Mann–Whitney U test	U = 0	0.003
12. Apoptosis rate between SH-SY5Y and SH-SY5Y+LPS BV2 (Fig. 2H)	Mann–Whitney U test	U = 0	0.001
13. ROS production (Fig. 3F)	Kruskal–Wallis test	Kruskal–Wallis H statistic = 27.87	<0.001
14. CD11b protein expression (Fig. 4B)	Kruskal–Wallis test	Kruskal–Wallis H statistic = 25.16	<0.001
15. Iba-1 protein expression (Fig. 4B)	Kruskal–Wallis test	Kruskal–Wallis H statistic = 24.13	<0.001
16. NLRP3 protein expression (Fig. 4C)	Kruskal–Wallis test	Kruskal–Wallis H statistic = 22.58	<0.001
17. Caspase-1 protein expression (Fig. 4C)	Kruskal–Wallis test	Kruskal–Wallis H statistic = 29.16	<0.001
18. ASC protein expression (Fig. 4C)	Kruskal–Wallis test	Kruskal–Wallis H statistic = 28.47	<0.001
19. STAT3 protein expression (Fig. 4D)	Kruskal–Wallis test	Kruskal–Wallis H statistic = 20.15	<0.001
20. p-STAT3 protein expression (Fig. 4D)	Kruskal–Wallis test	Kruskal–Wallis H statistic = 22.46	<0.001
21. TNF- $\alpha$ ELISA (Fig. 5A)	Kruskal–Wallis test	Kruskal–Wallis H statistic = 23.15	<0.001
22. IL-1 $\beta$ ELISA (Fig. 5B)	Kruskal–Wallis test	Kruskal–Wallis H statistic = 29.18	<0.001
23. IL-6 ELISA (Fig. 5C)	Kruskal–Wallis test	Kruskal–Wallis H statistic = 30.23	<0.001
24. STAT3 WT relative luciferase activity (Fig. 6B)	Kruskal–Wallis test	Kruskal–Wallis H statistic = 19.55	<0.001
25. STAT3 MUT relative luciferase activity (Fig. 6B)	Kruskal–Wallis test	Kruskal–Wallis H statistic = 0.43	0.933
26. STAT3 mRNA expression (Fig. 6D)	Kruskal–Wallis test	Kruskal–Wallis H statistic = 19.59	<0.001
27. CircHIPK3 WT relative luciferase activity (Fig. 7B)	Kruskal–Wallis test	Kruskal–Wallis H statistic = 19.51	<0.001
28. CircHIPK3 MUT relative luciferase activity (Fig. 7B)	Kruskal–Wallis test	Kruskal–Wallis H statistic = 0.41	0.935
29. MiR-124 relative expression (Fig. 7D)	Kruskal–Wallis test	Kruskal–Wallis H statistic = 22.68	<0.001
30. MiR-124 RIP (Fig. 8B)	Kruskal–Wallis test	Kruskal–Wallis H statistic = 11.67	<0.001
31. CircHIPK3 RIP (Fig. 8B)	Kruskal–Wallis test	Kruskal–Wallis H statistic = 11.63	<0.001
32. MiR-124 RNA pull-down (Fig. 8C)	Mann–Whitney U test	U = 0	0.002
33. CircHIPK3 RNA pull-down (Fig. 8D)	Mann–Whitney U test	U = 0	0.002

CSF – cerebrospinal fluid; PD – Parkinson's disease; circHIPK3 – circRNA homeodomain interacting protein kinase 3; miR-124 – microRNA-124; LPS – lipopolysaccharide; ROS – reactive oxygen species; CD11b – cluster of differentiation molecule 11b; Iba-1 – ionized calcium-binding adapter molecule 1; NLRP3 – NLR family pyrin domain containing 3; ASC – apoptosis-associated speck-like protein containing C-terminal caspase recruitment domain; STAT3 – signal transducer and activator of transcription 3; p-STAT3 – phosphorylated STAT3; TNF- $\alpha$  – tumor necrosis factor alpha; ELISA – enzyme-linked immunosorbent assay; IL – interleukin; MTT – 3-(4,5-dimethyl-2-thiazolyl)-2,5-diphenyl-2-H-tetrazolium bromide; RIP – RNA-binding protein immunoprecipitation; MUT – mutant-type; WT – wild-type.

As shown in Fig. 6A, the potential binding sites between miR-124 and the 3'-UTR regions of STAT3 were found. The sequences of MUT-STAT-3'-UTR are shown in Fig. 6A. Luciferase demonstrated that in comparison to the control cells (Kruskal–Wallis test,  $H(3) = 19.55$ ,  $p < 0.001$ ), miR-124 mimic transfection significantly reduced the activity of luciferase (Dunn's post hoc test:  $p = 0.033$ ). Also,

the transfection of anta-miR-124 dramatically enhanced the luciferase activity in cells transfected with WT-STAT-3'-UTR (Dunn's post hoc test:  $p = 0.027$ ). However, no changes were observed among the group of cells transfected with MUT-STAT-3'-UTR, suggesting the direct interaction of miR-124 with the 3'UTR region of STAT3 (Fig. 6B). Western blot and qRT-PCR assays showed that

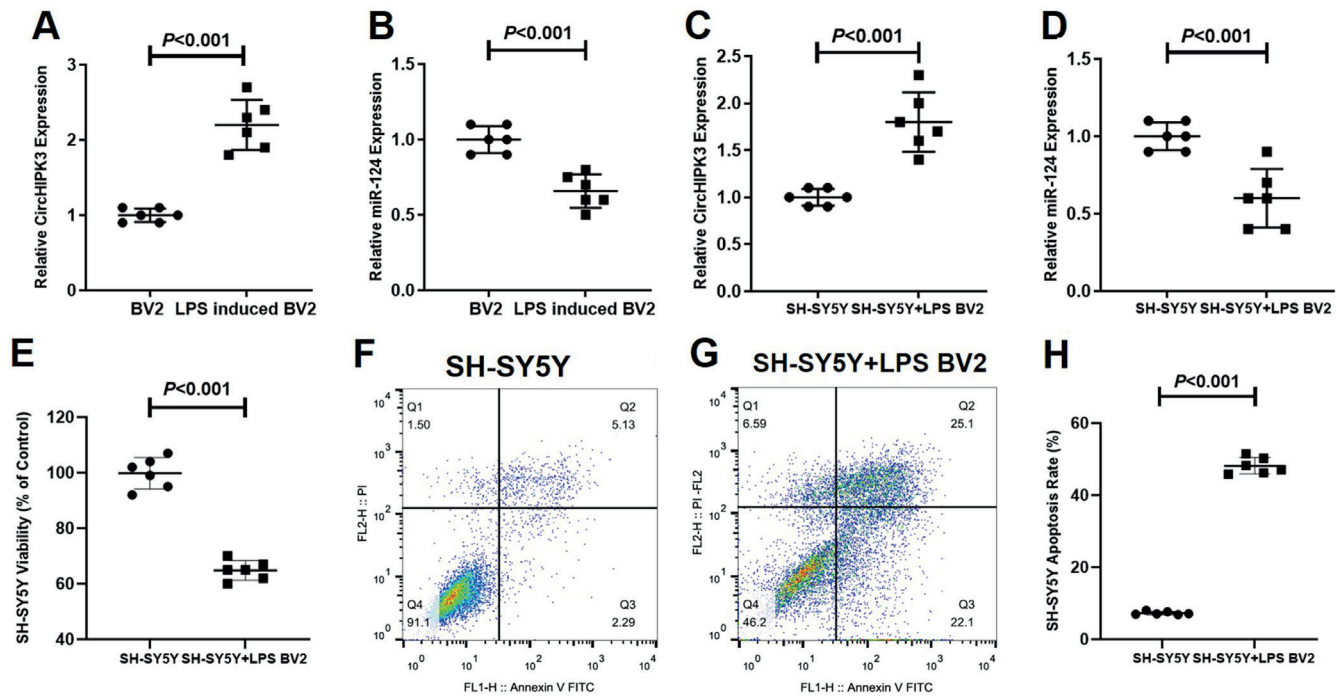


**Fig. 2.** A. Comparison of relative circular RNA homeodomain interacting protein kinase 3 (circHIPK3) expression between BV2 cells and lipopolysaccharide (LPS)-induced BV2 cells; B. Comparison of relative microRNA-124 (miR-124) expression between BV2 cells and LPS-induced BV2 cells; C. Comparison of relative circHIPK3 expression between SH-SY5Y cells with different treatments; D. Comparison of relative miR-124 expression between SH-SY5Y cells with different treatments; E. Comparison of SH-SY5Y cell viability between SH-SY5Y cells with different treatments; F. Representative figure of the apoptosis rate of SH-SY5Y cells; G. Representative figure of the apoptosis rate of SH-SY5Y cells adding conditioned LP2-BV2 medium; H. Comparison of the apoptosis rates between SH-SY5Y cells with different treatment. Results were statistically analyzed using Mann–Whitney U test. Data were expressed as data point plots, from the minimum to the maximum value ( $n = 6$ ) for each group. The interval represents the median value. The ends of the interval represent the interquartile range (IQR)

the overexpression of miR-124 inhibited the expression of STAT3 protein and mRNA (Kruskal–Wallis test,  $H(4) = 19.59$ ,  $p < 0.001$ ; Dunn's post hoc test:  $p = 0.030$ ), while miR-124-silenced cells exhibited an elevated STAT3 expression at mRNA and protein levels (Kruskal–Wallis test,  $H(4) = 19.59$ ,  $p < 0.001$ ; Dunn's post hoc test:  $p = 0.024$ ) (Fig. 6C,D).

### CircHIPK3 sponged miR-124 in LPS-induced BV2 cells

To elucidate whether circHIPK3 could act as a miR-124 sponge in LPS-induced BV2 cells, a prediction for the potential target miRNA of circHIPK3 was conducted using circBase (Fig. 7A). The relative activity of luciferase in the WT-circHIPK3 reporter-contained BV2 cells was significantly increased and reduced, respectively (Kruskal–Wallis test,  $H(3) = 19.51$ ,  $p < 0.001$ ) after miR-124 mimic (Dunn's post hoc test:  $p = 0.017$ ) and anta-miR-124 transfections (Dunn's post hoc test:  $p = 0.030$ , Fig. 7B), suggesting an interaction between circHIPK3 and miR-124. To explore the connection between circHIPK3 and the expression of miR-124, we overexpressed and silenced the expression of circHIPK3 in BV2 cells. Suppressed and elevated miR-124 expression in cells with circHIPK3 overexpression and silencing were observed in our northern blot results. Moreover, the expressions of circHIPK3 in circHIPK3-overexpressed (Kruskal–Wallis

test,  $H(3) = 19.51$ ,  $p < 0.001$ , Dunn's post hoc test:  $p = 0.025$ ) and circHIPK3-silenced cells (Dunn's post hoc test:  $p = 0.033$ ) were verified using qRT-PCR (Fig. 7D, Table 2 – No. 27–29).

To further verify the sponge between circHIPK3 and miR-124, a FISH experiment was conducted. As shown in Fig. 8A, the co-localization of circHIPK3 and miR-124 was discovered in BV2 cells. Moreover, in comparison to the IgG-treated control group, the argonaute RISC catalytic component 2 (Ago2) antibody-treated group exhibited dramatically elevated circHIPK3 and miR-124 expression (Fig. 8B, miR-124 RIP: Kruskal–Wallis test,  $H(2) = 11.67$ ,  $p < 0.001$ ; circHIPK3: Kruskal–Wallis test,  $H(2) = 11.63$ ,  $p < 0.001$ ; miR-124: Dunn's post hoc test,  $p = 0.008$ ; circHIPK3: Dunn's post hoc test:  $p = 0.006$ , respectively). The RNA pull-down results showed that miR-124 and circHIPK3 could pull down each other (miR-124: Mann–Whitney U test,  $U = 0$ ,  $p = 0.002$ ; circHIPK3: Mann–Whitney U test,  $U = 0$ ,  $p = 0.002$ , Fig. 8C,D), suggesting a direct sponge between miR-124 and circHIPK3 (Table 2 – No. 30–33).

## Discussion

Recently, researchers looking for a consensus opinion in regard to the pathogenesis of PD have been devoting more attention to the role of the inflammatory component.<sup>34</sup>

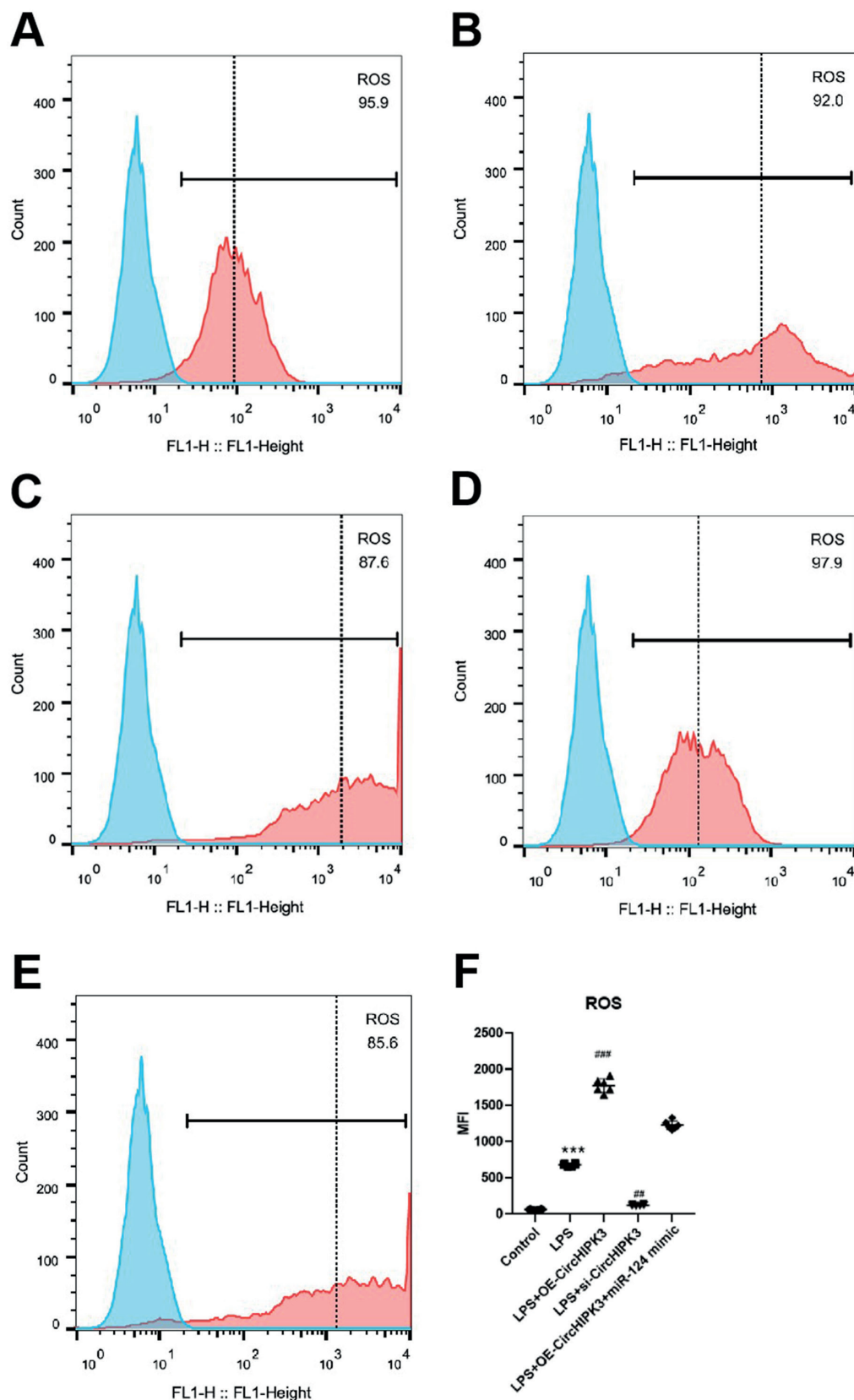


**Fig. 3.** Reactive oxygen species (ROS) production following circular RNA homeodomain interacting protein kinase 3 (circHIPK3) transfection.

A. Production of ROS in the control group; B. Production of ROS in the lipopolysaccharide (LPS) group; C. Production of ROS in the LPS+OE-circHIPK3 group; D. Production of ROS in the LPS+si-circHIPK3 group; E. Production of ROS in the LPS+OE-circHIPK3+microRNA-124 (miR-124) mimic group; F. Quantitative analysis of ROS production in each group (\*\**p* < 0.001 compared to the control group; ### *p* < 0.001 and ## *p* < 0.01 compared to the LPS group). Results were statistically analyzed using Kruskal–Wallis test followed by Dunn’s post hoc test. Data were expressed as data point plots, from the minimum to the maximum value (*n* = 6) for each group. The interval represents the median value. The ends of the interval represent the interquartile range (IQR)

MFI – mean fluorescence intensity; OE – overexpression; si – silencing.

Studies have demonstrated that PD is not only a neurodegenerative problem related to the progressive loss of dopamine but also a neuroinflammatory disease.<sup>35</sup> As a kind of programmed cell death, pyroptosis was associated with inflammatory responses dependent on caspase-1 and

activated by NLRP3.<sup>36</sup> It has been identified that the activation of pyroptosis was positively correlated with inflammatory cytokine production, which plays an important role in the pathogenesis of PD.<sup>37</sup> However, the process of pyroptosis regulation in PD remains poorly understood.

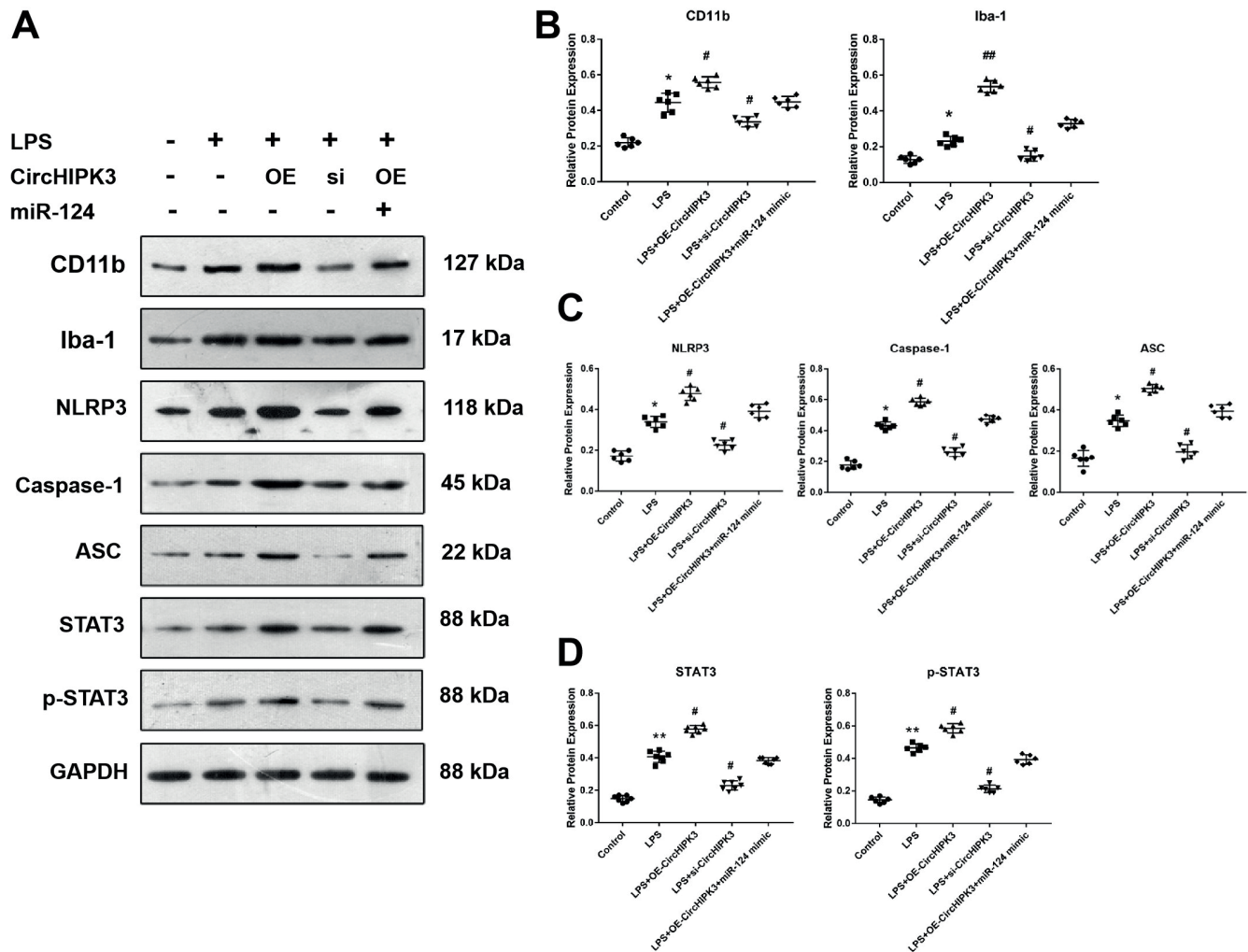


**Fig. 4.** Circular RNA homeodomain interacting protein kinase 3 (cirHIPK3) promoted microglial activation and pyroptosis through the activation of signal transducer and activator of transcription 3 (STAT3) signaling. **A.** Representative blots showing the production of cluster of differentiation molecule 11b (CD11b) and ionized calcium-binding adapter molecule 1 (Iba-1), pyroptosis-related factors, family pyrin domain containing 3 (NLRP3), caspase-1, apoptosis-associated speck-like protein containing C-terminal caspase recruitment domain (ASC), STAT3, and phosphorylated STAT3 (p-STAT3) in the cells after the indicated treatment; **B.** Expression of microglia markers CD11b and Iba-1 after the cirHIPK3 transfection; **C.** Expression of pyroptosis-related factors, NLRP3, caspase-1, and ASC after the cirHIPK3 transfection; **D.** Expression of STAT3 and p-STAT3 after the cirHIPK3 transfection (\*  $p < 0.05$  compared to control; #  $p < 0.05$  and ##  $p < 0.01$  compared to the lipopolysaccharide (LPS) group). Results were statistically analyzed using Kruskal–Wallis test followed by Dunn's post hoc test. Data were expressed as data point plots from the minimum to the maximum value ( $n = 6$ ) for each group. The interval represents the median value. The ends of the interval represent the interquartile range (IQR)

GAPDH – glyceraldehyde-3-phosphate dehydrogenase; OE – overexpression; si – silencing.

In the present study, we found that a novel circular RNA, cirHIPK3, was elevated in PD patients, LPS-induced BV2 cells and conditioned SH-SY5Y medium. Furthermore, our study suggested that cirHIPK3 is related to the activation and inflammation of LPS-induced BV2 microglia. Additionally, our study demonstrated that cirHIPK3 could directly interact with miR-124 and subsequently regulate the expression of STAT3, which is affected by miR-124, and activate the generation of a NLRP3 inflammasome. An accurately controlled expression of miR-124 was tightly connected with the neurogenesis, physiology and normal development of the CNS. Additionally, miR-124 participated in keeping  $\alpha$ -synuclein within a physiologic level. The association of dopaminergic neurodegeneration with significantly reduced expression of miR-124 in the brain

was observed in PD patients and PD-induced animals using 1-Methyl-4-phenyl-1,2,3,6-tetrahydropyridine (MPTP).<sup>38</sup> Furthermore, researchers discovered that miR-124 was significantly involved in the neuroinflammation involved in the pathogenesis of PD.<sup>39</sup> Therefore, the connection between cirHIPK3 and miR-124 in PD patients was explored. We observed a significantly decreased expression of miR-124 in PD patients, BV2 cells after LPS stimulation, and SH-SY5Y cells treated with CM collected from LPA-treated BV2 cells. Through bioinformatic analysis, the potential binding sites between miR-124 and cirHIPK3 were discovered and verified using a dual-luciferase assay. At the same time, a negative correlation between the expression of cirHIPK3 and miR-124 was observed, and the overexpression of miR-124 significantly reversed the expression



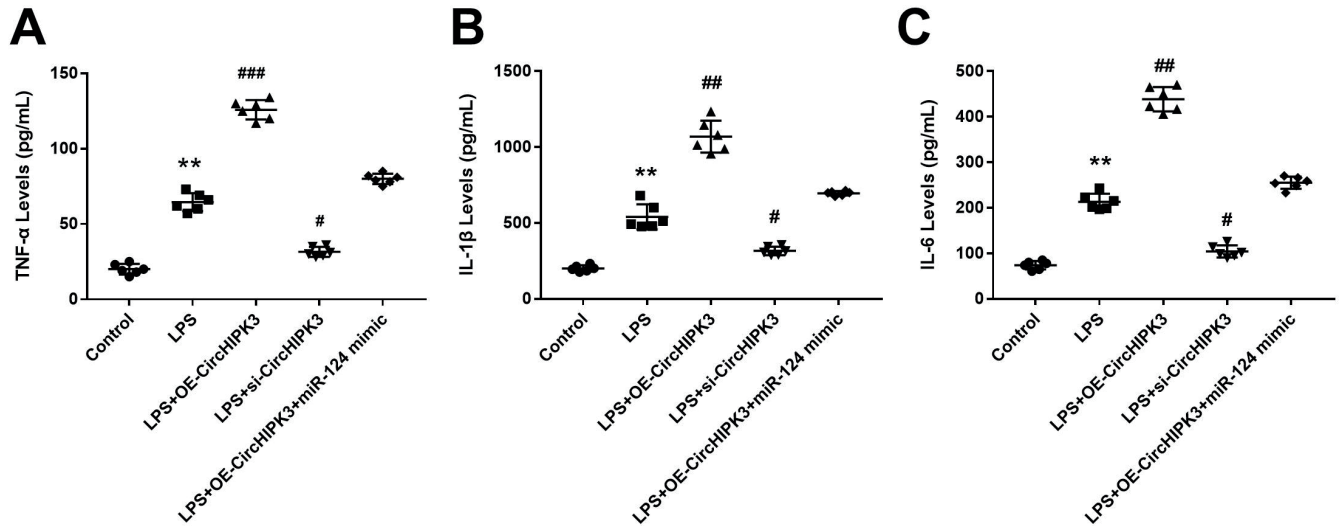


Fig. 5. Effect of circular RNA homeodomain interacting protein kinase 3 (circHIPK3) on the expression of inflammatory factors. A–C. Representative bar graphs showing the expression of tumor necrosis factor alpha (TNF-α) (A), interleukin (IL)-1β (B) and IL-6 (C) in cells after different treatments (\*\* p < 0.01 compared to the control group; # p < 0.05, ## p < 0.01 and ### p < 0.001 compared to the lipopolysaccharide (LPS) group). Results were statistically analyzed using Kruskal–Wallis test followed by Dunn’s post hoc test. Data were expressed as data point plots from the minimum to the maximum value (n = 6) for each group. The interval represents the median value. The ends of the interval represent the interquartile range (IQR)

OE – overexpression; si – silencing.

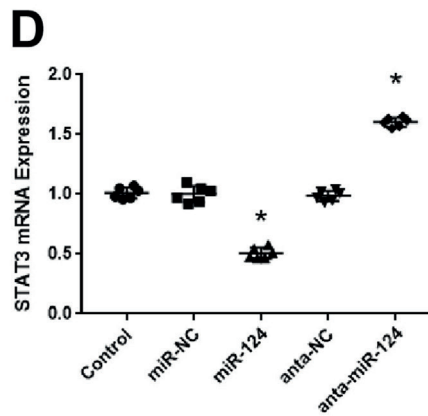
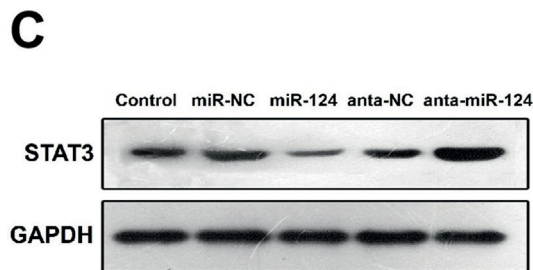
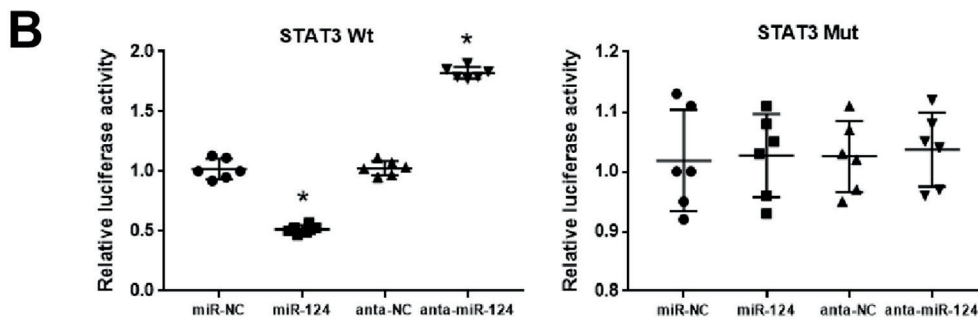
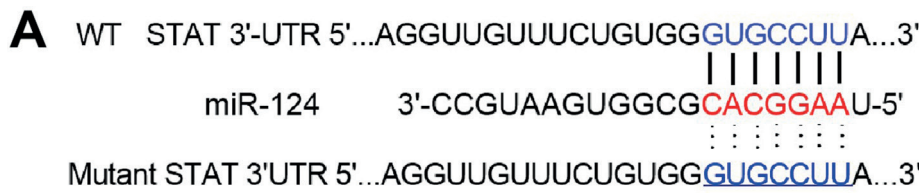
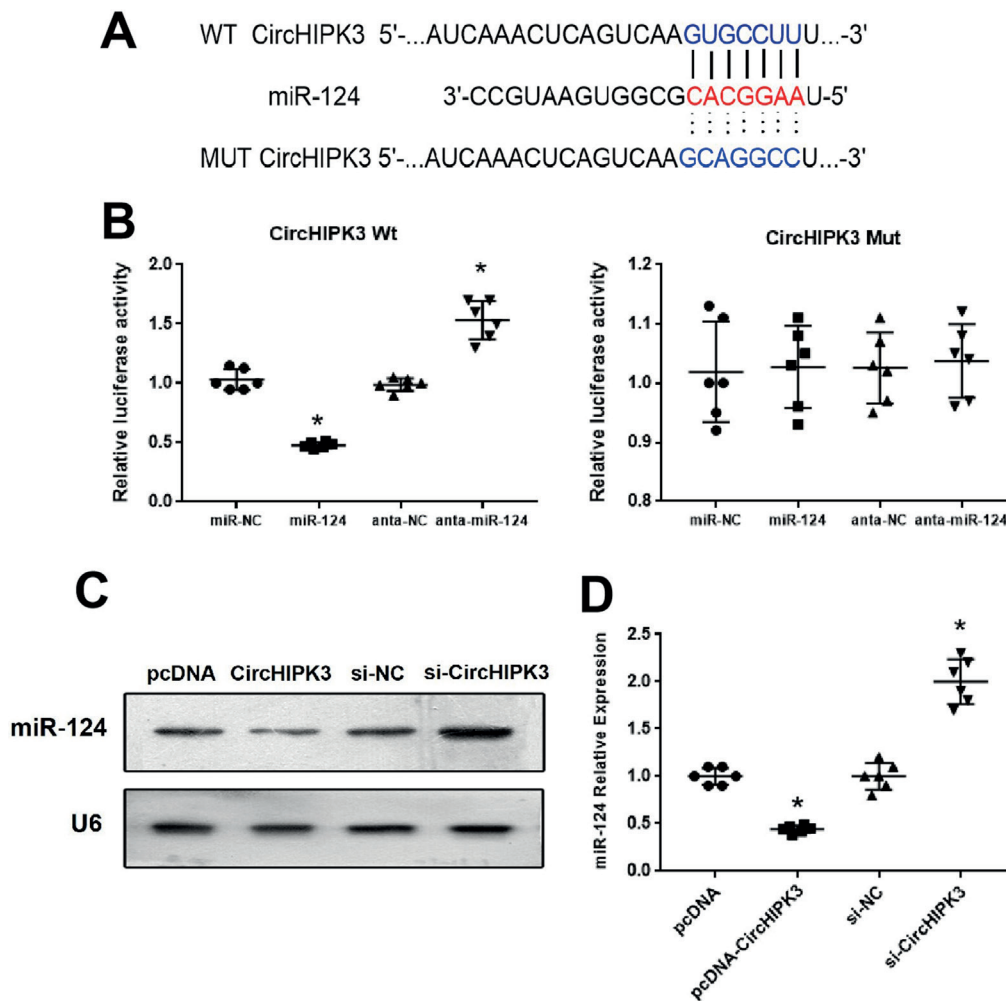


Fig. 6. MicroRNA-124 (miR-124) directly targeted signal transducer and activator of transcription 3 (STAT3). A. Binding sites of miR-124 with the 3'-UTR of STAT3 and the sequences of MUT-STAT3-3'-UTR; B. Relative luciferase activities of cells co-transfected with WT-STAT3-3'UTR or MUT-STAT3-3'-UTR with miR-124 mimic or miR-NC or anta-miR-124 or anta-NC (\* p < 0.05 compared to miR-NC); C. Representative western blot results showing the expression of STAT3 in cells with different treatments; D. Representative bar graph showing the mRNA levels of STAT3 after different transfections (\* p < 0.05 compared to controls). Results were statistically analyzed using Kruskal–Wallis test followed by Dunn’s post hoc test. Data were expressed as data point plots from the minimum to the maximum value (n = 6) for each group. The interval represents the median value. The ends of the interval represent the interquartile range (IQR)

GAPDH – glyceraldehyde-3-phosphate dehydrogenase; WT – wild-type; MUT – mutant-type; NC – negative control.

of circHIPK3-induced CD11b and Iba-1. On the other hand, the activation of STAT3 was observed in microglia after brain ischemia,<sup>40</sup> as well as in spinal cord microglia after nerve injury.<sup>41</sup> The activation of STAT3 was significantly

involved in the inflammatory responses and inflammation induced by thrombin in microglia in vitro.<sup>42</sup> The blockage of STAT3 pathway activation was associated with the suppression of neuroinflammation mediated by microglia.<sup>42</sup>



**Fig. 7.** The interaction between circular RNA homeodomain interacting protein kinase 3 (circHIPK3) and microRNA-124 (miR-124). **A.** Predicted binding site of circHIPK3 and miR-124; **B.** Representative bar graph showing the relative activities of luciferase in cells after the indicated transfection (\*  $p < 0.05$  compared to miR-negative control (miR-NC)); **C.** Representative northern blot results showing miR-124 expression in cells with the indicated treatment; **D.** Representative bar graph showing the mRNA levels of circHIPK3 in the cells after the indicated treatment (\*  $p < 0.05$  compared to plasmid cloning (pcDNA)). Results were statistically analyzed using Kruskal–Wallis test followed by Dunn's post hoc test. Data were expressed as data point plots from the minimum to the maximum value ( $n = 6$ ) for each group. The interval represents the median value. The ends of the interval represent the interquartile range (IQR) si – silencing.

We found that the overexpression of circHIPK3 increased the total STAT3 as well as p-STAT3 expression. In conclusion, our observations suggest that circHIPK3 exerts a promotive effect on the activation of microglia through impairing miR-124/STAT3/NLRP3 expression.

Reactive oxygen species are deeply involved in the development, expression and transduction of signals in cells.<sup>43</sup> However, an excessive production or accumulation of ROS in cells results in damage to cell membranes, DNA and protein molecules.<sup>44</sup> The cell death caused by excessive ROS production is activated by the mitochondrial apoptosis pathway.<sup>45</sup> Due to lower antioxidative enzymes and higher oxidative metabolism, neurons are more sensitive to ROS-induced cell death.<sup>46,47</sup> In recent years, oxidative stress and excessive ROS production were observed in the pathogenesis of PD and found to be significantly associated with the degeneration of dopaminergic neurons.<sup>48</sup> In vitro and in vivo studies have revealed that inflammatory responses and oxidative stress significantly participated in the activation of glial cells, as well as the subsequent damage to dopaminergic neurons.<sup>49</sup> Herein, we observed that the overexpression of circHIPK3 enhanced ROS production in LPS-stimulated BV2 cells, and adding miR-124 alleviated this effect. The circHIPK3 has been demonstrated to increase ROS production in other studies. For example,

the overexpression of circHIPK3 significantly promoted hypoxia/reoxygenation-induced cardiomyocyte cell injury by increasing intracellular ROS production.<sup>50</sup> In addition, silencing circHIPK3 partially impaired inflammation and oxidative injuries caused by LPS.<sup>51</sup>

## Limitations

There were several limitations of the present study that should be taken into account. First, we only detected the expression of circHIPK3 in PD patients. The investigation of other circRNAs may reveal much more information about non-coding RNAs in PD progression. Second, we only performed in vitro cell studies; thus, further in vivo animal studies are needed to verify this finding.

## Conclusions

We demonstrated that the circHIPK3 expression was increased in PD patients as well as LPS-induced BV2 cells. The circHIPK3 could promote the inflammatory response by sponging miR-124 and affecting the activation of STAT-3- and NLRP3-mediated inflammatory signaling pathways. In addition, circHIPK3 silencing decreased ROS

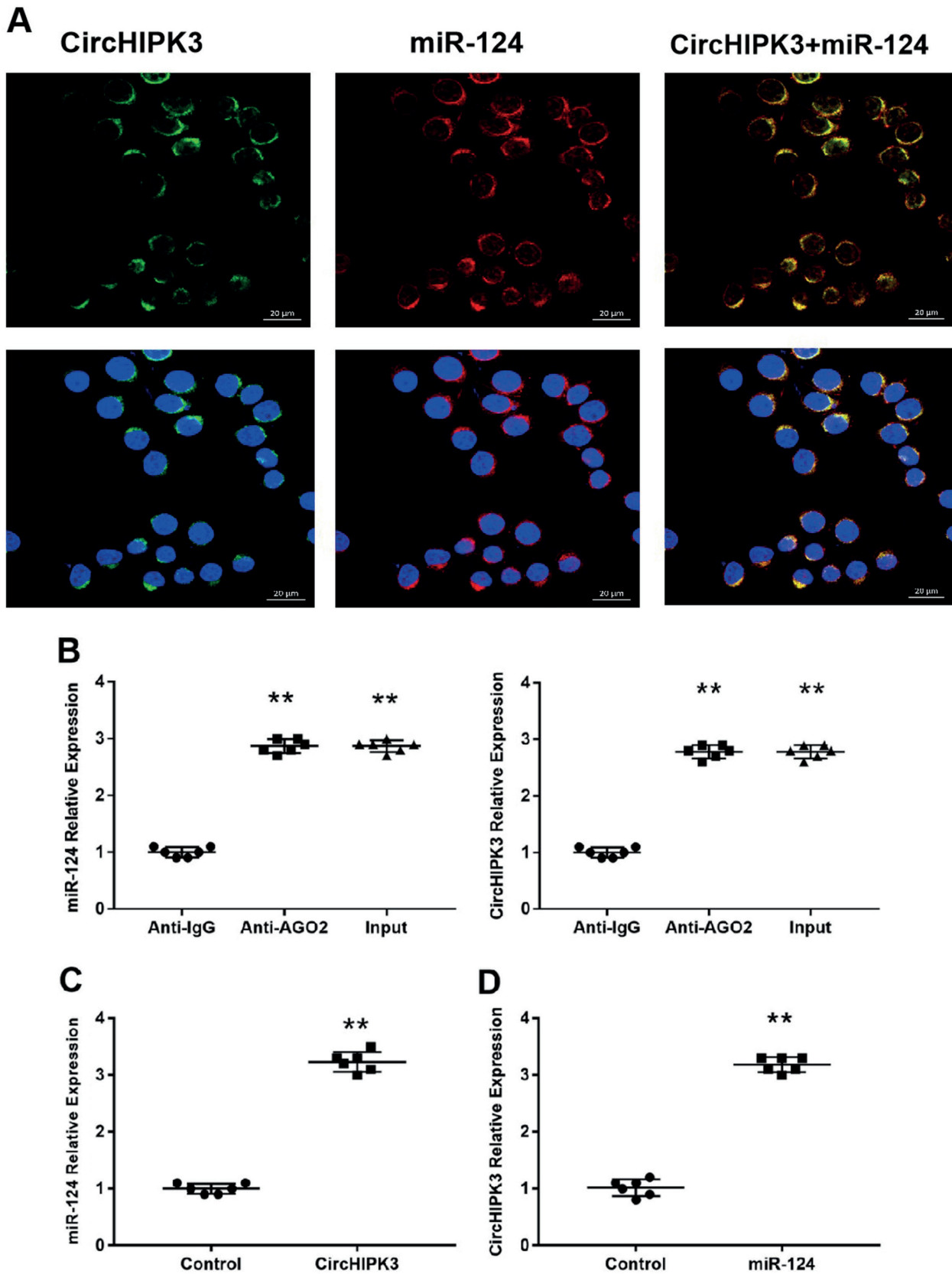


**Fig. 8.** A. Representative images showing the localization of circular RNA homeodomain interacting protein kinase 3 (circHIPK3) and microRNA-124 (miR-124) in BV2 cells (green: circHIPK3, red: miR-124, blue: 4',6-diamidino-2-phenylindole (DAPI), scale bar: 20  $\mu$ m); B. Representative summarized results showing the relative expression of miR-124 and circHIPK3 in cells after different treatments (\*\*  $p < 0.01$  compared to anti-immunoglobulin G (anti-IgG)). Results were statistically analyzed using Kruskal–Wallis test followed by Dunn’s post hoc test. Data were expressed as data point plots; C,D. Representative bar graphs showing the relative levels of miR-124 (C) and circHIPK3 (D) in pellets pulled down with circHIPK3 (C) and miR-124 (D), and their controls (\*\*  $p < 0.01$  compared to controls). Results were statistically analyzed using JMann–Whitney U test. Data were expressed as data point plots from the minimum to the maximum value ( $n = 6$ ) for each group. The interval represents the median value. The ends of the interval represent the interquartile range (IQR)

production. This study provides evidence that circHIPK3 functions as a miR-124 sponge to STAT3, and could be a potential target in the treatment of PD.

## Supplementary materials

The supplementary materials are available at <https://doi.org/10.5281/zenodo.7074360>. The package contains the following files:

Supplementary File. Results of normality and homogeneity tests for respective Figures.

Supplementary Table. Results of statistical tests.

## ORCID iDs

Yu-Juan Zhang  <https://orcid.org/0000-0003-0358-1691>

Wen-Kai Zhu  <https://orcid.org/0000-0002-5651-7709>

Fa-Ying Qi  <https://orcid.org/0000-0002-4046-6687>

Feng-Yuan Che  <https://orcid.org/0000-0001-6551-2072>

## References

- Jankovic J, Tan EK. Parkinson's disease: Etiopathogenesis and treatment. *J Neuro Neurol Psychiatry*. 2020;91(8):795–808. doi:10.1136/jnnp-2019-322338
- Antony PMA, Diederich NJ, Krüger R, Balling R. The hallmarks of Parkinson's disease. *FEBS J*. 2013;280(23):5981–5993. doi:10.1111/febs.12335
- Kalia LV, Lang AE. Parkinson's disease. *Lancet*. 2015;386(9996):896–912. doi:10.1016/S0140-6736(14)61393-3
- Gelders G, Baekelandt V, Van der Perren A. Linking neuroinflammation and neurodegeneration in Parkinson's disease. *J Immunol Res*. 2018;2018:4784268. doi:10.1155/2018/4784268
- Liu B, Gao HM, Hong JS. Parkinson's disease and exposure to infectious agents and pesticides and the occurrence of brain injuries: Role of neuroinflammation. *Environ Health Perspect*. 2003;111(8):1065–1073. doi:10.1289/ehp.6361
- Yan YQ, Fang Y, Zheng R, Pu JL, Zhang BR. NLRP3 inflammasomes in Parkinson's disease and their regulation by parkin. *Neuroscience*. 2020;446:323–334. doi:10.1016/j.neuroscience.2020.08.004
- Subhramanyam CS, Wang C, Hu Q, Dheen ST. Microglia-mediated neuroinflammation in neurodegenerative diseases. *Semin Cell Dev Biol*. 2019;94:112–120. doi:10.1016/j.semcdb.2019.05.004
- Xu L, He D, Bai Y. Microglia-mediated inflammation and neurodegenerative disease. *Mol Neurobiol*. 2016;53(10):6709–6715. doi:10.1007/s12035-015-9593-4
- Gustin A, Kirchmeyer M, Koncina E, et al. NLRP3 inflammasome is expressed and functional in mouse brain microglia but not in astrocytes. *PLoS One*. 2015;10(6):e0130624. doi:10.1371/journal.pone.0130624
- Chen LL, Yang L. Regulation of circRNA biogenesis. *RNA Biol*. 2015;12(4):381–388. doi:10.1080/15476286.2015.1020271
- Du WW, Zhang C, Yang W, Yong T, Awan FM, Yang BB. Identifying and characterizing circRNA-protein interaction. *Theranostics*. 2017;7(17):4183–4191. doi:10.7150/thno.21299
- Zhang Z, Yang T, Xiao J. Circular RNAs: Promising biomarkers for human diseases. *EBioMedicine*. 2018;34:267–274. doi:10.1016/j.ebiom.2018.07.036
- Zhang Y, Zhao Y, Liu Y, Wang M, Yu W, Zhang L. Exploring the regulatory roles of circular RNAs in Alzheimer's disease. *Transl Neurodegener*. 2020;9(1):35. doi:10.1186/s40035-020-00216-z
- Wang Y, Wang Y, Zhang H, He Z. The role of circular RNAs in brain and stroke. *Front Biosci (Landmark Ed)*. 2021;26(5):36. doi:10.52586/4923
- Kong F, Lv Z, Wang L, et al. RNA-sequencing of peripheral blood circular RNAs in Parkinson disease. *Medicine (Baltimore)*. 2021;100(23):e25888. doi:10.1097/MD.00000000000025888
- Kuo MC, Liu SCH, Hsu YF, Wu RM. The role of noncoding RNAs in Parkinson's disease: Biomarkers and associations with pathogenic pathways. *J Biomed Sci*. 2021;28(1):78. doi:10.1186/s12929-021-00775-x
- Hanan M, Simchovitz A, Yayon N, et al. A Parkinson's disease circRNAs resource reveals a link between circSLC8A1 and oxidative stress. *EMBO Mol Med*. 2020;12(9):e11942. doi:10.15252/emmm.201911942
- Kumar L, Shamsuzzama, Jadiya P, Haque R, Shukla S, Nazir A. Functional characterization of novel circular RNA molecule, circzip-2 and its synthesizing gene zip-2 in *C. elegans* model of Parkinson's disease. *Mol Neurobiol*. 2018;55(8):6914–6926. doi:10.1007/s12035-018-0903-5
- Ghosal S, Das S, Sen R, Basak P, Chakrabarti J. Circ2Traits: A comprehensive database for circular RNA potentially associated with disease and traits. *Front Genet*. 2013;10(4):283. doi:10.3389/fgene.2013.00283
- Zheng Q, Bao C, Guo W, et al. Circular RNA profiling reveals an abundant circHIPK3 that regulates cell growth by sponging multiple miRNAs. *Nat Commun*. 2016;7(1):11215. doi:10.1038/ncomms11215
- Lian C, Sun J, Guan W, et al. Circular RNA circHIPK3 activates macrophage NLRP3 inflammasome and TLR4 pathway in gouty arthritis via sponging miR-561 and miR-192. *Inflammation*. 2021;44(5):2065–2077. doi:10.1007/s10753-021-01483-2
- Fan S, Hu K, Zhang D, Liu F. Interference of circRNA HIPK3 alleviates cardiac dysfunction in lipopolysaccharide-induced mice models and apoptosis in H9C2 cardiomyocytes. *Ann Transl Med*. 2020;8(18):1147. doi:10.21037/atm-20-5306
- Wang L, Luo T, Bao Z, Li Y, Bu W. Intrathecal circHIPK3 shRNA alleviates neuropathic pain in diabetic rats. *Biochem Biophys Res Commun*. 2018;505(3):644–650. doi:10.1016/j.bbrc.2018.09.158
- Angelopoulos E, Paudel YN, Piperi C. miR-124 and Parkinson's disease: A biomarker with therapeutic potential. *Pharmacol Res*. 2019;150:104515. doi:10.1016/j.phrs.2019.104515
- Wang H, Ye Y, Zhu Z, et al. MiR-124 regulates apoptosis and autophagy process in MPTP model of Parkinson's disease by targeting to Bim. *Brain Pathol*. 2016;26(2):167–176. doi:10.1111/bpa.12267
- Li N, Pan X, Zhang J, et al. Plasma levels of miR-137 and miR-124 are associated with Parkinson's disease but not with Parkinson's disease with depression. *Neuro Sci*. 2017;38(5):761–767. doi:10.1007/s10072-017-2841-9
- Zhang F, Yao Y, Miao N, Wang N, Xu X, Yang C. Neuroprotective effects of microRNA 124 in Parkinson's disease mice. *Arch Gerontol Geriatr*. 2022;99:104588. doi:10.1016/j.archger.2021.104588
- Hillmer EJ, Zhang H, Li HS, Watowich SS. STAT3 signaling in immunity. *Cytokine Growth Factor Rev*. 2016;31:1–15. doi:10.1016/j.cytogfr.2016.05.001
- Przanowski P, Dabrowski M, Ellert-Miklaszewska A, et al. The signal transducers Stat1 and Stat3 and their novel target Jmjd3 drive the expression of inflammatory genes in microglia. *J Mol Med*. 2014;92(3):239–254. doi:10.1007/s00109-013-1090-5
- Tanaka S, Ishii A, Ohtaki H, Shioda S, Yoshida T, Numazawa S. Activation of microglia induces symptoms of Parkinson's disease in wild-type, but not in IL-1 knockout mice. *J Neuroinflammation*. 2013;10(1):907. doi:10.1186/1742-2094-10-143
- Jiang Q, Tang G, Zhong X, Ding D, Wang H, Li J. Role of Stat3 in NLRP3/caspase-1-mediated hippocampal neuronal pyroptosis in epileptic mice. *Synapse*. 2021;75(12):e22221. doi:10.1002/syn.22221
- Hirsch EC, Hunot S. Neuroinflammation in Parkinson's disease: A target for neuroprotection? *Lancet Neurol*. 2009;8(4):382–397. doi:10.1016/S1474-4422(09)70062-6
- Kustrimovic N, Marino F, Cosentino M. Peripheral immunity, immunaging and neuroinflammation in Parkinson's disease. *Curr Med Chem*. 2019;26(20):3719–3753. doi:10.2174/0929867325666181009161048
- Pajares M, I. Rojo IA, Manda G, Boscá L, Cuadrado A. Inflammation in Parkinson's disease: Mechanisms and therapeutic implications. *Cells*. 2020;9(7):1687. doi:10.3390/cells9071687
- Lünemann JD, Malhotra S, Shinohara ML, Montalban X, Comabella M. Targeting inflammasomes to treat neurological diseases. *Ann Neurol*. 2021;90(2):177–188. doi:10.1002/ana.26158
- Hirsch EC, Vyas S, Hunot S. Neuroinflammation in Parkinson's disease. *Parkinsonism Relat Disord*. 2012;18:S210–S212. doi:10.1016/S1353-8020(11)70065-7
- Tansey MG, Goldberg MS. Neuroinflammation in Parkinson's disease: Its role in neuronal death and implications for therapeutic intervention. *Neurobiol Dis*. 2010;37(3):510–518. doi:10.1016/j.nbd.2009.11.004
- Kanagaraj N, Beiping H, Dheen ST, Tay SSW. Downregulation of miR-124 in MPTP-treated mouse model of Parkinson's disease and MPP iodide-treated MN9D cells modulates the expression of the calpain/cdk5 pathway proteins. *Neuroscience*. 2014;272:167–179. doi:10.1016/j.neuroscience.2014.04.039



39. Liu F, Qiu F, Chen H. miR-124-3p ameliorates isoflurane-induced learning and memory impairment via targeting STAT3 and inhibiting neuroinflammation. *Neuroimmunomodulation*. 2021;28(4):248–254. doi:10.1159/000515661
40. Planas AM, Soriano MA, Berrueto M, et al. Induction of Stat3, a signal transducer and transcription factor, in reactive microglia following transient focal cerebral ischaemia. *Eur J Neurosci*. 1996;8(12):2612–2618. doi:10.1111/j.1460-9568.1996.tb01556.x
41. Lindborg JA, Tran NM, Chenette DM, et al. Optic nerve regeneration screen identifies multiple genes restricting adult neural repair. *Cell Rep*. 2021;34(9):108777. doi:10.1016/j.celrep.2021.108777
42. Huang C, Ma R, Sun S, et al. JAK2-STAT3 signaling pathway mediates thrombin-induced proinflammatory actions of microglia in vitro. *J Neuroimmunol*. 2008;204(1–2):118–125. doi:10.1016/j.jneuroim.2008.07.004.
43. Kolodkin A, Sharma RP, Colangelo AM, et al. ROS networks: Designs, aging, Parkinson's disease and precision therapies. *NPJ Syst Biol Appl*. 2020;6(1):34. doi:10.1038/s41540-020-00150-w
44. Zorov DB, Juhaszova M, Sollott SJ. Mitochondrial reactive oxygen species (ROS) and ROS-induced ROS release. *Physiol Rev*. 2014;94(3):909–950. doi:10.1152/physrev.00026.2013
45. Sinha K, Das J, Pal PB, Sil PC. Oxidative stress: The mitochondria-dependent and mitochondria-independent pathways of apoptosis. *Arch Toxicol*. 2013;87(7):1157–1180. doi:10.1007/s00204-013-1034-4
46. Vicente-Gutiérrez C, Jiménez-Blasco D, Quintana-Cabrera R. Intertwined ROS and metabolic signaling at the neuron-astrocyte interface. *Neurochem Res*. 2021;46(1):23–33. doi:10.1007/s11064-020-02965-9
47. Kennedy KAM, Sandiford SDE, Skerjanc IS, Li SSC. Reactive oxygen species and the neuronal fate. *Cell Mol Life Sci*. 2012;69(2):215–221. doi:10.1007/s00018-011-0807-2
48. Guo J, Zhao X, Li Y, Li G, Liu X. Damage to dopaminergic neurons by oxidative stress in Parkinson's disease (review). *Int J Mol Med*. 2018;41(4):1817–1825. doi:10.3892/ijmm.2018.3406
49. Miller RL, James-Kracke M, Sun GY, Sun AY. Oxidative and inflammatory pathways in Parkinson's disease. *Neurochem Res*. 2009;34(1):55–65. doi:10.1007/s11064-008-9656-2
50. Qiu Z, Wang Y, Liu W, et al. CircHIPK3 regulates the autophagy and apoptosis of hypoxia/reoxygenation-stimulated cardiomyocytes via the miR-20b-5p/ATG7 axis. *Cell Death Discov*. 2021;7(1):64. doi:10.1038/s41420-021-00448-6
51. Fan S, Hu K, Zhang D, Liu F. Interference of circRNA HIPK3 alleviates cardiac dysfunction in lipopolysaccharide-induced mice models and apoptosis in H9C2 cardiomyocytes. *Ann Transl Med*. 2020;8(18):1147–1147. doi:10.21037/atm-20-5306



# Prevalence and factors predisposing to potential drug–drug interactions in a Polish community-dwelling geriatric population: An observational, cross-sectional study

Emilia Bleszyńska-Marunowska<sup>1,A–D,F</sup>, Łukasz Wierucki<sup>2,A–C,F</sup>, Kacper Jagiełło<sup>2,B,C,F</sup>,  
Krzysztof Rewiuk<sup>3,E,F</sup>, Katarzyna Mitrega<sup>4,E,F</sup>, Zbigniew Kalarus<sup>5,E,F</sup>

<sup>1</sup> Department of Occupational, Metabolic and Internal Diseases, Medical University of Gdańsk, Poland

<sup>2</sup> Department of Preventive Medicine and Education, Medical University of Gdańsk, Poland

<sup>3</sup> Department of Internal Medicine and Gerontology, Jagiellonian University Medical College, Kraków, Poland

<sup>4</sup> Department of Cardiology, Silesian Center for Heart Diseases, Zabrze, Poland

<sup>5</sup> Division of Medical Sciences in Zabrze, Medical University of Silesia, Katowice, Poland

A – research concept and design; B – collection and/or assembly of data; C – data analysis and interpretation;  
D – writing the article; E – critical revision of the article; F – final approval of the article

Advances in Clinical and Experimental Medicine, ISSN 1899–5276 (print), ISSN 2451–2680 (online)

*Adv Clin Exp Med.* 2023;32(3):331–339

## Address for correspondence

Emilia Bleszyńska-Marunowska  
E-mail: e.bleszynska@gumed.edu.pl

## Funding sources

The study was funded by the National Centre for Research and Development under a grant agreement (No. STRATEGMED2/269343/18/NCBR/2016).

## Conflict of interest

None declared

Received on May 14, 2022

Reviewed on August 13, 2022

Accepted on September 15, 2022

Published online on October 12, 2022

## Cite as

Bleszyńska-Marunowska E, Wierucki Ł, Jagiełło K, Rewiuk K, Mitrega K, Kalarus Z. Prevalence and factors predisposing to potential drug–drug interactions in a Polish community-dwelling geriatric population: An observational, cross-sectional study. *Adv Clin Exp Med.* 2023;32(3):331–339. doi:10.17219/acem/154624

## DOI

10.17219/acem/154624

## Copyright

Copyright by Author(s)

This is an article distributed under the terms of the Creative Commons Attribution 3.0 Unported (CC BY 3.0) (<https://creativecommons.org/licenses/by/3.0/>)

## Abstract

**Background.** Due to advanced age, multimorbidity and polypharmacotherapy, older patients are predisposed to drug interactions and the adverse effects of inappropriate drug combinations.

**Objectives.** To provide up-to-date data on predisposing factors and the prevalence of possible drug interactions in the Polish geriatric population and to promote automated analysis programs as part of safe pharmacotherapy.

**Materials and methods.** We used the Lexicomp® Drug Interactions database to assess pharmacological interactions between active substances included in all types of preparations (prescription drugs, over-the-counter drugs, vitamins, nutritional preparations, and dietary supplements) used at least once in the 2 weeks preceding the study, among 2633 home-dwelling people aged >65 years. The variables measured included age, sex, place of residence, level of education, and multimorbidity. Post-stratification was used to weigh the sample structure against the Polish population in 2017.

**Results.** Drug interactions were identified in 81.2% of all individuals. The mean number (with 95% confidence interval (95% CI)) of all drug interactions was 4.24 (4.02–4.46), and the median value (with 1<sup>st</sup> and 3<sup>rd</sup> quartiles (Q1–Q3)) was 3 (1–6). At least 1 category C interaction was observed in 75.8% of all study participants, 24.3% had 1 or more category D interaction, and 4.3% had 1 or more category X interaction. The most important predisposing factor to drug interactions was multimorbidity.

**Conclusions.** This study identified a high prevalence of potential drug interactions in the Polish geriatric population. Automated analysis systems deliver useful information on pharmacological interactions and should be promoted in the Polish healthcare community as tools to support pharmacotherapy.

**Key words:** polypharmacy, geriatric, drug interactions, multimorbidity, medication errors, medical error prevention, control

## Background

A pharmacological interaction is an interaction of 2 drugs that can lead to a quantitative and/or qualitative change in the action of one of them.<sup>1</sup> Older adults are particularly prone to adverse drug interactions due to advanced age, multimorbidity and polypharmacy.<sup>2</sup> Of pertinent concern is the growing interest among older adults in over-the-counter drugs, which are widely advertised on the pharmaceutical market.<sup>3</sup> Properly conducted pharmacotherapy increases the likelihood of achieving the desired therapeutic effect and improving quality of life by avoiding the side effects associated with improperly combined preparations.<sup>4–6</sup> Appropriate pharmacotherapy is also associated with a decreased risk of rehospitalization<sup>7</sup> and death,<sup>8</sup> which reduces the financial burden on the healthcare system.<sup>2</sup> The cost of iatrogenic pharmacotherapy errors in Europe (11–38% of which are avoidable) has been estimated between €290 and €850 million per year.<sup>9–11</sup> Data from the USA also indicate high financial expenditure (\$200 billion per year) to treat the side effects of pharmacotherapy in people over 65 years of age.<sup>12</sup> Therefore, knowledge about the prevalence of pharmacological interactions in older patients, as well as the preventive methods available, is very important in terms of clinical practice and the efficient functioning of the healthcare system.

The topics of polypharmacy and pharmacological interactions have been analyzed extensively in Western Europe and the USA, but data from Central and Eastern Europe are limited. Most of the previous studies were conducted in the inpatient setting and were based on the Beers criteria,<sup>13</sup> the Screening Tool of Older Persons' potentially inappropriate Prescriptions (STOPP) criteria, the Screening Tool to Alert doctors to the Right Treatment (START) criteria,<sup>14</sup> or the Fit OR The Aged (FORTA) list.<sup>15</sup> The percentage of inappropriate drug combinations in European studies ranges from 9.8% to 38.5%, while it is 21.3% to 28.8% in the USA.<sup>16–19</sup>

Automated interaction analysis systems are a solution that could increase the recognition of drug interactions. Along with the computerization of healthcare systems, various forms of dedicated programs are available worldwide, such as online tools, applications for mobile telephone devices and software modules, even as part of a medical information network (e.g., the Surescripts network in the USA).<sup>20–23</sup> However, no such solution has yet been introduced on a national level in the Polish healthcare system.

## Objectives

This study was performed to provide up-to-date data on the predisposing factors and prevalence of possible drug interactions in the Polish geriatric population. In addition, we aimed to popularize automated interaction analysis systems as auxiliary tools for conducting safe pharmacotherapy.

## Materials and methods

### Ethics approval

All participants provided written informed consent prior to participation in the study. The study was approved by the Independent Bioethics Committee for Scientific Research at the Medical University of Gdańsk (approval No. 13/2020; 2020-04-21) and the Bioethics Commission at the Silesian Medical Chamber in Katowice (approval No. 26/2015; 2015-07-01). The study was conducted in compliance with the Declaration of Helsinki.

### Study design

The study group consisted of participants from the nationwide, cross-sectional observational study NONinvasive Monitoring for Early Detection of Atrial Fibrillation (NOMED-AF). The main objective of the NOMED-AF study was to evaluate the prevalence of atrial fibrillation and its associated comorbidities. It included electrocardiographic monitoring, completion of a detailed questionnaire, a follow-up survey, blood pressure measurements, and blood/urine sample collection. A detailed description of the methodology and sampling of the NOMED-AF study was presented in a separate publication.<sup>24</sup>

### Setting

The study was conducted from March 2017 to March 2019. Respondents were selected randomly by the Ministry of Digitization of the Republic of Poland based on a social security number database; therefore, they constituted a representative sample for Poland in terms of sex, age and place of residence. Based on a detailed questionnaire, the data were obtained by a trained nurse directly from the respondents, their families or their caregivers, followed by a presentation of the packaging of all of their drugs. The interview covered all preparations (prescription drugs, over-the-counter drugs, vitamins, nutritional preparations, and dietary supplements) taken at least once in the 2 weeks preceding the study (including drug name, form, single dose, and dosing frequency). The respondents provided information on diagnosed chronic diseases and were asked to present discharge cards from previous hospitalizations. Based on these data, individuals were assigned codes from the International Classification of Diseases, 10<sup>th</sup> Revision (ICD-10).

### Participants and sample size

The specific inclusion criteria for this study were the use of at least 2 active substances included in the preparations and an agreement to provide information on the drugs taken. The study group comprised 2633 respondents aged  $\geq 65$  years, and consisted of 1309 women and



1324 men. The mean  $\pm$  standard deviation ( $M \pm SD$ ) age of the entire sample was 78.0 ( $\pm 7.9$ ) years (78.9 ( $\pm 7.9$ ) years for women and 78.0 ( $\pm 7.8$ ) years for men).

## Variables

The analysis of drug interactions between active substances was performed using Lexicomp® Drug Interactions by Wolters Kluwer Clinical Drug Information ([www.wolterskluwer.com/en/solutions/lexicomp/](http://www.wolterskluwer.com/en/solutions/lexicomp/)), which enables a simultaneous analysis of 50 active substances. Detected interactions are classified into one of the 5 categories: A – no known interaction; B – no action required; C – monitor therapy; D – consider modifying therapy; X – avoid combination.

A further analysis of the detected drug interactions was based on the following variables: sex (male, female), age (in cohorts: 65–69, 70–74, 75–79, 80–84, 85–89,  $\geq 90$  years old), place of residence (village, small city with less than 50,000 inhabitants, medium-sized city with 50,000–200,000 inhabitants, large city with more than 200,000 inhabitants), level of education (primary, secondary/vocational, higher) and multimorbidity (determined using the Charlson Comorbidity Index (CCI)).

Qualitative analysis of pharmacotherapy was performed according to the Anatomical Therapeutic Chemical (ATC) classification.<sup>25</sup> The 2 most commonly used definitions were applied: taking 5 or more drugs was considered polypharmacy (PP), while excessive polypharmacy (EPP) was defined as taking more than 10 drugs.<sup>26</sup>

## Statistical analyses

Post-stratification was used to adjust the sample structure against the Polish population in 2017. Data normality was verified using the Shapiro–Wilk test. The results are presented as percentages and median values with 1<sup>st</sup> and 3<sup>rd</sup> quartiles (Q1–Q3). A simple single-factor analysis based on the  $\chi^2$  test was performed in order to assess the relationship between one variable in relation to another. Multivariate logistic regression was performed for the whole set of variables, and odds ratios (ORs) were calculated together with 95% confidence intervals (95% CIs). The quality of the overall regression models was measured using Nagelkerke's  $R^2$ , and p-values for the models were calculated. A value of  $p < 0.05$  was considered statistically significant. The analysis was performed using the statistical package R v. 3.6.3 (R Foundation for Statistical Computing, Vienna, Austria) and SAS v. 9.4 TS Level 1M5 (SAS Institute, Inc., Cary, USA).

## Results

The obtained results were stratified according to age structure in order to reflect the distribution of the Polish population over 65 years old in 2017; therefore, they reflect

the geriatric population of Poland. A detailed description of the sampling and subsequent weighing can be found in the methodological publication.<sup>24</sup>

## Analyses of all drug interactions

### Number of drug interactions

At least 1 drug interaction was found in 81.2% of all individuals aged  $\geq 65$  years, with a median value of 3 (Q1–Q3: 1–6). Most often, older adults had 1–4 interactions (47.6%). At least 5 interactions were found in 33.7% of all respondents, more than 10 interactions in 12.3% of participants, and 4.7% of seniors had  $\geq 15$  interactions. Detailed data are presented in Table 1,2.

### Drug interactions and number of drugs

The median value of interactions and the frequency of multiple interactions (5, 10 and 15) increased with the number of medications taken. Detailed data are presented in Table 1,2. A single-factor analysis showed a significant correlation between the number of interactions and the number of drugs taken ( $p < 0.001$ ).

### Drug interactions and sex

The median value of interactions was higher in men than in women: 3 (Q1–Q3: 1–7) and 2 (Q1–Q3: 1–6), respectively. Detailed data are presented in Table 1,2. The multivariate logistic regression model also showed that being male predisposed the participants to having  $\geq 10$  interactions ( $p < 0.05$ ) (Table 3–5). The Nagelkerke's  $R^2$  values for all 3 multivariate logistic regression models were relatively small.

### Drug interactions and age

The median value of all interactions was the highest among seniors aged 85–89 years. The frequency of multiple interactions (5, 10 and 15) increased with age. Detailed data are presented in Table 1,2. A single-factor analysis showed a significant positive correlation between the number of interactions and age ( $p < 0.001$ ); however, this was not confirmed by the multivariate logistic regression model (Table 3–5).

### Drug interactions and place of residence

There were no noticeable differences in the median value of all interactions in relation to the place of residence. People living in rural areas had a lower frequency of multiple drug interactions (5, 10 and 15) than those living in urban areas. Detailed data are presented in Table 1,2. A single-factor analysis showed a significant correlation between the number of interactions and place of residence ( $p < 0.001$ ); however, this was not confirmed by the multivariate logistic regression model (Table 3–5).

**Table 1.** Percentage of older people with drug interactions by gender (%)

Variable	All					Women					Men				
	number of all interactions					number of all interactions					number of all interactions				
	0	1-4	5-9	10-14	≥15	0	1-4	5-9	10-14	≥15	0	1-4	5-9	10-14	≥15
All	18.8	47.6	21.4	7.6	4.7	21.1	47.0	21.5	6.3	4.0	15.1	48.5	21.2	9.6	5.7
Age [years]															
65-69	25.0	48.4	18.0	5.5	3.1	30.8	47.4	17.8	2.9	1.1	17.2	49.5	18.4	9.0	5.8
70-74	22.7	45.7	19.8	6.9	4.9	26.5	44.5	18.7	6.1	4.2	17.2	47.5	21.3	8.0	6.0
75-79	12.9	47.9	25.0	9.1	5.1	14.3	47.7	25.1	7.3	5.6	10.6	48.3	25.0	11.8	4.4
80-84	13.8	48.5	22.7	9.4	5.6	13.2	47.6	25.4	9.5	4.3	15.2	50.2	17.1	9.2	8.4
85-89	8.8	50.4	26.2	9.1	5.5	7.3	50.8	27.3	8.4	6.2	12.4	49.3	23.7	10.7	4.0
90+	19.2	42.2	23.1	8.8	6.7	22.8	44.2	17.7	7.4	7.9	7.1	35.5	41.1	13.4	2.8
Number of drugs															
2-4	46.7	52.7	0.6	0.0	0.0	49.6	50.1	0.3	0.0	0.0	41.4	57.4	1.2	0.0	0.0
5-9	4.7	54.1	32.7	7.4	1.1	5.7	53.9	33.6	5.9	0.8	3.1	54.4	31.3	9.5	1.6
10+	0.0	3.6	31.6	30.6	34.2	0.0	4.7	33.9	28.9	32.5	0.0	2.1	28.5	32.9	36.6
Education															
Primary	15.0	49.0	22.0	9.7	4.4	15.6	48.8	22.4	8.4	4.8	13.6	49.4	21.1	12.5	3.4
Secondary/vocational	21.1	45.5	21.8	6.8	4.9	25.0	43.8	21.7	5.4	4.1	15.4	47.8	21.9	8.9	6.0
Higher	19.3	52.2	18.9	5.1	4.5	22.7	55.4	18.0	3.0	0.9	15.9	49.1	19.7	7.1	8.2
Residence															
Village	15.9	51.2	20.9	8.3	3.6	17.2	50.8	19.8	8.3	4.0	13.9	51.8	22.7	8.5	3.1
City <50 M	21.4	45.2	22.3	7.3	3.8	23.5	47.4	22.6	4.5	2.0	17.8	41.5	21.7	11.9	7.0
City 50-200 M	21.6	42.9	21.9	9.1	4.5	25.4	41.1	22.2	8.0	3.2	15.1	46.0	21.4	10.9	6.7
City >200 M	18.3	48.0	21.0	5.5	7.2	21.2	45.3	22.6	3.9	7.0	14.0	52.1	18.4	7.8	7.7

M – 1000. The results consider the use of a complex scheme of randomizing respondents. The data are presented after weighing the sample in relation to the structure of the Polish population aged 65 and over in 2017.

**Table 2.** Number of all drug interactions

Variable	Sample size, n			Median value (Q1-Q3)		
	women	men	all	women	men	all
All	1309	1324	2633	2 (1-6)	3 (1-7)	3 (1-6)
Age [years]						
65-69	226	218	444	1 (0-4)	3 (1-6)	2 (1-5)
70-74	273	257	530	2 (0-5)	3 (1-7)	2 (1-6)
75-79	243	285	528	3 (1-6)	4 (1-7)	3 (1-7)
80-84	255	228	483	4 (1-7)	3 (1-7)	3 (1-7)
85-89	181	225	406	4 (2-6)	4 (1-7)	4 (1-6)
90+	131	111	242	2 (1-7)	5 (2-8)	3 (1-7)
Number of drugs						
2-4	437	401	838	1 (0-1)	1 (0-2)	1 (0-1)
5-9	716	730	1446	4 (2-6)	4 (2-7)	4 (2-6)
10+	156	193	349	11 (8-16)	13 (9-18)	12 (8-17)
Education						
Primary	598	424	1022	3 (1-6)	3 (1-7)	3 (1-6)
Secondary/vocational	590	680	1270	2 (0-6)	3 (1-7)	3 (1-6)
Higher	115	216	331	2 (1-4)	3 (1-7)	2 (1-5)
Residence						
Village	528	461	989	3 (1-6)	3 (1-6)	3 (1-6)
City <50 M	315	327	642	2 (1-5)	3 (1-7)	3 (1-6)
City 50-200 M	246	261	507	2 (0-6)	3 (1-8)	2 (1-7)
City >200 M	220	275	495	3 (1-6)	3 (1-7)	3 (1-6)

M – 1000. The results are presented as medians with the 1<sup>st</sup> and 3<sup>rd</sup> quartile (Q1-Q3). The results take into account the use of a complex scheme of randomizing respondents. The data are presented after weighing the sample in relation to the structure of the Polish population aged 65 and over in 2017.

**Table 3.** Logistic regression model results for predisposing factors to at least 5 drug interactions

Variable	OR	95% CI	p-value
Sex			
Women (ref)	–	–	–
Men	1.18	0.98–1.43	0.088
Age [years]			
65–69 (ref)	–	–	–
70–74	0.84	0.56–1.27	0.053
75–79	0.68	0.45–1.02	0.792
80–84	0.50	0.32–0.78	0.181
85–89	0.63	0.39–1.01	0.097
90+	0.94	0.55–1.61	0.702
Education			
Primary (ref)	–	–	–
Secondary/occupational	1.17	0.96–1.43	0.120
Higher	1.16	0.86–1.56	0.334
Charlson Comorbidity Index			
2 (ref)	–	–	–
3–6	4.62	2.67–8.01	<0.001
7+	13.21	7.40–23.57	<0.001
Residence			
Village (ref)	–	–	–
City <50 M	1.00	0.80–1.25	0.990
City 50–200 M	1.05	0.82–1.34	0.687
City >200 M	1.00	0.77–1.29	0.976

OR – odds ratio; 95% CI – 95% confidence interval; M – 1000; ref – reference. Nagelkerke's  $R^2$ : 0.11;  $p < 0.001$ . The results take into account the use of a complex scheme of randomizing respondents. The data are presented after weighing the sample in relation to the structure of the Polish population aged 65 in 2017.

### Drug interactions and education

There were no noticeable differences in the median value of all interactions in relation to the education level. As education level increased, there was a reduction in the frequency of  $\geq 5$  and  $\geq 10$  interactions. A different trend was observed in the case of  $\geq 15$  interactions: the lowest percentage was found among people with primary education and the highest among people with secondary/vocational education. Detailed data are presented in Table 1,2. A single-factor analysis showed a significant correlation between the number of interactions and education level ( $p < 0.001$ ), but this was not confirmed by the multivariate logistic regression model (Table 3–5).

### Analysis of drug interactions by category

The percentage distribution among different categories of detected drug interactions was 0.6% in category A, 11.6% in category B, 77.9% in category C, 8.7% in category D, and 1.2% in category X. Further analysis focused on categories

**Table 4.** Logistic regression model results for predisposing factors to at least 10 drug interactions

Variable	OR	95% CI	p-value
Gender			
Women (ref)	–	–	–
Men	1.50	1.14–1.96	0.003
Age [years]			
65–69 (ref)	–	–	–
70–74	0.77	0.50–1.20	0.254
75–79	0.94	0.61–1.44	0.763
80–84	0.84	0.54–1.31	0.442
85–89	0.66	0.41–1.06	0.082
90+	0.66	0.39–1.13	0.133
Education			
Primary (ref)	–	–	–
Secondary/occupational	1.04	0.79–1.38	0.778
Higher	1.06	0.71–1.60	0.764
Charlson Comorbidity Index			
2 (ref)	–	–	–
3–6	11.05	2.63–46.50	0.001
7+	36.08	8.45–154.09	<0.001
Residence			
Village (ref)	–	–	–
City <50 M	1.02	0.74–1.40	0.915
City 50–200 M	1.15	0.82–1.61	0.420
City >200 M	1.06	0.74–1.51	0.758

OR – odds ratio; 95% CI – 95% confidence interval; M – 1000; ref – reference. Nagelkerke's  $R^2$ : 0.10;  $p < 0.001$ . The results take into account the use of a complex scheme of randomizing respondents. The data are presented after weighing the sample in relation to the structure of the Polish population aged 65 in 2017.

C, D and X due to their clinical importance and the possibility/necessity of intervention.

We found that 75.8% of all study participants had  $\geq 1$  interaction from category C, with the highest percentage among respondents aged 85–89 years, living in rural areas, with primary education, who took  $\geq 10$  drugs. Detailed percentage data are presented in Supplementary Fig. 1. Factors predisposing to interactions from category C included male sex, a high number of drugs and multimorbidity, whereas living in a small city had a protective effect.

The analysis showed that 24.3% of all study participants had  $\geq 1$  interaction from category D, with the highest percentage among respondents aged 85–89 years, living in rural areas, with primary education, who took  $\geq 10$  drugs. Detailed percentage data are presented in Supplementary Fig. 2. A high number of drugs taken predisposed respondents to interactions from category D, whereas male sex and living in small and big cities had protective effects.

We found that 4.3% of all study participants had  $\geq 1$  interaction from category X, with the highest percentage

**Table 5.** Logistic regression model results for predisposing factors to at least 15 drug interactions

Variable	OR	95% CI	p-value
Sex			
Women (ref)	–	–	–
Men	1.37	0.89–2.10	0.151
Age [years]			
65–69 (ref)	–	–	–
70–74	1.01	0.51–2.01	0.973
75–79	0.98	0.49–1.95	0.947
80–84	0.92	0.46–1.87	0.825
85–89	0.75	0.35–1.60	0.458
90+	0.44	0.17–1.15	0.093
Education			
Primary (ref)	–	–	–
Secondary/occupational	1.41	0.89–2.22	0.144
Higher	1.42	0.75–2.67	0.282
Charlson Comorbidity Index			
2 (ref)	–	–	–
3–6	4804075.21	0.00–Inf	0.975
7+	14383699.59	0.00–Inf	0.974
Residence			
Village (ref)	–	–	–
City <50 M	1.01	0.60–1.70	0.974
City 50–200 M	1.12	0.65–1.94	0.690
City >200 M	1.53	0.90–2.61	0.116

OR – odds ratio; 95% CI – 95% confidence interval; M – 1000; ref – reference; Inf – infinite. Nagelkerke's  $R^2$ : 0.08;  $p < 0.001$ . The results take into account the use of a complex scheme of randomizing respondents. The data are presented after weighing the sample in relation to the structure of the Polish population aged 65 in 2017

among the oldest individuals ( $\geq 90$  years), from large cities, with primary education, who took  $\geq 10$  drugs. Detailed percentage data are presented in Supplementary Fig. 3. Factors predisposing to interactions from category X included a high number of drugs taken and advanced age ( $\geq 90$  years).

### Analysis of drugs being taken

The median value (Q1–Q3) of all drugs consumed was 5 (4–8); it was slightly higher in men (6 (4–8)) than in women (5 (3–8)). Polypharmacy was reported in 63.4% of all individuals over 65 years of age, whereas EPP was reported in 10.4%. The median value (Q1–Q3) was 5 (3–7) for prescription drugs and 1 (0–1) for nonprescription drugs. Detailed data concerning the consumption of all drugs are presented in Supplementary Table 1,2.

A qualitative analysis of pharmacotherapy based on the ATC classification showed that older adults most often used preparations affecting the cardiovascular system, with drugs acting on the renin–angiotensin–aldosterone system being used most often, followed by  $\beta$ -blockers,

hypolipidemic drugs and diuretics. The 2<sup>nd</sup> main group of drugs were preparations influencing blood and the hematopoietic system, including anticoagulants and preparations used in the treatment of anemia. The 3<sup>rd</sup> main group of drugs included preparations affecting the gastrointestinal tract, such as antidiabetic drugs, followed by preparations to reduce gastric juice acidity and supplements for mineral deficiency. Detailed characteristics of the pharmacotherapy in relation to the ATC classification are presented in Supplementary Table 3.

### Comorbidities

The median value (Q1–Q3) of the CCI was 4 points (3–6); it was 4 points (3–6) in men and 4 points (3–5) in women. A result of  $\geq 7$  points (estimated chance of 10-year survival at level of 0%) was obtained for 16.3% of participants, while 6 points (2% chance of surviving 10 years) was achieved by just over every tenth respondent (11.1%). In comparison, a 90% chance of surviving 10 years (2 points) was estimated for 11.7% of all seniors. The distribution of the CCI is presented in Supplementary Fig. 4. The most common chronic diseases were arterial hypertension, osteoarthritis, ischemic heart disease, and diabetes.

### Discussion

In its 2019 report, the World Health Organization (WHO) underlined that PP is a widespread concern in many countries around the world.<sup>27</sup> In this study, the prevalence of PP among people over 65 years was similar to the PP rate reported in the national study assessing health conditions of elderly Poles – “PolSenior2”.<sup>28</sup> The data from both studies show that more than half of all seniors were taking at least 5 or more drugs.

Multimorbidity is a well-documented factor predisposing to PP.<sup>6</sup> An average senior in our study group was diagnosed with 4 chronic conditions and was being treated with 5 drugs. The most frequently used drug groups, as well as the most prevalent chronic diseases in our study, were similar to other geriatric populations.<sup>29</sup> The literature provides a broad and accurate description of the negative medical, economic and social consequences of adverse drug reactions emerging from polypharmacy and numerous drug interactions. The most dangerous are cognitive impairment, weight loss and malnutrition, falls and fractures, rehospitalization, reduced quality of life, and death.<sup>30–32</sup>

Several studies have been conducted to assess the prevalence of drug interactions in older adults using the Lexi-comp® Drug Interactions Tool. Compared to our study, a study in Croatia, which included 354 people over 65 years of age, showed not only a higher number of clinically important drug interactions but also a higher percentage of participants with  $\geq 1$  category C (91.2% compared



to 75.8%), category D (50.8% compared to 24.3%) and category X interactions (9.1% compared to 4.3%). These differences may be explained by the fact that the Croatian respondents were inpatients, and the analysis considered medications upon hospital discharge. In contrast, the participants in our study were home-dwelling adults, presumably with relatively lower morbidity.

In a study conducted in Bulgaria, 248 participants diagnosed with heart failure (New York Heart Association (NYHA) class 2–4) were assessed for drug interactions upon hospital discharge. The number of all detected drug interactions (categories A, B, C, D, and X) was higher than that determined in our study. In both studies, the number of category D interactions was similar; however, our population was characterized by a higher occurrence of category X interactions.<sup>34</sup> These differences may be explained by the inclusion of younger adults (aged <60 years, 15% of the study cohort) in the Bulgarian research.

A study in Slovenia on a group of 243 adults over 65 years old in an ambulatory setting with a diagnosed cardiovascular disease (according to the ICD-10 classification) revealed a higher percentage of the most dangerous drug interactions (category X) than that in our study (16.5% compared to 4.3%).<sup>35</sup> This difference could be explained by the fact that the authors included only older adults with EPP ( $\geq 10$  drugs) who carried a greater risk of drug interactions than participants who were taking fewer drugs.

Data on the frequency of possible drug interactions assessed with an automated analysis program concerning the Polish geriatric population are lacking. To our knowledge, this is the first study to report the prevalence of drug interactions using the Lexicomp® Drug Interactions Tool.

Our findings indicate that there is a significant correlation between the increasing number of interactions and the high number of drugs taken, advanced age, primary level of education, living in rural areas, and multimorbidity. The influence of age and the number of drugs taken on the frequency of drug interactions has already been documented, and our results are consistent with the current literature.<sup>14,36–38</sup> Studies defining a direct relationship between drug interactions and level of education are lacking. However, the connection between low educational attainment and polypharmacy,<sup>39</sup> noncompliance with treatment<sup>40</sup> and less positive beliefs toward medication<sup>41</sup> has been confirmed, which may explain the more frequent prevalence of drug interactions in our study. An increased risk of drug interactions in older adults from rural areas has been observed in other studies,<sup>42</sup> but the reasons are unclear. Presumably, areas with a larger population have greater access to healthcare and academic medical centers, which may lead to a lower prevalence of drug interactions.<sup>43</sup> Finally, the results of the multivariate logistic regression model showed that the strongest predisposing factor to drug interactions was multimorbidity, which has been observed in other populations.<sup>44,45</sup>

## Limitations

There are some limitations that need to be acknowledged and addressed regarding the present study. The use of an automatic interaction analysis system led to low specificity.<sup>46,47</sup> Furthermore, unlike the START/STOPP criteria, the Beers criteria or the FORTA list, we were not able to fully address the clinical context of the detected drug interactions. This is particularly important in older patients with multiple morbidities who require multidrug regimens to treat chronic diseases in accordance with the guidelines of evidence-based medicine. Finally, the clinical picture of drug interactions consists not only of drug–drug interactions but also drug–diet, drug–disease and drug–patient interactions,<sup>48–50</sup> which we did not investigate.

## Conclusions

Our study delivers up-to-date data from a representative sample of older, home-dwelling adults in Poland. Despite being based on theoretical knowledge, our results highlight the important problem of possible drug interactions in the Polish geriatric population, which constitutes a major challenge for clinicians and disrupts the therapeutic process. Tools supporting the identification of patients with inappropriate polypharmacy<sup>51</sup> should be further developed and popularized in the healthcare community, along with other preventive measures, such as systematic reviews of pharmacotherapy and support from clinical pharmacologists. Future studies are needed to assess the clinical context of drug interactions detected with automated analysis systems.

## Supplementary materials

The supplementary materials are available at <https://doi.org/10.5281/zenodo.7027709>. The package contains the following files:

Supplementary Fig. 1. Percentage of people with at least 1 drug interaction from category C (monitor therapy) broken down by main variables.

Supplementary Fig. 2. Percentage of people with at least 1 drug interaction from category D (consider modifying therapy) broken down by main variables.

Supplementary Fig. 3. Percentage of people with at least 1 drug interaction from category X (avoid combination) broken down by main variables.

Supplementary Fig. 4. Distribution of the Charlson Comorbidity Index (CCI) values in the entire population by gender.

Supplementary Table 1. Percentage of older people taking drugs.

Supplementary Table 2. Number of all drug interactions.

Supplementary Table 3. Percentage of people taking drugs based on the Anatomical Therapeutic Chemical

(ATC) classification (%). Detailed results in subgroups are presented for values above 5%.

Supplementary Table 4. Results of data normality checked with the Shapiro–Wilk test.

## ORCID iDs

Emilia Bleszyńska-Marunowska  <https://orcid.org/0000-0001-7816-189X>  
 Łukasz Wierucki  <https://orcid.org/0000-0003-2995-6180>  
 Kacper Jagiełło  <https://orcid.org/0000-0001-7138-5049>  
 Krzysztof Rewiuk  <https://orcid.org/0000-0001-6451-5730>  
 Katarzyna Mitreęa  <https://orcid.org/0000-0002-0312-6122>  
 Zbigniew Kalarus  <https://orcid.org/0000-0003-3921-7234>

## References

- Pazan F, Wehling M. Polypharmacy in older adults: A narrative review of definitions, epidemiology and consequences. *Eur Geriatr Med.* 2021;12(3):443–452. doi:10.1007/s41999-021-00479-3
- Kim J, Parish AL. Polypharmacy and medication management in older adults. *Nurs Clin North Am.* 2017;52(3):457–468. doi:10.1016/j.cnur.2017.04.007
- Mielke N, Huscher D, Douros A, et al. Self-reported medication in community-dwelling older adults in Germany: Results from the Berlin Initiative Study. *BMC Geriatr.* 2020;20(1):22. doi:10.1186/s12877-020-1430-6
- Montiel-Luque A, Núñez-Montenegro AJ, Martín-Aurioles E, et al. Medication-related factors associated with health-related quality of life in patients older than 65 years with polypharmacy. *PLoS One.* 2017;12(2):e0171320. doi:10.1371/journal.pone.0171320
- Verde Z, García de Diego L, Chicharro LM, et al. Physical performance and quality of life in older adults: Is there any association between them and potential drug interactions in polymedicated octogenarians. *Int J Environ Res Public Health.* 2019;16(21):4190. doi:10.3390/ijerph16214190
- Wastesson JW, Morin L, Tan ECK, Johnell K. An update on the clinical consequences of polypharmacy in older adults: A narrative review. *Exp Opin Drug Safety.* 2018;17(12):1185–1196. doi:10.1080/14740338.2018.1546841
- Patel NS, Patel TK, Patel PB, Naik VN, Tripathi C. Hospitalizations due to preventable adverse reactions: A systematic review. *Eur J Clin Pharmacol.* 2017;73(4):385–398. doi:10.1007/s00228-016-2170-6
- Muhlack DC, Hoppe LK, Weberpals J, Brenner H, Schöttker B. The association of potentially inappropriate medication at older age with cardiovascular events and overall mortality: A systematic review and meta-analysis of cohort studies. *J Am Med Dir Assoc.* 2017;18(3):211–220. doi:10.1016/j.jamda.2016.11.025
- Veeran JC, Weiss M. Trends in emergency hospital admissions in England due to adverse drug reactions: 2008–2015. *J Pharm Health Serv Res.* 2017;8(1):5–11. doi:10.1111/jphs.12160
- Hartholt KA, van der Velde N, Looman CWN, et al. Adverse drug reactions related hospital admissions in persons aged 60 years and over, The Netherlands, 1981–2007: Less rapid increase, different drugs. *PLoS One.* 2010;5(11):e13977. doi:10.1371/journal.pone.0013977
- Scripcaru G, Mateus C, Nunes C. Adverse drug events: Analysis of a decade. A Portuguese case-study, from 2004 to 2013 using hospital database. *PLoS One.* 2017;12(6):e0178626. doi:10.1371/journal.pone.0178626
- Tariq RA, Vashisht R, Sinha A, Scherbak Y. Medication dispensing errors and prevention. In: *StatPearls*. Treasure Island, USA: StatPearls Publishing; 2022. <http://www.ncbi.nlm.nih.gov/books/NBK519065/>. Accessed September 22, 2022.
- 2019 American Geriatrics Society Beers Criteria® Update Expert Panel. American Geriatrics Society 2019 Updated AGS Beers Criteria® for Potentially Inappropriate Medication Use in Older Adults: 2019. *J Am Geriatr Soc.* 2019;67(4):674–694. doi:10.1111/jgs.15767
- O'Mahony D. STOPP/START criteria for potentially inappropriate medications/potential prescribing omissions in older people: Origin and progress. *Exp Rev Clin Pharmacol.* 2020;13(1):15–22. doi:10.1080/17512433.2020.1697676
- Pazan F, Weiss C, Wehling M, et al. The FORTA (Fit FOR The Aged) List 2021: Fourth version of a validated clinical aid for improved pharmacotherapy in older adults. *Drugs Aging.* 2022;39(3):245–247. doi:10.1007/s40266-022-00922-5
- Zhan C, Sangl J, Bierman AS, et al. Potentially inappropriate medication use in the community-dwelling elderly: Findings from the 1996 Medical Expenditure Panel survey. *JAMA.* 2001;286(22):2823. doi:10.1001/jama.286.22.2823
- Simon SR, Chan KA, Soumerai SB, et al. Potentially inappropriate medication use by elderly persons in U.S. health maintenance organizations, 2000–2001. *J Am Geriatr Soc.* 2005;53(2):227–232. doi:10.1111/j.1532-5415.2005.53107.x
- Curtis LH, Østbye T, Sendersky V, et al. Inappropriate prescribing for elderly Americans in a large outpatient population. *Arch Intern Med.* 2004;164(15):1621. doi:10.1001/archinte.164.15.1621
- Jungo KT, Streit S, Lauffenburger JC. Patient factors associated with new prescribing of potentially inappropriate medications in multimorbid US older adults using multiple medications. *BMC Geriatr.* 2021;21(1):163. doi:10.1186/s12877-021-02089-x
- Patel RI, Beckett RD. Evaluation of resources for analyzing drug interactions. *J Med Libr Assoc.* 2017;104(4):290–295. doi:10.5195/jmla.2016.142
- Clauson KA, Marsh WA, Polen HH, Seamon MJ, Ortiz BI. Clinical decision support tools: Analysis of online drug information databases. *BMC Med Inform Decis Mak.* 2007;7(1):7. doi:10.1186/1472-6947-7-7
- Kheshtri R, Aalipour M, Namazi S. A comparison of five common drug–drug interaction software programs regarding accuracy and comprehensiveness. *J Res Pharm Pract.* 2016;5(4):257. doi:10.4103/2279-042X.192461
- Skelton T. Surescripts CEO sees “a much more interconnected and digitized healthcare system” ahead. *Mod Healthc.* 2016;46(38):30–31. PMID:30399301.
- Kalarus Z, Balsam P, Bandsz P, et al. Noninvasive Monitoring for Early Detection of Atrial Fibrillation: Rationale and design of the NOMED-AF study. *Kardiol Pol.* 2018;76(10):1482–1485. doi:10.5603/KP.a2018.0193
- World Health Organization. Anatomical Therapeutic Chemical (ATC) classification. 2019. <https://www.who.int/tools/atc-ddd-toolkit/atc-classification>. Accessed March 22, 2022.
- Masnoon N, Shakib S, Kalisch-Ellett L, Caughey GE. What is polypharmacy? A systematic review of definitions. *BMC Geriatr.* 2017;17(1):230. doi:10.1186/s12877-017-0621-2
- World Health Organization. *Medication Safety in Polypharmacy: Technical Report*. Geneva, Switzerland: World Health Organization; 2019. <https://www.who.int/publications/i/item/WHO-UHC-SDS-2019.11>. Accessed March 22, 2022.
- Wierucki Ł, Bleszyńska E, Gaciong M, et al. Farmakoterapia. In: Błęadowski P, Grodzicki T, Mossakowska M, Zdrojewski T, eds. *Badanie poszczególnych obszarów stanu zdrowia osób starszych, w tym jakości życia związanej ze zdrowiem*. Gdańsk, Poland: Gdański Uniwersytet Medyczny; 2021:737–760. [https://polsenior2.gumed.edu.pl/attachment/attachment/82370/Polsenior\\_2.pdf](https://polsenior2.gumed.edu.pl/attachment/attachment/82370/Polsenior_2.pdf).
- Chiapella LC, Montemarani Menna J, Mamprin ME. Assessment of polypharmacy in elderly patients by using data from dispensed medications in community pharmacies: Analysis of results by using different methods of estimation. *Int J Clin Pharm.* 2018;40(5):987–990. doi:10.1007/s11096-018-0663-3
- Davies LE, Spiers G, Kingston A, Todd A, Adamson J, Hanratty B. Adverse outcomes of polypharmacy in older people: Systematic review of reviews. *J Am Med Dir Assoc.* 2020;21(2):181–187. doi:10.1016/j.jamda.2019.10.022
- Sandoval T, Martínez M, Miranda F, Jirón M. Incident adverse drug reactions and their effect on the length of hospital stay in older inpatients. *Int J Clin Pharm.* 2021;43(4):839–846. doi:10.1007/s11096-020-01181-3
- Shinohara M, Yamada M. Drug-induced cognitive impairment [in Japanese]. *Brain Nerve.* 2012;64(12):1405–1410. PMID:23209067.
- Marinović I, Bačić Vrca V, Samardžić I, Marušić S, Grgurević I. Potentially inappropriate medications involved in drug–drug interactions at hospital discharge in Croatia. *Int J Clin Pharm.* 2021;43(3):566–576. doi:10.1007/s11096-020-01164-4
- Georgiev KD, Hvarchanova N, Georgieva M, Kanazirev B. The role of the clinical pharmacist in the prevention of potential drug interactions in geriatric heart failure patients. *Int J Clin Pharm.* 2019;41(6):1555–1561. doi:10.1007/s11096-019-00918-z
- Stuhec M, Flegar I, Zelko E, Kovačić A, Zabavnik V. Clinical pharmacist interventions in cardiovascular disease pharmacotherapy in elderly patients on excessive polypharmacy: A retrospective pre–post observational multicentric study. *Wien Klin Wochenschr.* 2021;133(15–16):770–779. doi:10.1007/s00508-020-01801-y

36. Jenkins S. A profile of older Americans: 2015. 2016. <https://acl.gov/sites/default/files/Aging%20and%20Disability%20in%20America/2015-Profile.pdf>. Accessed March 22, 2022.
37. Woo SD, Yoon J, Doo GE, et al. Common causes and characteristics of adverse drug reactions in older adults: A retrospective study. *BMC Pharmacol Toxicol*. 2020;21(1):87. doi:10.1186/s40360-020-00464-9
38. Rodrigues MCS, de Oliveira C. Drug-drug interactions and adverse drug reactions in polypharmacy among older adults: An integrative review. *Rev Lat Am Enfermagem*. 2016;24:e2800. doi:10.1590/1518-8345.1316.2800
39. Saum KU, Schöttker B, Meid AD, et al. Is polypharmacy associated with frailty in older people? Results from the ESTHER cohort study. *J Am Geriatr Soc*. 2017;65(2):e27–e32. doi:10.1111/jgs.14718
40. Oscanoa TJ, Lizaraso F, Carvajal A. Hospital admissions due to adverse drug reactions in the elderly: A meta-analysis. *Eur J Clin Pharmacol*. 2017;73(6):759–770. doi:10.1007/s00228-017-2225-3
41. Vilhelmsdóttir H, Jóhannsson M. Icelanders' beliefs about medicines: Use of BMQ [in Icelandic]. *Laeknabladid*. 2017;103(2):67–72. doi:10.17992/lbl.2017.02.120
42. Sikdar KC, Dowden J, Alaghebandan R, MacDonald D, Wang PP, Gadag V. Adverse drug reactions in elderly hospitalized patients: A 12-year population-based retrospective cohort study. *Ann Pharmacother*. 2012;46(7–8):960–971. doi:10.1345/aph.1Q529
43. Shepherd G, Mohorn P, Yacoub K, May DW. Adverse drug reaction deaths reported in United States Vital Statistics, 1999–2006. *Ann Pharmacother*. 2012;46(2):169–175. doi:10.1345/aph.1P592
44. Baré M, Herranz S, Jordana R, et al. Multimorbidity patterns in chronic older patients, potentially inappropriate prescribing and adverse drug reactions: Protocol of the multicentre prospective cohort study MoPIM. *BMJ Open*. 2020;10(1):e033322. doi:10.1136/bmjopen-2019-033322
45. Jennings E, Gallagher P, O'Mahony D. Detection and prevention of adverse drug reactions in multi-morbid older patients. *Age Ageing*. 2019;48(1):10–13. doi:10.1093/ageing/afy157
46. Muhić N, Mrhar A, Brvar M. Comparative analysis of three drug–drug interaction screening systems against probable clinically relevant drug–drug interactions: A prospective cohort study. *Eur J Clin Pharmacol*. 2017;73(7):875–882. doi:10.1007/s00228-017-2232-4
47. Shen C, Jiang B, Yang Q, et al. Mobile apps for drug–drug interaction checks in Chinese app stores: Systematic review and content analysis. *JMIR Mhealth Uhealth*. 2021;9(6):e26262. doi:10.2196/26262
48. Ased S, Wells J, Morrow LE, Malesker MA. Clinically significant food-drug interactions. *Consult Pharm*. 2018;33(11):649–657. PMID:30458907.
49. Schmidt-Mende K, Andersen M, Wettermark B, Hasselström J. Drug–disease interactions in Swedish senior primary care patients were dominated by non-steroid anti-inflammatory drugs and hypertension: A population-based registry study. *Scand J Prim Health Care*. 2020;38(3):330–339. doi:10.1080/02813432.2020.1794396
50. Ylä-Rautio H, Siissalo S, Leikola S. Drug-related problems and pharmacy interventions in non-prescription medication, with a focus on high-risk over-the-counter medications. *Int J Clin Pharm*. 2020;42(2):786–795. doi:10.1007/s11096-020-00984-8
51. Stewart D, Mair A, Wilson M, et al. Guidance to manage inappropriate polypharmacy in older people: Systematic review and future developments. *Exp Opin Drug Safety*. 2016;16(2):203–213. doi:10.1080/14740338.2017.1265503





# CLIC1 plasma concentration is associated with lymph node metastases in oral squamous cell carcinoma

Bartosz Paweł Wojtera<sup>1,A–D</sup>, Agnieszka Sobecka<sup>1,2,A–C</sup>, Mateusz Szewczyk<sup>1,A,B,E</sup>,  
Piotr Machczyński<sup>1,B,E</sup>, Wiktoria Maria Suchorska<sup>2,3,A,E,F</sup>, Wojciech Golusiński<sup>1,A,E,F</sup>

<sup>1</sup> Department of Head and Neck Surgery, Greater Poland Cancer Centre, Poznan University of Medical Sciences, Poland

<sup>2</sup> Radiobiology Lab, Department of Medical Physics, Greater Poland Cancer Centre, Poznań, Poland

<sup>3</sup> Department of Electroradiology, Poznan University of Medical Sciences, Poland

A – research concept and design; B – collection and/or assembly of data; C – data analysis and interpretation;

D – writing the article; E – critical revision of the article; F – final approval of the article

Advances in Clinical and Experimental Medicine, ISSN 1899–5276 (print), ISSN 2451–2680 (online)

*Adv Clin Exp Med.* 2023;32(3):341–347

## Address for correspondence

Bartosz Paweł Wojtera

E-mail: bartosz.wojtera96@gmail.com

## Funding sources

The study was funded by Poznan University Students Scientific Association grant No. 3549 titled "CLIC1 in laryngeal and oral squamous cell carcinoma patients' plasma".

## Conflict of interest

None declared

Received on December 12, 2021

Reviewed on June 29, 2022

Accepted on September 15, 2022

Published online on October 17, 2022

## Cite as

Wojtera BP, Sobecka A, Szewczyk M, Machczyński P, Suchorska WM, Golusiński W. CLIC1 plasma concentration is associated with lymph node metastases in oral squamous cell carcinoma. *Adv Clin Exp Med.* 2023;32(3):341–347. doi:10.17219/acem/154621

## DOI

10.17219/acem/154621

## Copyright

Copyright by Author(s)

This is an article distributed under the terms of the Creative Commons Attribution 3.0 Unported (CC BY 3.0) (<https://creativecommons.org/licenses/by/3.0/>)

## Abstract

**Background.** Previous studies have shown that the chloride intracellular channel 1 (CLIC1) protein is overexpressed in oral squamous cell carcinoma (OSCC) and nasopharyngeal carcinoma. Patients with these diseases had significantly higher CLIC1 plasma levels than healthy controls.

**Objectives.** To determine the plasma concentration of CLIC1 in patients with OSCC and laryngeal squamous cell carcinoma (LSCC).

**Materials and methods.** We collected blood samples from patients diagnosed with OSCC (n = 13) and LSCC (n = 7), as well as from healthy controls (n = 8). The blood samples were centrifuged to obtain plasma and stored at –80°C. The CLIC1 plasma concentration was determined using enzyme-linked immunosorbent assay (ELISA).

**Results.** The mean CLIC1 plasma concentration was higher in the OSCC group than in the LSCC and control groups. Patients with OSCC and nodal metastases had significantly higher CLIC1 plasma concentration levels than nonmetastatic patients (p < 0.0001; Tukey's multiple comparisons test) and controls (p = 0.0004). The CLIC1 concentration correlated significantly with the presence of nodal spread (p = 0.0003; Spearman's r = 0.8613) and overall TNM staging (p = 0.0167; Spearman's r = 0.6620). No differences in CLIC1 plasma levels were observed between the LSCC and control groups. The CLIC1 plasma concentration was not associated with age, sex, tumor stage, or tumor grade.

**Conclusions.** There were no differences in CLIC1 plasma concentration between healthy controls and patients with LSCC. However, our findings suggest that the presence of this protein in plasma may be associated with lymphatic metastasis in patients with OSCC. More research is needed to confirm this possible association.

**Key words:** HNSCC, oral squamous cell carcinoma, OSCC, CLIC1, cancer plasma marker

## Background

Head and neck squamous cell carcinoma (HNSCC) is a common malignancy with a poor prognosis. It is estimated that HNSCC accounts for more than 750,000 cases and 340,000 deaths annually worldwide.<sup>1</sup> Currently, there are only 2 widely accepted prognostic biomarkers for HNSCC, namely human papillomavirus (HPV) infection/p16 expression and programmed death-ligand 1 (PD-L1) expression.<sup>2</sup> Further research on the biological factors associated with HNSCC progression, recurrence and metastases is an important aim of contemporary oncology.

Numerous studies have evaluated biomarkers for the early diagnosis of cancer and to actively monitor treatment response. Recently, ion channels are being investigated as biomarkers of various diseases, including cancer.<sup>3</sup> Ion channels are integral membrane proteins present on the plasma membrane and within intracellular membranes. In the human genome, there are more than 400 genes encoding ion channel proteins.<sup>3</sup>

The chloride intracellular channel 1 (CLIC1) protein, which is representative of the chloride ion channel family, is one such biomarker. The CLIC1 is present in cells in both membrane and soluble forms.<sup>4,5</sup> It is widely distributed throughout the body and can be found in various epithelial tissues in apical domains.<sup>6</sup> This protein is involved in mitogen-activated protein kinase (MAPK) signaling pathways as well as in carcinogenic processes.<sup>7-9</sup> The CLIC1 is also considered to be a sensor and effector during oxidative stress in microglial cells.<sup>10</sup> The role of CLIC1 has been determined in several cancers, such as gallbladder cancer, glioblastoma multiforme, gastric cancer, colon cancer, ovarian cancer, breast cancer, liver cancer, pancreatic cancer, and others.<sup>3,7</sup>

Recent findings have shown that CLIC1 is overexpressed in patients with oral squamous cell carcinoma (OSCC) and is associated with a poor prognosis.<sup>7</sup> Cell culture studies have shown that *CLIC1* promotes cell viability, proliferation, migration, and invasion, as well as in vitro cell-mediated angiogenesis, in OSCC cells.<sup>8</sup> Although CLIC1 tissue activity has been identified in several cancer types,<sup>7</sup> elevated plasma levels have only been confirmed in 2 cancer types, namely nasopharyngeal carcinoma and OSCC.<sup>11</sup>

A cell culture study reported that the *CLIC1* gene is up-regulated in laryngeal squamous cell carcinoma (LSCC).<sup>12</sup> Another cell culture study found that *CLIC1* suppression results in an increased radiosensitivity of laryngeal cancer cells.<sup>13</sup> However, CLIC1 plasma levels in laryngeal cancer have yet to be determined.

## Objectives

This prospective study was performed to measure the concentration of CLIC1 in plasma obtained from patients diagnosed with LSCC and OSCC in order

to determine whether this protein could serve as a potential biomarker in patients with HNSCC.

## Materials and methods

### Patients

The study group consisted of 20 patients (14 males and 6 females), with a mean age of  $62.7 \pm 7.95$  years (range: 48–75 years). All patients were histologically diagnosed with either oral or laryngeal HNSCC (Table 1). Pathological tumor staging was performed according to the 8<sup>th</sup> edition of the TNM classification published by the Union for International Cancer Control (UICC).<sup>14</sup> Patients were prospectively recruited between November 2019 and August 2020 at the Department of Head and Neck Surgery at Poznan University of Medical Sciences and the Greater

Table 1. Study group characteristics

Characteristics	Total (n = 28)
<b>Cancer patients (n = 20)</b>	
Age	
M $\pm$ SD	62.7 $\pm$ 7.95
Median	63
Range	48–75
Sex	
Male	14
Female	6
T-stage	
T1	3
T2	6
T3	7
T4	4
N-stage	
N0	11
N1	1
N2	7
N3	1
Anatomical site	
Larynx	7
Oral cavity	13
<b>Healthy individuals (n = 8)</b>	
Age	
M $\pm$ SD	65.8 $\pm$ 3.93
Median	67
Range	60–72
Sex	
Male	5
Female	3

M  $\pm$ SD – mean  $\pm$  standard deviation; T – tumor; N – lymph node.

Poland Cancer Centre in Poznań, Poland. Blood samples from patients with primary tumors were collected prior to the surgical treatment. The control group consisted of 8 healthy age- and sex-matched volunteers.

We measured and compared CLIC1 plasma concentrations in 4 groups: LSCC, OSCC, HNSCC (all patients from the LSCC and OSCC groups combined), and healthy controls.

The study protocol was in compliance with the Declaration of Helsinki and approved by the Ethics Committee of Poznan University of Medical Sciences (decision No. 598/19). Written informed consent was obtained from the participating individuals.

## Exclusion criteria

Patients with any of the following were excluded from the study: second primary tumor, local recurrence, previous treatment with chemotherapy or radiotherapy, and positive HPV status.

## Sample preparation

Blood samples were collected preoperatively following a standardized protocol. Plasma samples were prepared by collecting blood in ethylenediaminetetraacetic acid (EDTA) tubes and centrifuging them at 2000 g for 20 min at 4°C. After centrifugation, the plasma samples were apportioned into 0.5 mL aliquots and stored at –80°C for further analysis.

## Enzyme-linked immunosorbent assay

The CLIC1 protein levels in plasma were measured with the Human CLIC1 enzyme-linked immunosorbent assay (ELISA) Kit (cat. No. orb438684; Biorbyt, Cambridge, UK), according to the manufacturer's instructions. Each sample was evaluated 3 times in order to confirm the consistency of the test. Briefly, 100 µL of samples and standards were added to the wells of microtiter plates pre-coated with anti-CLIC1 antibody and were incubated for 2 h at 37°C. The samples were removed, and 100 µL of biotin-conjugated detection antibody was added. The plates were incubated for 1 h at 37°C and washed 3 times with 1× Wash Solution (Biorbyt). Next, 100 µL of avidin conjugated to horseradish peroxidase (HRP) was added to each microplate well and incubated for 1 h at 37°C. The plate wells were washed 5 times using 1× Wash Solution, and 90 µL of tetramethylbenzidine peroxidase substrate was added. After 25 min of incubation at 37°C, the reaction was terminated with adding sulfuric acid solution. An automated plate reader (Multiskan™ FC Microplate Photometer; Thermo Fisher Scientific, Waltham, USA) was used to measure the absorbance at 450 nm. The CLIC1 levels were determined using a standard curve.

## Statistical analyses

The GraphPad Prism v. 8 software program (GraphPad Software, San Diego, USA) was used to perform the statistical analyses. The value of  $p < 0.05$  was considered statistically significant. The Kolmogorov–Smirnov normality test was performed to check for distribution normality. The Student's t-test, Kruskal–Wallis test, Dunn's multiple comparisons test, and Tukey's multiple comparisons test were used to calculate the differences in CLIC1 plasma levels between the groups. The Spearman's rank correlation coefficient was used to calculate the correlation between CLIC1 plasma concentration and TNM staging.

## Results

### Tumor

We found no significant differences in CLIC1 concentration levels between the HNSCC patients and the controls ( $p = 0.6178$ ; unpaired t-test), nor between the OSCC ( $p = 0.7023$ ), LSCC ( $p = 0.7295$ ) and control groups ( $p = 0.9973$ ; Tukey's multiple comparisons test) (Fig. 1A,B). The tumor stage was not correlated with the CLIC1 concentration ( $p = 0.9749$ ; Kruskal–Wallis test) (Fig. 1C).

### Lymph node metastases

The CLIC1 plasma concentration was significantly higher in OSCC patients with nodal metastases than in non-metastatic patients ( $p < 0.0001$ ) and controls ( $p = 0.0004$ ; Tukey's multiple comparisons test) (Fig. 1D). The CLIC1 plasma concentration was significantly correlated with the presence of nodal metastases in the HNSCC group ( $p = 0.0043$ ; Spearman's  $r = 0.6098$ ) and the OSCC group ( $p = 0.0003$ ; Spearman's  $r = 0.8613$ ) (Fig. 1D, Fig. 2A–C).

### TNM staging

The TNM stage correlated significantly with the CLIC1 plasma concentration in the OSCC group ( $p = 0.0167$ ; Spearman's  $r = 0.6620$ ). In the HNSCC group, there was a nonsignificant trend toward the correlation ( $p = 0.0860$ ; Spearman's  $r = 0.3936$ ).

### Grading

Tumor grade was not correlated with CLIC1 concentration in the HNSCC, OSCC or LSCC groups ( $p = 0.1356$ ,  $p = 0.2923$  and  $p = 0.7597$ , respectively; Kruskal–Wallis test) (Fig. 2D–F).

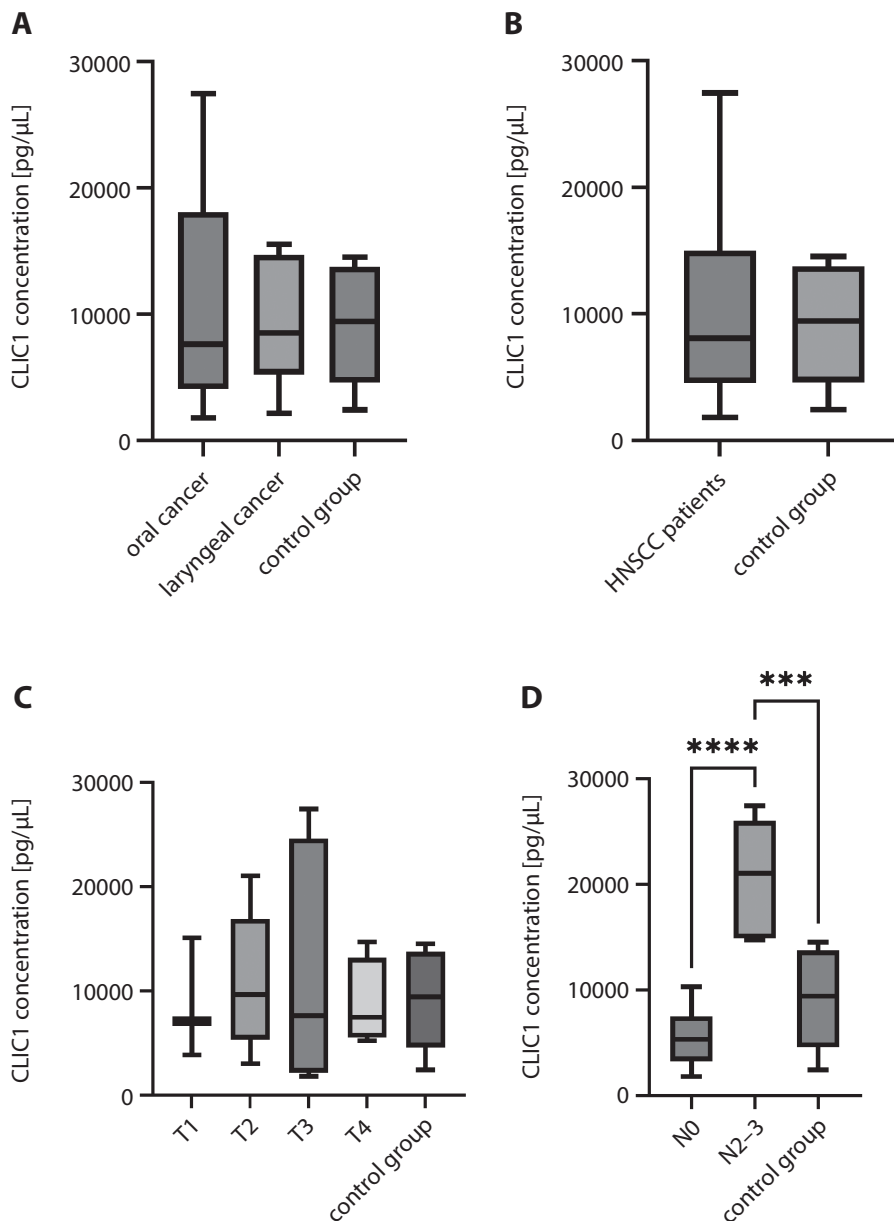


**Fig. 1.** A. CLIC1 plasma concentration in patients with oral cancer, laryngeal cancer and control group; B. CLIC1 plasma concentration in patients with head and neck squamous cell carcinoma (HNSCC) compared to controls; C. HNSCC patients compared to the control group); D. CLIC1 plasma concentration in patients with non-metastatic (N0) and metastatic (N2–N3) oral cancer compared to controls; \*\*\*  $p = 0.0004$ , \*\*\*\*  $p < 0.0001$  (Tukey's multiple comparisons test)

## Patient characteristics

The mean and median CLIC1 concentration levels were higher among women but the results were not statistically significant ( $p = 0.2761$ ; unpaired *t*-test) (Fig. 2G,H). Age was not correlated with CLIC1 plasma concentration ( $p = 0.9349$ ; Kruskal–Wallis test) (Fig. 2I).

## Discussion

In this study, we measured CLIC1 plasma concentrations in patients with oral and laryngeal cancer and healthy controls. The mean CLIC1 plasma concentration was higher in the OSCC group than in the LSCC and control groups, but the results were not statistically significant. Patients with metastatic OSCC had significantly higher CLIC1 plasma concentrations than nonmetastatic patients

( $p < 0.0001$ ). The CLIC1 concentration was significantly correlated with nodal metastases ( $p = 0.0003$ ; Spearman's  $r = 0.8613$ ) and overall TNM stage ( $p = 0.0167$ ; Spearman's  $r = 0.6620$ ). No differences in CLIC1 plasma levels were observed between the LSCC and control groups. The CLIC1 plasma concentration was not associated with age, sex, tumor stage, or tumor grade. These findings suggest that plasma CLIC1 concentration could be a useful biomarker in patients with OSCC but not in those with LSCC.

The CLIC family comprises 6 proteins (CLIC1–CLIC6).<sup>3,15</sup> Other members of the CLIC family have also been investigated as molecular targets in oncology.<sup>16</sup> Karsani et al. found an association between CLIC1 and the development and progression of OSCC.<sup>17</sup> Other studies have suggested that CLIC1 is involved in numerous cancers (nasopharyngeal, esophageal, stomach, liver, pancreatic, colorectal, lung, breast, gallbladder, prostate, ovarian, and brain cancers).<sup>11,18–28</sup> Two studies reported



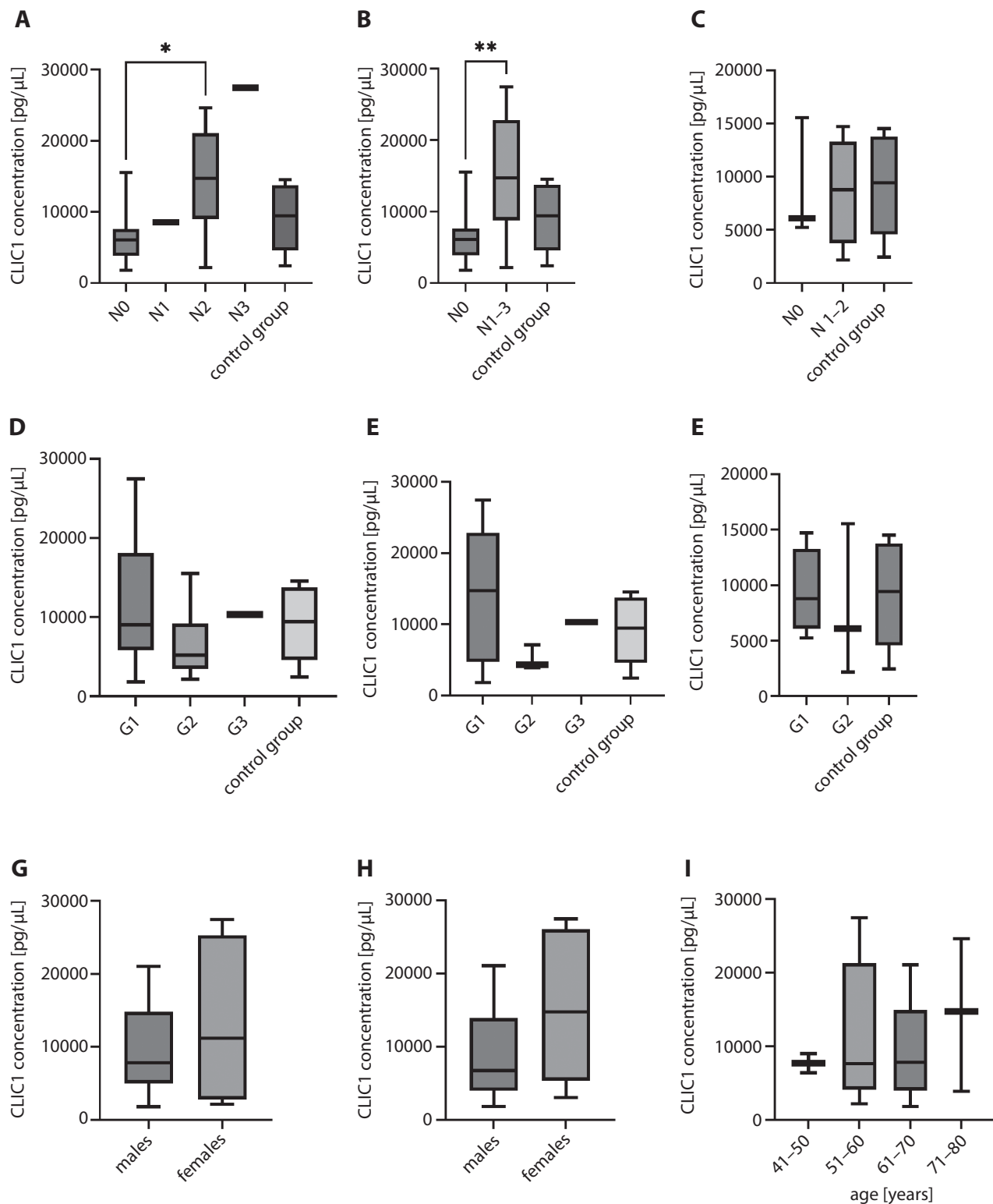


**Fig. 2.** A. CLIC1 plasma concentration by metastatic lymph node (N) stage in patients with HNSCC compared to controls; \*  $p = 0.0463$  (Dunn’s multiple comparisons test); B. CLIC1 plasma concentration in patients with non-metastatic (N0) and metastatic (N1–N3) HNSCC compared to controls; \*\*  $p = 0.006$  (Tukey’s multiple comparisons test); C. CLIC1 plasma concentration in patients with non-metastatic (N0) and metastatic (N1–N2) laryngeal cancer compared to controls; D. CLIC1 plasma concentration by grading in HNSCC patients; E. CLIC1 plasma concentration by grading in oral cancer patients; F. CLIC1 plasma concentration by grading in laryngeal cancer patients; G. CLIC1 plasma concentration by gender in HNSCC patients; H. CLIC1 plasma concentration by gender in oral cancer patients; I. CLIC1 plasma concentration by age group

a possible association between *CLIC1* and laryngeal cancer.<sup>12,13</sup> In the present study, we investigated plasma CLIC1 concentration in patients with LSCC and found

that the plasma CLIC1 concentration in these patients was similar to the healthy controls. These results suggest that further study of CLIC1 as a potential biomarker of LSCC

may not be beneficial. However, this biomarker may be useful in patients with OSCC, given the higher specificity of raised CLIC1 plasma levels in these patients. It is important to note that the plasma expression of this protein is also elevated in nasopharyngeal carcinoma, which was not investigated in this study.<sup>11</sup>

The lack of significant differences in CLIC1 plasma levels between the OSCC and control group may be due to the small sample size of the study (13 patients with OSCC and 8 healthy controls). However, the CLIC1 plasma concentration was significantly correlated with TNM staging, a finding that is in line with a previous report by Xu et al.<sup>7</sup> Nonetheless, this correlation was only significant for nodal staging (N), not tumor staging (T).

Xu et al. did not observe any correlation between the CLIC1 expression and the presence of metastatic lymph nodes in patients with OSCC.<sup>7</sup> By contrast, Feng et al. found that the upregulation of *CLIC1* was associated with the viability and proliferation of OSCC cells.<sup>8</sup> In that study, silencing of *CLIC1* inhibited these processes and promoted apoptosis. We found a strong correlation ( $p = 0.0003$ ; Spearman's  $r = 0.8613$ ) between CLIC1 plasma concentration and metastatic nodal staging, a finding that may have diagnostic and prognostic implications.

The role of *CLIC1* in metastatic lesions has been investigated in other cancer types. One study revealed that *CLIC1* knockdown inhibits gallbladder cancer metastasis by reducing migration and invasion of cells.<sup>21</sup> Other studies have demonstrated that the expression of *CLIC1* is correlated with metastatic spread in colon<sup>9</sup> and breast cancers,<sup>28</sup> as well as with nodal dissemination in gastric cancer.<sup>19</sup>

The CLIC1 plasma expression in patients with OSCC tends to change during the course of cancer treatment, which suggests that this protein could potentially play a valuable role in monitoring treatment response. In the study by Xu et al., CLIC1 concentration levels were lower in patients who underwent tumor resection than in those with ongoing disease.<sup>7</sup> Relevantly, tumor resection followed by adjuvant chemotherapy lowered plasma CLIC1 expression levels even further.<sup>7</sup> According to Feng et al., *CLIC1* knockdown increased the susceptibility of OSCC cells to cisplatin.<sup>8</sup>

## Limitations

This study has several limitations, mainly the small patient population and the use of an ELISA test based on a single kit only, which could explain the lack of significant intergroup differences in some of the comparisons.

## Conclusions

This study demonstrates that the CLIC1 plasma concentration is associated with metastatic nodal spread in patients with OSCC and, consequently, with overall TNM

stage. These findings suggest that CLIC1 could be a feasible plasma biomarker to diagnose and monitor patients with oral cancer with nodal involvement. However, these findings need to be confirmed in larger studies.

## ORCID iDs

Bartosz Paweł Wojtera  <https://orcid.org/0000-0003-4677-0783>  
 Agnieszka Sobiecka  <https://orcid.org/0000-0003-0976-1802>  
 Mateusz Szewczyk  <https://orcid.org/0000-0002-6834-5369>  
 Piotr Machczyński  <https://orcid.org/0000-0002-3196-2427>  
 Wiktoria Maria Suchorska  <https://orcid.org/0000-0003-4742-2465>  
 Wojciech Golusiński  <https://orcid.org/0000-0002-6075-3464>

## References

- Sung H, Ferlay J, Siegel RL, et al. Global Cancer Statistics 2020: GLOBOCAN estimates of incidence and mortality worldwide for 36 cancers in 185 countries. *CA Cancer J Clin.* 2021;71(3):209–249. doi:10.3322/caac.21660
- De Keukeleire SJ, Vermassen T, Hilgert E, Creyten D, Ferdinande L, Rottey S. Immuno-oncological biomarkers for squamous cell cancer of the head and neck: Current state of the art and future perspectives. *Cancers (Basel).* 2021;13(7):1714. doi:10.3390/cancers13071714
- Gururaja Rao S, Patel NJ, Singh H. Intracellular chloride channels: Novel biomarkers in diseases. *Front Physiol.* 2020;11:96. doi:10.3389/fphys.2020.00096
- Jentsch TJ, Günther W. Chloride channels: An emerging molecular picture. *Bioessays.* 1997;19(2):117–126. doi:10.1002/bies.950190206
- Harrop SJ, DeMaere MZ, Fairlie WD, et al. Crystal structure of a soluble form of the intracellular chloride ion channel CLIC1 (NCC27) at 1.4-Å resolution. *J Biol Chem.* 2001;276(48):44993–45000. doi:10.1074/jbc.M107804200
- Ulmasov B, Bruno J, Woost PG, Edwards JC. Tissue and subcellular distribution of CLIC1. *BMC Cell Biol.* 2007;8(1):8. doi:10.1186/1471-2121-8-8
- Xu Y, Xu J, Feng J, et al. Expression of CLIC1 as a potential biomarker for oral squamous cell carcinoma: A preliminary study. *Onco Targets Ther.* 2018;11:8073–8081. doi:10.2147/OTT.S181936
- Feng J, Xu J, Xu Y, et al. CLIC1 promotes the progression of oral squamous cell carcinoma via integrins/ERK pathways. *Am J Transl Res.* 2019;11(2):557–571. PMID:30899362.
- Wang P, Zeng Y, Liu T, et al. Chloride intracellular channel 1 regulates colon cancer cell migration and invasion through ROS/ERK pathway. *World J Gastroenterol.* 2014;20(8):2071–2078. doi:10.3748/wjg.v20.i8.2071
- Averaimo S, Milton RH, Duchon MR, Mazzanti M. Chloride intracellular channel 1 (CLIC1): Sensor and effector during oxidative stress. *FEBS Lett.* 2010;584(10):2076–2084. doi:10.1016/j.febslet.2010.02.073
- Chang YH, Wu CC, Chang KP, Yu JS, Chang YC, Liao PC. Cell secretome analysis using hollow fiber culture system leads to the discovery of CLIC1 protein as a novel plasma marker for nasopharyngeal carcinoma. *J Proteome Res.* 2009;8(12):5465–5474. doi:10.1021/pr900454e
- Peyvandi H, Peyvandi AA, Safaei A, Zamanian Azodi M, Rezaei-Tavirani M. Introducing potential key proteins and pathways in human laryngeal cancer: A system biology approach. *Iran J Pharm Res.* 2018; 17(1):415–425. PMID:29755572.
- Kim JS, Chang JW, Yun HS, et al. Chloride intracellular channel 1 identified using proteomic analysis plays an important role in the radiosensitivity of HEP-2 cells via reactive oxygen species production. *Proteomics.* 2010;10(14):2589–2604. doi:10.1002/pmic.200900523
- Brierley J, Gospodarowicz MK, Wittekind C. TNM classification of malignant tumours. Chichester, UK: Wiley; 2017. ISBN: 978-1-119-26357-9
- Al Khamici H, Brown LJ, Hossain KR, et al. Members of the chloride intracellular ion channel protein family demonstrate glutaredoxin-like enzymatic activity. *PLoS One.* 2015;10(1):e115699. doi:10.1371/journal.pone.0115699
- Suh KS, Mutoh M, Gerdes M, Yuspa SH. CLIC4, an intracellular chloride channel protein, is a novel molecular target for cancer therapy. *J Invest Dermatol Symp Proc.* 2005;10(2):105–109. doi:10.1111/j.1087-0024.2005.200402.x

17. Karsani S, Saihen N, Zain R, Cheong SC, Abdul Rahman M. Comparative proteomics analysis of oral cancer cell lines: Identification of cancer associated proteins. *Proteome Sci.* 2014;12(1):3. doi:10.1186/1477-5956-12-3
18. Petrova DT, Asif AR, Armstrong VW, et al. Expression of chloride intracellular channel protein 1 (CLIC1) and tumor protein D52 (TPD52) as potential biomarkers for colorectal cancer. *Clin Biochem.* 2008; 41(14–15):1224–1236. doi:10.1016/j.clinbiochem.2008.07.012
19. Chen CD, Wang CS, Huang YH, et al. Overexpression of CLIC1 in human gastric carcinoma and its clinicopathological significance. *Proteomics.* 2007;7(1):155–167. doi:10.1002/pmic.200600663
20. Huang JS, Chao CC, Su TL, et al. Diverse cellular transformation capability of overexpressed genes in human hepatocellular carcinoma. *Biochem Biophys Res Commun.* 2004;315(4):950–958. doi:10.1016/j.bbrc.2004.01.151
21. Wang JW, Peng SY, Li JT, et al. Identification of metastasis-associated proteins involved in gallbladder carcinoma metastasis by proteomic analysis and functional exploration of chloride intracellular channel 1. *Cancer Lett.* 2009;281(1):71–81. doi:10.1016/j.canlet.2009.02.020
22. Tang HY, Beer LA, Tanyi JL, Zhang R, Liu Q, Speicher DW. Protein isoform-specific validation defines multiple chloride intracellular channel and tropomyosin isoforms as serological biomarkers of ovarian cancer. *J Proteomics.* 2013;89:165–178. doi:10.1016/j.jprot.2013.06.016
23. Kobayashi T, Shiozaki A, Nako Y, et al. Chloride intracellular channel 1 as a switch among tumor behaviors in human esophageal squamous cell carcinoma. *Oncotarget.* 2018;9(33):23237–23252. doi:10.18632/oncotarget.25296
24. Lu J, Dong Q, Zhang B, et al. Chloride intracellular channel 1 (CLIC1) is activated and functions as an oncogene in pancreatic cancer. *Med Oncol.* 2015;32(6):616. doi:10.1007/s12032-015-0616-9
25. Wang W, Xu X, Wang W, et al. The expression and clinical significance of CLIC1 and HSP27 in lung adenocarcinoma. *Tumour Biol.* 2011;32(6):1199–1208. doi:10.1007/s13277-011-0223-0
26. Tian Y, Guan Y, Jia Y, Meng Q, Yang J. Chloride intracellular channel 1 regulates prostate cancer cell proliferation and migration through the MAPK/ERK pathway. *Cancer Biother Radiopharm.* 2014;29(8): 339–344. doi:10.1089/cbr.2014.1666
27. Setti M, Savalli N, Osti D, et al. Functional role of CLIC1 ion channel in glioblastoma-derived stem/progenitor cells. *J Natl Cancer Inst.* 2013;105(21):1644–1655. doi:10.1093/jnci/djt278
28. Nanaware PP, Ramteke MP, Somavarapu AK, Venkatraman P. Discovery of multiple interacting partners of gankyrin, a proteasomal chaperone and an oncoprotein: Evidence for a common hot spot site at the interface and its functional relevance. *Proteins.* 2014;82(7): 1283–1300. doi:10.1002/prot.24494





# The impact of IGF-1 on alveolar bone remodeling and BMP-2 expression in orthodontic tooth movement in diabetic rats

Mengxi Wang<sup>1,D,E</sup>, Yanfen Qiu<sup>2,A,F</sup>, Lili Gao<sup>1,B</sup>, Feng Qi<sup>1,D</sup>, Liangjia Bi<sup>1,A,E</sup>

<sup>1</sup> Department of Stomatology, The Fourth Affiliated Hospital of Harbin Medical University, China

<sup>2</sup> Department of Oral Radiology, School of Stomatology, Harbin Medical University, China

A – research concept and design; B – collection and/or assembly of data; C – data analysis and interpretation; D – writing the article; E – critical revision of the article; F – final approval of the article

Advances in Clinical and Experimental Medicine, ISSN 1899–5276 (print), ISSN 2451–2680 (online)

*Adv Clin Exp Med.* 2023;32(3):349–356

## Address for correspondence

Mengxi Wang

E-mail: nftphlvnl@sina.com

## Funding sources

None declared

## Conflict of interest

None declared

Received on July 27, 2018

Reviewed on May 14, 2022

Accepted on September 9, 2022

Published online on November 24, 2022

## Abstract

**Background.** Orthodontic tooth movement is linked to alveolar bone reconstruction.

**Objectives.** As a regulator of cell proliferation, insulin-like growth factor 1 (IGF-1) plays an important role in osteoporotic fracture healing. This study aims to investigate the effect of IGF-1 on alveolar bone remodeling in diabetic rats.

**Materials and methods.** Sprague Dawley (SD) rats were randomly divided into 3 groups, including a control group, a model group established with streptozotocin (STZ) injection to prepare the diabetic rats (type 1 diabetes), and an IGF-1 group of diabetic rats receiving daily intraperitoneal injections of 1.0 mg/kg IGF-1. Nickel–titanium coil springs were used to pull the first molar forward to establish the model. The maxillary first to third molars and the surrounding alveolar bone were collected to measure tooth movement distance. Hematoxylin and eosin (H&E) staining was applied to detect the pathological changes in the periodontal tissue. Real-time polymerase chain reaction (PCR) and western blot were adopted to measure bone morphogenetic protein 2 (BMP-2) mRNA and protein expression. Enzyme-linked immunosorbent assays (ELISAs) were used to measure interleukin-1 $\alpha$  (IL-1 $\alpha$ ) levels in the serum.

**Results.** The tooth movement distance was significantly decreased, BMP-2 expression was downregulated, and IL-1 $\alpha$  levels were enhanced in the model group compared to the control group ( $p < 0.05$ ). However, the tooth movement distance was increased, BMP-2 expression was increased, and IL-1 $\alpha$  levels were reduced in the IGF-1 group compared to the model group ( $p < 0.05$ ). Hematoxylin and eosin staining showed that alveolar bone destruction was attenuated in the IGF-1 group, while the new bone was not active in the model group.

**Conclusions.** Diabetes can damage alveolar bone remodeling in orthodontic tooth movement. The IGF-1 promotes alveolar bone remodeling by inhibiting inflammation and upregulating BMP-2 expression.

**Key words:** diabetes mellitus, IGF-1, BMP-2, alveolar bone remodeling, IL-1 $\alpha$

## Cite as

Wang M, Qiu Y, Gao L, Qi F, Bi L. The impact of IGF-1 on alveolar bone remodeling and BMP-2 expression in orthodontic tooth movement in diabetic rats.

*Adv Clin Exp Med.* 2023;32(3):349–356.

doi:10.17219/acem/153956

## DOI

10.17219/acem/153956

## Copyright

Copyright by Author(s)

This is an article distributed under the terms of the Creative Commons Attribution 3.0 Unported (CC BY 3.0) (<https://creativecommons.org/licenses/by/3.0/>)

## Background

The teeth are fixed in the alveolar fossa by attaching to the alveolar bone via the periodontal ligament. The orthodontic process is aimed at the correction of teeth and removal of malocclusions, and depends on the usage of correction devices inside or outside the mouth.<sup>1,2</sup> It adjusts dental deformities and coordinates facial bone, maxillofacial, teeth, nerve, and muscle realignment. Moreover, it corrects the abnormal state between the upper and lower teeth, the upper and lower jaw, the teeth and the jaws, as well as the nerves and muscles, to ensure the balance, stability and beauty of the stomatognathic system.<sup>3,4</sup> Through a corrective force on the teeth, alveolar bone and jaw, the device makes the misaligned teeth physically move to achieve a normal alignment and more natural beauty.<sup>5</sup> People in many countries are more and more aware of the importance of aesthetic teeth and oral health, as a consequence the number of orthodontic patients continues to rise year after year.<sup>6</sup> Alveolar bone reconstruction is critical in orthodontic tooth movement and the simultaneous changes in periodontal tissue caused by the tooth movement.<sup>6,7</sup> Identifying the key factors in alveolar bone remodeling is beneficial in accelerating the orthodontic process. Acceleration of alveolar bone remodeling can be assisted by surgery, drugs and other treatment strategies.<sup>8</sup> Periodontal disease, caries and other risks may escalate due to factors such as difficult physiological transformation, poor regeneration ability, and longer time required for adult alveolar bone reconstruction.<sup>9,10</sup> Therefore, speeding up orthodontic tooth movement and shortening the orthodontic treatment time is crucial.

Diabetes mellitus (DM) can lead to metabolic disorders of minerals, in which increased blood glucose further aggravates vitamin, bone and other metabolic disorders.<sup>11</sup> A deficiency of insulin-like growth factor 1 (IGF-1) and other growth factors induces a variety of diabetic complications.<sup>12,13</sup> Diabetes mellitus causes delayed union of the fracture, mainly due to the occurrence of diabetic osteopenia, which further increases the difficulty of adult orthodontics.<sup>14</sup> Insulin-like growth factor 1 is an important bioactivity factor that plays an important role in the healing of osteoporotic fractures.<sup>15,16</sup> However, the effect of IGF-1 on alveolar bone remodeling and bone morphogenetic protein 2 (BMP-2) expression in orthodontic tooth movement in diabetic rats has not been reported.

## Objectives

Through establishing a type 1 diabetic rat model, this study investigated the influence of IGF-1 on alveolar bone remodeling.

## Materials and methods

### Experimental animals

A total of 60 healthy male Sprague Dawley (SD) rats at 3 months of age and weighing  $250 \pm 30$  g were acquired from the experimental animal center at the Harbin Medical University, China. The feeding conditions included a temperature of  $21 \pm 1^\circ\text{C}$ , humidity of 50–70%, and a 12-hour day/night cycle.

The experiments on rats used for the experiments were approved by the Animal Ethics Committee of the Forth Affiliated Hospital of Harbin Medical University, China (approval No. ZWLLSC-08).

### Main reagents and instruments

Streptozotocin (STZ) was purchased from Sigma-Aldrich (St. Louis, USA). Trizol reagents were bought from Invitrogen (Shanghai, China). Polyvinylidene fluoride (PVDF) membranes were obtained from Pall Life Sciences Inc. (Port Washington, USA). Western blot-related chemical reagents were obtained from Beyotime (Shanghai, China). Enhanced chemiluminescence (ECL) reagents were provided by Amersham Biosciences (Amersham, UK). Mouse anti-rat BMP-2 monoclonal antibodies and goat anti-mouse horseradish peroxidase (HRP)-labeled immunoglobulin G (IgG) secondary antibodies were purchased from Cell Signaling Technology (Danvers, USA). The RNA extraction kits and reverse transcription kits were bought from Axygen (Union City, USA). Interleukin-1 $\alpha$  (IL-1 $\alpha$ ) enzyme-linked immunosorbent assay (ELISA) kits were obtained from R&D Systems (Minneapolis, USA). Rat urine protein detection reagents were obtained from Beijing Furu Bioengineering Company (Beijing, China). The Lab-system v. 1.3.1 microplate reader was provided by Bio-Rad Laboratories (Hercules, USA). The ABI 7700 Fast Fluorescence Quantitative PCR was purchased from ABI (Foster City, USA). The DNA amplifier PE Gene Amp PCR System 2400 was purchased from Perkin Elmer (Waltham, USA). An electronic blood glucose meter was purchased from Advantage (Indianapolis, USA). Surgical equipment was purchased from the Suzhou Medical Equipment Factory (Suzhou, China). A surgical microscope was bought from the Jiangsu Zhenjiang Optical Instrument Company (model LZL-21; Zhenjiang, China). Automatic Biochemistry Analyzer BK-200 (Shandong Boke Biological Industry, Jinan, China) was used. Urine glucose test paper was obtained from the Pearl River Biochemical Reagents Company (Guangzhou, China). Other commonly used reagents were purchased from Sangon Biotech (Shanghai, China).

### Grouping

Sixty SD rats were randomly and equally divided into 3 groups, including a control group, a model group

established by injecting STZ to prepare a diabetic rat, and an IGF-1 group, in which diabetic rats received daily intraperitoneal injections of 1.0 mg/kg IGF-1.

## DM model preparation

Diabetes mellitus rats were used for modeling after adaptive breeding for 1 week. The rats fasted for 12 h and received 1% STZ solution as a single intraperitoneal injection using a dose of 60 mg/kg. Blood and urine glucose levels were tested after 48 h. Blood glucose > 16.7 mmol/L and urine glucose above +++ (>55.0 mmol/L) were considered successful modeling.<sup>17</sup>

## Establishment of rat orthodontics model

The rats were anesthetized with 10% chloral hydrate via intraperitoneal injection and fixed. Next, a 0.2-mm concavity was ground into the distal axis angle of bilateral upper jaws, the lips, the tongue, and the gingival margin between the mesial surface of the first molar and the axial angle. Nickel-titanium coil springs were measured for the initial length out of the mouth and remeasured within the mouth after force proofing to ensure their accuracy. Then, the coil springs were fixed in the concave by a 0.2-mm ligation wire and 50 g of force was added to both sides to pull the first molar forward.<sup>18</sup>

## Specimen collection

The rats were euthanized on the 16<sup>th</sup> day after treatment. Aorta blood was collected and stored at room temperature for 30 min. Then, the blood was centrifuged at 3600 rpm for 10 min at 4°C and the serum was stored at -20°C. The specimens of bilateral maxillary first to third molars and surrounding alveolar bone were collected and fixed in 4% paraformaldehyde for 24 h. After measuring the distance of the experimental tooth movement, the specimens were decalcified using a 10% ethylenediaminetetraacetic acid (EDTA) solution.

## ELISA

Enzyme-linked immunosorbent assay was used to test IL-1 $\alpha$  content in the supernatant. A total of 50  $\mu$ L of diluted standard substance were added into each well to establish a standard curve. Next, a 50- $\mu$ L sample was added to the plate and washed 5 times. Then, 50  $\mu$ L of conjugate reagent were added and incubated at 37°C for 30 min. After being washed 5 times, 50  $\mu$ L of color agents A and B were added and incubated at 37°C for 30 min in the dark, followed by the addition of 50  $\mu$ L of buffer to stop the reaction and subsequent measurement of the optical density (OD) value at a wavelength of 450 nm. The OD value of the standard substance was used to prepare the linear regression

equation, which was adopted to calculate the concentration of samples.

## Real-time PCR

Total RNA was extracted from alveolar bone and reversely transcribed into cDNA. The primers were designed using Primer Premier v. 6.0 software (PREMIER Biosoft, San Francisco, USA) based on the mRNA sequence (BMP-2: accession number: NM\_017178.1 and glyceraldehyde-3-phosphate dehydrogenase (GAPDH): accession number: NM\_017008.4) and synthesized by Invitrogen (Table 1). Using SYBR Green qPCR SuperMix, the real-time polymerase chain reaction (PCR) was performed at 56°C for 1 min, followed by 35 cycles at 92°C for 30 s, 35 cycles at 58°C for 45 s, and 35 cycles at 72°C for 35 s. Glyceraldehyde-3-phosphate dehydrogenase was selected as an internal reference. The relative expression of mRNA was calculated using the  $2^{-\Delta\Delta CT}$  method.

Table 1. Primer sequences

Gene	Forward 5'-3'	Reverse 5'-3'
GAPDH	AGTACCAGTCTGTTGCTGG	TAATAGACCCGGATGTCTGGT
BMP-2	TGCACCTACTCTCGATCCAT	GTGTAGGACCTCATACCTT

## Western blot

Radioimmunoprecipitation assay (RIPA) lysis buffer was added to the alveolar bone and cracked on ice for 15–30 min. Next, the tissue was treated 4 times with ultrasound lasting 5 s, and centrifuged at 10,000 g for 15 min. The protein was transferred to a new Eppendorf (Ep) tube and quantified using the Bradford method. The protein was separated using 10% sodium dodecyl sulfate-polyacrylamide gel electrophoresis (SDS-PAGE) and transferred to a PVDF membrane using 100 mA for 1.5 h. After blocking with 5% skim milk for 2 h, the membrane was incubated with BMP-2 antibodies (1:2000) at 4°C overnight. Then, the membrane was incubated with HRP-conjugated goat anti-rabbit secondary antibody (1:2000) at room temperature for 30 min. After that, the ECL reagent was added to the membrane and incubated for 1 min, followed by exposure. The film was scanned using Quantity One software (Bio-Rad Laboratories) and analyzed with a protein image processing system. Four independent experiments were performed for each assay.

## Hematoxylin and eosin staining

The alveolar bone tissue was decalcified in 10% EDTA, dehydrated in ethanol, dewaxed with xylene, embedded in paraffin, and stained with hematoxylin and eosin (H&E). At last, the samples were observed under a light microscope (Olympus BX51; Olympus Corp., Tokyo, Japan).

## Statistical analyses

The R software package v. 3.6.1 (R Foundation for Statistical Computing, Vienna, Austria) was used for statistical analyses of all the data, and the Shapiro–Wilk test was used to evaluate the normality of the data. The results were shown in Supplementary Table 1. A value of  $p > 0.05$  indicates that the orthodontic tooth movement distance, BMP-2 mRNA expression, BMP-2 protein expression, and serum IL-1 $\alpha$  levels all conformed to a normal distribution and are expressed as a mean  $\pm$  standard deviation. In addition, the Levene's test was consistent with the homogeneity of variance of normally distributed data; the results of the Levene's test are shown in Supplementary Table 2. One-way analysis of variance (ANOVA) and the Tukey's post hoc test were used to compare the differences between the groups, degrees of freedom (df) =  $K-1$ , where  $K$  is the number of groups. The  $p$ -value smaller than 0.05 indicated statistically significant differences between the groups.

## Results

### Orthodontic tooth movement distance

The comparison results of orthodontic tooth movement distances are shown in Fig. 1 and Table 2. Under the action of orthodontic force, the tooth movement distance of the 3 groups gradually increased. A comparison of tooth movement distances between the control group, model group and IGF-1 group was performed using ANOVA and Tukey's post hoc test. The results showed that  $F = 389.40$ ,  $p < 0.001$ ,  $df = 2$ , and the difference between the 3 groups was statistically significant. The results of the Tukey's post hoc tests are shown in Supplementary Table 3. The tooth movement distance in the model group ( $0.3 \pm 0.06$  mm) was significantly shorter than in the control group ( $0.8 \pm 0.05$  mm,  $p < 0.001$ ). Compared to the model group, the distance in the IGF-1 group significantly increased ( $0.62 \pm 0.06$  mm,  $p < 0.001$ ). The tooth movement distance in the IGF-1 group was significantly shorter than in the control group ( $p < 0.001$ ).

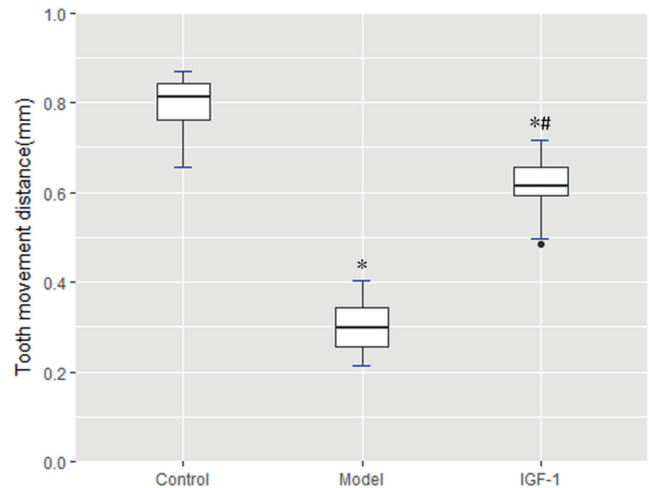


Fig. 1. Orthodontic tooth movement distance. Comparison between the model group and the control group, \* $p < 0.001$ ; the insulin-like growth factor 1 (IGF-1) group and the control group, \* $p < 0.001$ ; the IGF-1 group compared with the model group, # $p < 0.001$ . The upper and lower boundaries of the main body of the box diagram are the upper and the lower quartile, the horizontal line in the middle is the median, the whiskers extend to a maximum of  $1.5 \times$  interquartile range (IQR) beyond the box, and the black dots represent outliers

### Histological analysis with H&E staining

The rats in each group showed periodontal membrane narrowing and alveolar bone resorption on the pressure side. Increased bone deposits and new bone formation were found in the bone resorption pit on the tension side of the control group. The number of osteoclasts increased in the model group. Osteoclasts were decreased in the IGF-1 group and the periodontal and dental tissue began to repair. A small number of osteoblasts were seen arranged in the IGF-1 group (Fig. 2).

### BMP-2 mRNA expression

Real-time PCR was used to detect BMP-2 mRNA expression in rat alveolar bone, and the results are shown in Fig. 3 and Table 3. The BMP-2 mRNA expression levels in the control group, model group and IGF-1 group were compared using one-way ANOVA and Tukey's post hoc test ( $F = 270.52$ ,  $p < 0.001$ ,  $df = 2$ ), and the differences among the 3 groups were statistically significant. The results of the Tukey's post hoc test are shown in Supplementary Table 4. The BMP-2 mRNA expression in the model

Table 2. Orthodontic tooth movement distance

Group	n	Orthodontic tooth movement distance [mm]	F	df	p-value
Control group	20	$0.80 \pm 0.05$	389.395	2	<0.001
Model group	20	$0.30 \pm 0.06$			
IGF-1 group	20	$0.62 \pm 0.06$			

IGF-1 – insulin-like growth factor 1; df – degrees of freedom.



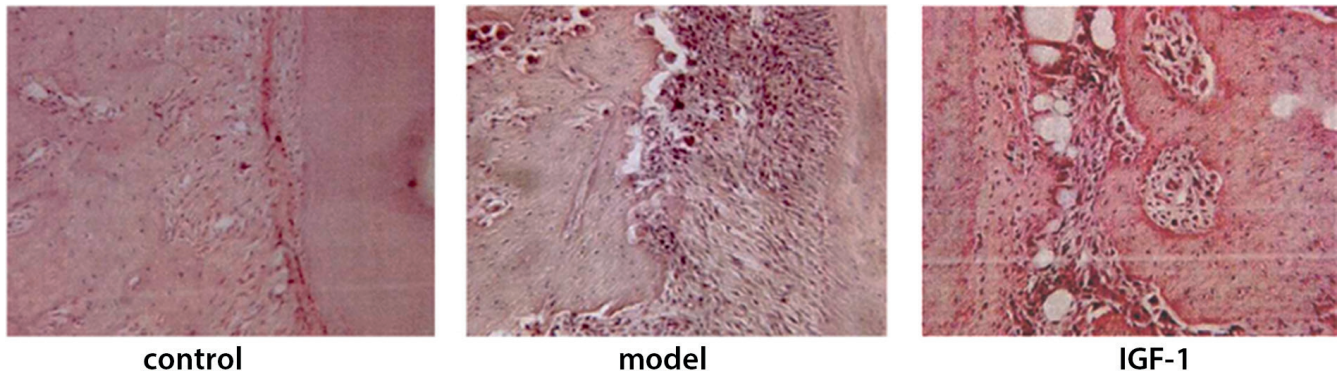


Fig. 2. Histological changes observed using hematoxylin and eosin (H&E) staining (x200 magnification)

IGF-1 – insulin-like growth factor 1.

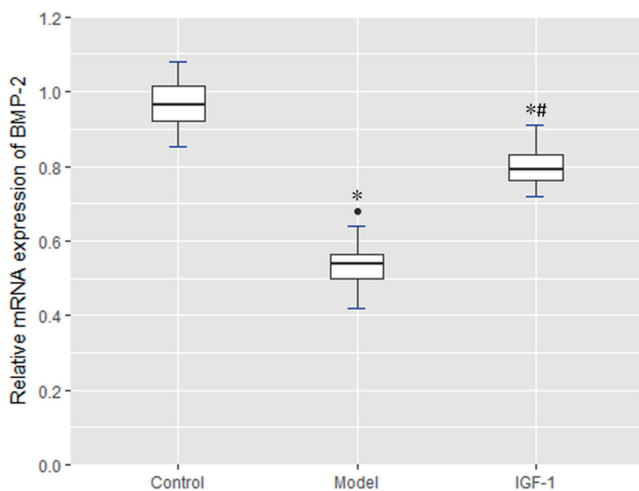


Fig. 3. Bone morphogenetic protein 2 (BMP-2) mRNA expression changes. Comparison between the model group and the control group, \* $p < 0.001$ ; the insulin-like growth factor 1 (IGF-1) group and the control group, \* $p < 0.001$ ; the IGF-1 group and the model group, # $p < 0.001$ . The upper and lower boundaries of the main body of the box diagram are the upper and the lower quartile, the horizontal line in the middle is the median, the whiskers extend to a maximum of  $1.5 \times$  interquartile range (IQR) beyond the box, and the black dots represent outliers

group ( $0.53 \pm 0.06$ ) was significantly lower than in the control group ( $0.96 \pm 0.06$ ,  $p < 0.001$ ). However, compared with the model group, BMP-2 mRNA expression in the IGF-1 group was significantly increased ( $0.8 \pm 0.05$ ,  $p < 0.001$ ), and the BMP-2 mRNA expression in the IGF-1 group was significantly lower than in the control group ( $p < 0.001$ ).

### BMP-2 protein expression

Western blot was used to detect the expression of BMP-2 protein in rat alveolar bone, and the results are presented in Fig. 4 and Table 4. The expression levels of BMP-2 protein in the control group, model group and IGF-1 group were compared using one-way ANOVA and Tukey’s post hoc test ( $F = 224.54$ ,  $p < 0.001$ ,  $df = 2$ ), and the differences among the 3 groups were statistically significant. The results of the Tukey’s post hoc test are shown in Supplementary Table 5. The expression of BMP-2 protein in the model group ( $0.72 \pm 0.07$ ) was significantly lower than in the control group ( $1.2 \pm 0.08$ ,  $p < 0.001$ ). However, BMP-2 protein expression in the IGF-1 group ( $0.91 \pm 0.06$ ) was significantly higher than in the model group ( $p < 0.001$ ), and in the IGF-1 group it was significantly lower than in the control group ( $p < 0.001$ ).

Table 3. BMP-2 mRNA expression changes

Group	n	BMP-2 mRNA expression changes	F	df	p-value
Control group	20	$0.96 \pm 0.06$	270.520	2	<0.001
Model group	20	$0.53 \pm 0.06$			
IGF-1 group	20	$0.80 \pm 0.05$			

IGF-1 – insulin-like growth factor 1; df – degrees of freedom; BMP-2 – bone morphogenetic protein 2.

Table 4. BMP-2 protein expression changes

Group	n	BMP-2 protein expression changes	F	df	p-value
Control group	20	$1.20 \pm 0.08$	224.542	2	<0.001
Model group	20	$0.72 \pm 0.07$			
IGF-1 group	20	$0.91 \pm 0.06$			

IGF-1 – insulin-like growth factor 1; df – degrees of freedom; BMP-2 – bone morphogenetic protein 2.

Table 5. Serum IL-1 $\alpha$  levels

Group	n	Serum IL-1 $\alpha$ levels [pg/mL]	F	df	p-value
Control group	20	107.86 $\pm$ 26.66	242.797	2	<0.001
Model group	20	276.11 $\pm$ 23.26			
IGF-1 group	20	217.21 $\pm$ 23.44			

IL-1 $\alpha$  – interleukin-1 $\alpha$ ; IGF-1 – insulin-like growth factor 1; df – degrees of freedom.

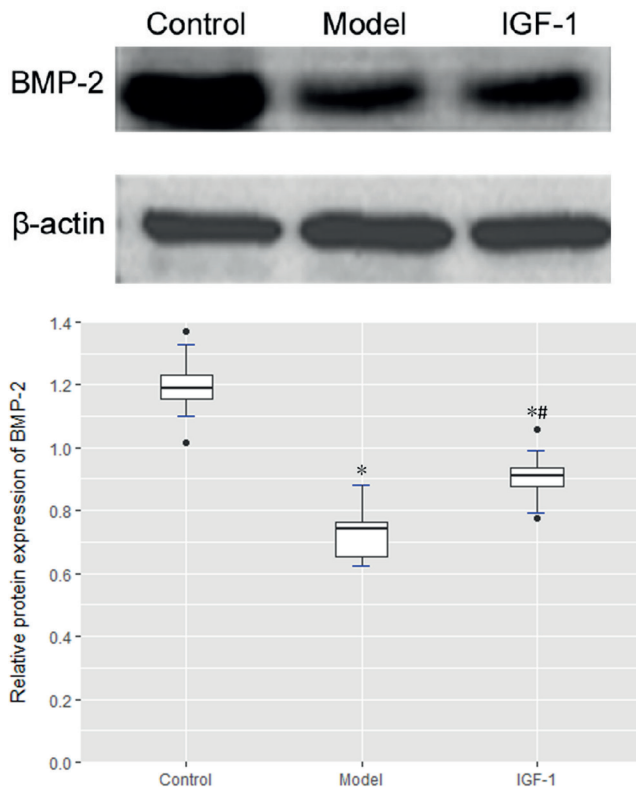


Fig. 4. Bone morphogenetic protein 2 (BMP-2) expression changes. Comparison between the model group and the control group, \* $p < 0.004$ ; the insulin-like growth factor 1 (IGF-1) group and the control group, \* $p < 0.001$ ; the IGF-1 group and the model group, # $p < 0.001$ . The upper and lower boundaries of the main body of the box diagram are the upper and the lower quartile, the horizontal line in the middle is the median, the whiskers extend to a maximum of 1.5  $\times$  interquartile range (IQR) beyond the box, and the black dots represent outliers

## The expression of IL-1 $\alpha$ in serum

The expression of IL-1 $\alpha$  in serum was detected with ELISA, and the results were shown in Fig. 5 and Table 5. The serum IL-1 $\alpha$  levels of the control group, model group and IGF-1 group were compared using one-way ANOVA and Tukey's post hoc test ( $F = 242.80$ ,  $p < 0.001$ ,  $df = 2$ ), and the differences among the 3 groups were statistically significant. The results of the Tukey's post hoc test are shown in Supplementary Table 6. The serum IL-1 $\alpha$  levels in the model group ( $276.11 \pm 23.26$  pg/mL) were significantly higher than in the control group ( $107.86 \pm 26.66$  pg/mL,  $p < 0.001$ ). The level of IL-1 $\alpha$  in the IGF-1 group was  $217.21 \pm 23.44$  pg/mL, which was significantly lower than in the model group ( $p < 0.001$ ).

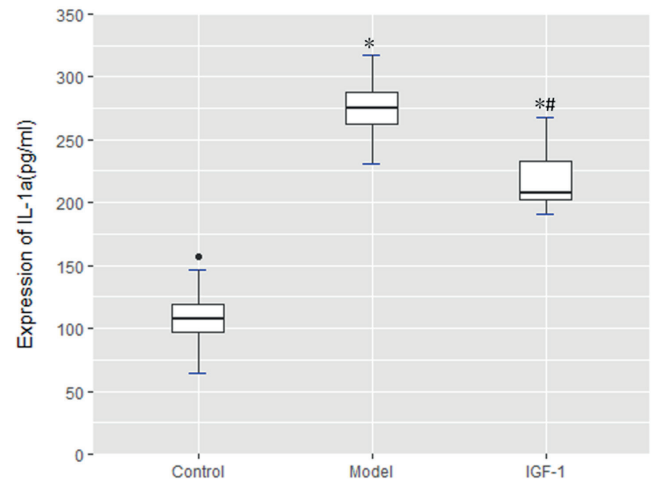


Fig. 5. Serum interleukin-1 $\alpha$  (IL-1 $\alpha$ ) levels. Comparison between the model group and the control group, \* $p < 0.001$ ; the IGF-1 group and the control group, \* $p < 0.001$ ; the IGF-1 group and the model group, # $p < 0.001$ . The upper and lower boundaries of the main body of the box diagram are the upper and the lower quartile, the horizontal line in the middle is the median, the whiskers extend to a maximum of 1.5  $\times$  interquartile range (IQR) beyond the box, and the black dots represent outliers

The level of IL-1 $\alpha$  in the IGF-1 group was significantly higher than in the control group ( $p < 0.001$ ).

## Discussion

Reduced physical activity and overeating can cause endocrine and metabolic disorders, resulting in the occurrence and development of DM. Diabetes mellitus causes damage to multiple tissues and organs and induces microvascular disease, as well as cardiovascular and cerebrovascular diseases, which seriously affect the prognosis. Diabetes mellitus is an enormous challenge faced by the endocrine disciplines.<sup>19</sup> On the other hand, DM-induced metabolic disorders, increased blood glucose, and insulin deficiency further aggravate abnormal bone metabolism, leading to osteoporosis which affects orthodontics.<sup>20</sup> This study showed a reduced distance of tooth movement and formed bone resorption lacunae, an increased number of osteoclasts, as well as enhanced secretion of IL-1 $\alpha$  during the orthodontic process in DM rats. These factors affect orthodontic tooth movement during alveolar bone reconstruction.

The IGF-1, also known as somatostatin C, is regulated by pituitary growth hormone together with growth

hormone C. The IGF-1 is synthesized and secreted by osteoblasts, osteoclasts and other cells.<sup>21</sup> It regulates bone metabolism by binding to receptors on the surface of specific target cells mainly through autocrine and paracrine pathways. It induces bone marrow stromal cells and osteoblast differentiation, and promotes the synthesis of type I collagen fibers that can promote differentiation, leading to the facilitation of bone metabolism.<sup>22</sup> Therefore, this study explored the role of IGF-1 during the orthodontic process in DM rats and showed that IGF-1 accelerated the movement of teeth, promoted new bone formation, reduced the number of osteoclasts, and inhibited the secretion of inflammatory factors resulting in enhanced reconstruction of alveolar bone during orthodontic tooth movement. Further investigations found that IGF-1 increased BMP-2 mRNA and protein expression. It has been proven that BMP-2 plays an important role in the process of fracture healing. The BMP-2 promotes the expression of bone matrix proteins by regulating bone alkaline phosphatase, thereby contributing to the mineralization of the extracellular matrix and the promotion of the orthodontics process.<sup>23,24</sup>

## Limitations

This study has some limitations. Although the role of IGF-1 in orthodontic alveolar bone remodeling in DM rats has been demonstrated, the exact molecular mechanisms by which IGF-1 is involved in alveolar bone remodeling in DM require further investigations. In addition, whether IGF-1 plays a role in alveolar bone remodeling in DM patients needs to be verified.

## Conclusions

Diabetes mellitus destroys alveolar bone remodeling in orthodontic tooth movement and IGF-1 promotes alveolar bone remodeling, possibly by promoting BMP-2 expression and inhibiting inflammation.

## Supplementary data

The Supplementary data are available at <https://doi.org/10.5281/zenodo.7317395>. The package contains the following files:

- Supplementary Table 1. Results of Shapiro–Wilk test.
- Supplementary Table 2. Results of Levene's test.
- Supplementary Table 3. Results of Tukey's post hoc test of orthodontic tooth movement distance.
- Supplementary Table 4. Results of Tukey's post hoc test of BMP-2 mRNA expression changes.
- Supplementary Table 5. Results of Tukey's post hoc test of BMP-2 protein expression changes.
- Supplementary Table 6. Results of Tukey's post hoc test of serum IL-1 $\alpha$  levels.

## ORCID iDs

Mengxi Wang  <https://orcid.org/0000-0001-9709-3378>  
 Yanfen Qiu  <https://orcid.org/0000-0002-8955-2623>  
 Lili Gao  <https://orcid.org/0000-0001-6412-6516>  
 Feng Qi  <https://orcid.org/0000-0002-4863-6492>  
 Liangjia Bi  <https://orcid.org/0000-0001-9691-0903>

## References

1. Arun M, Usman Q, Johal A. Orthodontic treatment modalities: A qualitative assessment of Internet information. *J Orthod.* 2017;44(2):82–89. doi:10.1080/14653125.2017.1313546
2. Al-Zoubi H, Alharbi AA, Ferguson DJ, Zafar MS. Frequency of impacted teeth and categorization of impacted canines: A retrospective radiographic study using orthopantomograms. *Eur J Dent.* 2017;11(1):117–121. doi:10.4103/ejd.ejd\_308\_16
3. Tehranchi A, Motamedian SR, Saedi S, Kabiri S, Shidfar S. Correlation between frontal sinus dimensions and cephalometric indices: A cross-sectional study. *Eur J Dent.* 2017;11(1):64–70. doi:10.4103/1305-7456.202630
4. Saleh M, Hajeer MY, Muessig D. Acceptability comparison between Hawley retainers and vacuum-formed retainers in orthodontic adult patients: A single-centre, randomized controlled trial. *Eur J Orthod.* 2017;39(4):453–461. doi:10.1093/ejo/cjx024
5. Vicente A, Ortiz Ruiz AJ, González Paz BM, García López J, Bravo-González LA. Efficacy of fluoride varnishes for preventing enamel demineralization after interproximal enamel reduction: Qualitative and quantitative evaluation. *PLoS One.* 2017;12(4):e0176389. doi:10.1371/journal.pone.0176389
6. Yi J, Xiao J, Li Y, Li X, Zhao Z. Efficacy of piezocision on accelerating orthodontic tooth movement: A systematic review. *Angle Orthod.* 2017;87(4):491–498. doi:10.2319/01191-751.1
7. Li Y, Hu Z, Zhou C, et al. Intermittent parathyroid hormone (PTH) promotes cementogenesis and alleviates the catabolic effects of mechanical strain in cementoblasts. *BMC Cell Biol.* 2017;18(1):19. doi:10.1186/s12860-017-0133-0
8. Savoldi F, Visconti L, Dalessandri D, et al. In vitro evaluation of the influence of velocity on sliding resistance of stainless steel arch wires in a self-ligating orthodontic bracket. *Orthod Craniofac Res.* 2017;20(2):119–125. doi:10.1111/ocr.12156
9. Rashid A, ElSharaby FA, Nassef EM, Mehanni S, Mostafa YA. Effect of platelet-rich plasma on orthodontic tooth movement in dogs. *Orthod Craniofac Res.* 2017;20(2):102–110. doi:10.1111/ocr.12146
10. Angelieri F, Franchi L, Cevidanes LHS, Hino CT, Nguyen T, McNamara JA. Zygomaticomaxillary suture maturation: A predictor of maxillary protraction? Part I. A classification method. *Orthod Craniofac Res.* 2017;20(2):85–94. doi:10.1111/ocr.12143
11. Mostafavinia A, Ahadi R, Abdollahifar M, Ghorishi SK, Jalalifirouzkouhi A, Bayat M. Evaluation of the effects of photobiomodulation on biomechanical properties and Hounsfield unit of partial osteotomy healing in an experimental rat model of type I diabetes and osteoporosis. *Photomed Laser Surg.* 2017;35(10):520–529. doi:10.1089/pho.2016.4191
12. Canda MT, Demir N, Sezer O. Fetal nasal bone length as a novel marker for prediction of adverse perinatal outcomes in the first trimester of pregnancy. *Balkan Med J.* 2017;34(2):127–131. doi:10.4274/balkanmedj.2016.0133
13. Mishra R, Cano E, Venkatram S, Diaz-Fuentes G. An interesting case of mycoplasma pneumonia associated multisystem involvement and diffuse alveolar hemorrhage. *Respir Med Case Rep.* 2017;21:78–81. doi:10.1016/j.rmcr.2017.03.022
14. Raška I, Rašková M, Zikán V, Škrha J. Prevalence and risk factors of osteoporosis in postmenopausal women with type 2 diabetes mellitus. *Cent Eur J Public Health.* 2017;25(1):3–10. doi:10.21101/cejph.a4717
15. Ogundele OM, Ebenezer PJ, Lee CC, Francis J. Stress-altered synaptic plasticity and DAMP signaling in the hippocampus-PFC axis: Elucidating the significance of IGF-1/IGF-1R/CaMKII $\alpha$  expression in neural changes associated with a prolonged exposure therapy. *Neuroscience.* 2017;353:147–165. doi:10.1016/j.neuroscience.2017.04.008
16. Weischendorff S, Kielsen K, Sengeløv H, et al. Associations between levels of insulin-like growth factor 1 and sinusoidal obstruction syndrome after allogeneic haematopoietic stem cell transplantation. *Bone Marrow Transplant.* 2017;52(6):863–869. doi:10.1038/bmt.2017.43

17. Hazell TJ, Olver TD, Kowalchuk H, et al. Aerobic endurance training does not protect bone against poorly controlled type 1 diabetes in young adult rats. *Calcif Tissue Int.* 2017;100(4):374–381. doi:10.1007/s00223-016-0227-2
18. Faienza MF, Ventura A, Delvecchio M, et al. High sclerostin and Dickkopf-1 (DKK-1) serum levels in children and adolescents with type 1 diabetes mellitus. *J Clin Endocrinol Metab.* 2017;102(4):1174–1181. doi:10.1210/jc.2016-2371
19. Domouky AM, Hegab AS, Al-Shahat A, Raafat N. Mesenchymal stem cells and differentiated insulin producing cells are new horizons for pancreatic regeneration in type I diabetes mellitus. *Int J Biochem Cell Biol.* 2017;87:77–85. doi:10.1016/j.biocel.2017.03.018
20. Pogliacomì F, Pellegrini A, Tacci F, et al. Risks of subsequent contralateral fractures of the trochanteric region in elderly. *Acta Biomed.* 2016;87(3):275–281. PMID:28112694.
21. Mehrpour M, Rahatlou H, Hamzehpur N, Kia S, Safdarian M. Association of insulin-like growth factor-I with the severity and outcomes of acute ischemic stroke. *Iran J Neurol.* 2016;15(4):214–218. PMID:28435630.
22. Shahbazi M, Abdolmohammadi R, Ebadi H, Farazmandfar T. Novel functional polymorphism in *IGF-1* gene associated with multiple sclerosis: A new insight to MS. *Multiple Scler Relat Dis.* 2017;13:33–37. doi:10.1016/j.msard.2017.02.002
23. Dohan Ehrenfest DM, Pinto NR, Pereda A, et al. The impact of the centrifuge characteristics and centrifugation protocols on the cells, growth factors, and fibrin architecture of a leukocyte- and platelet-rich fibrin (L-PRF) clot and membrane. *Platelets.* 2018;29(2):171–184. doi:10.1080/09537104.2017.1293812
24. López-Cebral R, Civantos A, Ramos V, et al. Gellan gum based physical hydrogels incorporating highly valuable endogen molecules and associating BMP-2 as bone formation platforms. *Carbohydrate Polym.* 2017;167:345–355. doi:10.1016/j.carbpol.2017.03.049

# Hydrogen suppresses oxidative stress by inhibiting the p38 MAPK signaling pathway in preeclampsia

Lili Guo<sup>1,B-D</sup>, Ming Liu<sup>2,E</sup>, Tao Duan<sup>1,A,F</sup>

<sup>1</sup> Shanghai Key Laboratory of Maternal Fetal Medicine, Shanghai Institute of Maternal-Fetal Medicine and Gynecologic Oncology, Shanghai First Maternity and Infant Hospital, School of Medicine, Tongji University, China

<sup>2</sup> Department of Obstetrics, Shanghai East Hospital, Tongji University School of Medicine, Shanghai, China

A – research concept and design; B – collection and/or assembly of data; C – data analysis and interpretation;

D – writing the article; E – critical revision of the article; F – final approval of the article

Advances in Clinical and Experimental Medicine, ISSN 1899–5276 (print), ISSN 2451–2680 (online)

*Adv Clin Exp Med.* 2023;32(3):357–367

## Address for correspondence

Tao Duan

E-mail: yxgll1985@163.com

## Funding sources

None declared

## Conflict of interest

None declared

Received on April 23, 2022

Reviewed on June 5, 2022

Accepted on September 15, 2022

Published online on November 4, 2022

## Abstract

**Background.** Hypertensive disorders complicating pregnancy (HDCP) are one of the most serious medical disorders during pregnancy.

**Objectives.** To investigate the effects of hydrogen on the mitogen-activated protein kinase (MAPK) signaling pathway in preeclampsia (PE).

**Materials and methods.** The N(omega)-nitro-L-arginine methyl ester (L-NAME)-induced PE model with Sprague Dawley (SD) rats was employed. An inhibitor of MAPK signaling pathways (SB203580) was used as a p38 MAPK inhibitor. The SD rats were randomized into 5 groups: non-pregnant (NP); normal pregnancy (P); pregnancy + L-NAME (L); pregnancy + L-NAME + hydrogen-rich saline (LH); and pregnancy + L-NAME + hydrogen-rich saline + SB203580 (LHS). The pregnancies were terminated on day 22 of gestation, and the placentas and kidneys were microscopically inspected. Tumor necrosis factor alpha (TNF- $\alpha$ ), interleukin-1 $\beta$  (IL-1 $\beta$ ) and malondialdehyde (MDA) levels were assessed. The mean systolic blood pressure (SBP) and level of proteinuria were recorded. The p38 MAPK mRNA expression and p-p38 MAPK protein levels were measured using real-time polymerase chain reaction (RT-PCR) and western blot, respectively.

**Results.** It was found that hydrogen-rich saline (LH group) decreased placental MDA, proteinuria, TNF- $\alpha$ , and IL-1 $\beta$  levels in the placental tissues compared with the L group (all  $p < 0.05$ ). Additionally, hydrogen-rich saline (LH group) treatment significantly decreased the p38 MAPK mRNA expression and p-p38 MAPK protein levels compared with the L group ( $p < 0.05$ ). The p38 MAPK inhibitor SB203580 (LHS group) further decreased the p38 MAPK mRNA expression and p-p38 MAPK protein levels compared with the LH group ( $p < 0.05$ ).

**Conclusions.** Hydrogen can decrease the reactive oxygen species (ROS) content and inhibit the MAPK pathway. The protective effect of hydrogen may be associated with the inhibition of the p38 MAPK signaling pathway.

**Key words:** preeclampsia, antioxidant, reactive oxygen species, hydrogen, p38 MAPK pathway

## Cite as

Guo L, Liu M, Duan T. Hydrogen suppresses oxidative stress by inhibiting the p38 MAPK signaling pathway in preeclampsia. *Adv Clin Exp Med.* 2023;32(3):357–367. doi:10.17219/acem/154623

## DOI

10.17219/acem/154623

## Copyright

Copyright by Author(s)

This is an article distributed under the terms of the Creative Commons Attribution 3.0 Unported (CC BY 3.0) (<https://creativecommons.org/licenses/by/3.0/>)



## Background

Preeclampsia (PE) is a serious disease for pregnant women. It can lead to placental disorders, fetal growth restriction and other unfavorable outcomes.<sup>1</sup> Its etiology remains complex.

The presence of oxidative stress, such as placental oxidative stress<sup>2</sup> or periodontal oxidative stress,<sup>3</sup> may increase the risk of PE in pregnant women. As a novel antioxidant, hydrogen selectively reduced toxic reactive oxygen levels,<sup>4</sup> which was observed in a PE rat model in our previous study,<sup>5</sup> indicating that hydrogen is a potential therapeutic antioxidant that could be clinically applied in treating PE. Its mechanism of action remains to be investigated.

Previous studies found that oxidative stress activated mitogen-activated protein kinase (MAPK) signaling and increased the expression of apoptosis receptors.<sup>6</sup> The p38 MAPK activity was observed to be significantly higher in women with PE placentas.<sup>7</sup> These findings imply that reactive oxygen species (ROS) could activate the p38 MAPK signaling pathway in the placenta, followed by the over-expression of sFlt-1 and sEng in maternal serum<sup>8</sup> and a systemic inflammatory reaction, giving rise to endothelial dysfunction and the clinical symptoms of PE. Therefore, hydrogen, as an antioxidant agent, may have an effect on the MAPK signaling pathway by blocking ROS, thereby reducing the inflammatory reaction and apoptosis, and ultimately improving the prognosis of PE patients.

To explore the mechanism of molecular hydrogen in the pathogenesis of hypertensive disorders complicating pregnancy (HDCP), we investigated the influence of hydrogen on ROS content, apoptosis and the MAPK signaling pathway at the mRNA and protein levels by employing a previously established N(omega)-nitro-L-arginine methyl ester (L-NAME)-induced gestational hypertension rat model.

To further confirm the role of the MAPK signaling pathways in the pathogenesis of HDCP, an inhibitor of MAPK signaling pathways (SB203580) was employed in the L-NAME-induced gestational hypertension rat model.

The investigation of the mechanism of molecular hydrogen could potentially promote novel treatment strategies in the PE and HDCP patient populations.

## Objectives

The objective of this study was to explore the mechanism of molecular hydrogen in the pathogenesis of PE by investigating the influence of hydrogen on ROS content, apoptosis and the MAPK signaling pathway at the mRNA and protein levels. We employed a previously established gestational hypertension rat model<sup>5</sup> and an inhibitor of MAPK signaling pathways (SB203580).<sup>9</sup>

## Materials and methods

The experiment was approved by animal ethical committee of Tongji University, Shanghai, China (approval No. TJLAC-020-010).

### Animals and drugs

Fifty female and 50 male Sprague Dawley (SD) rats weighing 220–250 g and aged 9–10 weeks were employed. They were kept under light-, air- and temperature-controlled conditions for 7 days before the experiment. The rats were mated separately overnight. The first day of finding spermatozoa using vaginal smear in the female rat was defined as day 0 of gestation for the female rat. Each pregnant rat was raised in a separate metabolic cage. On the 21<sup>st</sup> gestational day, the metabolic cages were used to collect 24-hour urine samples.

Hydrogen was dissolved in physiological saline for 6 h under 0.4 MPa, followed by sterilization. The prepared hydrogen saline was stored in an aluminum bag at 4°C. Gas chromatography was used to measure the concentration of hydrogen.<sup>4</sup> Hydrogen saline above 0.6 mmol/L, L-NAME and SB203580 (both from Sigma-Aldrich, St. Louis, USA) were used in the experiment.

### Intervention

The rats were randomized into 5 groups on the 15<sup>th</sup> day of pregnancy: non-pregnant (NP); normal pregnancy (P); pregnancy + L-NAME (L); pregnancy + L-NAME + hydrogen-rich saline (LH); and pregnancy + L-NAME + hydrogen-rich saline + SB203580 (LHS). Each group had 10 rats. The NP rats and P rats as control groups received an intraperitoneal injection of normal saline (5 mL/kg). The PE group (L) and hydrogen intervention group (LH) received L-NAME at a dose of 60 mg/kg dissolved in normal saline or hydrogen-rich saline, respectively. In the LHS group, the pregnant rats received 10 mg/kg/d of SB203580 1 h before receiving L-NAME at a dose of 60 mg/kg dissolved in hydrogen-rich saline.

All rats were anesthetized with ether on the 22<sup>nd</sup> day of pregnancy. The systolic blood pressure (SBP) of the right carotid artery was measured with a polyethylene catheter connected to a Medlab pressure transducer (Nanjing Biotech Co., Jiangsu, China). All rats were sacrificed on the same day under ketamine anesthesia. The pregnant rats underwent cesarean section. The resorption and weight of each pup were determined.

Partial tissues of the placenta, kidney, liver, and aorta were fixed with paraformaldehyde (40 g/L), and the remaining tissues were stored in liquid nitrogen for a subsequent analysis.

## Biochemical factors and cytokines

Following the manufacturer's instructions for the malondialdehyde (MDA) kit (Nanjing Biotech Co.), placental MDA was measured in 100 mg of wet tissue. Twenty-four-hour urine samples were collected and quantified with a total protein kit (Sigma-Aldrich). Placental cytokines, including tumor necrosis factor alpha (TNF- $\alpha$ ) and interleukin-1 $\beta$  (IL-1 $\beta$ ), were measured using an enzyme-linked immunosorbent assay (ELISA) kit (Biosource International, Inc., Camarillo, USA). Based on a standard curve, the TNF- $\alpha$  and IL-1 $\beta$  concentrations were calculated using an absorbance reader (Denley Dragon; Thermo Fisher Scientific, Helsinki, Finland).

## Real-time polymerase chain reaction

Total RNA was extracted from tissues preserved in liquid nitrogen with TRIpure Total RNA Extraction Reagent (ELK Biotechnology Co., Wuhan, China). The EntiLink™ Synthesis Kit (EQ003; ELK Biotechnology) was employed to synthesize the first strand of cDNA, followed by real-time fluorescence quantitative polymerase chain reaction (RT-PCR) with the EnTurbo™ SYBR Green PCR SuperMax Kit (EQ001; ELK Biotechnology), which was performed on a StepOne™ Real-Time PCR Instrument (Life Technologies, Carlsbad, USA). The comparative CT method ( $\Delta\Delta$ CT) was used for relative gene expression analysis. All PCR reactions were performed in duplicate. Primer Premier v. 5.0 software (PREMIER Biosoft International Co., San Francisco, USA) was used for the design of the primer sequences.

## Western blot

Western blot was performed as previously described.<sup>10</sup> The total protein of the placental tissue was extracted using whole cell lysis buffer. The protein samples were resolved on sodium dodecyl sulfate–polyacrylamide gel electrophoresis (SDS–PAGE) gels (Beyotime Biotechnology, Shanghai, China). The proteins were transferred to polyvinylidene fluoride (PVDF) membranes. Rabbit anti-rat primary antibody was probed on the membranes after blocking. Using the ECL detection system (GeneCopia Inc., Rockville, USA), we determined the immune complexes by incubation with a secondary antibody, which was conjugated with horseradish peroxidase (HRP).

## Statistical analyses

The SPSS v. 13.0 (SPSS Inc., Chicago, USA) and GraphPad v. 6.0 (GraphPad Software, San Diego, USA) software was used for statistical analysis. Data distribution was analyzed using the Shapiro–Wilk method. The Student's t-test was used for comparison between the 2 groups for normally distributed data, and the Mann–Whitney

U test was used for non-normally distributed data between the 2 groups. The Levene's test was used to determine the homogeneity of variance for the normally distributed data. Statistical significance was defined as  $p \leq 0.05$ . All statistical data can be found in the Supplementary files (<https://doi.org/10.5281/zenodo.7074902>).

## Results

### Basic parameters

The number of resorptions, fetal weight, protein excretion, and SBP are shown in Table 1. Administration of L-NAME (L group) caused a significant increase in the number of resorptions, SBP and 24-hour urine protein excretion, as well as a decrease in fetal weight, compared with the normal pregnant rats (P group). The hydrogen intervention resulted in an improvement in pregnancy outcomes in terms of fetal weight, resorptions, urine protein excretion, and SBP. However, there were no differences in all indices between the LH and LHS group.

### Lipid peroxidation product levels

The L-NAME-treated group (L group) showed a marked increase in the level of placental MDA on the terminal day ( $p < 0.001$ ; Fig. 1), while the hydrogen-treated rats showed a significant decrease of MDA in both the LH and LHS groups when compared with L group, respectively ( $p < 0.001$ ). Malondialdehyde levels were lower in the P group than in the other groups ( $p < 0.001$ ).

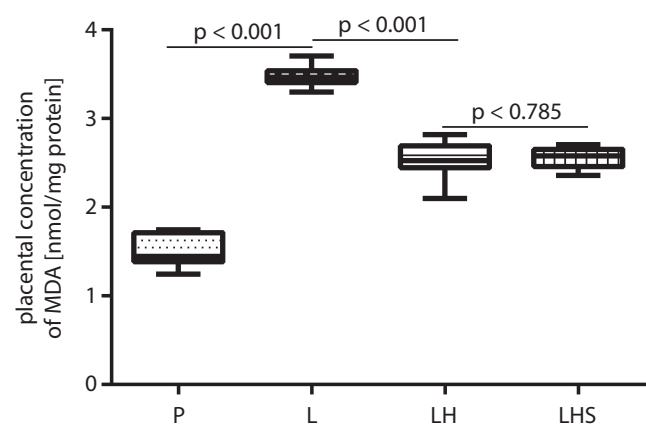


Fig. 1. Malondialdehyde (MDA) assays on day 22 in the placentas

P – normal pregnancy; L – pregnancy + N(omega)-nitro-L-arginine methyl ester (L-NAME); LH – pregnancy + L-NAME + hydrogen saline; LHS – pregnancy + L-NAME + hydrogen saline + SB203580 (n = 10 per group). The p-values were calculated using the Student's t-test.

### Inflammatory factor levels

The L-NAME-treated group (L group) showed elevated placental TNF- $\alpha$  and IL-1 $\beta$  levels, which was in contrast

**Table 1.** Conditions of resorptions, fetal weight, protein excretion, and systolic blood pressure (SBP) in different groups of animals

Group	Number of resorptions, median (range)	Fetal weight [g]	Protein excretion [mg/24 h]	SBP [mm Hg]
NP	–	–	1.02 ±0.50	103.03 ±5.16
P	0 (0–1)	3.13 ±0.53	0.99 ±0.29	106.90 ±3.05
Levene's test	–	–	0.025	0.108
t	–	–	0.190	–2.042
P <sup>1</sup>	–	–	0.852	0.056
L	2 (0–4)	1.93 ±0.58	3.92 ±0.49	157.89 ±7.15
Levene's test	–	0.707	0.093	0.013
t or U	0.000	4.790	–16.193	–20.745
P <sup>2</sup>	<0.001	<0.001	<0.001	<0.001
LH	0 (0–1)	2.53 ±0.38	2.39 ±0.59	137.05 ±6.02
Levene's test	–	0.218	0.378	0.433
t or U	0.000	–2.730	6.247	7.047
P <sup>3</sup>	<0.001	0.015	<0.001	<0.001
LHS	0 (0–1)	2.70 ±0.15	2.27 ±0.45	139.70 ±6.70
Levene's test	–	0.005	0.181	0.540
t or U	45.000	–1.255	0.512	–0.930
P <sup>4</sup>	0.739	0.234	0.615	0.365

NP – non-pregnancy; P – normal pregnancy; L – pregnancy + N(omega)-nitro-L-arginine methyl ester (L-NAME); LH – pregnancy + L-NAME + hydrogen saline rats; LHS – pregnancy + L-NAME + hydrogen saline + SB203580 rats (n = 10 per group). The P<sup>1</sup> comparison was made between NP and P groups. The P<sup>2</sup> comparison was made between P and L groups. The P<sup>3</sup> comparison was made between L and LH groups. The P<sup>4</sup> comparison was made between LH and LHS groups. The Levene's test was used for homogeneity of variance for normally distributed data. The analysis was made using the Student's t-test for normally distributed data. Non-normally distributed data were analyzed using the Mann-Whitney U test. All data were normally distributed except for the number of resorptions.

with the P group (both  $p < 0.001$ , Table 2). However, the hydrogen intervention considerably depressed the L-NAME-mediated increase in placental TNF- $\alpha$  and IL-1 $\beta$  levels. The LHS group showed an even further decrease of inflammatory factor levels compared with the LH group ( $p < 0.001$  and  $p = 0.002$ , respectively).

## Histopathology outcome

When compared with NP and P groups (Fig. 2A,B), reduced Bowman's capsule space and hyperplasia in the glomerular epithelium, in addition to degenerative changes in the proximal convoluted tubules, were significant in the L group (Fig. 2C). This result was consistent with the elevated urine protein levels caused by the administration of L-NAME. Interestingly, the pathological changes were markedly alleviated in the LH and LHS groups (Fig. 2D,E). Similarly, abnormalities were absent in both the NP and P control groups (Fig. 2A,B). Compared with the P group (Fig. 3A), L-NAME caused a remarkable degeneration in the junctional zone of placenta (Fig. 3B), but such degeneration was not found in the P, LH and LHS groups (Fig. 3A,C,D). Similarly, the result of apoptosis in the L group was consistent with findings from the hematoxylin and eosin (H&E)-stained specimens ( $p < 0.001$ , Fig. 4,5). When compared with NP and P groups (Fig. 6A,B), the continuous structure

**Table 2.** Levels of tumor necrosis factor alpha (TNF- $\alpha$ ) and interleukin-1 $\beta$  (IL-1 $\beta$ ) in placenta

Group	TNF- $\alpha$ [pg/mL]	IL-1 $\beta$ [pg/mL]
P	10.09 ±1.25	4.36 ±0.73
L	17.68 ±1.27	11.48 ±0.69
Levene's test	0.533	0.774
t	–13.475	–22.390
P <sup>1</sup>	<0.001	<0.001
LH	15.54 ±0.80	7.98 ±1.61
Levene's test	0.415	0.009
t	4.532	6.321
P <sup>2</sup>	<0.001	<0.001
LHS	12.51 ±0.87	5.82 ±0.61
Levene's test	0.468	0.006
t	8.104	3.977
P <sup>3</sup>	<0.001	0.002

P – normal pregnancy; L – pregnancy + N(omega)-nitro-L-arginine methyl ester (L-NAME); LH – pregnancy + L-NAME + hydrogen saline rats; LHS – pregnancy + L-NAME + hydrogen saline + SB203580 rats (n = 10 per group). The P<sup>1</sup> comparison was made between P and L groups using the Student's t-test. The P<sup>2</sup> comparison was made between L and LH groups using the Student's t-test. The P<sup>3</sup> comparison was made between LH and LHS groups using the Student's t-test. The Levene's test was used for homogeneity of variance. All data were normally distributed.



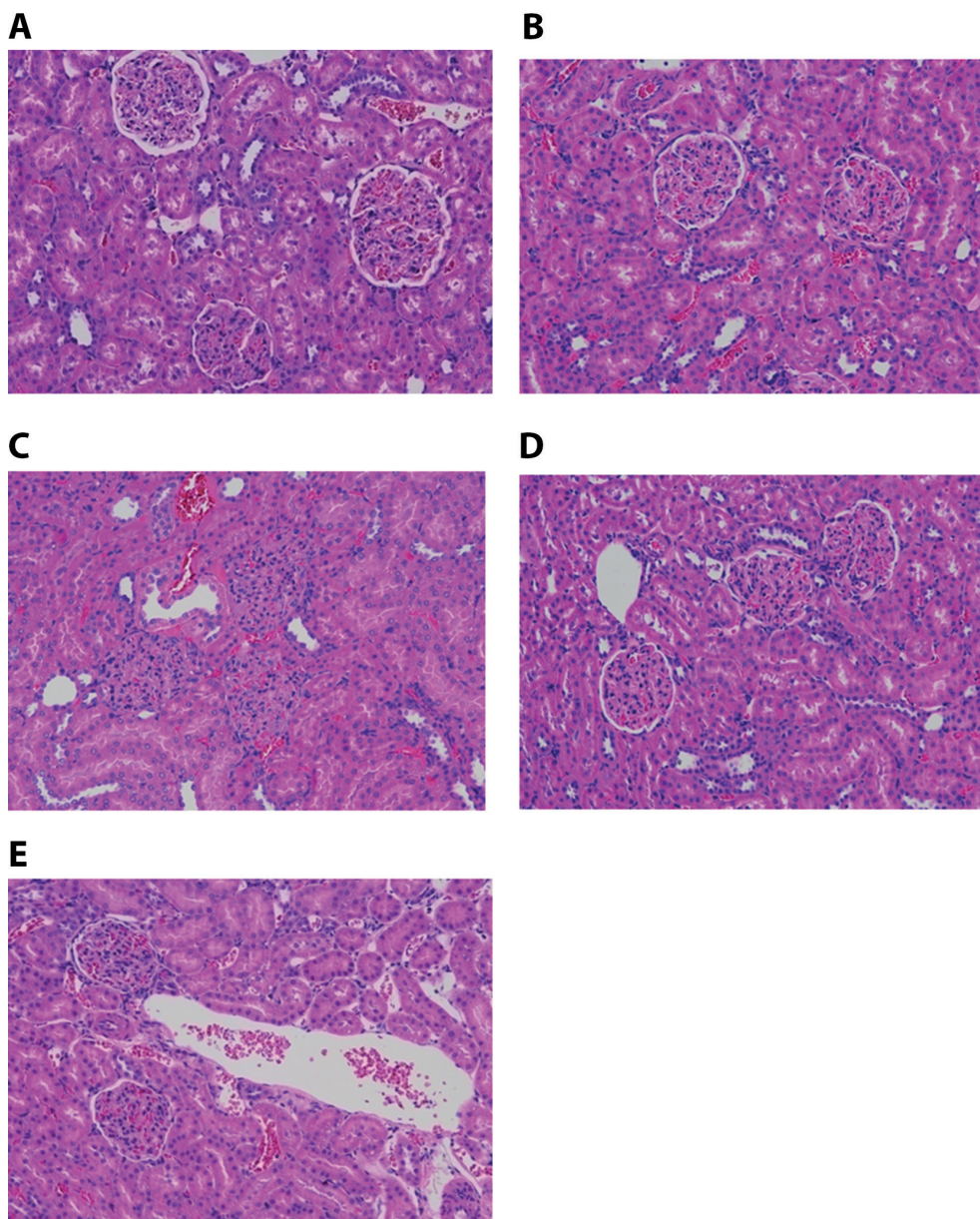


**Fig. 2.** Hematoxylin and eosin (H&E) stain for renal pathological analysis (x40 magnification). Photomicrographs of the left kidney from: A. non-pregnancy; B. normal pregnancy; C. pregnancy + N(omega)-nitro-L-arginine methyl ester (L-NAME); D. pregnancy + L-NAME + hydrogen saline; E. pregnancy + L-NAME + hydrogen saline + SB203580

of the hepatic lobules was interrupted, accompanied by hepatocyte edema in the L group (Fig. 6C). Moderate edema was found in the LH and LHS groups (Fig. 6D,E). No significant differences were observed in the aorta between the groups (Fig. 7).

### Real-time PCR outcome

The L-NAME intervention in the L group caused higher p38 mRNA expression when compared with the P group ( $p < 0.001$ , Fig. 8). The p38 mRNA in the placenta was depressed in LH and LHS groups ( $p < 0.001$ ). We also noticed that the p38 MAPK inhibitor SB203580 (LHS group) decreased p38 MAPK mRNA expression more than the hydrogen-only intervention (LH group,  $p < 0.001$ ). The p38 MAPK mRNA expression did not differ significantly between P and LHS groups.

### Western blot outcome

Group L showed an elevation of placental p-p38 MAPK protein level compared to the P group ( $p < 0.001$ , Fig. 9). Lower p-p38 MAPK protein levels in placental tissues were found in the LH and LHS groups compared to the L group ( $p < 0.001$ ). The p38 MAPK inhibitor SB203580 (LHS group) further decreased the p-p38 MAPK protein level compared with the hydrogen-only intervention (LH group,  $p < 0.001$ ).

### Discussion

Abnormal invasion of the spiral arteries<sup>11</sup> in PE patients was shown to result in blood resistance changes,<sup>12</sup> placental oxidative stress and elevated ROS generation.<sup>12,13</sup> As a “second messenger” in intracellular signaling cascades,



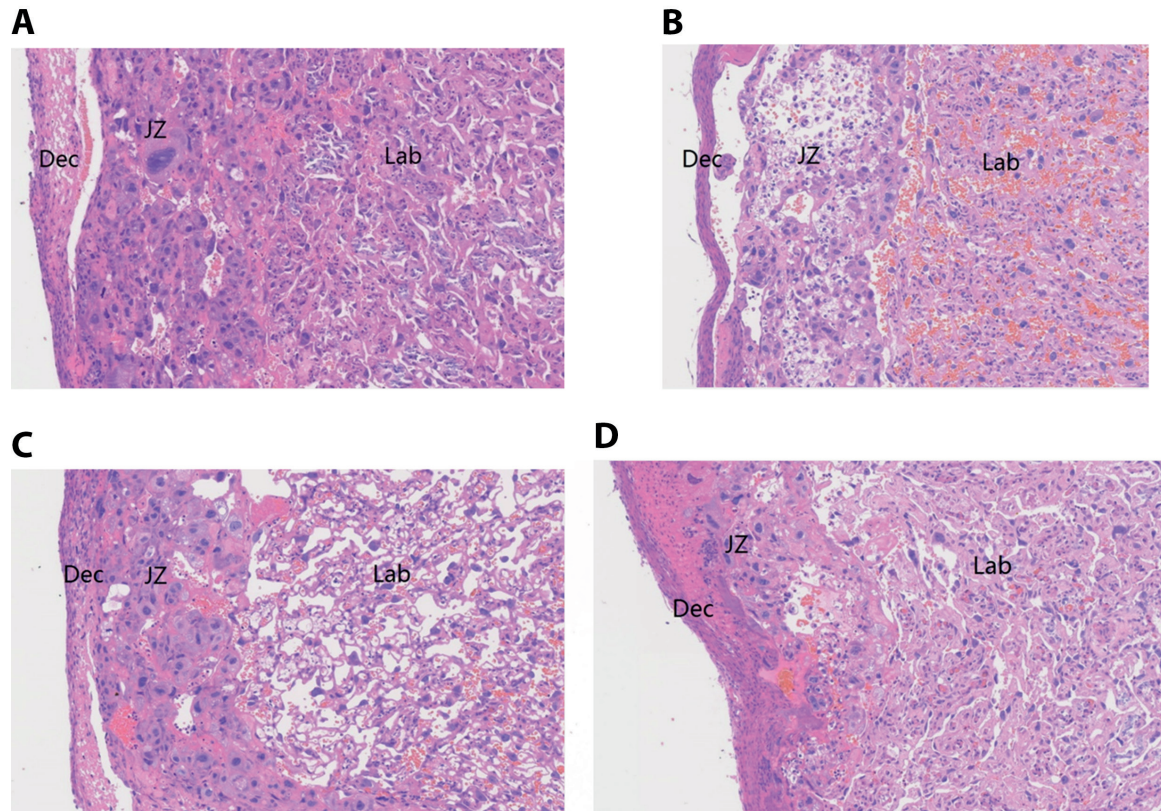


**Fig. 3.** Hematoxylin and eosin (H&E) stain for placental pathological analysis (x40 magnification). Photomicrographs of the placental tissue from: A. normal pregnancy; B. pregnancy + N(omega)-nitro-L-arginine methyl ester (L-NAME); C. pregnancy + L-NAME + hydrogen saline; D. pregnancy + L-NAME + hydrogen saline + SB203580

Dec – decidua; Lab – labyrinth; JZ – junctional zone.

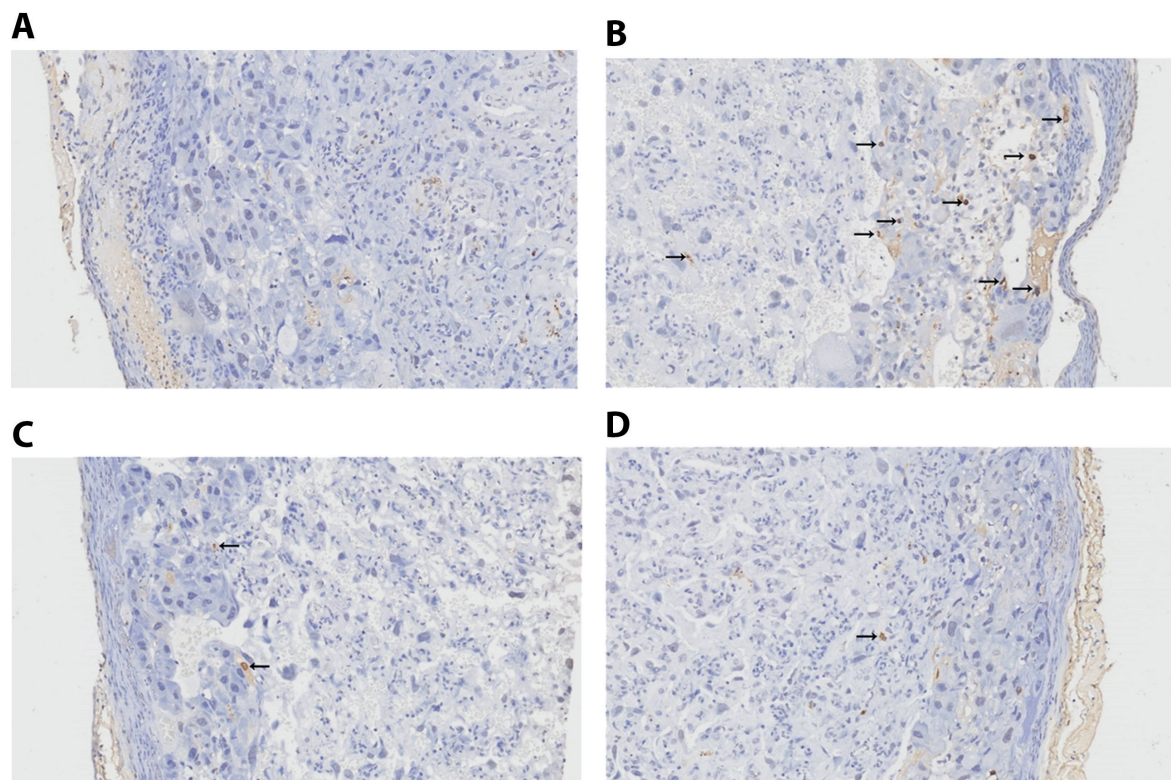


**Fig. 4.** Terminal deoxynucleotidyl transferase dUTP nick end labeling (TUNEL) stain for placental pathological analysis (x40 magnification). Photomicrographs of the placental tissue from: A. normal pregnancy; B. pregnancy + N(omega)-nitro-L-arginine methyl ester (L-NAME); C. pregnancy + L-NAME + hydrogen saline; D. pregnancy + L-NAME + hydrogen saline + SB203580. Apoptosis is indicated by an arrow



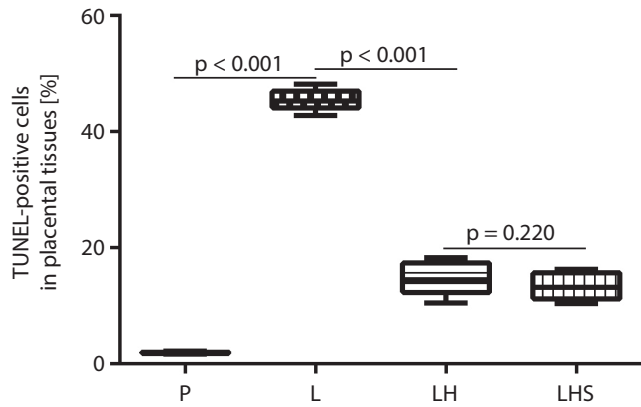


**Fig. 5.** Number of terminal deoxynucleotidyl transferase dUTP nick end labeling (TUNEL)-positive cells in placental tissue

P – normal pregnancy; L – pregnancy + N(omega)-nitro-L-arginine methyl ester (L-NAME); LH – pregnancy + L-NAME + hydrogen saline; LHS – pregnancy + L-NAME + hydrogen saline + SB203580 (n = 10 per group). The p-values were calculated using the Student’s t-test.

ROS influenced cell apoptosis or proliferation<sup>14</sup> and played an important role in regulating cellular signaling.<sup>15</sup> Among the potential cellular signaling pathways that could be impacted by ROS, the p38 MAPK pathway is a crucial candidate; it was shown to conduct signal transduction from the cell surface to the nucleus,<sup>16–18</sup> which would affect cellular survival, migration, proliferation, and differentiation.<sup>19–21</sup> Accumulated evidence indicates that the p38 MAPK pathway is one of the key signal pathways related to PE pathogenesis.<sup>8,19,20</sup> It has been demonstrated that nitration of phospho-p38 MAPK was higher in PE placentas.<sup>22</sup> Reduced phospho-p38 MAPK concentration and p38 MAPK catalytic activity were also found in placentas from PE cases.<sup>22</sup> Trophoblastic p38 signaling may be activated by hypoxic and ischemic stress, thus impacting villous trophoblastic functions in the placentas of PE patients.<sup>23</sup> Due to hypoxic stress generated by ROS, the p38-Wip1 feedback regulatory loop is dysregulated in PE patients.<sup>20</sup>

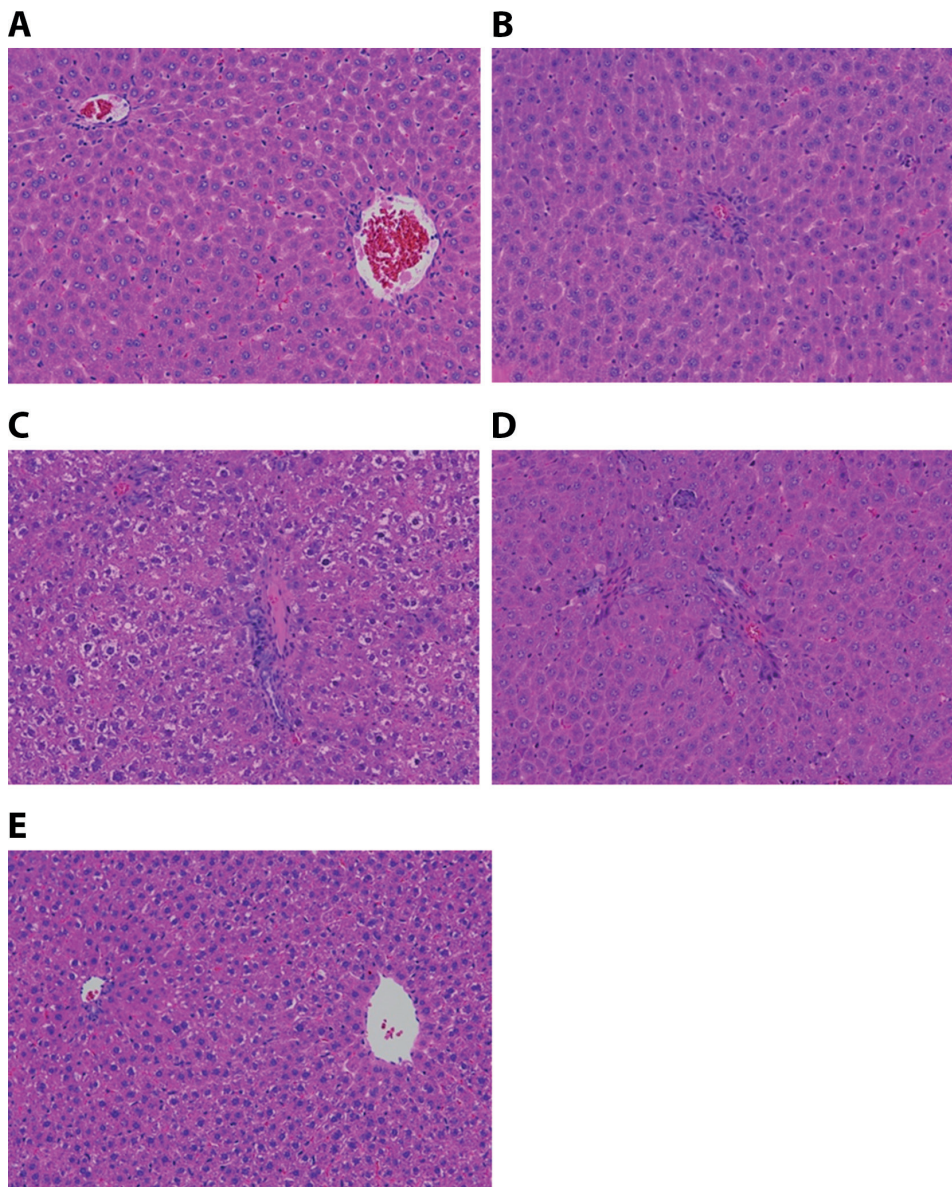


**Fig. 6.** Hematoxylin and eosin (H&E) staining for hepatic pathological analysis (×40 magnification). Photomicrographs of the liver from: A. non-pregnancy; B. normal pregnancy; C. pregnancy + N(omega)-nitro-L-arginine methyl ester (L-NAME); D. pregnancy + L-NAME + hydrogen saline; E. pregnancy + L-NAME + hydrogen saline + SB203580

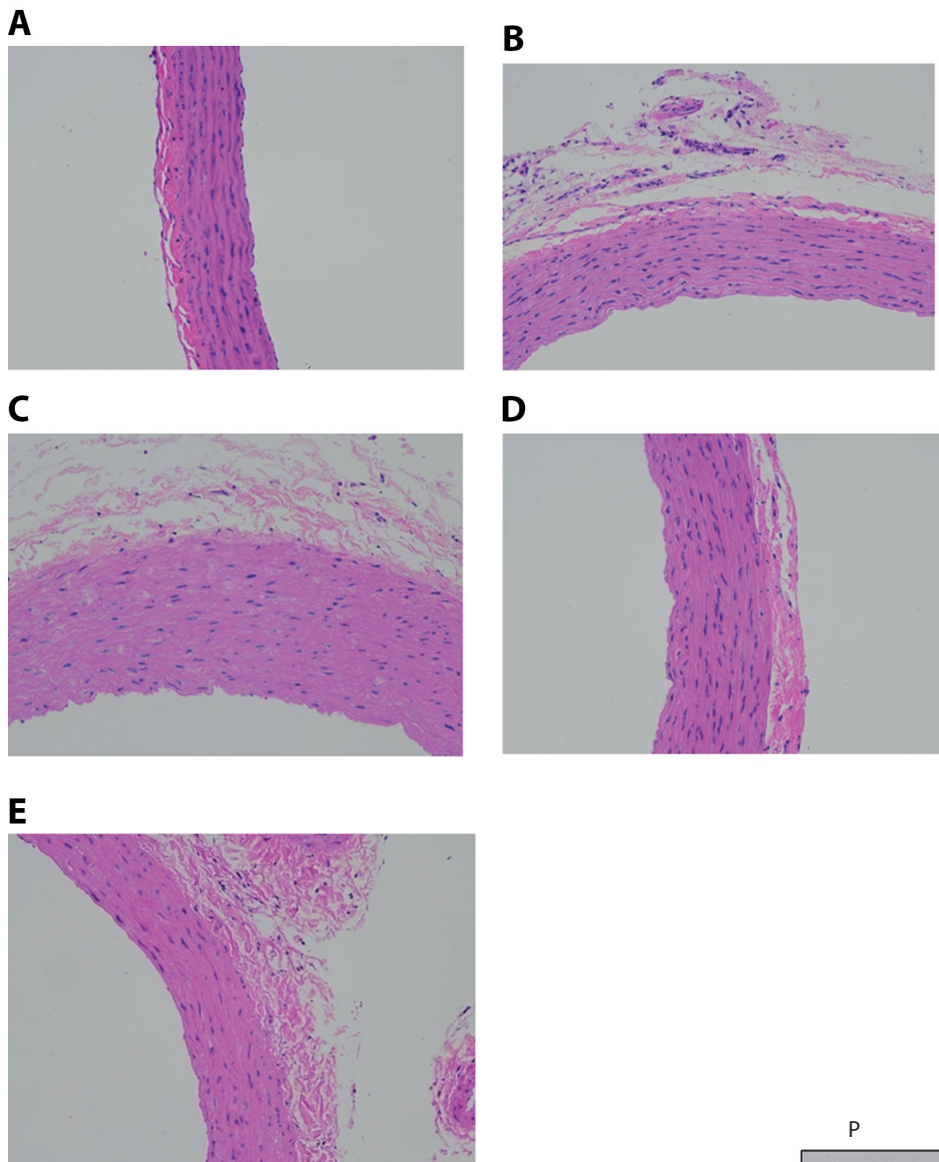


**Fig. 7.** Hematoxylin and eosin (H&E) staining for aorta pathological analysis (x40 magnification). Photomicrographs of the aorta from: A. non-pregnancy; B. normal pregnancy; C. pregnancy + N(omega)-nitro-L-arginine methyl ester (L-NAME); D. pregnancy + L-NAME + hydrogen saline; E. pregnancy + L-NAME + hydrogen saline + SB203580

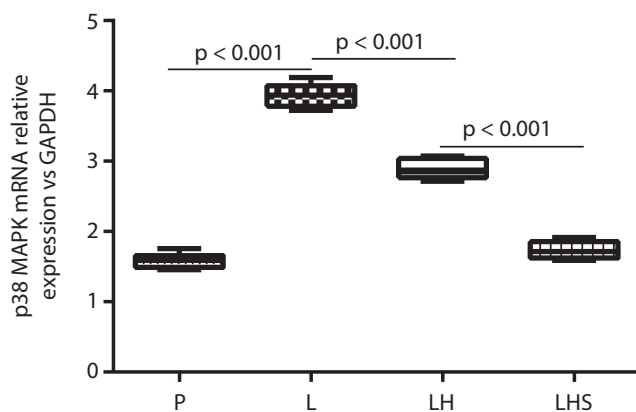


**Fig. 8.** The p38 mitogen-activated protein kinase (MAPK) mRNA relative expression

P – normal pregnancy; L – pregnancy + N(omega)-nitro-L-arginine methyl ester (L-NAME); LH – pregnancy + L-NAME + hydrogen saline; LHS – pregnancy + L-NAME + hydrogen saline + SB203580 (n = 10 per group); GAPDH – glyceraldehyde 3-phosphate dehydrogenase. The p-values were calculated using the Student's t-test.

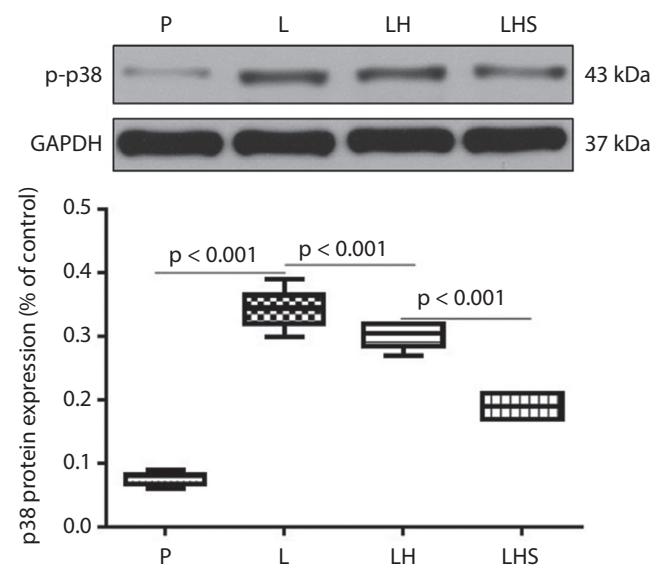


**Fig. 9.** The p-p38 protein expression levels

P – normal pregnancy; L – pregnancy + N(omega)-nitro-L-arginine methyl ester (L-NAME); LH – pregnancy + L-NAME + hydrogen saline; LHS – pregnancy + L-NAME + hydrogen saline + SB203580 (n = 10 per group); GAPDH – glyceraldehyde 3-phosphate dehydrogenase. The p-values were calculated using the Student's t-test.

In this study, we confirmed the role of p38 MAPK in the pathogenesis of PE by employing a rat model. We found that p38 mRNA expression and p-p38 MAPK protein levels in the placenta were significantly elevated in the L-NAME-induced PE rats, which could be associated with increased ROS levels, as indicated by higher MDA. Our findings are consistent with clinical evidence. First, p38 MAPK activity was observed to be significantly higher in women with PE placentas.<sup>7</sup> Second, p38 MAPK signaling could be activated through oxidative stress and increased apoptosis receptor expression.<sup>6</sup>

Interestingly, the expression of p38 was upregulated in the upper uterine segment of pregnant non-laboring or spontaneously laboring uteri, but uniformly distributed in non-pregnant uteri.<sup>24</sup> We proposed a hypothesis that placental oxidative stress is elevated in normal pregnancy compared with non-pregnancy status. The p38 expression change in pregnancy could be self-adaption to placental oxidative stress.

As dysregulated TNF- $\alpha$  synthesis may be a consequence of the p38 MAPK activation,<sup>25</sup> we also observed abnormal elevation of inflammatory cytokines, including TNF- $\alpha$  and IL-1 $\beta$  in the placenta of the rat model, which may be due to the activation of p38 MAPK cascades. In addition, the p38 MAPK pathway has been regarded as one of the key pathways for a significant decline of microvessel density<sup>8</sup> and excessive apoptosis<sup>20</sup> in placentas. Similarly, we found that remarkable degeneration and excessive apoptosis in the placentas of the PE rat model and adverse pregnancy outcomes were associated with p38 MAPK signal activation. Furthermore, the activation of the p38 MAPK pathway in PE followed by placental nicotinamide adenine dinucleotide phosphate (NADPH) oxidase<sup>19</sup> induced elevated sFlt-1 and sEng expression in the maternal circulation.<sup>8</sup> This led to systemic vascular endothelial cell dysfunction<sup>8</sup> and the pathogenesis of PE.<sup>26</sup> In the present study, the renal dysfunction (indicated by 24-hour urine protein excretion) and renal pathological degeneration may result from systemic vascular endothelial cell dysfunction related to p38 MAPK signal activation.

We also investigated the mechanism of action of hydrogen, a novel selective antioxidant. Although various antioxidants used to balance ROS, including vitamin E and vitamin C, have been investigated, the clinical outcomes are still controversial. Considering their permeability limitations and their potential detrimental effects, such as decreased human chorionic gonadotropin secretion, elevated TNF- $\alpha$  levels and depressed cell viability,<sup>27</sup> novel antioxidants have not yet been investigated. Hydrogen may have potential as a novel selective antioxidant. It has the advantages of selectively reducing toxic ROS, such as hydroxyl radical and peroxynitrite anion, and better penetration into cell membranes,<sup>28</sup> with no detrimental effects on other free radicals and normal physiological function.<sup>29</sup> Hydrogen may act as a therapeutic

antioxidant in the prevention or treatment of PE in vivo<sup>5</sup> and in vitro.<sup>30</sup> At the same time, hydrogen showed no negative effects on cell proliferation and TNF- $\alpha$  expression,<sup>27</sup> indicating that hydrogen is a potential antioxidant candidate in the management of PE. Our findings suggest that saturated hydrogen saline treatment effectively decreased p38 activation. We observed a significant reduction in p38 mRNA expression and p-p38 MAPK protein levels in the placentas of the hydrogen-treated groups, suggesting the involvement of MAPK cascades in saturated hydrogen saline-mediated protection. Similarly, p38 MAPK activation has been considered a potential target for therapeutic interventions to prevent adverse pregnancy outcomes mediated by stress factors,<sup>31</sup> and a novel therapeutic target for pregnancy complications arising from placental endothelial dysfunction.<sup>32</sup> Other drugs have been employed to suppress oxidative stress in PE by inhibiting the p38 MAPK signaling pathway, such as alpha-1-antitrypsin (AAT).<sup>33</sup>

Hydrogen, as an antioxidant agent, may affect the MAPK signaling pathway by blocking ROS, thereby reducing the inflammatory reaction and apoptosis, and ultimately improving the prognosis in HDCP. It has also been observed to improve vascular remodeling diseases via the downregulation of the p38 MAPK signaling pathway.<sup>34</sup> In this study, hydrogen moderated degeneration and apoptosis in the placenta in the PE rat model and decreased p38 MAPK activation. Considering that placental vascular remodeling plays a critical role in PE, hydrogen may improve placental vascular remodeling by suppressing the p38 MAPK signaling pathway.

To confirm the role of the p38 MAPK signaling pathway in suppressing oxidative stress by hydrogen in PE, we employed SB203580, an inhibitor of the MAPK signaling pathway. Together with hydrogen, the LHS exhibited an even further decrease in p38 MAPK mRNA expression and p-p38 MAPK protein levels compared with the LH group. Furthermore, the LHS group showed a more pronounced depression of TNF- $\alpha$  and IL-1 $\beta$  expression compared with the LH group. By inhibiting p38 MAPK with SB203580, we demonstrated that the p38 protein plays a role in the pathology of PE. As reported, p38 inhibition by SB203580 also decreases sFlt-1/sEng secretions by suppressing oxidative stress, and activates p38 MAPK signaling.<sup>26</sup> Activation of p38 MAPK was followed by affecting the invasion of trophoblast cells and increasing the secretions of sFlt-1/sEng, which then participate in the pathogenesis of PE.<sup>26</sup>

## Limitations

First, although L-NAME, as a nitric oxide synthase inhibitor, could induce symptoms of PE in pregnant rats (including hypertension and pathological changes in the placenta and kidney), it may be difficult to accurately reproduce the pathogenesis of PE in humans. Therefore,



the findings of this study should be interpreted carefully if clinical application of hydrogen in PE patients is to be considered. Second, hydrogen was administered through intraperitoneal injection in this study, but a satisfactory alternative route may need to be investigated in clinical studies.

## Conclusions

Hydrogen, as an antioxidant agent, may suppress the MAPK signaling pathway by blocking ROS, thereby reducing the inflammatory reaction and apoptosis, and ultimately improving the prognosis of HDCP. Nevertheless, the potential association between the MAPK signaling pathway and oxidative stress or inflammatory responses in HDCP needs to be further clarified.

## Supplementary materials

The supplementary tables are available at <https://doi.org/10.5281/zenodo.7074902>. The package contains the following files:

Supplementary Table 1. Shapiro–Wilk test results for protein excretion and SBP in different groups

Supplementary Table 2. Shapiro–Wilk test results for number of resorptions, fetal weight, TNF- $\alpha$ , IL-1 $\beta$ , MDA, TUNEL-positive cells, p-38 mRNA, and p-p38 protein in different groups

Supplementary Table 3. Student's t-test for Fig. 1, Fig. 5, Fig. 8, and Fig. 9.

## ORCID iDs

Lili Guo  <https://orcid.org/0000-0001-8606-3405>

Ming Liu  <https://orcid.org/0000-0002-6480-3035>

Tao Duan  <https://orcid.org/0000-0001-5320-4611>

## References

- Ness RB, Sibai BM. Shared and disparate components of the pathophysiologies of fetal growth restriction and preeclampsia. *Am J Obstet Gynecol*. 2006;195(1):40–49. doi:10.1016/j.ajog.2005.07.049
- Yang X, Guo L, Li H, Chen X, Tong X. Analysis of the original causes of placental oxidative stress in normal pregnancy and pre-eclampsia: A hypothesis. *J Matern Fetal Neonatal Med*. 2012;25(7):884–888. doi:10.3109/14767058.2011.601367
- Mahendra J, Mahendra L, Mugri MH, et al. Role of periodontal bacteria, viruses, and placental mir155 in chronic periodontitis and pre-eclampsia: A genetic microbiological study. *Curr Issues Mol Biol*. 2021; 43(2):831–844. doi:10.3390/cimb43020060
- Ohsawa I, Ishikawa M, Takahashi K, et al. Hydrogen acts as a therapeutic antioxidant by selectively reducing cytotoxic oxygen radicals. *Nat Med*. 2007;13(6):688–694. doi:10.1038/nm1577
- Yang X, Guo L, Sun X, Chen X, Tong X. Protective effects of hydrogen-rich saline in preeclampsia rat model. *Placenta*. 2011;32(9):681–686. doi:10.1016/j.placenta.2011.06.020
- Schattenberg JM, Galle PR, Schuchmann M. Apoptosis in liver disease. *Liver Int*. 2006;26(8):904–911. doi:10.1111/j.1478-3231.2006.01324.x
- Hannke-Lohmann A, von Steinburg S, Dehne K, et al. Downregulation of a mitogen-activated protein kinase signaling pathway in the placentas of women with preeclampsia. *Obstet Gynecol*. 2000;96(4): 582–587. doi:10.1016/S0029-7844(00)00986-8
- Luo X, Liu DD, Qi HB, Yao ZW. Study on p38 mitogen activated protein kinase in vascular endothelial cells dysfunction in preeclampsia [in Chinese]. *Zhonghua Fu Chan Ke Za Zhi*. 2011;46(1):36–40. PMID:21429433.
- Gao X, Li N, Zhang J. SB203580, a p38MAPK inhibitor, attenuates olfactory dysfunction by inhibiting OSN apoptosis in AR mice (activation and involvement of the p38 mitogen-activated protein kinase in olfactory sensory neuronal apoptosis of OVA-induced allergic rhinitis). *Brain Behav*. 2019;9(6):e01295. doi:10.1002/brb3.1295
- Yang Y, Fukui K, Koike T, Zheng X. Induction of autophagy in neurite degeneration of mouse superior cervical ganglion neurons. *Eur J Neurosci*. 2007;26(10):2979–2988. doi:10.1111/j.1460-9568.2007.05914.x
- Granger JP, Alexander BT, Llinas MT, Bennett WA, Khalil RA. Pathophysiology of hypertension during preeclampsia linking placental ischemia with endothelial dysfunction. *Hypertension*. 2001;38(3 Pt 2): 718–722. doi:10.1161/01.HYP.38.3.718
- Ogita H, Liao JK. Endothelial function and oxidative stress. *Endothelium*. 2004;11(2):123–132. doi:10.1080/10623320490482664
- Wassmann S, Laufs U, Bäumer AT, et al. HMG-CoA reductase inhibitors improve endothelial dysfunction in normocholesterolemic hypertension via reduced production of reactive oxygen species. *Hypertension*. 2001;37(6):1450–1457. doi:10.1161/01.HYP.37.6.1450
- Thannickal VJ, Fanburg BL. Reactive oxygen species in cell signaling. *Am J Physiol Lung Cell Mol Physiol*. 2000;279(6):L1005–L1028. doi:10.1152/ajplung.2000.279.6.L1005
- Paravicini TM, Touyz RM. NADPH oxidases, reactive oxygen species, and hypertension: Clinical implications and therapeutic possibilities. *Diabetes Care*. 2008;31(Suppl 2):S170–S180. doi:10.2337/dc08-s247
- Rhyu DY, Yang Y, Ha H, et al. Role of reactive oxygen species in TGF- $\beta$ 1-induced mitogen-activated protein kinase activation and epithelial-mesenchymal transition in renal tubular epithelial cells. *J Am Soc Nephrol*. 2005;16(3):667–675. doi:10.1681/ASN.2004050425
- Davis RJ. Signal transduction by the JNK group of MAP kinases. *Cell*. 2000;103(2):239–252. doi:10.1016/S0092-8674(00)00116-1
- Son Y, Cheong YK, Kim NH, Chung HT, Kang DG, Pae HO. Mitogen-activated protein kinases and reactive oxygen species: How can ROS activate MAPK pathways? *J Signal Transduct*. 2011;2011:792639. doi:10.1155/2011/792639
- Hernandez I, Chissey A, Guibourdenche J, et al. Human placental NADPH oxidase mediates sFlt-1 and PlGF secretion in early pregnancy: Exploration of the TGF- $\beta$ 1/p38 MAPK pathways. *Antioxidants (Basel)*. 2021;10(2):281. doi:10.3390/antiox10020281
- Tan B, Tong C, Yuan Y, et al. The regulation of trophoblastic p53 homeostasis by the p38-Wip1 feedback loop is disturbed in placentas from pregnancies complicated by preeclampsia. *Cell Physiol Biochem*. 2019;52(2):315–335. doi:10.33594/000000023
- Wagner EF, Nebreda ÁR. Signal integration by JNK and p38 MAPK pathways in cancer development. *Nat Rev Cancer*. 2009;9(8):537–549. doi:10.1038/nrc2694
- Webster RP, Brockman D, Myatt L. Nitration of p38 MAPK in the placenta: Association of nitration with reduced catalytic activity of p38 MAPK in pre-eclampsia. *Mol Hum Reprod*. 2006;12(11):677–685. doi:10.1093/molehr/gal071
- Szabo S, Mody M, Romero R, et al. Activation of villous trophoblastic p38 and ERK1/2 signaling pathways in preterm preeclampsia and HELLP syndrome. *Pathol Oncol Res*. 2015;21(3):659–668. doi:10.1007/s12253-014-9872-9
- Otun HA, MacDougall MWJ, Bailey J, Europe-Finner GN, Robson SC. Spatial and temporal expression of the myometrial mitogen-activated protein kinases p38 and ERK1/2 in the human uterus during pregnancy and labor. *J Soc Gynecol Investig*. 2005;12(3):185–190. doi:10.1016/j.jsg.2004.11.008
- Thirunavukkarasu C, Watkins SC, Gandhi CR. Mechanisms of endotoxin-induced NO, IL-6, and TNF- $\alpha$  production in activated rat hepatic stellate cells: Role of p38 MAPK. *Hepatology*. 2006;44(2):389–398. doi:10.1002/hep.21254
- Liu X, Deng Q, Luo X, Chen Y, Shan N, Qi H. Oxidative stress-induced Gadd45a inhibits trophoblast invasion and increases sFlt1/sEng secretions via p38 MAPK involving in the pathology of pre-eclampsia. *J Matern Fetal Neonatal Med*. 2016;29(23):3776–3785. doi:10.3109/14767058.2016.1144744
- Guan Z, Li HF, Guo LL, Yang X. Effects of vitamin C, vitamin E, and molecular hydrogen on the placental function in trophoblast cells. *Arch Gynecol Obstet*. 2015;292(2):337–342. doi:10.1007/s00404-015-3647-8



28. Hayashida K, Sano M, Ohsawa I, et al. Inhalation of hydrogen gas reduces infarct size in the rat model of myocardial ischemia–reperfusion injury. *Biochem Biophys Res Commun*. 2008;373(1):30–35. doi:10.1016/j.bbrc.2008.05.165
29. Buchholz BM, Kaczorowski DJ, Sugimoto R, et al. Hydrogen inhalation ameliorates oxidative stress in transplantation induced intestinal graft injury. *Am J Transplant*. 2008;8(10):2015–2024. doi:10.1111/j.1600-6143.2008.02359.x
30. Guo L, Guan Z, Li H, Yang X. Hydrogen inhibits cytotrophoblast cells apoptosis in hypertensive disorders complicating pregnancy. *Cell Mol Biol (Noisy-le-grand)*. 2016;62(6):59–64. PMID:27262804.
31. Menon R, Papaconstantinou J. p38 mitogen activated protein kinase (MAPK): A new therapeutic target for reducing the risk of adverse pregnancy outcomes. *Expert Opin Ther Targets*. 2016;20(12):1397–1412. doi:10.1080/14728222.2016.1216980
32. Luo X, Yao ZW, Qi HB, et al. Gadd45 $\alpha$  as an upstream signaling molecule of p38 MAPK triggers oxidative stress-induced sFlt-1 and sEng upregulation in preeclampsia. *Cell Tissue Res*. 2011;344(3):551–565. doi:10.1007/s00441-011-1164-z
33. Feng YL, Yin YX, Ding J, et al. Alpha-1-antitrypsin suppresses oxidative stress in preeclampsia by inhibiting the p38MAPK signaling pathway: An in vivo and in vitro study. *PLoS One*. 2017;12(3):e0173711. doi:10.1371/journal.pone.0173711
34. Zhang YX, Xu JT, You XC, et al. Inhibitory effects of hydrogen on proliferation and migration of vascular smooth muscle cells via down-regulation of mitogen/activated protein kinase and ezrin-radixin-moesin signaling pathways. *Chin J Physiol*. 2016;59(1):46–55. doi:10.4077/CJP.2016.BAE365



# The role of the 47-kDa membrane lipoprotein of *Treponema pallidum* in promoting maturation of peripheral blood monocyte-derived dendritic cells without enhancing C-C chemokine receptor type 7-mediated dendritic cell migration

Wenhao Cheng<sup>A–E</sup>, Yumo Lu<sup>B,C</sup>, Renqiong Chen<sup>A</sup>, Hong Ren<sup>A,E,F</sup>, Wenlong Hu<sup>A,E,F</sup>

Department of Dermatology and Venereology, The Affiliated Lianyungang Hospital of Xuzhou Medical University, China

A – research concept and design; B – collection and/or assembly of data; C – data analysis and interpretation; D – writing the article; E – critical revision of the article; F – final approval of the article

Advances in Clinical and Experimental Medicine, ISSN 1899–5276 (print), ISSN 2451–2680 (online)

Adv Clin Exp Med. 2023;32(3):369–377

## Address for correspondence

Wenlong Hu  
E-mail: lyghuwl@163.com

## Funding sources

The study was supported by National Natural Science Foundation of China (grant No. 82002181), Jiangsu Key Laboratory of Immunity and Metabolism (grant No. JSKIM201903), Lianyungang Health Science and Technology Project (grant No. 202010), and Lianyungang 521 Project (grant No. LYG06521202156).

## Conflict of interest

None declared

Received on February 14, 2022

Reviewed on February 27, 2022

Accepted on September 22, 2022

Published online on November 4, 2022

## Abstract

**Background.** The 47-kDa membrane lipoprotein (Tp47) is the most representative membrane protein of *Treponema pallidum* (*T. pallidum*). Dendritic cells (DCs) are the most potent professional antigen-presenting cells (APCs) that connect innate and acquired immunity. The regulatory role of Tp47 on DCs remains unclear.

**Objectives.** To evaluate the effects of Tp47 on DC maturation and migration, and research the changes of the main chemokine C-C chemokine receptor type 7 (CCR7) involved in DC migration.

**Materials and methods.** A transwell assay was applied to assess the migration of DCs. Cytokines (interleukin (IL)-6, IL-10, IL-12, and tumor necrosis factor alpha (TNF- $\alpha$ )) in the supernatants were measured using enzyme-linked immunosorbent assay (ELISA), and the expression of cell surface markers (CD80, CD86, CD40, and human leukocyte antigen (HLA)-DR) and CCR7 was assessed using flow cytometry. The expression of CCR7 in DCs was analyzed using quantitative real-time polymerase chain reaction (qRT-PCR).

**Results.** The Tp47 promoted DC phenotypic maturation, such as increased CD40, CD80, CD86, and HLA-DR expression, as well as DC functional maturation, thus stimulating DCs to secrete inflammatory cytokines, including IL-6, IL-10, IL-12, and TNF- $\alpha$ . At the same time, Tp47 did not enhance DC migration and did not increase the expression of CCR7.

**Conclusions.** The Tp47 promoted the maturation of DCs while not enhancing CCR7-mediated DC migration ability. This may be one of the mechanisms by which *T. pallidum* escapes host immune clearance.

**Key words:** dendritic cells, migration, *Treponema pallidum*, syphilis, C-C chemokine receptor type 7

## Cite as

Cheng W, Lu Y, Chen R, Ren H, Hu W. The role of the 47-kDa membrane lipoprotein of *Treponema pallidum* in promoting maturation of peripheral blood monocyte-derived dendritic cells without enhancing C-C chemokine receptor type 7-mediated dendritic cell migration. *Adv Clin Exp Med*. 2023;32(3):369–377. doi:10.17219/acem/154857

## DOI

10.17219/acem/154857

## Copyright

Copyright by Author(s)

This is an article distributed under the terms of the Creative Commons Attribution 3.0 Unported (CC BY 3.0) (<https://creativecommons.org/licenses/by/3.0/>)

## Background

Syphilis is a human infectious disease attributed to sexual transmission of the spirochete *Treponema pallidum* (*T. pallidum*). Its clinical manifestations are complex and can develop in stages. In the advanced stage, it can lead to multiple organ damage, seriously threatening the health of the host.<sup>1,2</sup> Previous studies have shown that *T. pallidum* can escape clearance by the human immune system and coexist with the host for a long time, which leads to asymptomatic and persistent infection, enabling sexual transmission of syphilis and causing physical and mental health problems.<sup>3–5</sup> Different studies have suggested different mechanisms by which *T. pallidum* can evade immune control, thereby damaging host tissues. It is believed that antigenic variation and the paucity of outer membrane antigenic targets can promote the spread of *T. pallidum*.<sup>6–9</sup> In recent years, progressively more studies have suggested that host immune imbalance and immunosuppression are responsible for immune evasion of *T. Pallidum*.<sup>10–12</sup>

Dendritic cells (DCs), the most potent professional antigen-presenting cells (APCs), play an important role in the initiation and amplification of innate and adaptive immunity.<sup>13–15</sup> The ability of DCs to migrate and activate naïve T cells is closely related to the efficiency of their immunomodulatory activity.<sup>16–18</sup> Dendritic cells gradually mature after recognizing and ingesting antigens, and the expression of their surface molecule C-C chemokine receptor type 7 (CCR7) is upregulated. When CCR7 binds effectively to its ligand chemokine CCL21/CCL19, the resulting chemotaxis enables DCs to migrate into lymph nodes, triggering an adaptive immune response.<sup>19</sup> The CCR7 is the major receptor on DCs to present antigens to naïve T lymphocytes, and it plays a key role in promoting the migration and nesting of DCs.<sup>20–22</sup>

Dendritic cells have been reported as one of the major immunocompetent cells that encounter bacterial antigens at primary sites of early syphilitic infection (e.g., mucous membranes or skin); they play a crucial role in clearing *T. pallidum*.<sup>23,24</sup> However, until now, there has been no study on the migratory capacity of DCs following *T. pallidum* infection. Previous studies have demonstrated that the outer membrane proteins and lipoproteins of *T. pallidum* constitute the main immune response components to *T. pallidum*.<sup>25,26</sup> Among them, the 47-kDa membrane lipoprotein (Tp47) is the most abundant membrane protein of *T. pallidum*. It has strong antigenicity and good specificity, mainly modulating the inflammation induced by *T. pallidum*.<sup>27–30</sup> Therefore, we chose Tp47 to induce a *T. pallidum* infection model in this study.

## Objectives

This study aimed to evaluate the effects of Tp47 on the maturation and CCR7-mediated migration of DCs,

which is expected to provide a preliminary explanation for why *T. pallidum* can escape clearance by the host immune system.

## Materials and methods

### Production of recombinant *T. pallidum* Tp47 protein after removal of endotoxin

Before the experiments, the recombinant *T. pallidum* Tp47 protein (0.6 g/L; Boson Biotech Co., Ltd., Xiamen, China) was treated to remove endotoxin contamination using an EtEraser™ endotoxin removal kit (Chinese Horseshoe Crab Reagent Manufactory Co., Ltd., Xiamen, China). The endotoxin content was detected using tachypleus amoebocyte lysate (Chinese Horseshoe Crab Reagent Manufactory Co., Ltd.). The endotoxin content in the Tp47 preparation was limited to <0.05 endotoxin units/mL.

### In vitro generation of dendritic cells

Through standard density gradient centrifugation using Ficoll-Paque™ PLUS (Cytiva, Marlborough, USA), human peripheral blood mononuclear cells (PBMCs) were isolated from 9 healthy blood donors (5 males and 4 females aged 18–55 years; all provided written informed consent). Then, cells from each donor sample were cultured in Dulbecco's Modified Eagle's Medium (DMEM; Gibco, Waltham, USA) with 1% penicillin/streptomycin (Gibco) and 10% fetal bovine serum (FBS; Gibco), in a 6-well tissue culture plate, in a 37°C incubator with 5% CO<sub>2</sub>. Fresh medium containing 50 ng/mL recombinant human granulocyte-macrophage colony-stimulating factor (GM-CSF; R&D Systems, Minneapolis, USA) and 50 ng/mL recombinant interleukin (IL)-4 (R&D Systems) was replaced every 2 days. According to pre-experiments, we found that the confluence of DCs could reach 92.5 ± 8.4% after human PBMCs were cultured in vitro in the presence of IL-4 and GM-CSF for 7 days.

On day 7, DCs were divided into 6 groups. The experimental group was stimulated with different concentrations of Tp47 (120, 300, 600, and 1200 ng/mL) based on previous studies.<sup>28,30</sup> Cells treated with 1 µg/mL lipopolysaccharide (LPS) or phosphate-buffered saline (PBS) were assigned to the positive control group or the negative control group, respectively. After 24 h of culturing, DCs in each group were collected for subsequent experiments.

### Dendritic cell migration assay

Dendritic cell migration capacity was determined using a 5-µm pore size culture insert (Merck Millipore, Burlington, USA), which was placed into a 24-well culture plate as described elsewhere.<sup>20</sup> Briefly, DCs in each group were harvested, washed twice with PBS and resuspended



into a concentration of  $1 \times 10^6$  cells/mL medium. Thereafter, 100  $\mu$ L of DC suspension was seeded into the upper chamber, and 600  $\mu$ L of medium complemented with 100 ng/mL CCL21 (PeproTech, Cranbury, USA) was added into the lower chamber. Three replicates for each cell type were placed in a 37°C, 5% CO<sub>2</sub> incubator. At 1 h, 2 h, 3 h, and 4 h, 10  $\mu$ L of the lower chamber culture, medium was obtained and counted on a hemocytometer under a light microscope (model CX33; Olympus Corp., Tokyo, Japan), and 10  $\mu$ L of medium containing 100 ng/mL CCL21 was simultaneously added to the lower chamber. The DC migration rate was considered the ratio of migrated cells within the lower chamber to the total number of cells added to the upper chamber.

## Cytokine assay

Using an enzyme-linked immunosorbent assay (ELISA) kit (R&D Systems) in accordance with the manufacturer's instructions, the IL-6, IL-10, IL-12, and tumor necrosis factor alpha (TNF- $\alpha$ ) concentrations in the DC culture supernatants were assessed. The absorbance was measured at 460 nm.

## Flow cytometry

In each group, dendritic cells ( $1 \times 10^5$ /mL) were resuspended in 100  $\mu$ L PBS supplemented with 10  $\mu$ g/mL fluoro-chrome-conjugated antibodies. The cells were stained with the following monoclonal antibodies: CCR7-PE (clone G043H7; BioLegend, San Diego, USA), CD86-APC (clone BU63; BioLegend), CD80-PE (clone 2D10.4; eBioscience, San Diego, USA), CD40-PE-Cy7 (clone 5C3; BioLegend), human leukocyte antigen (HLA)-DR-Alexa Fluor<sup>®</sup> 488 (clone LN3; BioLegend). After incubation with the antibodies in the dark for 30 min at 4°C, the cells were washed twice, resuspended in PBS (300  $\mu$ L), and subjected to flow cytometry analysis (FACSCanto™ II; BD Biosciences, Franklin Lakes, USA).

## Quantitative real-time polymerase chain reaction

The expression of CCR7 on DCs was analyzed using quantitative real-time polymerase chain reaction (qRT-PCR). With the use of a TRIzol kit (Invitrogen, Waltham, USA), we extracted total RNA from the incubated cells. Using a Nanodrop™ 2000 spectrophotometer (Thermo Fisher Scientific, Waltham, USA), RNA purity and concentration were tested. The RNA was reverse-transcribed into cDNA with the PrimeScript™ RT reagent kit (TaKaRa, Beijing, China), and amplification was conducted with TB Green Premix Ex Taq II (TaKaRa) in accordance with the manufacturer's instructions. The qRT-PCR was performed with a PRISM 7300 Sequence Detection System

(Applied Biosystems, Waltham, USA) using the following amplification conditions: 95°C for 30 s, followed by 40 cycles at 60°C for 1 min, 60°C for 34 s, 95°C for 15 s, 95°C for 5 s, and 95°C for 15 s. Glyceraldehyde 3-phosphate dehydrogenase (GAPDH) acted as an internal reference. Sangon Biotech Co., Ltd. (Shanghai, China) provided all primers. The primer sequences included: 5'-AGCAG-CAGTGAGCAAGCGATG-3' (forward) and 5'-GGGT-GCGGATGATGACAAGGTAAC-3' (reverse) for CCR7; and 5'-GCACCGTCAAGGCTAGAAC-3' (forward) and 5'-TGGTGAAGACGCCAGTGGA-3' (reverse) for GAPDH. The specificity of amplification was controlled using melting curve analysis. The  $2^{-\Delta\Delta CT}$  method was adopted to analyze the data.<sup>31</sup>

## Statistical analyses

Each experiment was repeated 3 times independently ( $n = 3$ ). Variables were expressed as mean  $\pm$  standard deviation ( $M \pm SD$ ), and the results were analyzed based on the "gemtc 1.4-2" package of R software (v. 4.1.2; R Foundation for Statistical Computing, Vienna, Austria). The statistical analysis was performed with the Wilcoxon–Mann–Whitney test, and the permutation test was employed to obtain the p-value. The Holm–Bonferroni method was used for post hoc corrections. A value of  $p < 0.05$  was considered statistically significant. The full results (including p-values, test statistics and degrees of freedom, where appropriate) are available as Supplementary material for inspection (<https://doi.org/10.5281/zenodo.7249173>).

## Results

### Tp47 prompted DCs to secrete high levels of IL-6, IL-10, IL-12, and TNF- $\alpha$

The maturation of DCs in response to pathogens mainly involves an increased expression of pro-inflammatory cytokines. As indicated by the ELISA results, the levels of IL-6, IL-10, IL-12, and TNF- $\alpha$  in the supernatants of cultured DCs in the presence of Tp47 (120, 300, 600, and 1200 ng/mL) were remarkably higher compared with those of the control group (Fig. 1).

### Tp47 upregulated the expression of CD80, CD86, CD40, and HLA-DR on DCs

In order to determine the effect of Tp47 on the phenotypic maturation of DCs, flow cytometry was carried out to detect the expression of surface molecules (CD80, CD86, CD40, and HLA-DR) on DCs. The results showed that the expression of surface molecules on DCs was upregulated under stimulation by Tp47 (120, 300, 600, and 1200 ng/mL) compared with the control group (Fig. 2).

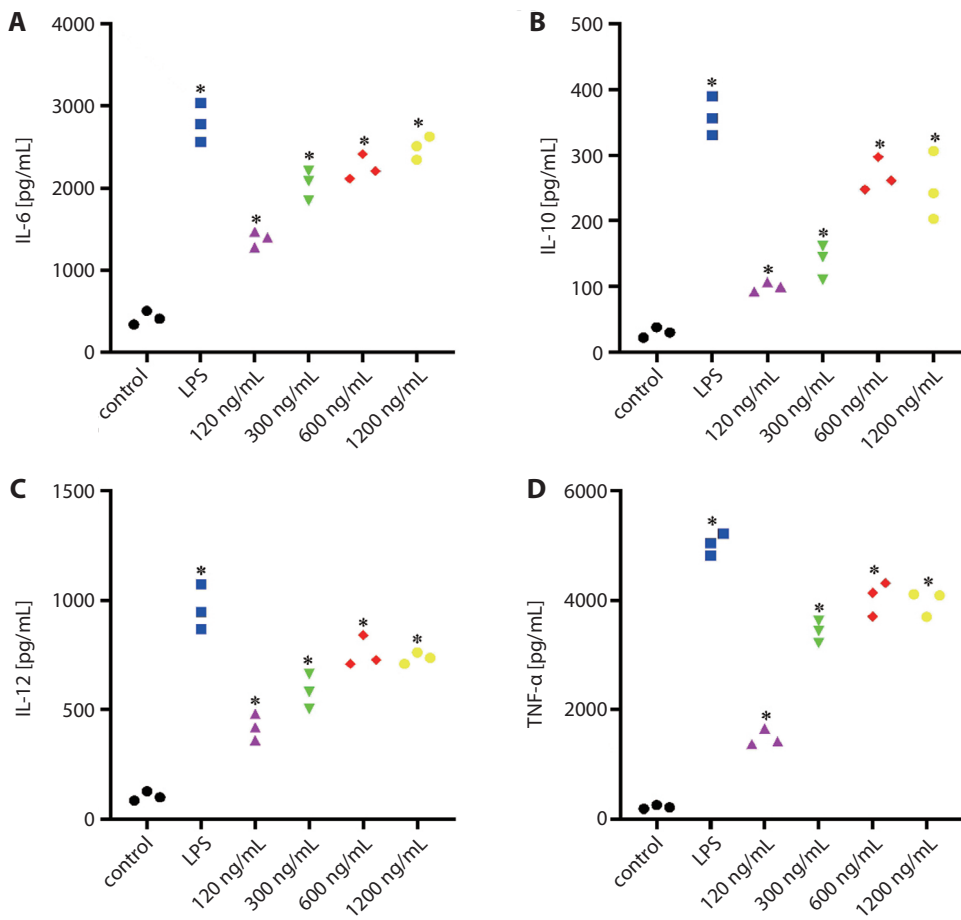


**Fig. 1.** Levels of cytokines – interleukin (IL)-6 (A), IL-10 (B), IL-12 (C), and tumor necrosis factor alpha (TNF- $\alpha$ ) (D) – in the supernatants of cultured dendritic cells, measured using enzyme-linked immunosorbent assay (ELISA) 24 h after phosphate-buffered saline (PBS) (control group), lipopolysaccharide (LPS) (1  $\mu$ g/mL), and different concentrations of 47-kDa membrane lipoprotein of *Treponema pallidum* (Tp47) (120, 300, 600, and 1200 ng/mL) stimulation

n = 3; \*p < 0.05 compared to control.

## Tp47 did not promote DC migration

Using the transwell assay, we examined the migration ability of DCs in response to the chemokine CCL21. The results showed that the proportion of DCs that migrated to the lower chamber after 24 h of stimulation by Tp47 (120, 300, 600, and 1200 ng/mL) did not increase significantly compared with that of the control group. However, the proportion of DCs that, after stimulation with 1  $\mu$ g/mL LPS, migrated to the lower chamber was significantly increased at 2 h, 3 h and 4 h compared to the control group (Fig. 3).

## Tp47 did not increase CCR7 expression

Next, we verified whether CCR7 impacted DC migration after Tp47 stimulation. We assessed the CCR7 expression level in DCs using 2 approaches. First, the qPCR results showed that after co-culturing with Tp47 (120, 300, 600, and 1200 ng/mL), the expression level of CCR7 mRNA in DCs did not increase significantly compared with the control group (Fig. 4A). Flow cytometry showed that the CCR7 level on DCs was not significantly up-regulated after the stimulation with Tp47 at different concentrations in comparison with the control group (Fig. 4B).

## Discussion

Dendritic cells, as the most important APCs, have the ability to activate naïve T cells to generate adaptive immune responses only after maturation.<sup>32,33</sup> The maturation of DCs manifests as both phenotypic and functional.<sup>34</sup> Phenotypic maturation implies that multiple surface molecules can be expressed at high levels, such as CD40, CD80, CD86, and HLA-DR, while functional maturation suggests the ability to secrete various inflammatory cytokines, including TNF- $\alpha$ , IL-6, IL-10, and IL-12.<sup>35</sup> We found that for DCs stimulated by Tp47, not only the abovementioned surface molecule expression levels increased but also the ability of the DCs to secrete inflammatory cytokines significantly improved, indicating that Tp47 could simultaneously promote phenotypic and functional maturation of DCs. This result is consistent with previously reported studies on DCs in most pathogenic infections.<sup>36–38</sup> After DCs uptake and process antigens, they undergo phenotypic and functional changes and gradually differentiate into mature DCs, which can provide the 2<sup>nd</sup> signal necessary for T-cell activation.<sup>39,40</sup>

Immune cell migration serves as a key link between immune regulation and host defense. It has an indispensable role in eliminating the inflammatory responses triggered by foreign pathogens.<sup>41,42</sup> Previous studies have

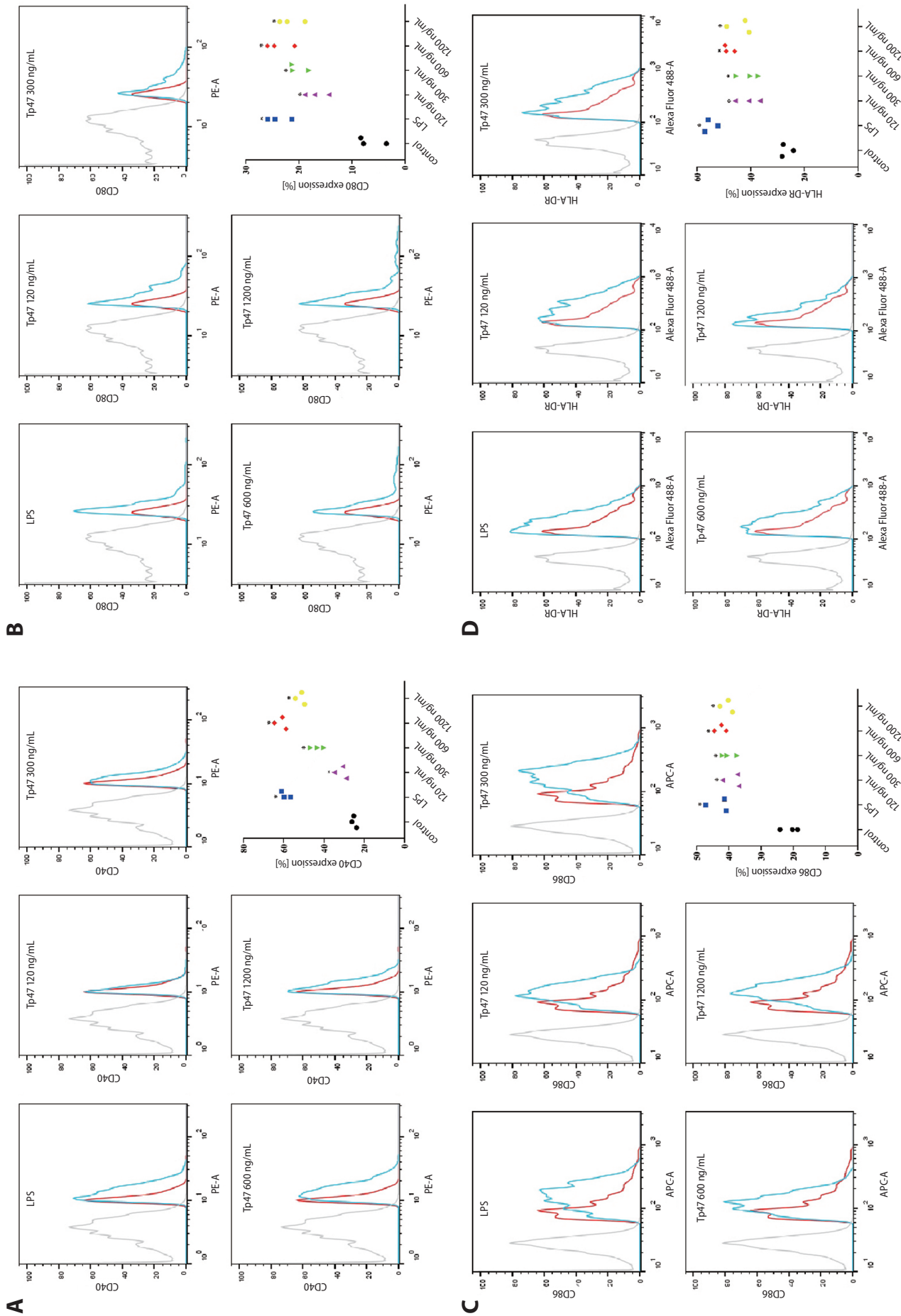


**Fig. 2.** Expression of dendritic cell surface markers CD40 (A), CD80 (B), CD86 (C), and human leukocyte antigen (HLA)-DR (D) was detected using flow cytometry 24 h after phosphate-buffered saline (PBS) (control group), lipopolysaccharide (LPS) (1 µg/mL) and different concentrations of 47-kDa membrane lipoprotein of *Treponema pallidum* (Tp47) (120, 300, 600, and 1200 ng/mL) stimulation. The control group is indicated as a red line, LPS and different concentrations of Tp47 groups are represented by blue lines, and the unstained group is marked in gray  
n = 3; \*p < 0.05 compared to control. PE-A – phycoerythrin-A; APC-A – allophycocyanin-A.

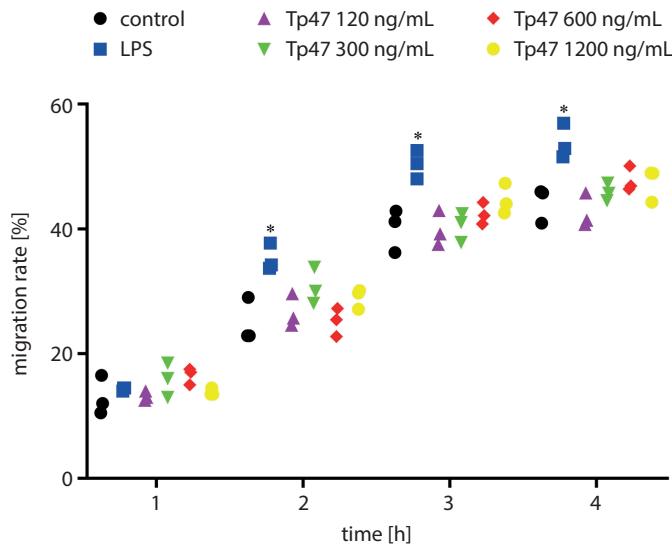


**Fig. 3.** Migration rates of dendritic cells at 1 h, 2 h, 3 h, and 4 h were detected using transwell assay 24 h after phosphate-buffered saline (PBS) (control group), lipopolysaccharide (LPS) (1  $\mu\text{g}/\text{mL}$ ) and different concentrations of 47-kDa membrane lipoprotein of *Treponema pallidum* (Tp47) (120, 300, 600, and 1200 ng/mL) stimulation

$n = 3$ ; \* $p < 0.05$  compared to control.

found that Tp47 can promote the migration and adherence of THP-1 cells to human dermal vascular smooth muscle cells by inducing the expression of monocyte chemoattractant protein-1 (MCP-1) and intercellular adhesion molecule-1 (ICAM-1).<sup>43</sup> In our study, we explored the effect of Tp47 on migratory activity of DCs and found that the migratory ability of DCs did not significantly increase

after they were stimulated by Tp47 compared to the control group. At the same time, we used *Escherichia coli* LPS stimulation as a positive control in all experiments. The results indicated that LPS could significantly promote the migration of DCs to the lower chamber in the transwell assay. Thus, it could be deduced that DCs did not fully exert their migratory ability to fulfill the mission of antigen presentation after Tp47 stimulation. During the maturation process, the migration of DCs to secondary lymphoid organs and their interactions with antigen-specific T cells are prerequisites for the induction of a primary immune response,<sup>44,45</sup> which plays an important role in anti-infective immunity. Numerous studies have shown that pathogenic microbes have evolved strategies to evade and/or suppress host inflammatory responses in order to infect and spread into other tissues and to other hosts. One of these strategies, as shown in *Salmonella* infection, is to inhibit DC migration.<sup>46,47</sup> In addition, Angeli et al. found that *Schistosoma* parasites inhibited DC migration to lymph nodes after infection through skin by producing prostaglandin D2.<sup>48</sup> Our study indicated that Tp47, the most abundant *T. pallidum* protein, did not promote the migration of DCs, which might be one strategy by which *T. pallidum* evades host immune clearance.

It is well established that the interaction between CCR7 on the DC surface and its ligands has been proven to be a key driver for DC migration.<sup>49,50</sup> To further validate the impact of Tp47 on DC migration, we studied the change in the CCR7 expression level in DCs after Tp47 stimulation. The results showed that there was no increase in the DC surface CCR7 expression level and CCR7 mRNA

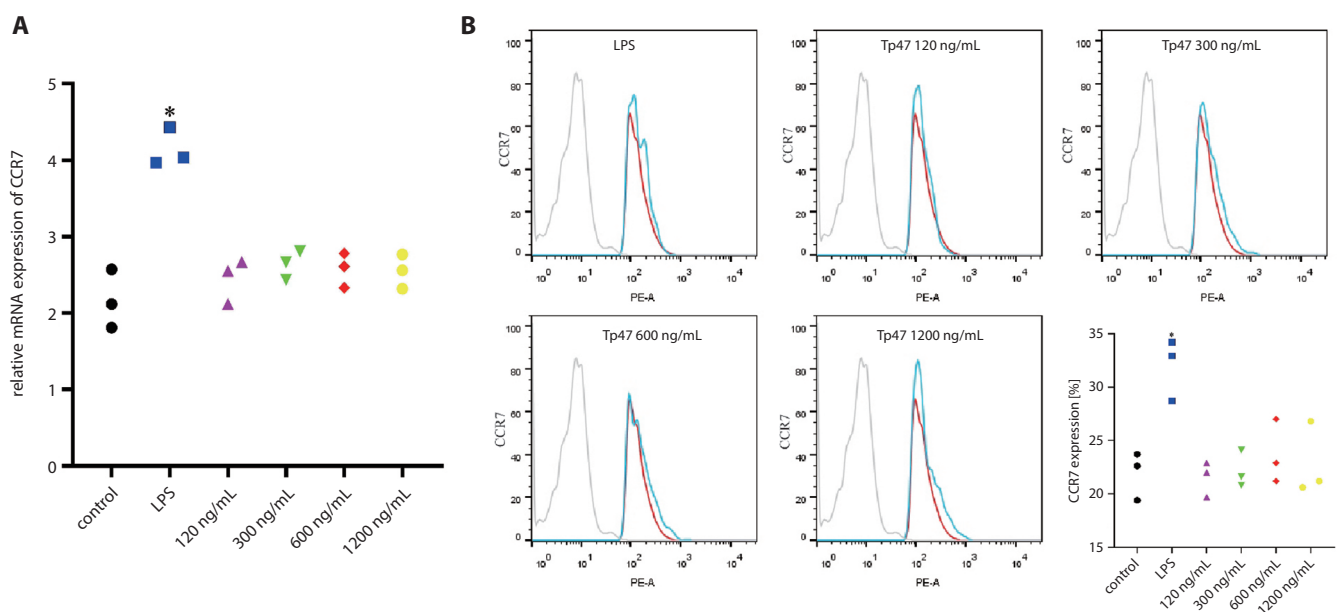


**Fig. 4.** Expression of C-C chemokine receptor type 7 (CCR7) in dendritic cells was detected 24 h after phosphate-buffered saline (PBS) (control group), lipopolysaccharide (LPS) (1  $\mu\text{g}/\text{mL}$ ) and different concentrations of 47-kDa membrane lipoprotein of *Treponema pallidum* (Tp47) (120, 300, 600, and 1200 ng/mL) stimulation. A. Quantitative polymerase chain reaction (qPCR) quantification of CCR7 in dendritic cells; B. Surface CCR7 expression levels on dendritic cells. The control group is indicated as a red line, the LPS and different concentrations of Tp47 groups are represented by blue lines, and the unstained group is marked in gray

$n = 3$ ; \* $p < 0.05$  compared to control. PE-A – phycoerythrin-A; APC-A – allophycocyanin-A.



content following Tp47 stimulation. Additionally, we found that LPS, as a positive control, significantly promoted the expression of CCR7. The chemotaxis jointly mediated by CCR7 and its ligands was the fundamental force driving DC migration that played an indispensable role in regulating the DC migration process. Studies have shown that the migration of DCs and the function of lymph nodes are significantly limited in the CCR7-knockout mice.<sup>51,52</sup> Our results reveal that Tp47 did not increase the CCR7 expression and, consequently, could not facilitate CCR7-mediated DC migration like LPS, which might be the mechanism underlying why Tp47 did not promote the migration of mature DCs. Interestingly, one of the important strategies utilized by pathogenic microorganisms to escape immune clearance is to modulate the CCR7 molecule on the surface of immune cells. Kling et al. found that the absence of CCR7 resulted in dysregulated monocyte migration and immunosuppression, facilitating chronic cutaneous leishmaniasis.<sup>53</sup> Hartiala et al. reported that *Borrelia garinii*, one of the causative agents of Lyme borreliosis, impeded the migratory ability of DCs by significantly downregulating CCR7 expression in DCs.<sup>54</sup> Therefore, Tp47, as previously confirmed by pathogenic microbes, could restrict the migration of DCs by reducing CCR7 expression to mitigate the impact of a robust immune response against itself.

## Limitations

This study assessed the effects of Tp47 on DC maturation and migration. Despite the new findings presented here, our study has some limitations. First, immune evasion is a complex process that is not limited to the parameters evaluated above. Second, the suggested specific molecular mechanism underlying how Tp47 affects DC migration needs more studies to be confirmed. Finally, this study only included cell experiments in vitro with a small sample size, thus further confirmation of the findings with larger in vivo experiments is required.

## Conclusions

In conclusion, the current findings indicate that the 47-kDa membrane lipoprotein of *T. pallidum* promoted the maturation of DCs without enhancing the CCR7-mediated DC migration. This study provides novel insights into the mechanisms by which *T. pallidum* escapes host immune clearance.

## Supplementary files

The complete statistical results (including p-values, test statistics, and degrees of freedom where appropriate) are available as Supplementary material: <https://doi.org/10.5281/zenodo.7249173>.

Supplementary Table 1. Difference of IL-6 levels between other groups and the control group.

Supplementary Table 2. Difference of IL-10 levels between other groups and the control group.

Supplementary Table 3. Difference of IL-12 levels between other groups and the control group.

Supplementary Table 4. Difference of TNF- $\alpha$  levels between other groups and the control group.

Supplementary Table 5. Difference of CD40 levels between other groups and the control group.

Supplementary Table 6. Difference of CD80 levels between other groups and the control group.

Supplementary Table 7. Difference of CD86 levels between other groups and the control group.

Supplementary Table 8. Difference of HLA-DR levels between other groups and the control group.

Supplementary Table 9. Difference of CCR7 levels between other groups and the control group.

Supplementary Table 10. Difference of the relative CCR7 mRNA expression between other groups and the control group.

Supplementary Table 11. Differences of DCs migration rate between other groups and the control group at 1 h.


Supplementary Table 12. Differences of DCs migration rate between other groups and the control group at 2 h.


Supplementary Table 13. Differences of DCs migration rate between other groups and the control group at 3 h.

Supplementary Table 14. Differences of DCs migration rate between other groups and the control group at 4 h.


## ORCID iDs

Wenhao Cheng  <https://orcid.org/0000-0001-6197-8510>

Yumo Lu  <https://orcid.org/0000-0002-8929-9701>

Renqiong Chen  <https://orcid.org/0000-0002-4191-0057>

Hong Ren  <https://orcid.org/0000-0003-3156-6640>

Wenlong Hu  <https://orcid.org/0000-0001-9706-3769>

## References

1. Kojima N, Klausner JD. An update on the global epidemiology of syphilis. *Curr Epidemiol Rep*. 2018;5(1):24–38. doi:10.1007/s40471-018-0138-z
2. Stamm LV. Syphilis: Re-emergence of an old foe. *Microb Cell*. 2016;3(9):363–370. doi:10.15698/mic2016.09.523
3. Peeling RW, Mabey D, Kamb ML, Chen XS, Radolf JD, Benzaken AS. Syphilis. *Nat Rev Dis Primers*. 2017;3(1):17073. doi:10.1038/nrdp.2017.73
4. LaFond RE, Lukehart SA. Biological basis for syphilis. *Clin Microbiol Rev*. 2006;19(1):29–49. doi:10.1128/CMR.19.1.29-49.2006
5. Radolf JD, Deka RK, Anand A, Šmajš D, Norgard MV, Yang XF. *Treponema pallidum*, the syphilis spirochete: Making a living as a stealth pathogen. *Nat Rev Microbiol*. 2016;14(12):744–759. doi:10.1038/nrmicro.2016.141
6. Reid TB, Molini BJ, Fernandez MC, Lukehart SA. Antigenic variation of TprK facilitates development of secondary syphilis. *Infect Immun*. 2014;82(12):4959–4967. doi:10.1128/IAI.02236-14
7. Centurion-Lara A, Giacani L, Godornes C, Molini BJ, Brinck Reid T, Lukehart SA. Fine analysis of genetic diversity of the TPR gene family among treponemal species, subspecies and strains. *PLoS Negl Trop Dis*. 2013;7(5):e22222. doi:10.1371/journal.pntd.0002222
8. Giacani L, Molini BJ, Kim EY, et al. Antigenic variation in *Treponema pallidum*: TprK sequence diversity accumulates in response to immune pressure during experimental syphilis. *J Immunol*. 2010;184(7):3822–3829. doi:10.4049/jimmunol.0902788

9. Chan K, Nasereddin T, Alter L, Centurion-Lara A, Giacani L, Parveen N. *Treponema pallidum* lipoprotein TP0435 expressed in *Borrelia burgdorferi* produces multiple surface/periplasmic isoforms and mediates adherence. *Sci Rep*. 2016;6(1):25593. doi:10.1038/srep25593
10. Luo X, Zhang X, Gan L, et al. The outer membrane protein Tp92 of *Treponema pallidum* induces human mononuclear cell death and IL-8 secretion. *J Cell Mol Med*. 2018;22(12):6039–6054. doi:10.1111/jcmm.13879
11. Cruz AR, Ramirez LG, Zuluaga AV, et al. Immune evasion and recognition of the syphilis spirochete in blood and skin of secondary syphilis patients: Two immunologically distinct compartments. *PLoS Negl Trop Dis*. 2012;6(7):e1717. doi:10.1371/journal.pntd.0001717
12. Pastuszczak M, Gozdzińska A, Jakiela B, Obtulowicz A, Jaskiewicz J, Wojas-Pelc A. Robust pro-inflammatory immune response is associated with serological cure in patients with syphilis: An observational study. *Sex Transm Infect*. 2017;93(1):11–14. doi:10.1136/sextrans-2016-052681
13. Collin M, Bigley V. Human dendritic cell subsets: An update. *Immunology*. 2018;154(1):3–20. doi:10.1111/imm.12888
14. Théry C, Amigorena S. The cell biology of antigen presentation in dendritic cells. *Curr Opin Immunol*. 2001;13(1):45–51. doi:10.1016/S0952-7915(00)00180-1
15. Waisman A, Lukas D, Clausen BE, Yogev N. Dendritic cells as gatekeepers of tolerance. *Semin Immunopathol*. 2017;39(2):153–163. doi:10.1007/s00281-016-0583-z
16. Chudnovskiy A, Pasqual G, Victora GD. Studying interactions between dendritic cells and T cells in vivo. *Curr Opin Immunol*. 2019;58:24–30. doi:10.1016/j.coi.2019.02.002
17. Seyfzadeh N, Muthuswamy R, Mitchell DA, Nierkens S, Seyfzadeh N. Migration of dendritic cells to the lymph nodes and its enhancement to drive anti-tumor responses. *Crit Rev Oncol Hematol*. 2016;107:100–110. doi:10.1016/j.critrevonc.2016.09.002
18. Worbs T, Hammerschmidt SI, Förster R. Dendritic cell migration in health and disease. *Nat Rev Immunol*. 2017;17(1):30–48. doi:10.1038/nri.2016.116
19. Rodríguez-Fernández JL, Criado-García O. The chemokine receptor CCR7 uses distinct signaling modules with biased functionality to regulate dendritic cells. *Front Immunol*. 2020;11:528. doi:10.3389/fimmu.2020.00528
20. Guak H, Al Habyan S, Ma EH, et al. Glycolytic metabolism is essential for CCR7 oligomerization and dendritic cell migration. *Nat Commun*. 2018;9(1):2463. doi:10.1038/s41467-018-04804-6
21. Ohl L, Mohaupt M, Czeloth N, et al. CCR7 governs skin dendritic cell migration under inflammatory and steady-state conditions. *Immunity*. 2004;21(2):279–288. doi:10.1016/j.immuni.2004.06.014
22. Clarkson BD, Walker A, Harris MG, et al. CCR7 deficient inflammatory dendritic cells are retained in the central nervous system. *Sci Rep*. 2017;7(1):42856. doi:10.1038/srep42856
23. Bouis DA, Popova TG, Takashima A, Norgard MV. Dendritic cells phagocytose and are activated by *Treponema pallidum*. *Infect Immun*. 2001;69(1):518–528. doi:10.1128/IAI.69.1.518-528.2001
24. Shin JL, Chung KY, Kang JM, Lee TH, Lee MG. The effects of *Treponema pallidum* on human dendritic cells. *Yonsei Med J*. 2004;45(3):515. doi:10.3349/ymj.2004.45.3.515
25. Radolf JD, Kumar S. The *Treponema pallidum* outer membrane. In: Adler B, ed. *Spirochete Biology: The Post Genomic Era*. Vol. 415. Current Topics in Microbiology and Immunology. Cham, Switzerland: Springer International Publishing; 2017:1–38. [http://link.springer.com/10.1007/82\\_2017\\_44](http://link.springer.com/10.1007/82_2017_44). Accessed September 22, 2022.
26. Hawley KL, Montezuma-Rusca JM, Delgado KN, et al. Structural modeling of the *Treponema pallidum* outer membrane protein repertoire: A road map for deconvolution of syphilis pathogenesis and development of a syphilis vaccine. *J Bacteriol*. 2021;203(15):e0008221. doi:10.1128/JB.00082-21
27. Guan Y, Ding R, Zhou Y, et al. Sensitivity of nPCR for four types of membrane protein DNA and of two pairs of primers for Tpp47 DNA of *Treponema pallidum* in whole blood of congenital syphilis newborns. *J Matern Fetal Neonatal Med*. 2019;32(2):229–235. doi:10.1080/14767058.2017.1378321
28. Liu WN, Jiang XY, JunRen, et al. Tp47 induces cell death involving autophagy and mTOR in human microglial HMO6 cells. *Int Immunopharmacol*. 2019;74:105566. doi:10.1016/j.intimp.2019.04.013
29. de Miranda APF, Sato NS. Profile of Anti-Tp47 antibodies in patients with positive serology for syphilis analyzed by western blot. *Braz J Infect Dis*. 2008;12(2):139–143. doi:10.1590/S1413-8670200800200008
30. Gao ZX, Luo X, Liu LL, Lin LR, Tong ML, Yang TC. Recombinant *Treponema pallidum* protein Tp47 induces angiogenesis by modulating the matrix metalloproteinase/tissue inhibitor of metalloproteinase balance in endothelial cells. *J Eur Acad Dermatol Venereol*. 2019;33(10):1958–1970. doi:10.1111/jdv.15725
31. Livak KJ, Schmittgen TD. Analysis of relative gene expression data using real-time quantitative PCR and the  $2^{-\Delta\Delta CT}$  method. *Methods*. 2001;25(4):402–408. doi:10.1006/meth.2001.1262
32. Collin M, Ginhoux F. Human dendritic cells. *Semin Cell Dev Biol*. 2019;86:1–2. doi:10.1016/j.semcdb.2018.04.015
33. Angeli V, Randolph GJ. Inflammation, lymphatic function, and dendritic cell migration. *Lymph Res Biol*. 2006;4(4):217–228. doi:10.1089/lrb.2006.4406
34. Chung TW, Li YR, Huang WY, et al. Sinulariolide suppresses LPS-induced phenotypic and functional maturation of dendritic cells. *Mol Med Rep*. 2017;16(5):6992–7000. doi:10.3892/mmr.2017.7480
35. Cabeza-Cabrero M, Cardoso A, Minutti CM, Pereira da Costa M, Reis e Sousa C. Dendritic cells revisited. *Annu Rev Immunol*. 2021;39(1):131–166. doi:10.1146/annurev-immunol-061020-053707
36. Choi S, Choi HG, Lee J, Shin KW, Kim HJ. *Mycobacterium tuberculosis* protein Rv2220 induces maturation and activation of dendritic cells. *Cell Immunol*. 2018;328:70–78. doi:10.1016/j.cellimm.2018.03.012
37. Wang X, Zhang C, Wang S, et al. SND1 promotes Th1/17 immunity against chlamydial lung infection through enhancing dendritic cell function. *PLoS Pathog*. 2021;17(2):e1009295. doi:10.1371/journal.ppat.1009295
38. Lee A, Lim HX, Kim MS, et al. *Vibrio vulnificus* infection induces the maturation and activation of dendritic cells with inflammatory Th17-polarizing ability. *Int J Mol Med*. 2018;41(1):531–540. doi:10.3892/ijmm.2017.3230
39. Rizkallah G, Alais S, Futsch N, et al. Dendritic cell maturation, but not type I interferon exposure, restricts infection by HTLV-1, and viral transmission to T-cells. *PLoS Pathog*. 2017;13(4):e1006353. doi:10.1371/journal.ppat.1006353
40. Perot BP, García-Paredes V, Luka M, Ménager MM. Dendritic cell maturation regulates TSPAN7 function in HIV-1 transfer to CD4<sup>+</sup> T lymphocytes. *Front Cell Infect Microbiol*. 2020;10:70. doi:10.3389/fcimb.2020.00070
41. Willinger T. Metabolic control of innate lymphoid cell migration. *Front Immunol*. 2019;10:2010. doi:10.3389/fimmu.2019.02010
42. Kim D, Shaw AK. Migration and tolerance shape host behaviour and response to parasite infection. *J Anim Ecol*. 2021;90(10):2315–2324. doi:10.1111/1365-2656.13539
43. Gao ZX, Liu D, Liu LL, et al. Recombinant *Treponema pallidum* protein Tp47 promotes the migration and adherence of THP-1 cells to human dermal vascular smooth muscle cells by inducing MCP-1 and ICAM-1 expression. *Exp Cell Res*. 2019;381(1):150–162. doi:10.1016/j.yexcr.2019.04.035
44. Xu Y, Pektor S, Balkow S, et al. Dendritic cell motility and T cell activation requires regulation of Rho-cofilin signaling by the Rho-GTPase activating protein myosin IxB. *J Immunol*. 2014;192(8):3559–3568. doi:10.4049/jimmunol.1300695
45. Choo EH, Lee JH, Park EH, et al. Infarcted myocardium-primed dendritic cells improve remodeling and cardiac function after myocardial infarction by modulating the regulatory T cell and macrophage polarization. *Circulation*. 2017;135(15):1444–1457. doi:10.1161/CIRCULATIONAHA.116.023106
46. McLaughlin LM, Govoni GR, Gerke C, et al. The salmonella SPI2 effector Ssel mediates long-term systemic infection by modulating host cell migration. *PLoS Pathog*. 2009;5(11):e1000671. doi:10.1371/journal.ppat.1000671
47. Cerny O, Holden DW. Salmonella SPI-2 type III secretion system-dependent inhibition of antigen presentation and T cell function. *Immunol Lett*. 2019;215:35–39. doi:10.1016/j.imlet.2019.01.006
48. Angeli V, Daveeuw C, Roye O, et al. Role of the parasite-derived prostaglandin D2 in the inhibition of epidermal Langerhans cell migration during schistosomiasis infection. *J Exp Med*. 2001;193(10):1135–1148. doi:10.1084/jem.193.10.1135

49. Rodríguez-Fernández JL, Criado-García O. The chemokine receptor CCR7 uses distinct signaling modules with biased functionality to regulate dendritic cells. *Front Immunol.* 2020;11:528. doi:10.3389/fimmu.2020.00528
50. Ritter U, Wiede F, Mielenz D, Kiafard Z, Zwirner J, Körner H. Analysis of the CCR7 expression on murine bone marrow-derived and spleen dendritic cells. *J Leukoc Biol.* 2004;76(2):472–476. doi:10.1189/jlb.0104037
51. Fleige H, Bosnjak B, Permanyer M, et al. Manifold roles of CCR7 and its ligands in the induction and maintenance of bronchus-associated lymphoid tissue. *Cell Rep.* 2018;23(3):783–795. doi:10.1016/j.celrep.2018.03.072
52. Nico D, Martins Almeida F, Maria Motta J, et al. NH36 and F3 antigen-primed dendritic cells show preserved migrating capabilities and CCR7 expression and F3 is effective in immunotherapy of visceral leishmaniasis. *Front Immunol.* 2018;9:967. doi:10.3389/fimmu.2018.00967
53. Kling JC, Mack M, Körner H. The absence of CCR7 results in dysregulated monocyte migration and immunosuppression facilitating chronic cutaneous leishmaniasis. *PLoS One.* 2013;8(10):e79098. doi:10.1371/journal.pone.0079098
54. Hartiala P, Hytonen J, Pelkonen J, et al. Transcriptional response of human dendritic cells to *Borrelia garini*: Defective CD38 and CCR7 expression detected. *J Leukoc Biol.* 2007;82(1):33–43. doi:10.1189/jlb.1106709





# Time-to-event modeling for achieving a stable warfarin dose using genetic and non-genetic covariates

Kannan Sridharan<sup>1,A–F</sup>, Rashed Abdulla Al Banna<sup>2,B,E,F</sup>, Aisha Husain<sup>2,B,E,F</sup>

<sup>1</sup> Department of Pharmacology and Therapeutics, College of Medicine and Medical Sciences, Arabian Gulf University, Manama, Bahrain

<sup>2</sup> Department of Cardiology, Salmaniya Medical Complex, Manama, Bahrain

A – research concept and design; B – collection and/or assembly of data; C – data analysis and interpretation; D – writing the article; E – critical revision of the article; F – final approval of the article

Advances in Clinical and Experimental Medicine, ISSN 1899–5276 (print), ISSN 2451–2680 (online)

*Adv Clin Exp Med.* 2023;32(3):379–384

## Address for correspondence

Kannan Sridharan

E-mail: skannandr@gmail.com

## Funding sources

The study was funded by Arabian Gulf University and RCSI-Medical University of Bahrain (grant No. AGU RCSI-MUB 2019-02).

## Conflict of interest

None declared

## Acknowledgements

The authors would like to thank Dr. Yaseen Abbasi, Dr. Siti Ghadzi and Dr. Mwila Mulubwa for their assistance during the modeling.

Received on May 31, 2022

Reviewed on October 31, 2022

Accepted on February 12, 2023

Published online on March 10, 2023

## Cite as

Sridharan K, Al Banna RA, Husain A. Time-to-event modeling for achieving a stable warfarin dose using genetic and non-genetic covariates. *Adv Clin Exp Med.* 2023;32(3):379–384. doi:10.17219/acem/161155

## DOI

10.17219/acem/161155

## Copyright

Copyright by Author(s)

This is an article distributed under the terms of the Creative Commons Attribution 3.0 Unported (CC BY 3.0) (<https://creativecommons.org/licenses/by/3.0/>)

## Abstract

**Background.** Time-to-event modeling is gaining importance in drug dosage determination, particularly using pharmacometrics approaches.

**Objectives.** To evaluate the various time-to-event models for estimating the time to achieve a stable warfarin dose in the Bahraini population.

**Materials and methods.** A cross-sectional study evaluating the non-genetic and genetic covariates (single nucleotide polymorphisms (SNPs) in *CYP2C9*, *VKORC1* and *CYP4F2* genotypes) was conducted in patients receiving warfarin for at least 6 months. Time to achieving a stable dose of warfarin was defined as the duration (in days) from the day of initiating warfarin until 2 consecutive prothrombin time-international normalized ratio (PT-INR) values were observed in the therapeutic range with a gap of at least 7 days. Exponential, Gompertz, log-logistics, and Weibull models were tested, and the model with the lowest objective function value (OFV) was chosen. The covariate selection was carried out using the Wald test and OFV. A hazard ratio (HR) with a 95% confidence interval (95% CI) was estimated.

**Results.** A total of 218 participants were included in the study. The Weibull model was observed to have the lowest OFV (1989.82). The expected time to reach a stable dose in the population was 21.35 days. The *CYP2C9* genotypes were identified as the only significant covariate. The HR (95% CI) for achieving a stable warfarin dose within 6 months of initiation for individuals with *CYP2C9* \*1/\*2 was 0.2 (0.09, 0.3), 0.2 (0.1, 0.5) for *CYP2C9* \*1/\*3, 0.14 (0.04, 0.6) for *CYP2C9* \*2/\*2, 0.2 (0.03, 0.9) for *CYP2C9* \*2/\*3, and 0.8 (0.45, 0.9) for those with the C/T genotype for *CYP4F2*.

**Conclusions.** We estimated the population time-to-event parameters for achieving a stable warfarin dose in our population and observed *CYP2C9* genotypes to be the main predictor covariate followed by *CYP4F2*. The influence of these SNPs needs to be validated in a prospective study and an algorithm to predict a stable warfarin dose and the time to achieve it needs to be developed.

**Key words:** warfarin, Weibull, Gompertz, time-to-event, exponential

## Introduction

Warfarin, a commonly administered oral anticoagulant, poses a lot of challenges clinically, owing to inter- and intra-individual variabilities, drug and food interactions, and the influence of genetic polymorphisms on its metabolism and pharmacodynamic target enzymes.<sup>1</sup> Though several novel oral anticoagulants (NOACs) are more efficacious and safer, warfarin is still the preferred, cost-effective drug in most developing nations. Among genetic polymorphisms, cytochrome P450 2C9 (CYP2C9), CYP4F2 and vitamin K epoxide reductase complex subunit 1 (VKORC1) have been shown to affect the therapeutic response to warfarin.<sup>2</sup>

Pharmacometrics is the quantification of pharmacokinetic and pharmacodynamic data with the use of appropriate mathematical models to help determine dosage regimens. Pharmacometrics time-to-event modeling has recently gained importance, wherein various models can be applied to predict the median time for achieving an outcome and to identify factors that significantly affect the outcome variable.<sup>3</sup> Commonly used models include exponential – when the hazard ratio (HR) is expected to be constant – and Weibull, Gompertz and log-logistics, when the HR is expected to change over time.<sup>4</sup> Several clinical trials and observational studies evaluating the role of genetic and non-genetic factors included outcomes on the anticoagulation control, warfarin stable dose and bleeding episodes. However, hardly any studies assessed the time taken to reach a stable warfarin dose and the associated factors. Achieving a stable dose of warfarin is clinically important for optimized therapeutic goals so that the risk of thrombosis and/or hemorrhage can be minimized.

Previously, we conducted a warfarin pharmacogenetics study in the Bahraini population<sup>5</sup> and in the present study, we performed a secondary analysis of the data evaluating various time-to-event models for ascertaining the time to achieve a stable warfarin dose in the studied population.

## Objectives

To evaluate various time-to-event models for estimating the time to achieve a stable warfarin dose in the Bahraini population.

## Materials and methods

### Study design and ethics

The analysis was carried out as a part of the warfarin pharmacogenomics study that was cross-sectional in design. The approvals from the Institutional Ethics Committee of Arabian Gulf University (Manama, Bahrain; approval No. E-024-PI-11/18), and the Research Technical Support

Team of the Ministry of Health of Bahrain (approval No. AURS 301/2019) were granted. Consent was obtained from the study participants. This study was carried out in compliance with the latest Declaration of Helsinki guidelines.

### Study procedure

We included patients who were enrolled in the anticoagulation clinic in a tertiary care hospital receiving warfarin for at least 6 months and with the following details available: age, gender, CHA<sub>2</sub>DS<sub>2</sub>-VASc (congestive heart failure history, age, sex, hypertension history, stroke/transient ischemic attack/thromboembolism history, vascular disease history, and diabetes history) score, HASBLED (hypertension, abnormal renal/liver function, stroke, bleeding, labile international normalized ratio (INR), elderly, and interacting drugs/alcohol) score, and SAMe-TT<sub>2</sub>R<sub>2</sub> (sex, age, history of concomitant diseases, interacting drugs, tobacco use, and race) score. We evaluated genotypes of CYP2C9, VKORC1 and CYP4F2 using reverse transcription polymerase chain reaction (RT-PCR), as described previously.<sup>5</sup> Statins, proton pump inhibitors, carbamazepine, and amiodarone were considered as drugs with potential interaction with warfarin. The following genotypes were considered wild-type: \*1/\*1 for CYP2C9, C/C for VKORC1 and C/C for CYP4F2. Therapeutic prothrombin time (PT)-INR categories were defined as either between 2.5 and 3.5 for those with heart valve replacement, or between 2 and 3 for others.

### Outcome variable

Time to achieve a stable dose of warfarin was defined as the duration (in days) from the day of initiating warfarin until 2 consecutive PT-INR values were observed in the therapeutic range with a gap of at least 7 days.<sup>6</sup>

### Time-to-event modeling

Time to achieve a stable warfarin dose was the outcome variable with the following covariates: age, gender, CHA<sub>2</sub>DS<sub>2</sub>-VASc score, HASBLED score, SAMe-TT<sub>2</sub>R<sub>2</sub> score, presence of any drugs with potential interaction, PT-INR categories (either between 2.5 and 3.5 or between 2 and 3), and genotypes of CYP2C9, VKORC1 and CYP4F2. We explored the following base models: exponential, Gompertz, log-logistics, and Weibull. The model with the lowest (minimum) objective function value (OFV) was chosen. Both the Wald test and a decline in OFV by at least 3.84 points were used as criteria for defining significant covariates.<sup>7</sup> The HRs were calculated for the significant covariates using standard formulae.<sup>8</sup> A visual predictive check (VPC) was used for evaluating the model fit.

The Monolix v. 2021R1 (<http://lixoft.com/products/monolix/>; Lixoft SAS, Antony, France) was used for modeling the outcome variable.

## Results

### Demographics

The study involved 218 participants. Table 1 shows a summary of their demographic characteristics. Among the participants, 206 achieved a stable dose of warfarin within 6 months, with the median (range) time required for achieving the stable dose being 44 (14–171) days. The Kaplan–Meier

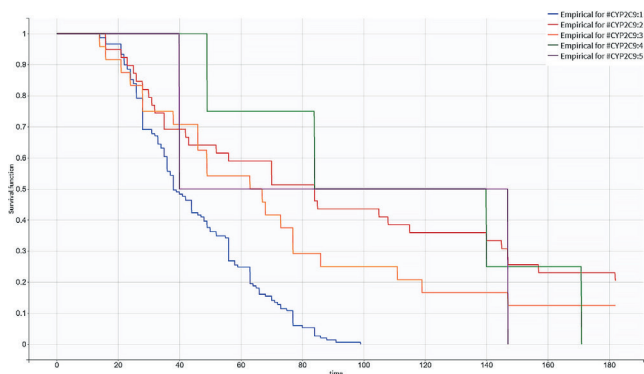


**Fig. 1.** Kaplan–Meier curve for achieving a stable warfarin dose according to CYP2C9 genotypes. The blue line represents the estimates for CYP2C9 \*1/\*1, the red line for \*1/\*2, the yellow line for \*1/\*3, the green line for \*2/\*2, and the purple line for \*2/\*3 genotypes

**Table 1.** Summary of demographic characteristics of study participants (n = 218)

Variables		Values
Age [years]		69 (21–89)
Male:female, n		116:102
CHA <sub>2</sub> DS <sub>2</sub> -VASc score		4 (0–8)
HASBLED score		2 (0–6)
SAME-TT <sub>2</sub> R <sub>2</sub> score		1 (0–3)
CYP2C9 genotypes, n (%)	*1/*1	149 (68.3)
	*1/*2	39 (17.9)
	*1/*3	24 (11)
	*2/*2	4 (1.8)
	*2/*3	2 (1)
VKORC1 genotypes, n (%)	C/C	94 (43.1)
	C/T	90 (41.3)
	T/T	34 (15.6)
CYP4F2 genotypes, n (%)	C/C	86 (39.6)
	C/T	99 (45.6)
	T/T	32 (14.8)
Number of participants with at least 1 drug with potential interaction, n (%)		134 (61.5)

Unless stated otherwise, numerical variables are expressed as median (range). CHA<sub>2</sub>DS<sub>2</sub>-VASc – congestive heart failure history, age, sex, hypertension history, stroke/transient ischemic attack/thromboembolism history, vascular disease history, and diabetes history; HASBLED – hypertension, abnormal renal/liver function, stroke, bleeding, labile international normalized ratio (INR), elderly, and interacting drugs/alcohol; SAME-TT<sub>2</sub>R<sub>2</sub> score – sex, age, history of concomitant diseases, interacting drugs, tobacco use, and race.

curve for achieving a stable warfarin dose as stratified by CYP2C9 genotype is depicted in Fig. 1, and the curves according to gender, potentially interacting drugs, and CYP4F2 and VKORC1 genotypes are depicted in Fig. 2–5.

### Time-to-event model

The Weibull model was found to have the lowest OFV among the base models (Table 2). The CYP2C9 improved the base model, followed by the addition of the CYP4F2 genotype. Population time-to-event parameters are listed in Table 3. The Wald statistics revealed a significant

**Table 2.** Comparison of objective function values (OFVs) between the models

Model	OFVs	
Base model	exponential	1996.22
	Gompertz	1995.89
	log-logistics	1994.17
	Weibull	1989.82
Weibull model with CYP2C9 genotype (significant covariate) selection	addition of CYP2C9 genotype to the base (Weibull) model	1944.97
	addition of CYP4F2 genotype to the Weibull model with CYP2C9 covariate included	1939.85
	Weibull model with all covariates included	1943.9
	removal of CYP2C9 genotype from the Weibull model with all covariates	1981.84
	removal of CYP4F2 genotype from the Weibull model with all covariates except CYP2C9 genotype	1985.15

**Table 3.** Population time-to-event parameters

Parameter	Estimate	RSE, %
Te <sub>pop</sub> [days]	21.35	14.5
Effect of CYP2C9 *1/*2 on Te <sub>pop</sub>	1.79	18.5
Effect of CYP2C9 *1/*3 on Te <sub>pop</sub>	1.43	26.7
Effect of CYP2C9 *2/*2 on Te <sub>pop</sub>	1.9	35.7
Effect of CYP2C9 *2/*3 on Te <sub>pop</sub>	1.58	63.7
Effect of CYP4F2 C/T on Te <sub>pop</sub>	0.26	103
Effect of CYP4F2 T/T on Te <sub>pop</sub>	–0.4	91
P <sub>pop</sub>	4.29	24.8
del <sub>pop</sub>	21.93	9.67
Between-subject variability		
ΩTe	1.13	9.75
ΩP	0.83	22.2
Ωdel	0.51	14.1

RSE – relative standard error; Te<sub>pop</sub> – time to event in the population; P<sub>pop</sub> – shape parameter in the population; del<sub>pop</sub> – delay before the time to event starts decreasing in the population; ΩTe – standard deviation of the random effects of time to event; ΩP – standard deviation of the random effects of the shape parameter; Ωdel – standard deviation of the random effects of time delay.

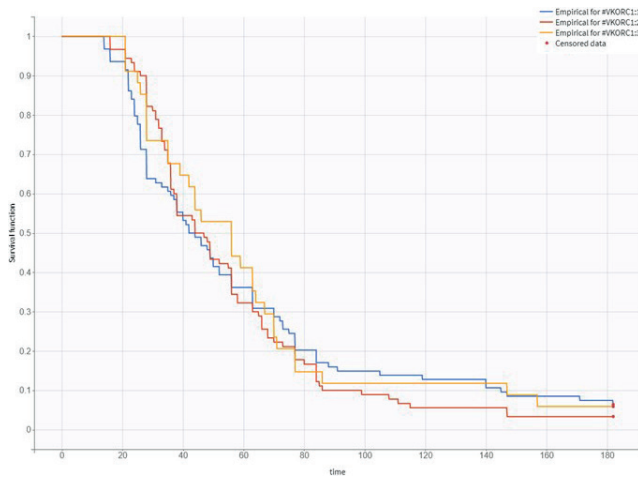


Fig. 2. Kaplan–Meier curve for achieving warfarin stable dose according to *VKORC1* genotypes

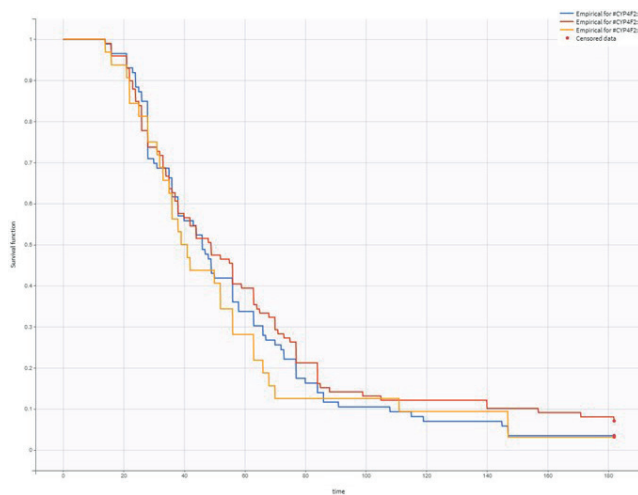


Fig. 3. Kaplan–Meier curve for achieving warfarin stable dose according to *CYP4F2* genotypes

prolongation of time to achieve a stable warfarin dose with *CYP2C9* genotypes and a shortened time with *CYP4F2* genotypes. The model used for evaluating the effect of significant genotype covariates is outlined as follows.

The HR (95% confidence interval (95% CI)) for achieving a stable warfarin dose within 6 months of initiation for individuals with *CYP2C9* \*1/\*2 was 0.2 (0.09, 0.3), 0.2 (0.1, 0.5) for *CYP2C9* \*1/\*3, 0.14 (0.04, 0.6) for *CYP2C9* \*2/\*2, and 0.2 (0.03, 0.9) for those with *CYP2C9* \*2/\*3. Similarly, the HR (95% CI) for the *CYP4F2* C/T genotype was 0.8 (0.45, 0.9), but it was not significant for the T/T genotype (1.4 (0.9, 1.3)) when compared to the C/C genotype.

The VPC revealed a good fit of the model to the observed data (Fig. 6). Those with *CYP2C9* \*1/\*1 and *CYP4F2* C/C genotypes were observed to have a shorter time to achieve a stable warfarin dose compared to other genotype categories (Fig. 7).

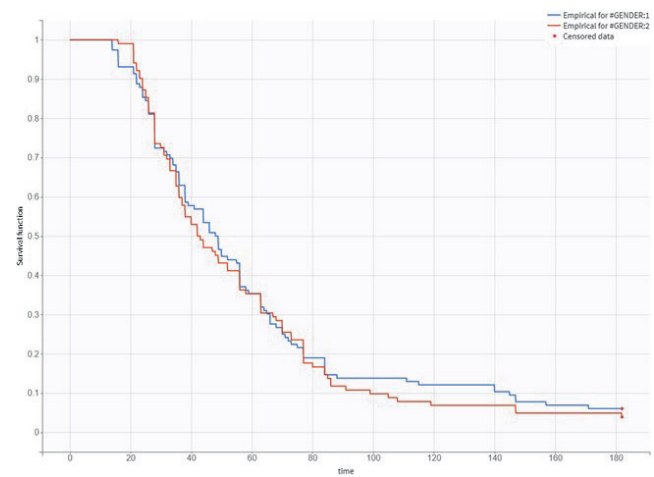


Fig. 4. Kaplan–Meier curve for achieving warfarin stable dose according to gender

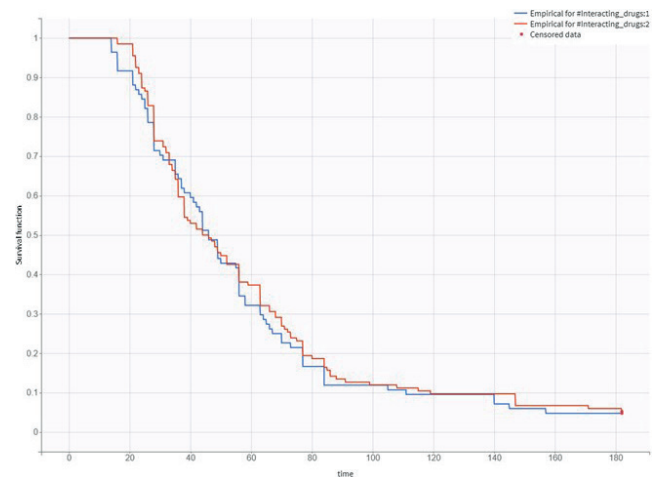


Fig. 5. Kaplan–Meier curve for achieving warfarin stable dose according to the presence of potentially interacting drugs

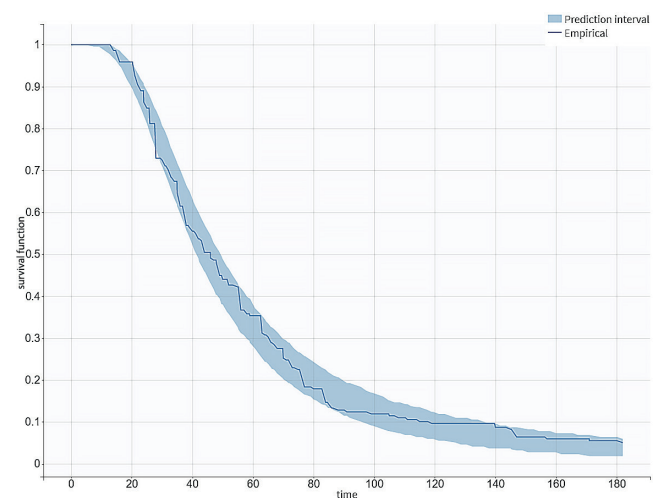


Fig. 6. Visual predictive check (VPC) for the time-to-event model. The black dotted line represents the median predicted time, and the area shaded in blue represents the 90% predicted interval



## Discussion

### Key findings from the study

This pharmacometrics-based modeling study was carried out to evaluate the time needed to achieve a stable warfarin dose in 218 patients. We established the population-specific parameters associated with time to reach a stable warfarin dose, and observed that CYP2C9 and CYP4F2 genotypes are the predominant predictor covariates. Those with CYP2C9\*1/\*1 and CYP4F2C/C genotypes were observed to achieve the stable warfarin dose much earlier, and those with genetic polymorphisms in CYP2C9 were less likely to reach the stable dose at 6 months.

### Comparison with existing literature

This is the first study evaluating the time needed to reach a stable warfarin dose using pharmacometrics time-to-event modeling. Combined CYP2C9 and VKORC1 polymorphisms are recommended by the US Food and Drug

Administration (FDA) for determining the appropriate warfarin dose.<sup>2</sup> We observed that those with the wild-type CYP2C9 genotype achieved the stable dose sooner compared to those with genetic polymorphisms. This finding reiterates the importance of determining the CYP2C9 genotype as soon as possible when a patient has been identified as requiring warfarin therapy, so that genotype-based warfarin dosing can be initiated to aid in achieving the stable dose sooner, particularly when genetic polymorphisms are identified. The existing standard of care is to initiate warfarin at a fixed dose (5 mg/day) and titrate based on the therapeutic response. In the same population, we have observed that genetic polymorphisms in CYP2C9 require lower warfarin doses for achieving therapeutic PT-INR.<sup>5</sup> Nearly 31.8% of the population was observed to carry at least 1 functionally variant CYP2C9 allele that necessitates a lower warfarin dose to be administered for achieving an optimal PT-INR value. Even then, those with at least 1 single nucleotide polymorphism (SNP) in CYP2C9 were observed to take a significantly longer time to achieve a stable dose. Such candidates are at an increased risk of thromboembolic

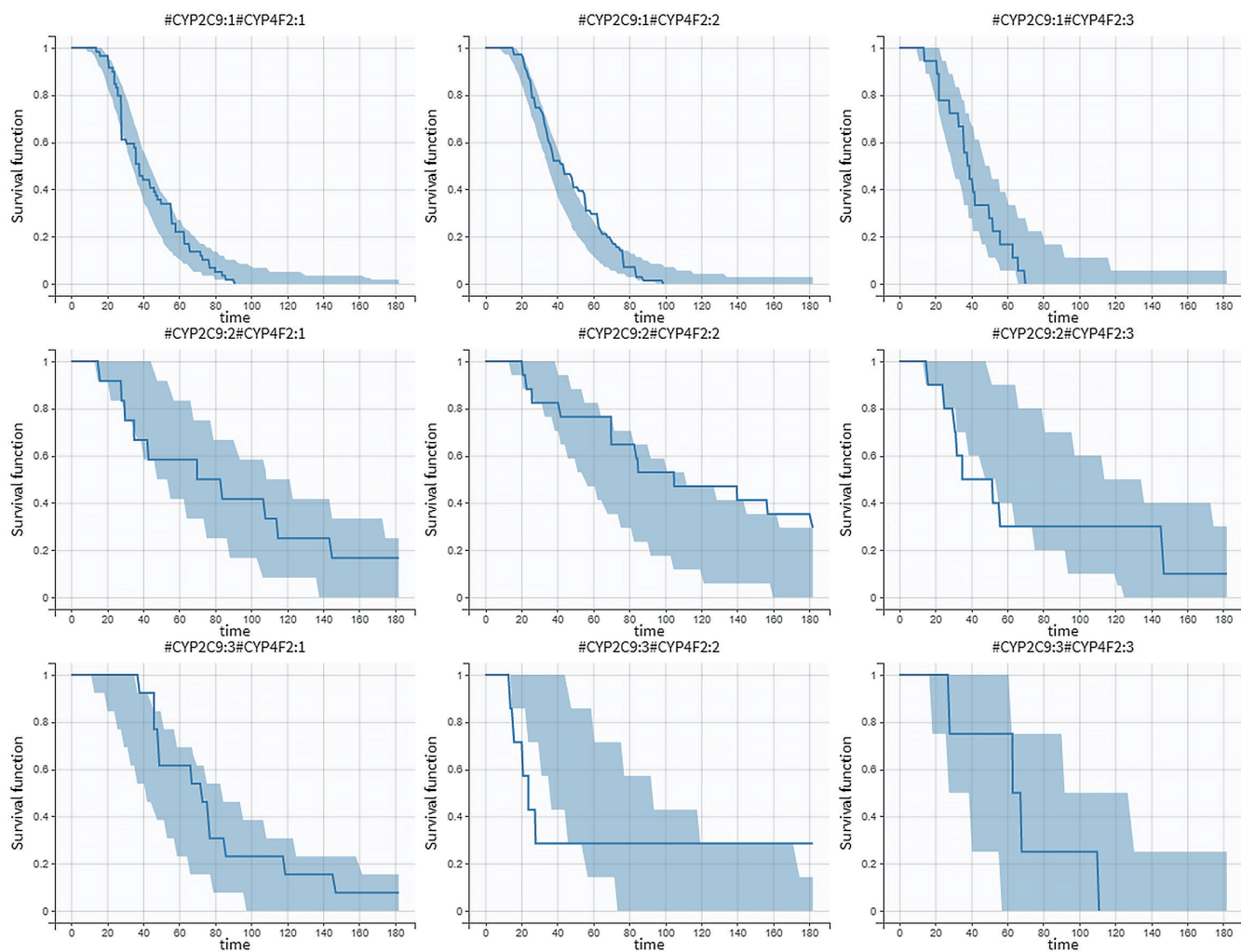


Fig. 7. Comparison of predicted time to achieve a stable warfarin dose. The blue line indicates the Kaplan–Meier-predicted curve after the simulation; CYP2C9:1 indicates \*1/\*1, CYP2C9:2 represents \*1/\*2, CYP2C9:3 represents \*1/\*3, CYP4F2:1 represents C/C, CYP4F2:2 represents C/T, and CYP4F2:3 represent T/T genotypes. The area shaded in blue represents the prediction interval

attacks for bleeding episodes until a stable dose is achieved, and thus need either intense monitoring or serve as likely candidates for receiving a NOAC.

## Limitations

The study is limited by a lack of external validation of the model using data from prospective patients.

## Conclusions

In this study, we have estimated the time-to-event parameters for achieving a stable warfarin dose in Bahraini population. The CYP2C9 has been observed to be the main predictor covariate, followed by the CYP4F2 genotype. Those with at least one SNP in CYP2C9 were observed to have a significantly lower likelihood of achieving a stable warfarin dose, as follows: CYP2C9 \*1/\*2: 0.2 (0.09, 0.3), CYP2C9 \*1/\*3: 0.2 (0.1, 0.5), CYP2C9 \*2/\*2: 0.14 (0.04, 0.6), and for those with CYP2C9 \*2/\*3: 0.2 (0.03, 0.9). There is a need to validate the influence of these SNPs in a prospective study and develop an algorithm predicting a stable warfarin dose and time to achieve it.

## Data availability statement

The data are available from the corresponding author upon reasonable request.

## ORCID iDs

Kannan Sridharan  <https://orcid.org/0000-0003-3811-6503>

## References

1. Patel S, Singh R, Preuss C, Patel N. Warfarin. In: *StatPearls*. Treasure Island, USA: StatPearls Publishing; 2022. <https://www.ncbi.nlm.nih.gov/books/NBK470313/>. Accessed June 1, 2022.
2. Dean L. Warfarin therapy and VKORC1 and CYP genotype. In: Dean L, Pratt V, Scott S, et al., eds. *Medical Genetic Summaries*. Bethesda, USA: National Center for Biotechnology Information (US); 2018. <https://www.ncbi.nlm.nih.gov/books/NBK84174/>.
3. Holford N. A time to event tutorial for pharmacometricians. *CPT Pharmacometrics Syst Pharmacol*. 2013;2(5):e43. doi:10.1038/psp.2013.18
4. Gong X, Hu M, Zhao L. Big data toolsets to pharmacometrics: Application of machine learning for time-to-event analysis. *Clin Transl Sci*. 2018;11(3):305–311. doi:10.1111/cts.12541
5. Sridharan K, Al Banna R, Malalla Z, et al. Influence of CYP2C9, VKORC1, and CYP4F2 polymorphisms on the pharmacodynamic parameters of warfarin: A cross-sectional study. *Pharmacol Rep*. 2021;73(5):1405–1417. doi:10.1007/s43440-021-00256-w
6. Sridharan K, Banny RA, Husain A. Evaluation of stable doses of warfarin in a patient cohort. *Drug Res (Stuttg)*. 2020;70(12):570–575. doi:10.1055/a-1228-5033
7. Teuscher N. What is the -2LL or the log-likelihood ratio? 2013. <https://www.certara.com/knowledge-base/what-is-the-2ll-or-the-log-likelihood-ratio/>. Accessed November 1, 2022.
8. Sedgwick P. Hazards and hazard ratios. *BMJ*. 2012;345:e5980. doi:10.1136/bmj.e5980

# An epidemiological and retrospective study in a cohort qualified for SARS-CoV-2 vaccination in the region of Lower Silesia, Poland

Monika Stępień<sup>1,A–F</sup>, Natalia Świątoniowska-Lonc<sup>2,A–F</sup>, Brygida Knysz<sup>1,A–F</sup>, Beata Jankowska-Polańska<sup>2,A–F</sup>, Amadeusz Kuźniarski<sup>3,A,D–F</sup>, Agnieszka Piwowa<sup>4,A,D–F</sup>, Małgorzata Zalewska<sup>1,A–F</sup>

<sup>1</sup> Department of Infectious Diseases, Liver Diseases and Acquired Immune Deficiencies, Wrocław Medical University, Poland

<sup>2</sup> Center for Research and Innovation, 4<sup>th</sup> Military Teaching Hospital, Wrocław, Poland

<sup>3</sup> Department of Prosthetic Dentistry, Wrocław Medical University, Poland

<sup>4</sup> Department of Toxicology, Wrocław Medical University, Poland

A – research concept and design; B – collection and/or assembly of data; C – data analysis and interpretation;

D – writing the article; E – critical revision of the article; F – final approval of the article

Advances in Clinical and Experimental Medicine, ISSN 1899–5276 (print), ISSN 2451–2680 (online)

*Adv Clin Exp Med.* 2023;32(3):385–389

## Address for correspondence

Monika Stępień

E-mail: lekmonkastepien@gmail.com

## Funding sources

None declared

## Conflict of interest

None declared

Received on October 29, 2022

Reviewed on December 27, 2022

Accepted on February 20, 2023

Published online on March 15, 2023

## Cite as

Stępień M, Świątoniowska-Lonc N, Knysz B, et al.

An epidemiological and retrospective study in a cohort qualified for SARS-CoV-2 vaccination in the region of Lower Silesia, Poland. *Adv Clin Exp Med.* 2023;32(3):385–389.

doi:10.17219/acem/161461

## DOI

10.17219/acem/161461

## Copyright

Copyright by Author(s)

This is an article distributed under the terms of the Creative Commons Attribution 3.0 Unported (CC BY 3.0) (<https://creativecommons.org/licenses/by/3.0/>)

## Abstract

**Background.** Since the beginning of the coronavirus disease (COVID-19) pandemic, numerous infections have been observed with various symptoms and degrees of severity. Not all patients have had a confirmation of infection made using reverse transcription polymerase chain reaction (RT-PCR) or antigen tests. It has been observed that some people, including convalescents or those without knowledge of a past infection, perform serological tests to detect anti-severe acute respiratory syndrome coronavirus 2 (SARS-CoV-2) antibodies.

**Objectives.** We aimed to evaluate the levels of anti-SARS-CoV-2 immunoglobulin G (IgG) antibodies in a cohort of convalescents and in individuals not previously infected, who were willing to get vaccinated. We also aimed to assess several socio-clinical factors associated with participants' humoral responses.

**Materials and methods.** We recruited 298 individuals from the region of Lower Silesia who were willing to get vaccinated for SARS-CoV-2. The participants were divided into 2 groups: convalescents (group I) and participants without a past infection (group II). Several seropositive individuals in group II were identified, and they were transferred to group I, resulting in a final distribution of 171 individuals in group I and 127 individuals in group II. For serological testing, the QuantiVac anti-SARS-CoV-2 (IgG) enzyme-linked immunosorbent assay (ELISA) was used.

**Results.** The results showed the presence of anti-SARS-CoV-2 IgG antibodies in participants from group I, with an average number of 190.3 IU/mL. Twenty-three participants (13.45%) did not have a detectable level of antibodies despite a previous SARS-CoV-2 infection. In 21 participants (12.28%), antibodies were detected despite no previous symptoms of infection (average level: 145.0 IU/mL).

**Conclusions.** Older participants were more likely to experience a symptomatic SARS-CoV-2 infection, and the severity of the symptoms was related to higher antibody titers seen later after COVID-19. Numerous individuals from group II were unaware of past SARS-CoV-2 infections. In several participants, antibodies were not detected despite a previous infection.

**Key words:** antibodies, serology, seronegative, SARS-CoV-2, asymptomatic

## Background

The first information about severe acute respiratory syndrome coronavirus 2 (SARS-CoV-2) emerged at the beginning of 2020. At present, over 12.88 billion vaccine doses have been administered worldwide, with 67.9% of the world's population having received at least 1 dose. In Poland, over 57 million vaccines were administered in the 2 years since their introduction.<sup>1</sup> However, we are still facing new infections in everyday clinical practice. Therefore, we are continuously in need of information regarding this topic.<sup>2</sup>

Serological tests have been used to detect antibodies produced as a result of infection. Severe disease, compared to mild disease, correlates with persistently higher antibody levels.<sup>3</sup> There is also a small group of people, mainly those with mild/asymptomatic infections, who do not produce antibodies.<sup>4</sup> However, it should be noted that the detection of the persistence of antibodies can vary depending on the assay used.<sup>5</sup>

## Objectives

We present preliminary data on a cohort of participants qualified to receive vaccination against SARS-CoV-2. This is the 1<sup>st</sup> part of a larger study evaluating the humoral immune response to vaccination against coronavirus disease (COVID-19). The 2<sup>nd</sup> part of the analysis, entitled “How humoral response and side effects depend on the type of vaccine and past SARS-CoV-2 infection” has also been published (*Vaccines*. 2022;10(7):1042) and is available online (<https://doi.org/10.3390/vaccines10071042>).

The main aim of this study is to evaluate the levels of anti-SARS-CoV-2 immunoglobulin G (IgG) antibodies in a cohort of convalescents and not previously infected individuals from the Lower Silesia region (Poland) who were willing to get vaccinated.

## Materials and methods

The inclusion criteria were: age >18 years, providing written informed consent to participate in the study and a willingness to get vaccinated. Two groups of participants were selected for the study: COVID-19 convalescents (group I) and naïve participants (group II). The exclusion criteria were: the presence of diabetes, any cancer detected within the last 5 years, chronic kidney, liver or lung diseases, acquired immunodeficiency syndrome (AIDS), or immunosuppression for any other reason.

Before each blood draw, the participants were asked to complete a questionnaire. The questions concerned previous SARS-CoV-2 infections and whether it was confirmed through testing, as well as general wellbeing, persistence of COVID-19 symptoms, adverse vaccine reactions, chronic diseases, and allergic reactions to drugs, substances and foods.

Overall, 298 participants were included in the study. After receiving results showing that 21 supposedly naïve participants had current IgG antibodies, we decided to analyze them together with the convalescent group, which resulted in the final division: group I (COVID-19 convalescents,  $n = 171$ ) and group II (naïve participants,  $n = 127$ ).

This single-center study was conducted from February 20, 2021, to May 19, 2021. The participants were inhabitants of the Lower Silesia region, aged 21–69 years, and were of both sexes. The participants were recruited by announcements in the local media. Due to changes in the registration rules and participants' individual contraindications at the moment, the interval between taking the blood sample for testing and the actual vaccination date varied from 1 day to 6 weeks, usually approx. 1 week (mean: 2.00, interquartile range (IQR): 0.25–6.00, standard deviation (SD): 8.54). Before vaccination, all participants were tested for the presence of anti-SARS-CoV-2 IgG antibodies.

Plasma samples were collected using heparin, centrifuged, and stored in aliquots at  $-70^{\circ}\text{C}$  for later use. The QuantiVac anti-SARS-CoV-2 (IgG) enzyme-linked immunosorbent assay (ELISA) (EUROIMMUN, Lübeck, Germany) was used for quantitative detection of anti-SARS-CoV-2 antibodies by means of 6-point calibration curve.

The ELISAs were performed and the results were evaluated as recommended by the manufacturer. Samples with an absorbance higher than the absorbance of the highest standard (386 international units (IU)/mL) were diluted and retested. The assay was standardized against the First WHO International Standard for anti-SARS-CoV-2 immunoglobulin (NIBSC 20/136) and the quantitative results are given in standardized units (IU/mL).

## Ethical approval

This study received approval from the Bioethics Committee of Wrocław Medical University, Poland (approval No. 51/2021). The study was performed in accordance with the Declaration of Helsinki and the principles of good clinical practice with respect to the rights and dignity of participants.

## Statistical analyses

Counts, percentages, means, medians, SDs, ranges, and lower and upper quartiles are reported where appropriate. The normality of the distributions was tested with the Shapiro–Wilk test.

Statistical significance between means for different groups was calculated using the non-parametric Kruskal–Wallis test, followed by Dunn's post hoc tests with Bonferroni correction. Statistical significance between frequencies was calculated using the  $\chi^2$  test.



**Table 1.** Characteristics of coronavirus disease (COVID-19) convalescents (group I) and naïve participants (group II)

Parameters		Group I convalescents (n = 171)	Group II (n = 127)	p-value
Age [years]	M ±SD	44.0 ±9.4	42.6 ±7.2	0.177 Mann–Whitney U test, U = 9715.0
	median (IQR)	44.0 (39.0–49.0)	43.0 (39.0–47.0)	
Sex, n (%)	female	101 (57.81)	74 (58.27)	0.828 $\chi^2 = 0.04$
	male	70 (42.19)	53 (41.73)	
Previous allergic reactions to vaccines, n (%)	yes	3 (1.75)	1 (0.79)	0.639 Fisher's exact test
	no	168 (98.25)	126 (99.21)	
Musculoskeletal pain, n (%)	yes	4 (2.34)	0 (0)	0.139 Fisher's exact test
	no	167 (97.66)	127 (100)	
Fatigue, n (%)	yes	9 (5.26)	0 (0)	0.012 Fisher's exact test
	no	162 (94.74)	127 (100)	
Taste and smell loss, n (%)	yes	15 (8.77)	0 (0)	0.002 $\chi^2 = 10.03$
	no	155 (90.64)	127 (100)	
Anti-SARS-CoV-2 antibodies level [IU/mL]	before vaccination, M ±SD	190.3 ±328.4 (n = 148)	0 (n = 127)	<0.001 Mann–Whitney U test, U = 1512.0
	median (IQR)	105.6 (38.4–198.4)	0	

SARS-CoV-2 – severe acute respiratory syndrome coronavirus 2; M ±SD – mean ± standard deviation; IQR – interquartile range.

A value of  $p < 0.05$  was required to reject the null hypothesis. Statistical analyses were performed using the Statistica v. 13.3 (StatSoft Inc., Tulsa, USA) software package.

## Results

All 298 participants were tested for anti-SARS-CoV-2 IgG antibodies, creating 2 groups: I (COVID-19 convalescents,  $n = 171$ ) and II (naïve participants,  $n = 127$ ). Tables 1,2 present characteristics of the groups.

After testing the blood samples, the results showed that anti-SARS-CoV-2 IgG antibodies were present in participants from group I with a median of 105.6 (38.4–198.4) IU/mL. In group II, no spike antibodies were found (0 IU/mL). The detailed data are presented in Fig. 1.

When describing our findings, we would like to underline the fact that, among the participants of group I, there can be found 3 specific subgroups based on antibody levels (Fig. 1). One consists of participants without knowledge or symptoms of a previous COVID-19 infection but with positive antibody results ( $n = 21$ ; 12.28% of group I, 7.05% of all participants). The 2<sup>nd</sup> group includes participants with a proven previous infection but with no antibodies found in the first blood sample ( $n = 23$ ; 13.45% of I group, 7.72% of all participants). The 3<sup>rd</sup> group consists of seropositive convalescents ( $n = 127$ ) with a median age of 45 (40.0–52.0) years, a maximum age of 69 years, and a median number of antibodies of 123.2 (58.7–252.8) IU/mL. In this subgroup, the time between sample collection and symptoms of the infection varied between 18 days and 7 months.

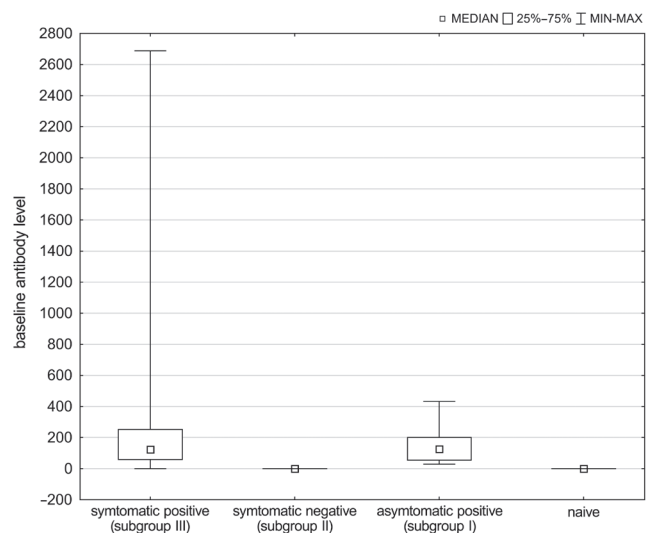


**Fig. 1.** Initial antibody levels in subgroup I (convalescents, asymptomatic), subgroup II (symptomatic, seronegative) and subgroup III (symptomatic, seropositive)

Subgroup I participants without knowledge of a previous infection were aged from 24 to 50 years, with antibody levels between 28.8 IU/mL and 432 IU/mL (median: 126.4 IU/mL, range: 54.4–2000.0 IU/mL). After receiving the serological results, we confirmed that the participants were not able to recall any possible COVID-19 manifestations.

Subgroup II includes participants with undetectable antibody levels despite the fact that they had a previous SARS-CoV-2 infection and were aged from 23 to 63 years ( $n = 23$ ). The time between COVID-19 and blood sampling varied from 2.5 months to 6.5 months.

**Table 2.** Characteristics of the subgroups of coronavirus disease (COVID-19) convalescents (group I)

Parameters		Subgroup I (n = 21)	Subgroup II (n = 23)	Subgroup III (n = 127)	Statistical analysis
Age [years]	M ±SD	41.5 ±7.1	40.6 ±9.9	45.0 ±9.5	K-W test H = 6.70, p = 0.0350 I R = 72.690; II R = 66.717; III R = 91.693 I compared to II: Z = 0.399737 I compared to III: Z = 1.629365 II compared to III: Z = 2.226194 I compared to II: p = 1.000000 I compared to III: p = 0.309708 II compared to III: p = 0.078004
	median (IQR)	42.0 (39.0–46.0)	43.0 (33.0–46.0)	45.0 (40.0–52.0)	
Sex, n (%)	female	11 (52.38)	13 (56.52)	77 (60.63)	I compared to II: p = 0.625 I compared to III: p = 0.0983 II compared to III: p = 0.0271
	male	10 (47.62)	10 (43.48)	50 (39.37)	
Previous allergic reactions to vaccines, n (%)	yes	0 (0)	1 (4.35)	2 (1.57)	I compared to II: p = 0.334 I compared to III: p = 0.563 II compared to III: p = 0.382
	no	0 (110)	22 (95.65)	125 (98.43)	
Musculoskeletal pain, n (%)	yes	0 (0)	0 (0)	4 (3.15)	I compared to III: p = 0.410 II compared to III: p = 0.388
	no	21 (100)	23 (100)	123 (96.85)	
Fatigue, n (%)	yes	0 (0)	0 (0)	9 (7.09)	I compared to III: p = 0.208 II compared to III: p = 0.188
	no	21 (100)	23 (100)	118 (92.91)	
Taste and smell loss, n (%)	yes	0 (0)	1 (4.35)	15 (11.81)	I compared to II: p = 0.334 I compared to III: p = 0.252 II compared to III: p = 0.557
	no	21 (100)	22 (95.65)	112 (88.19)	
Anti-SARS-CoV-2 antibodies level [IU/mL]	before vaccination M ±SD	145.0 ±112.1	0 ±0	233.0 ±367.7	K-W test H = 6.70, p = 0.0350 I R = 93.286; II R = 12.500; III R = 96.948 I compared to II: Z = 5.470218 I compared to III: Z = 0.317368 II compared to III: Z = 7.606769 I compared to II: p = 0.000000 I compared to III: p = 1.000000 II compared to III: p = 0.000000
	median (IQR)	126.4 (54.4–200.0)	0	123.2 (58.7–252.8)	

subgroup I – asymptomatic; subgroup II – symptomatic, seronegative; subgroup III – symptomatic, seropositive; SARS-CoV-2 – severe acute respiratory syndrome coronavirus 2; M ±SD – mean ± standard deviation; IQR – interquartile range; I – subgroup I; II – subgroup II; III – subgroup III; K-W test – Kruskal-Wallis test, was used when Shapiro-Wilk test result was  $p < 0.05$ . For other parameters, the Mann-Whitney U test was used.

## Discussion

Assuming that 4 main COVID-19 waves in 2020 and 2021 can be distinguished, the current study covers the 2<sup>nd</sup> (most convalescent participants suffered from a SARS-CoV-2 infection between October and December 2020) and 3<sup>rd</sup> wave (when we collected blood samples).

A precise analysis of group I (divided into: subgroup I – convalescents, asymptomatic; subgroup II – symptomatic, seronegative; and subgroup III – seropositive, symptomatic) showed that there was a significant age difference. In subgroup III, the age was significantly higher than in subgroup II (median 45.0 (40.0–52.0) years compared to 43.0 (33.0–46.0) years  $p = 0.0271$ , Mann-Whitney U test,  $U = 1038.5$ ) and than with group II (45.0 (40.0–52.0) compared to 43.0 (39.0–47.0)  $p = 0.0228$ , Mann-Whitney U test,  $U = 6675.5$ ). There was no such age difference between subgroups III and I ((45.0 (40.0–52.0) years compared to 42.0 (39.0–46.0) years,  $p = 0.0983$ , Mann-Whitney U test,  $U = 1032.5$ ). We also analyzed these data using the Scheffé's test (mean square error (MSE) = 57057,

degrees of freedom (df) = 290.00), which showed that, with regard to age, the antibody results differed between subgroup III and group II ( $p = 0.00000$ ), and between subgroups II and III ( $p = 0.000452$ ). These results are consistent with an earlier meta-analysis, which concluded that elderly or older participants (age  $\geq 50$  years) are at a higher risk of severe disease course.<sup>6</sup>

Furthermore, the asymptomatic subgroup may be an important link in the transmission of the virus. These participants took part in our study in mid-April–mid-May, so it is possible that they were infected during the so-called 3<sup>rd</sup> wave. It has been established that individuals without symptoms are capable of infecting others.<sup>7,8</sup> A similar situation occurs when participants are isolated with a delay due to developing symptoms 1–2 days after becoming infectious.<sup>9</sup>

The level of antibodies in group I differed across individuals, starting from 27.2 IU/mL, which is a borderline titer (blood sample taken 6.5 months after infection), and going up to 2688.2 IU/mL (blood sample taken 2.5 months after infection). The average titer was 190.3 IU/mL. These

differences in titer may be explained by the varying times between SARS-CoV-2 infection and testing. It has been observed that spike antibody levels are relatively stable for several months before waning.<sup>10</sup> In addition, antibody levels are better sustained in participants with severe symptoms.<sup>11</sup> Our participants with borderline titers had no or mild symptoms, whereas the participant with the highest result was hospitalized due to the severity of COVID-19.<sup>12</sup> These findings, together with the theory that some people are serological non-responders,<sup>13</sup> can also partially explain why a subgroup of 23 participants (subgroup II) did not have a detectable level of antibodies.

## Limitations


There are several limitations to the current study. First, there are uneven sample sizes due to the presence of asymptomatic convalescents. In addition, there were irregular time intervals between taking blood samples and receiving first vaccine dose.

## Conclusions


The symptoms of COVID-19 were more often observed in older participants, and the severity of the disease can correlate with higher antibody titers seen later after COVID-19 compared to a mild infection. One should be aware that numerous participants without symptoms of past SARS-CoV-2 infection can transmit the virus to other people. Serological data are not an unambiguous evidence of a past infection.

## ORCID iDs

Monika Stępień  <https://orcid.org/0000-0002-3725-3744>

Natalia Świątoniowska-Lonc  <https://orcid.org/0000-0003-4211-9205>

Brygida Knysz  <https://orcid.org/0000-0003-2605-1079>

Beata Jankowska-Polańska  <https://orcid.org/0000-0003-1120-3535>

Agnieszka Piwowar  <https://orcid.org/0000-0001-6971-3883>

## References

1. Our World in Data. Coronavirus (COVID-19) vaccinations. 2023. [https://ourworldindata.org/covid-vaccinations?country=OWID\\_WRL](https://ourworldindata.org/covid-vaccinations?country=OWID_WRL). Accessed December 17, 2022.
2. Zhou F, Yu T, Du R, et al. Clinical course and risk factors for mortality of adult inpatients with COVID-19 in Wuhan, China: A retrospective cohort study. *Lancet*. 2020;395(10229):1054–1062. doi:10.1016/S0140-6736(20)30566-3
3. Milani GP, Dioni L, Favero C, et al. Serological follow-up of SARS-CoV-2 asymptomatic subjects. *Sci Rep*. 2020;10(1):20048. doi:10.1038/s41598-020-77125-8
4. Rijkers G, Murk JL, Wintermans B, et al. Differences in antibody kinetics and functionality between severe and mild severe acute respiratory syndrome coronavirus 2 infections. *J Infect Dis*. 2020;222(8):1265–1269. doi:10.1093/infdis/jiaa463
5. Liu G, Rusling JF. COVID-19 antibody tests and their limitations. *ACS Sens*. 2021;6(3):593–612. doi:10.1021/acssensors.0c02621
6. Berek MdA, Aziz MdA, Islam MS. Impact of age, sex, comorbidities and clinical symptoms on the severity of COVID-19 cases: A meta-analysis with 55 studies and 10014 cases. *Heliyon*. 2020;6(12):e05684. doi:10.1016/j.heliyon.2020.e05684
7. Johansson MA, Quandelacy TM, Kada S, et al. SARS-CoV-2 transmission from people without COVID-19 symptoms. *JAMA Netw Open*. 2021;4(1):e2035057. doi:10.1001/jamanetworkopen.2020.35057
8. Bi Q, Lessler J, Eckerle I, et al. Insights into household transmission of SARS-CoV-2 from a population-based serological survey. *Nat Commun*. 2021;12(1):3643. doi:10.1038/s41467-021-23733-5
9. Hart WS, Maini PK, Thompson RN. High infectiousness immediately before COVID-19 symptom onset highlights the importance of continued contact tracing. *eLife*. 2021;10:e65534. doi:10.7554/eLife.65534
10. Wajnberg A, Amanat F, Firpo A, et al. Robust neutralizing antibodies to SARS-CoV-2 infection persist for months. *Science*. 2020;370(6521):1227–1230. doi:10.1126/science.abd7728
11. Horton DB, Barrett ES, Roy J, et al. Determinants and dynamics of SARS-CoV-2 infection in a diverse population: 6-month evaluation of a prospective cohort study. *J Infect Dis*. 2021;224(8):1345–1356. doi:10.1093/infdis/jiab411
12. den Hartog G, Vos ERA, van den Hoogen LL, et al. Persistence of antibodies to severe acute respiratory syndrome coronavirus 2 in relation to symptoms in a nationwide prospective study. *Clin Infect Dis*. 2021;73(12):2155–2162. doi:10.1093/cid/ciab172
13. Liu W, Russell RM, Bibollet-Ruche F, et al. Predictors of nonseroconversion after SARS-CoV-2 infection. *Emerg Infect Dis*. 2021;27(9):2454–2458. doi:10.3201/eid2709.211042

